

AL/EQ-TR-1996-0042



## UNITED STATES AIR FORCE ARMSTRONG LABORATORY

---

### Calibration of MADE-2 Groundwater Flow and Contaminant Transport Models

Dale F. Rucker and Donald D. Gray

DEPARTMENT OF CIVIL AND ENVIRONMENTAL ENGINEERING  
West Virginia University  
P.O. Box 6103  
Morgantown, West Virginia 26506-6103

November 1996

19961209 069

DTIC QUALITY INSPECTED 3

*Approved for public release; distribution is unlimited.*

EnviroNics Directorate  
Environmental Research Division  
139 Barnes Drive  
Tyndall Air Force Base FL  
32403-5323

## NOTICES

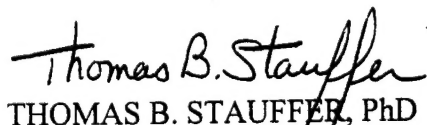
This report was prepared as an account of work sponsored by an agency of the United States Government. Neither the United States Government nor any agency thereof, nor any employees, nor any of their contractors, subcontractors, or their employees, make any warranty, expressed or implied, or assume any legal liability or responsibility for the accuracy, completeness, or usefulness of any privately owned rights. Reference herein to any specific commercial products, process, or service by trade name, trademark, manufacturer, or otherwise, does not necessarily constitute or imply its endorsement, recommendation, or favoring by the United States Government or any agency, contractor, or subcontractor thereof. The views and opinions of the authors expressed herein do not necessarily state or reflect those of the United States Government or any agency, contractor, or subcontractor thereof.

When Government drawings, specifications, or other data are used for any purpose other than in connection with a definitely Government-related procurement, the United States Government incurs no responsibility or any obligation whatsoever. The fact that the Government may have formulated or in any way supplied the said drawings, specifications, or other data, is not to be regarded by implication, or otherwise in any manner construed, as licensing the holder or any other person or corporation; or as conveying any rights or permission to manufacture, use, or sell any patented invention that may in any way be related thereto.

This technical report has been reviewed by the Public Affairs Office (PA) and is releasable to the National Technical Information Service, where it will be available to the general public, including foreign nationals.

This report has been reviewed and is approved for publication.

FOR THE COMMANDER:

  
THOMAS B. STAUFFER, PhD

Chief, Environmental Chemical Processes

  
JIMMY C. CORNETTE, PhD

Chief, Environmental Research Division

# REPORT DOCUMENTATION PAGE

Form Approved  
OMB No. 0704-0188

Public reporting burden for this collection of information is estimated to average 1 hour per response, including the time for reviewing instructions, searching existing data sources, gathering and maintaining the data needed, and completing and reviewing the collection of information. Send comments regarding this burden estimate or any other aspect of this collection of information, including suggestions for reducing this burden, to Washington Headquarters Services, Directorate for Information Operations and Reports, 1215 Jefferson Davis Highway, Suite 1204, Arlington, VA 22202-4302, and to the Office of Management and Budget, Paperwork Reduction Project (0704-0188), Washington, DC 20503.

|   |  |   |   |  |
|---|--|---|---|--|
| 1. AGENCY USE ONLY (Leave blank)  |  | 2. REPORT DATE<br>November 1996                     | 3. REPORT TYPE AND DATES COVERED<br>Final Report 1 Mar 94 - 31 Dec 95   |  |
| 4. TITLE AND SUBTITLE<br>Calibration of MADE-2 Groundwater Flow and Contaminant Transport Models  |  |   | 5. FUNDING NUMBERS<br>F0863794M6010                                     |  |
| 6. AUTHOR(S)<br>Dale F. Rucker<br>Donald D. Gray  |  |   |   |  |
| 7. PERFORMING ORGANIZATION NAME(S) AND ADDRESS(ES)<br>Department of Civil and Environmental Engineering<br>West Virginia University<br>P.O. Box 6103<br>Morgantown, WV 26506-6103   |  |   | 8. PERFORMING ORGANIZATION<br>REPORT NUMBER                             |  |
| 9. SPONSORING/MONITORING AGENCY NAME(S) AND ADDRESS(ES)<br>Armstrong Laboratory Environics Directorate (AL/EQ)<br>Tyndall AFB, FL 32403-5323  |  |   | 10. SPONSORING/MONITORING<br>AGENCY REPORT NUMBER<br>AL/EQ-Tn-1996-0042 |  |
| 11. SUPPLEMENTARY NOTES<br><br>AL/EQL Project Manager is Dr. Thomas Stauffer  |  |   |   |  |
| 12a. DISTRIBUTION/AVAILABILITY STATEMENT<br><br>Approved For Public Release<br>Distribution Unlimited   |  |   | 12b. DISTRIBUTION CODE  |  |
| 13. ABSTRACT (Maximum 200 words)<br><br>Public domain computer programs were used to simulate groundwater flow and contaminant migration through a site at the Columbus Air Force Base Mississippi. In the MADE-2 (Macrodispersion Experiment) experiment a pulse of dissolved contaminants in the saturated zone of an alluvial aquifer was monitored for 15 months. MODFLOW solved for head and seepage velocity for input to the transport code, MT3D. The contaminant transport equation was solved separately from the flow equation since buoyancy effects were assumed to be negligible. Initial simulations of the tritium plume did not extend far enough from the injection site. An ad hoc assumption of horizontal anisotropy applied to the conductivity field produced good agreement with the observed plumes. Although the simulated plumes were realistic, the horizontally anisotropic conductivity field used to achieve these predictions was not. The principal axes were not aligned with the directions suggested by pump tests or geology, the anisotropy ratio was in excess of any previously observed, and the effective conductivity was above what had been measured at the site. The use of public domain software to model contaminant transport at heterogeneous sites is technically practical; but in the absence of exhaustive field measurements, little confidence can be placed in the predictions.<br><br>DTIC QUALITY INSPECTED 3 |  |   |   |  |
| 14. SUBJECT TERMS<br><br>MODFLOW, MT3D, MADE-2, Groundwater, Numerical Modeling   |  |   | 15. NUMBER OF PAGES   |  |
|   |  |   | 16. PRICE CODE  |  |
| 17. SECURITY CLASSIFICATION<br>OF REPORT<br>Uncl.   | 18. SECURITY CLASSIFICATION<br>OF THIS PAGE<br>Uncl. | 19. SECURITY CLASSIFICATION<br>OF ABSTRACT<br>Uncl. | 20. LIMITATION OF ABSTRACT<br>Unlim.                                    |  |

## PREFACE

This report was prepared by the Department of Civil and Environmental Engineering, West Virginia University, P.O. Box 6103, Morgantown, WV 26506-6103. This research project was funded by the United States Air Force under contract F0863794M6010 with the 325 Contracting Squadron, Tyndall Air Force Base, FL 32403-5323. The Principal Investigator was Dr. Donald D. Gray. The point of contact was Dr. Thomas Stauffer, OL-AL/EQ. The work was conducted between March, 1994, and December, 1995.

This final report describes the use of public domain software to create numerical models of the groundwater flow and contaminant transport in the Macrodispersion Experiment 2 conducted at Columbus AFB, Mississippi.

The authors thank Dr. Robert Eli, Dr. Mohammed Gabr, and Mr. Mandar Sarangdhar of West Virginia University; Dr. Manfred Koch of Temple University; and Dr. Chunmiao Zheng of the University of Alabama.

The reverse of this page is intentionally blank.



## EXECUTIVE SUMMARY

Public domain numerical groundwater flow (MODFLOW) and contaminant transport (MT3D) computer programs were used to simulate groundwater flow and contaminant migration of a nonreactive tracer and four organic compounds through a site at Columbus Air Force Base in Columbus, Mississippi. The MADE-2 (Macrodispersion Experiment) experiment commenced with the pulse injection of the dissolved contaminants into the saturated zone of an alluvial aquifer through a series of five injection wells. The concentrations of the contaminants, hydraulic head, and net recharge were monitored for 15 months. Previous measurements of hydraulic conductivity, porosity, and other parameters were also used in the modeling process.

The finite-difference code, MODFLOW, solved the governing groundwater equation for hydraulic head and seepage velocity at discrete nodes. Kriging was employed to obtain initial and boundary conditions by extrapolating measured heads.

The head and flow velocities were used as input to the transport code. MT3D solved the contaminant transport equation separately from the flow equation since buoyancy effects were assumed to be negligible. Initial simulations of the tritium plume were unsatisfactory. The simulated plume did not extend far enough from the injection site to match the observations. An ad hoc assumption of horizontal anisotropy was applied to the conductivity field in order to increase the longitudinal velocities enough to push the plume downgradient. This produced realistic simulated plumes for tritium and the four organic chemicals.

Although the simulated plumes were realistic, the horizontally anisotropic conductivity field used to achieve these predictions was not. The assumed principal axes were not aligned with the directions suggested by pump tests or geologic history. In addition, the degree of anisotropy was far in excess of any previously observed. Finally, the magnitude of the effective conductivity was far above what had been measured at the site.

The use of public domain software to model contaminant transport at heterogeneous sites is technically practical; but in the absence of exhaustive field measurements, little confidence can be placed in the predictions.

## TABLE OF CONTENTS

| Section | Title  | Page |
|---------|--|------|
| I       | INTRODUCTION.....                                    | 1    |
|         | A. OBJECTIVE.....                                    | 1    |
|         | B. BACKGROUND.....                                   | 1    |
|         | C. SCOPE.....  | 5    |
|         | D. APPROACH.....                                     | 7    |
| II      | SITE DESCRIPTION.....                                | 10   |
|         | A. HYDROGEOLOGIC MEASUREMENTS.....                   | 10   |
|         | 1. Hydraulic Conductivity.....                       | 10   |
|         | 2. Aquifer Tests.....                                | 17   |
|         | 3. Hydraulic Head Monitoring.....                    | 19   |
|         | 4. Other Aquifer Measurements.....                   | 26   |
|         | B. HYDROLOGY.....                                    | 26   |
| III     | TRACER MONITORING.....                               | 29   |
| IV      | MADE-2 DATABASE.....                                 | 33   |
| V       | FLOW MODELING.....                                   | 37   |
|         | A. CODE SELECTION.....                               | 37   |
|         | B. DISCRETIZATION.....                               | 40   |
|         | C. INITIAL AND BOUNDARY CONDITIONS.....              | 43   |
|         | D. MODELING OF AQUIFER PARAMETERS.....               | 50   |
|         | 1. Hydraulic Conductivity and Vertical Leakance..... | 50   |
|         | 2. Horizontal Anisotropy.....                        | 54   |
|         | 3. Storage Parameters.....                           | 54   |
|         | E. HYDROLOGIC STRESSES.....                          | 55   |
|         | 1. Recharge.....                                     | 55   |
|         | 2. Well Simulation.....                              | 55   |
|         | F. SOLUTION METHOD.....                              | 56   |
|         | G. COMPUTER SIMULATIONS.....                         | 57   |
| VI      | TRANSPORT MODELING.....                              | 70   |
|         | A. THEORY.....                                       | 70   |
|         | 1. Advection.....                                    | 71   |
|         | 2. Dispersion.....                                   | 73   |
|         | 3. Chemical Reactions.....                           | 73   |
|         | 4. Sink and Sources.....                             | 74   |
|         | B. DISCRETIZATION.....                               | 74   |
|         | C. INITIAL AND BOUNDARY CONDITIONS.....              | 75   |
|         | D. TRANSPORT PARAMETERS.....                         | 75   |
|         | 1. Porosity.....                                     | 75   |
|         | 2. Dispersivity.....                                 | 76   |
|         | 3. Chemical Reactions.....                           | 76   |

|   |     |
|---|-----|
| 4. Contaminant Sources.....                           | 78  |
| E. MT3D OUTPUT .....                                  | 78  |
| F. COMPUTER SIMULATIONS .....                         | 79  |
| VII EFFECTS OF HORIZONTAL ANISOTROPY .....            | 90  |
| A. MT3D CODING MODIFICATIONS.....                     | 90  |
| B. HORIZONTAL ANISOTROPY.....                         | 91  |
| 1. Flow Modeling with Horizontal Anisotropy.....      | 91  |
| 2. Transport Modeling of M2-8-7.....                  | 102 |
| C. ANISOTROPY VARYING BY CONDUCTIVITY .....           | 104 |
| D. FURTHER CONSIDERATION OF ANISOTROPY.....           | 142 |
| VIII DISCUSSIONS.....                                 | 158 |
| A. BUOYANCY EFFECTS.....                              | 158 |
| B. GRID CONVERGENCE.....                              | 159 |
| IX CONCLUSION .....                                   | 164 |
| REFERENCES .....                                      | 166 |
| APPENDICES  |     |
| A KRIGED OBSERVED HEAD SURVEYS.....                   | 169 |
| B KRIGED TRANSMISSIVITY AND LEAKANCE FOR M2-8-8 ..... | 185 |
| C CHANGES TO MODFLOW SOURCE CODE FOR MF95.....        | 201 |

## LIST OF FIGURES

| Figure   | Page |
|--|------|
| 1. Location of MADE Site. ....   | 3    |
| 2. Borehole Flowmeter Locations. ....  | 12   |
| 3. Vertically Averaged Hydraulic Conductivity and Conductivity Profile Along Section A-A ..            | 14   |
| 4. Aerial Photograph of MADE Site. ....  | 15   |
| 5. Piezometer Locations. ....  | 20   |
| 6. Heads at Upper and Lower Piezometers, June 19, 1990. ....   | 22   |
| 7. Averaged Hydrographs of Piezometers P53A and P54B. ....   | 24   |
| 8. Cross Correlation of Piezometers P53 and P54 (Upper) and Piezometers<br>P53 and P61 (Lower). ....   | 25   |
| 9. Net Recharge Vs. Time. ....   | 28   |
| 10. Sampling Well Network. ....  | 31   |
| 11. Grid Used in MADE-2 Modeling. ....   | 41   |
| 12. Piezometers Used for Kriging. ....   | 46   |
| 13. Upper and Lower Kriged Heads of June 19, 1990. ....  | 47   |
| 14. Upper and Lower Kriged Heads of March 8, 1991. ....  | 48   |
| 15. Kriged Transmissivity [ $m^2/d$ ] and Leakance [ $1/d$ ] for M2-5. ....                            | 53   |
| 16. Left: M2-5-1, Day 270, Layer 4 Heads. Right: Upper Kriged Heads of March 8, 1991. ....             | 59   |
| 17. Left: M2-5-1, Day 270, Layer 9 Heads. Right: Lower Kriged Heads of March 8, 1991. ....             | 60   |
| 18. Observed and Simulation M2-5-1 Hydrographs of P53A. ....   | 61   |
| 19. Layer 3 Transmissivity [ $m/d$ ] of M2-8 (Left) and M2-5 (Right). ....                             | 64   |
| 20. M2-8-1, Day 270. Left: Layer 4, Right: Layer 9. ....   | 66   |
| 21. Nearest Grid Point Transmissivity Distribution for Layer 9. ....                                   | 68   |
| 22. M2-9-1 Heads for Day 270. Left: Layer 4; Right: Layer 9. ....                                      | 69   |
| 23. Two Dimensional Tritium Relative Concentration, Run M2-6-1.<br>Left: Day 148; Right: Day 344. .... | 82   |
| 24. Two Dimensional Tritium Relative Concentration, Run M2-6-2.<br>Left: Day 148; Right: Day 344. .... | 83   |
| 25. Observed Tritium Relative Concentration at 59.5 m MSL. Source: Boggs et al (1993). ....            | 84   |
| 26. Two Dimensional Tritium Relative Concentration, Run M2-6-3.<br>Left: Day 148; Right: Day 344. .... | 85   |
| 27. Normalized Tritium Concentration, M2-5-5, Run 1, Layer 4.<br>Left: Day 148; Right: Day 344. ....   | 87   |
| 28. Normalized Tritium Concentration, M2-9-1, Layer 4, Day 344. ....                                   | 89   |
| 29. Heads of M2-8-2, Day 270. Left: Layer 4; Right: Layer 9. ....                                      | 94   |
| 30. Heads of M2-8-3, Day 270. Left: Layer 4; Right: Layer 9. ....                                      | 95   |
| 31. Heads of M2-8-4, Day 270. Left: Layer 4; Right: Layer 9. ....                                      | 96   |
| 32. Heads of M2-8-5, Day 270. Left: Layer 4; Right: Layer 9. ....                                      | 97   |
| 33. Heads of M2-8-6, Day 270. Left: Layer 4; Right: Layer 9. ....                                      | 98   |
| 34. Kriged TRPY for M2-8-7. Left: Upper Levels; Right: Lower Levels. ....                              | 100  |
| 35. Heads of M2-8-7, Day 270. Left: Layer 4; Right: Layer 9. ....                                      | 101  |
| 36. Normalized Tritium Concentration, M2-8-7, Layer 4, Days 44, 148, 240, 344, and 456. ....           | 103  |

|   |     |
|---|-----|
| 37. Regions of TRPY = 15 Indicated By Shading. Left: Layer 3; Right: Layer 7 .....            | 106 |
| 38. Heads of M2-8-8, Day 270. Left: Layer 4; Right: Layer 9.....                              | 107 |
| 39. Normalized Tritium Concentration, M2-8-8, Layer 4, Days 44, 148, 240, 344, and 456... 108 |     |
| 40. M2-8-8 Normalized Concentration Profiles Along Column 11, Day 44. ....                    | 111 |
| 41. M2-8-8 Normalized Concentration Profiles Along Column 11, Day 148. ....                   | 112 |
| 42. M2-8-8 Normalized Concentration Profiles Along Column 11, Day 240. ....                   | 113 |
| 43. M2-8-8 Normalized Concentration Profiles Along Column 11, Day 344. ....                   | 114 |
| 44. M2-8-8 Normalized Concentration Profiles Along Column 11, Day 456. ....                   | 115 |
| 45. Observed Normalized Concentration Profiles, Day 44.....                                   | 116 |
| 46. Observed Normalized Concentration Profiles, Day 148.....                                  | 117 |
| 47. Observed Normalized Concentration Profiles, Day 240.....                                  | 118 |
| 48. Observed Normalized Concentration Profiles, Day 344.....                                  | 119 |
| 49. Observed Normalized Concentration Profiles, Day 456.....                                  | 120 |
| 50. M2-8-8 Normalized Organic Concentrations in Layer 4, Day 44. ....                         | 121 |
| 51. M2-8-8 Normalized Organic Concentrations in Layer 4, Day 148. ....                        | 122 |
| 52. M2-8-8 Normalized Organic Concentrations in Layer 4, Day 240. ....                        | 123 |
| 53. M2-8-8 Normalized Organic Concentrations in Layer 4, Day 344. ....                        | 124 |
| 54. M2-8-8 Normalized Organic Concentrations in Layer 4, Day 456. ....                        | 125 |
| 55. Observed and M2-8-8 Mass Ratio for Tritium. ....  | 131 |
| 56. Observed and M2-8-8 Mass Ratio for Benzene.....   | 132 |
| 57. Observed and M2-8-8 Mass Ratio for Naphthalene.....                                       | 133 |
| 58. Observed and M2-8-8 Mass Ratio for p-Xylene.....  | 134 |
| 59. Observed and M2-8-8 Mass Ratio for o-DCB.....   | 135 |
| 60. Observed and M2-8-8 Center of Mass Trajectory for Tritium. ....                           | 137 |
| 61. Observed and M2-8-8 Center of Mass Trajectory for Benzene.....                            | 138 |
| 62. Observed and M2-8-8 Center of Mass Trajectory for Naphthalene.....                        | 139 |
| 63. Observed and M2-8-8 Center of Mass Trajectory for p-Xylene.....                           | 140 |
| 64. Observed and M2-8-8 Center of Mass Trajectory for o-DCB.....                              | 141 |
| 65. Normalized Tritium Concentration for Layer 4, Day 344, M2-8-9, Rm 1. ....                 | 147 |
| 66. Head and Seepage Velocity in Layer 4, Day 298, M2-8-9, Rm 1.....                          | 149 |
| 67. Head and Seepage Velocity in Layer 4, Day 298, M2-8-9, Rm 2.....                          | 150 |
| 68. Head and Seepage Velocity in Layer 4, Day 298, M2-8-9, Rm 3.....                          | 151 |
| 69. Head and Seepage Velocity in Layer 4, Day 298, M2-8-9, Rm 4.....                          | 152 |
| 70. Head and Seepage Velocity in Layer 4, Day 298, M2-8-9, Rm 5.....                          | 153 |
| 71. Kriged Observed Heads of April 4, 1991. Left: Upper Level; Right: Lower Level .....       | 154 |
| 72. Head and Seepage Velocity in Layer 4, Day 298, M2-8-8.....                                | 155 |
| 73. Normalized Tritium Concentration in Layer 4, Day 344, M2-8-9, Rm 4. ....                  | 157 |
| A-1. Upper and Lower Kriged Heads of July 23, 1990. ....                                      | 170 |
| A-2. Upper and Lower Kriged Heads of August 13, 1990. ....                                    | 171 |
| A-3. Upper and Lower Kriged Heads of September 17, 1990.....                                  | 172 |
| A-4. Upper and Lower Kriged Heads of October 15, 1990.....                                    | 173 |
| A-5. Upper and Lower Kriged Heads of November 7, 1990.....                                    | 174 |
| A-6. Upper and Lower Kriged Heads of December 5, 1990.....                                    | 175 |
| A-7. Upper and Lower Kriged Heads of January 8, 1991.....                                     | 176 |
| A-8. Upper and Lower Kriged Heads of February 8, 1991.....                                    | 177 |

|  |     |
|--|-----|
| A-9. Upper and Lower Kriged Heads of April 4, 1991.....        | 178 |
| A-10. Upper and Lower Kriged Heads of May 10, 1991.....        | 179 |
| A-11. Upper and Lower Kriged Heads of May 20, 1991.....        | 180 |
| A-12. Upper and Lower Kriged Heads of June 13, 1991.....       | 181 |
| A-13. Upper and Lower Kriged Heads of July 9, 1991. ....       | 182 |
| A-14. Upper and Lower Kriged Heads of August 19, 1991. ....    | 183 |
| A-15. Upper and Lower Kriged Heads of September 11, 1991. .... | 184 |
| B-1. Hydraulic Conductivity [m/d] of Layer 1.....              | 186 |
| B-2. Transmissivity [ $m^2$ /d] of Layer 2.....                | 187 |
| B-3. Transmissivity [ $m^2$ /d] of Layer 4.....                | 188 |
| B-4. Transmissivity [ $m^2$ /d] of Layer 5.....                | 189 |
| B-5. Transmissivity [ $m^2$ /d] of Layer 6.....                | 190 |
| B-6. Transmissivity [ $m^2$ /d] of Layer 7.....                | 191 |
| B-7. Transmissivity [ $m^2$ /d] of Layer 8.....                | 192 |
| B-8. Transmissivity [ $m^2$ /d] of Layer 9.....                | 193 |
| B-9. Leakance [1/d] of Layer 1.....                            | 194 |
| B-10. Leakance [1/d] of Layer 2.....                           | 195 |
| B-11. Leakance [1/d] of Layer 4.....                           | 196 |
| B-12. Leakance [1/d] of Layer 5.....                           | 197 |
| B-13. Leakance [1/d] of Layer 6.....                           | 198 |
| B-14. Leakance [1/d] of Layer 7.....                           | 199 |
| B-15. Leakance [1/d] of Layer 8.....                           | 200 |

## LIST OF TABLES

| Table   | Title   | Page |
|---------|---|------|
| 1.      | CONDUCTIVITY AT MACRODISPERSION SITES.....                        | 2    |
| 2.      | SUMMARY OF HYDRAULIC CONDUCTIVITY MEASUREMENTS.....               | 19   |
| 3.      | INITIAL CONCENTRATIONS AND INJECTED MASS.....                     | 29   |
| 4.      | SUMMARY OF TRACER SAMPLING.....                                   | 32   |
| 5.      | EXAMPLE SNAPSHOT DATA.....  | 33   |
| 6.      | EXAMPLE SURVEY PIEZOMETRIC HEAD DATA.....                         | 34   |
| 7.      | EXAMPLE CONTINUOUS PIEZOMETRIC HEAD DATA.....                     | 34   |
| 8.      | EXAMPLE BOREHOLE FLOWMETER CONDUCTIVITY DATA.....                 | 35   |
| 9.      | AVAILABLE GROUNDWATER CODES IN JUNE 1992.....                     | 38   |
| 10.     | STRESS PERIODS FOR MADE-2 SIMULATIONS.....                        | 43   |
| 11 (A). | KRIGING PARAMETERS FOR THE UPPER MONTHLY HEAD SURVEYS.....        | 49   |
| 11 (B). | KRIGING PARAMETERS FOR THE LOWER MONTHLY HEAD SURVEYS.....        | 49   |
| 12.     | AVERAGE NET RECHARGE.....   | 55   |
| 13.     | SUMMARY OF MODFLOW CASES M2-5-1 THROUGH M2-5-5.....               | 57   |
| 14.     | OBSERVED HEADS VS. MODFLOW HEADS FOR M2-5-1,4,5.....              | 62   |
| 15.     | KRIGING PARAMETERS FOR TRANSMISSIVITY AND LEAKANCE.....           | 63   |
| 16.     | SUMMARY STATISTICS FOR M2-8.....                                  | 65   |
| 17.     | PARAMETERS FOR ORGANIC TRANSPORT SIMULATIONS.....                 | 77   |
| 18.     | MT3D SIMULATIONS BY GRAY AND RUCKER (1994).....                   | 80   |
| 19.     | SUMMARY OF 2-D TRANSPORT SIMULATIONS (M2-6).....                  | 81   |
| 20.     | SUCCESSFUL HORIZONTALLY ISOTROPIC TRANSPORT SIMULATIONS.....      | 86   |
| 21.     | UNIFORMLY HORIZONTALLY ANISOTROPIC FLOW SIMULATIONS.....          | 92   |
| 22 (A). | TRITIUM PLUME CHARACTERISTICS FROM SIMULATION M2-8-8.....         | 126  |
| 22 (B). | BENZENE PLUME CHARACTERISTICS FROM SIMULATION M2-8-8.....         | 126  |
| 22 (C). | NAPHTHALENE PLUME CHARACTERISTICS FROM SIMULATION M2-8-8.....     | 127  |
| 22 (D). | P-XYLENE PLUME CHARACTERISTICS FROM SIMULATION M2-8-8.....        | 127  |
| 22 (E). | O-DCB PLUME CHARACTERISTICS FROM SIMULATION M2-8-8.....           | 127  |
| 23 (A). | OBSERVED TRITIUM PLUME CHARACTERISTICS.....                       | 128  |
| 23 (B). | OBSERVED BENZENE PLUME CHARACTERISTICS.....                       | 128  |
| 23 (C). | OBSERVED NAPHTHALENE PLUME CHARACTERISTICS.....                   | 128  |
| 23 (D). | OBSERVED P-XYLENE PLUME CHARACTERISTICS.....                      | 129  |
| 23 (E). | OBSERVED O-DCB PLUME CHARACTERISTICS.....                         | 129  |
| 24.     | SIMULATIONS OF M2-8-9 (CORRECTED ANISOTROPIC TRANSMISSIVITY)..... | 146  |
| 25.     | RELATIVE DENSITIES OF CONTAMINANTS.....                           | 159  |
| 26.     | EXTRACTED HEADS FOR VARIOUS GRID SIZES.....                       | 161  |
| 27.     | GCI VALUES.....   | 162  |



## SECTION I

### INTRODUCTION

#### A. OBJECTIVE

Numerous Air Force sites have suffered groundwater contamination due to hydrocarbon spills. The design of optimal remediation programs requires reliable numerical modeling of contaminant transport, and this modeling should be carried out using the most widely available hardware and software. The objective of this study was to illustrate state-of-the-art modeling of dissolved contaminant transport in a heterogeneous surficial aquifer using public domain software on a microcomputer. This was accomplished by applying these techniques to the data obtained in an actual field-scale experiment.

#### B. BACKGROUND

Realizing the dangers associated with polluted groundwater, the Air Force has initiated several programs dedicated to understanding the physical processes involved with the fate of contaminants in the subsurface. Focusing mainly on organic solvents, such as cleaning solutions (e.g. trichloroethylene) and jet fuel constituents (e.g. naphthalene, toluene, xylene, benzene, etc.), these studies are aimed at developing a predictive capability for the transport of these harmful chemicals. By estimating the amount and location of the contaminant at any given time, remediation techniques can be implemented in a more cost-effective manner.

In the present study, a numerical model was applied to the MADE (Macrodispersion Experiment) site, located at Columbus Air Force Base (CAFB), Mississippi. Figure 1 shows the location of the site. The MADE site was the location of two natural-gradient, large-scale tracer experiments intended to quantify the effects of macrodispersivity in an extremely heterogeneous aquifer. Macrodispersion arises from spatial variability in the hydraulic properties of natural aquifers (Boggs et al., 1992), and its understanding requires controlled experimentation in which a detailed analysis is performed on a nonreactive tracer plume. Describing the motion of the plume

requires a three-dimensional sampling network to characterize the depth and areal extent of contamination. Extensive hydraulic conductivity measurements are also needed to accurately estimate the spatial variability of the conductivity. Together, these data allow the dispersion coefficients to be estimated, allowing a model to fit the observed phenomena.

The MADE site is the most heterogeneous site used to date for a natural-gradient experiment. Table 1, taken from Rehfeldt (1992), shows the variance in the natural logarithm of the conductivity ( $\ln(K)$ ) to be 4.5, translating to a range of over three orders of magnitude. This value was calculated from 2187 separate borehole flowmeter measurements in 49 different profiles by Rehfeldt et al. (1992).

TABLE 1. CONDUCTIVITY AT MACRODISPERSION SITES.

K = hydraulic conductivity (cm/s)  
 $L_h$  = horizontal correlation scale (meters)  
 $L_v$  = vertical correlation scale (meters)

| Location   | Variance ( $\ln(K)$ ) | $L_h$ | $L_v$ |
|------------|-----------------------|-------|-------|
| MADE       | 4.5                   | 12.8  | 1.6   |
| Borden     | 0.29                  | 2.8   | 0.12  |
| Cape Cod   | 0.26                  | 5.1   | 0.26  |
| Twin Lakes | 0.031                 | 3.0   | 0.91  |

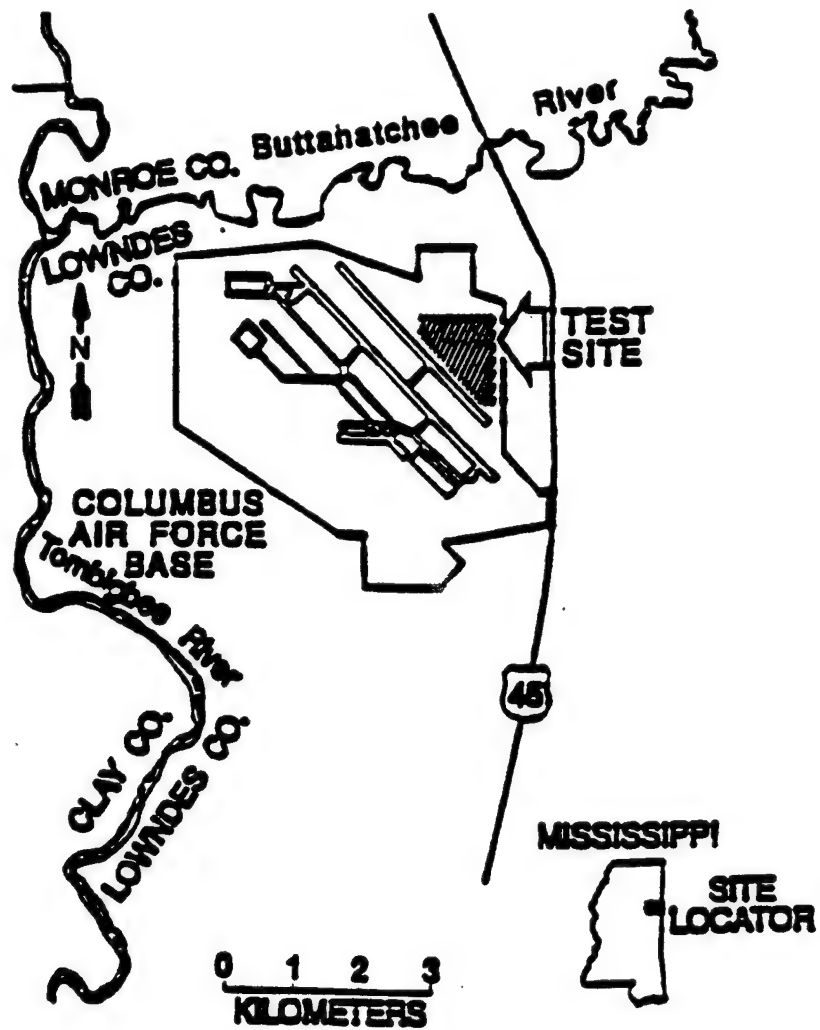


Figure 1. Location of MADE Site. Source: Boggs et al. (1993).

Two experiments took place at the MADE site, denoted as MADE-1, and MADE-2. The first, MADE-1, tracked a conservative tracer, bromide, for approximately 20 months. The experiment started with a pulse injection of a known quantity of solution, and concentrations were monitored periodically by use of multilevel samplers. The results of this experiment can be found in a series of journal articles (Boggs et al., 1992; Adams and Gelhar, 1992; Rehfeldt, Boggs, and Gelhar, 1992; Boggs and Adams, 1992).

The second experiment, MADE-2, sponsored by the Air Force and the Electric Power Research Institute (EPRI), is considered in this research. MADE-2 studied the transport of a conservative tracer, tritiated water, as well as the effects of sorption and biodegradation on four nonconservative dissolved organic compounds (benzene, naphthalene, p-xylene, and o-dichlorobenzene) in the saturated zone. The dissolved organic chemicals are of types found in jet fuels and cleaning solvents. MADE-2 started in June, 1990, with the pulse injection of the solution into five screened wells, spaced 1 meter apart. The injection of  $9.7 \text{ m}^3$  of solution lasted 48.5 hours. For 15 months, the concentrations of each contaminant were monitored by the Tennessee Valley Authority (TVA) using multilevel samplers dispersed somewhat regularly over the domain. The multilevel sampler network provided a detailed array of contaminant plume data. Five three-dimensional sampling events, referred to as "snapshots" were performed at intervals of approximately 100 days. The features of the observed plumes were characterized by the first three spatial moments: the zeroth (total mass), first (centroid), and second (concentration variance about the centroid) moments.

In addition to the extensive concentration data, several aquifer parameters were measured to determine the variability of the hydraulic conductivity field. First, the borehole flowmeter measured the horizontal hydraulic conductivity in 77 separate boreholes at 15 cm (6 inch) depth intervals. Hydraulic conductivity was often seen to range over four orders of magnitude in the same borehole, making the MADE site the most heterogeneous aquifer in which a natural-gradient tracer experiment has been conducted, including the Cape Cod (LeBlanc et al., 1991) and Borden sites (Sudicky, 1986). Over 2500 measurements allowed the use of geostatistical techniques to estimate conductivity values over the entire domain.

A soil grain analysis was also used to measure the hydraulic conductivity. The empirical method of Seiler (Boggs et al., 1990) was used to calculate the conductivity from grain-size distributions. However, only 214 soil samples from 30 separate coreholes were taken. The variance of the natural logarithm of conductivity measurements ( $\sigma^2_{\ln K}$ ) was calculated to be 3.1, outside of the confidence limits of the borehole flowmeter measurements, 3.4 to 5.6. This high degree of uncertainty in the variance estimates for the borehole flowmeter is unavoidable for practical problems involving extremely heterogeneous aquifers (Rehfeldt et al., 1992). Other methods used to measure conductivity at the MADE site were the slug, permeameter, and double-packer tests, having variances of 1.8, 5.5, and 0.47, respectively.

Hydraulic head measurements were taken to monitor the rise and fall of the water table. A total of 17 monthly surveys were taken in an array of 49 single- and multistaged piezometers. Continuous hydrographs were measured in 8 staged piezometers.

### C. SCOPE

The above data, supplied by the Tennessee Valley Authority and the United States Air Force, were used to apply and evaluate a numerical model of the MADE-2 plumes. During the Summer Faculty Research Program (SFRP) of 1992, Gray selected MODFLOW (McDonald and Harbaugh, 1988) as the code to simulate the three-dimensional groundwater flow (Gray, 1992). Preliminary steady state solutions were obtained at this time.

Gray (1993) continued his research during the summer of 1993 in the SFRP at Tyndall Air Force Base. He modeled the tritium plume using the mixed Eulerian-Lagrangian finite-difference program MT3D, which solves the contaminant transport equation using the MODFLOW-predicted flow field. Two transient flow fields were simulated, one assuming a uniform conductivity field, and the other a heterogeneous conductivity field based on kriging the borehole flowmeter data. The uniform conductivity flow model ran approximately three times faster to simulate a given time period. However, the MT3D transport simulations were unsuccessful

because numerical instabilities or grossly unrealistic predictions ended every simulation prematurely.

During the summer of 1994 at Tyndall Air Force Base, Gray and Rucker (1994) were able to formulate a more accurate depiction of the conductivity field by using a new geostatistical program, Geo-EAS. Again, MODFLOW and MT3D were used to solve the flow and concentration fields, respectively. Their successes in modeling the transport of tritium were limited, as the code ran excessively long. Numerical instability again ended every transport simulation before the desired completion time.

The authors continued work on the MADE-2 modeling project under the present contract. However, it was not until the spring of 1995 that the transport of tritium was modeled for the entire 468-day experiment. Excessive run times and inaccurate results did not allow many simulations to be completed. The transport code took up to 3 weeks to finish.

Rucker was invited for a second summer during 1995 to continue research at Tyndall Air Force Base. A modified version of MT3D, acquired from Dr. Manfred Koch of Temple University, reduced run times from weeks to hours. Additional modeling investigated the possibility of horizontal anisotropy in the conductivity. Early successful simulations showed the longitudinal migration of tritium to reach only 75 meters downgradient from the injection source. However, the field observations showed the plume to spread at least 225 m. By implementing horizontal anisotropy, the velocities were increased, thus increasing the plume movement. Continuing the work at WVU, the tritium plume was finally simulated fairly accurately, and other runs were conducted to simulate the dissolved organic contaminants.

In addition to the works of Gray (1992, 1993) and Gray and Rucker (1994), there have been other models of the MADE-2 plumes. Dr. Manfred Koch conducted independent modeling of MADE-2 while at Tyndall AFB. Koch (1994) was able to model the contaminants through the entire 468-day experiment, but could not match the field observations. Dr. C. Zheng and Dr. J. Jiao of the University of Alabama, and C. J. Neville of S. S. Papadopoulos and Associates (Zheng

et al., 1994) applied a steady-state model to the MADE-2 experiment. Their efforts proved that the simulated plume was more sensitive to the hydraulic conductivity field than to the dispersivity used. Each study greatly contributed to the present research.

#### D. APPROACH

A model is an approximate representation of an observed phenomenon. A mathematical model consists of the governing equations together with appropriate boundary and initial conditions. The mathematical equations may be solved analytically or numerically, with numerical solutions usually allowing for more complex boundaries and heterogeneous soil properties (Anderson and Woessner, 1992). This study concerns numerical modeling.

The partial differential equations which govern groundwater flow and contaminant transport can be discretized by the finite-difference method, the finite-element method, or some other schemes. The finite-difference method is the most easily understood and was used in this study. The domain is gridded into regularly shaped blocks or cells. Within each cell are nodes where the unknowns are to be calculated. The discretized equations are solved using numerical methods implemented in computer programs known as codes. The codes used in this research were the groundwater flow code MODFLOW and the contaminant transport code MT3D. Both are widely used public domain programs which can be executed on current personal computers.

This report provides a detailed explanation of a numerical model being applied to simulate the MADE-2 field data. The report moves from the site description to data analysis, modeling, and ends with the interpretation of results and suggestions for further research.

## SECTION II

### SITE DESCRIPTION

#### A. HYDROGEOLOGIC MEASUREMENTS

Figure 1 shows that the MADE-2 test site is located approximately 6 km east of the Tombigbee River and 2.5 km south of the Buttahatchee River at Columbus Air Force Base in Lowndes County, Mississippi. The site lies within the Columbus aquifer and is situated above the 100-year flood plain. Averaging 8 to 10 meters in depth, the Columbus aquifer is composed of alluvial deposits, primarily interfingering, discontinuous, lozenge-shaped lenses of poorly to well sorted gravely sand and sandy gravel with small amounts of clay and silt (Young, 1994). The lenses are typically on the order of 8 meters in the horizontal direction, and 1 meter in the vertical. Subsurface investigations show the soil to be mainly unconsolidated and cohesionless, however occasional small consolidated zones were encountered during exploratory drilling (Boggs et al., 1992). Beneath the alluvial aquifer lies the Eutaw formation, an aquitard consisting of clays, fine grained sands, and silts of marine origin, estimated to be 75 meters thick.

Data gathered at the MADE site included hydraulic conductivity, hydraulic head, aquifer porosity, and bulk density. These extensive measurements allowed analysis of the spatial distribution of hydraulic conductivity using geostatistical techniques. Moreover, the data have been used to infer the geologic history of the area.

##### 1. Hydraulic Conductivity

Hydraulic conductivity was measured using several direct and indirect methods. Of the direct methods, including borehole flowmeter, permeameter, slug, and double-packer tests, the borehole flowmeter tests provided the largest data set, with over 2500 measurements in 77 different locations. Borehole flowmeter measurements were originally made for the MADE-1 experiment, but 21 new wells have been tested since that time. The borehole flowmeter measures the discharge during pumping at discrete locations along the screened length of the well. This



provides the inflow to the well as a function of elevation. Since the inflow is assumed to be horizontal and radial, the discharge from each layer is proportional to the product of the layer hydraulic conductivity and the layer thickness. Using the layer flow rate and drawdown, the Cooper-Jacob well equation is employed incrementally to evaluate the hydraulic conductivity of each layer. The key assumptions underlying this procedure are (1) the aquifer is layered and each layer is homogeneous and of uniform thickness, (2) the storage coefficient of each layer is linearly related to the layer transmissivity, and (3) the well losses attributed to each layer can be estimated (Boggs et al., 1990). The heterogeneity of the MADE site limits the validity of these assumptions, especially assumption 1.

Flow measurements were made with an impeller-type flowmeter which was lowered down the borehole. The rotation of the impeller caused by vertical flow in the well was read by optical sensors and converted to a voltage which was directly proportional to the rate of rotation (Rehfeldt et al., 1989). The voltage passed through a coaxial cable to surface electronics. Calibration of the instrument was necessary before and after each flowmeter measurement to convert the recorded voltages to flow rates. The lower threshold of flow measurement for the impeller flowmeter is approximately 0.005 L/s, corresponding to a hydraulic conductivity of about  $10^{-4}$  cm/s (Rehfeldt et al., 1989).

The locations of the borehole flowmeter measurements can be seen in Figure 2. The origin of the plot lies at the center of the injection wells. Each conductivity well is labeled with a 'K' and a number corresponding to the order in which it was installed. The wells were constructed of 5.1 cm diameter flush PVC slotted pipe, and were screened over the entire saturated length of the aquifer, except for gaps where sections were joined (Rehfeldt et al., 1992). Within each well, flowmeter measurements were made at approximate 15.24 cm (6 inch) intervals. For a more detailed explanation of the borehole flowmeter method or the derivation of the model equations used to calculate the hydraulic conductivity, see Rehfeldt et al. (1989).

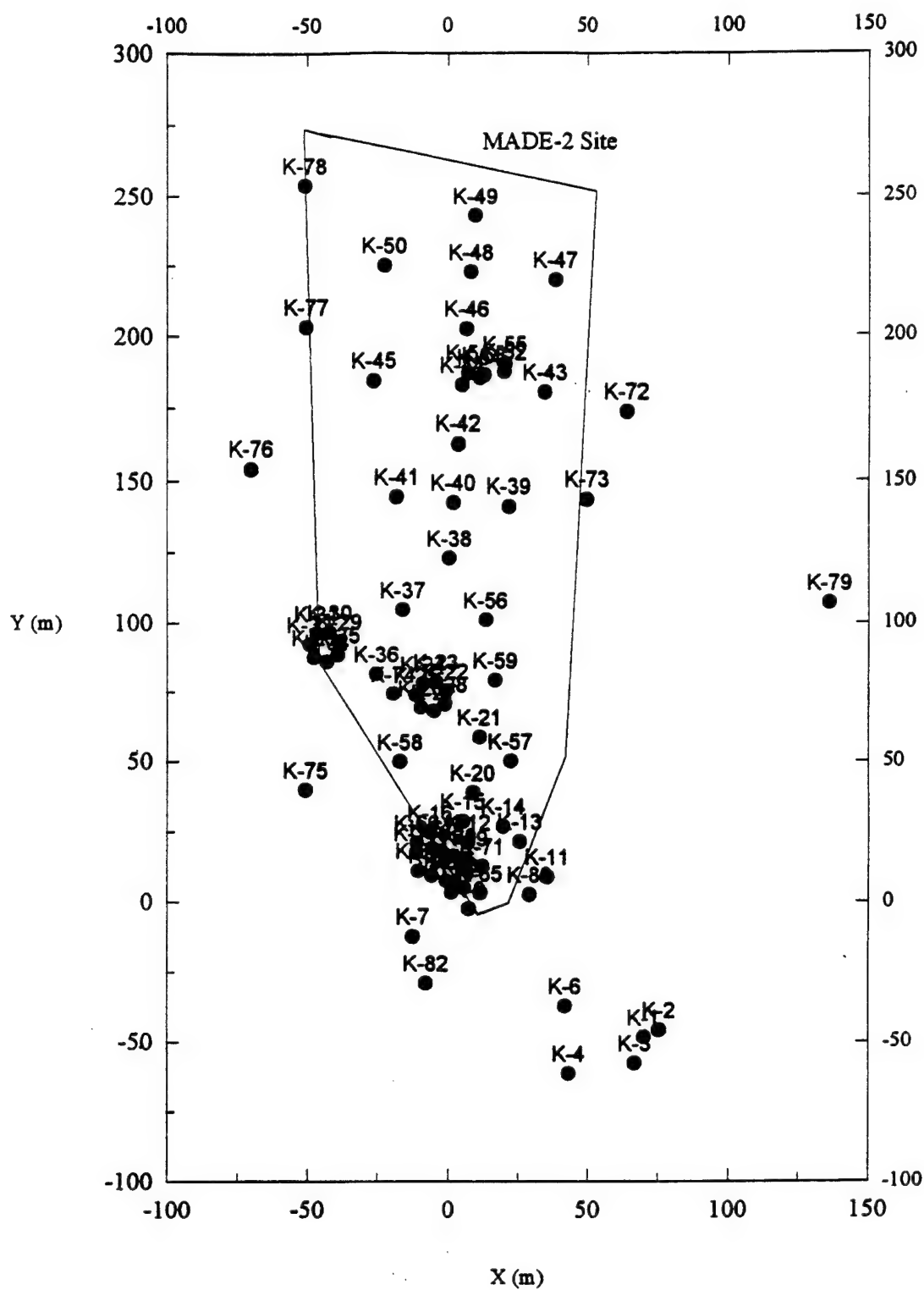


Figure 2. Borehole Flowmeter Locations.

Figure 3 shows the depth-averaged hydraulic conductivity variation and a profile along a vertical slice. The injection site lies within an area of relatively low hydraulic conductivity ( $10^{-3}$  cm/s), and the conductivity increases one to two orders of magnitude to the north. At the northern extreme of the domain the mean conductivity decreases to values noticed in the near field. The portion of the aquifer above 57 meters MSL shows a higher conductivity variation than the lower portion. A region of high conductivity from southwest to northeast through the midsection of the aquifer can also be seen.

The areas of high permeability within the aquifer have been attributed by Young (1994;1995) to a former meandering river channel, developed during the end of the Pleistocene period. Among the evidence cited by Young (1995) for this hypothesis is an aerial photograph of the test site (Figure 4) which shows a difference in vegetation crossing the site at about  $30^{\circ}$  east of north. The channel is said to lie above 58 meters MSL and is about 70 meters wide, corresponding to the zone of higher conductivity. The major argument used by Rehfeldt et al (1992) to interpret this band as nothing more than a regionally continuous zone of relatively high mean conductivity is that the observed groundwater flow does not seem to follow the axis of the channel, but moves perpendicularly to the northwest. These considerations will be seen to have a significant bearing on the modeling process.

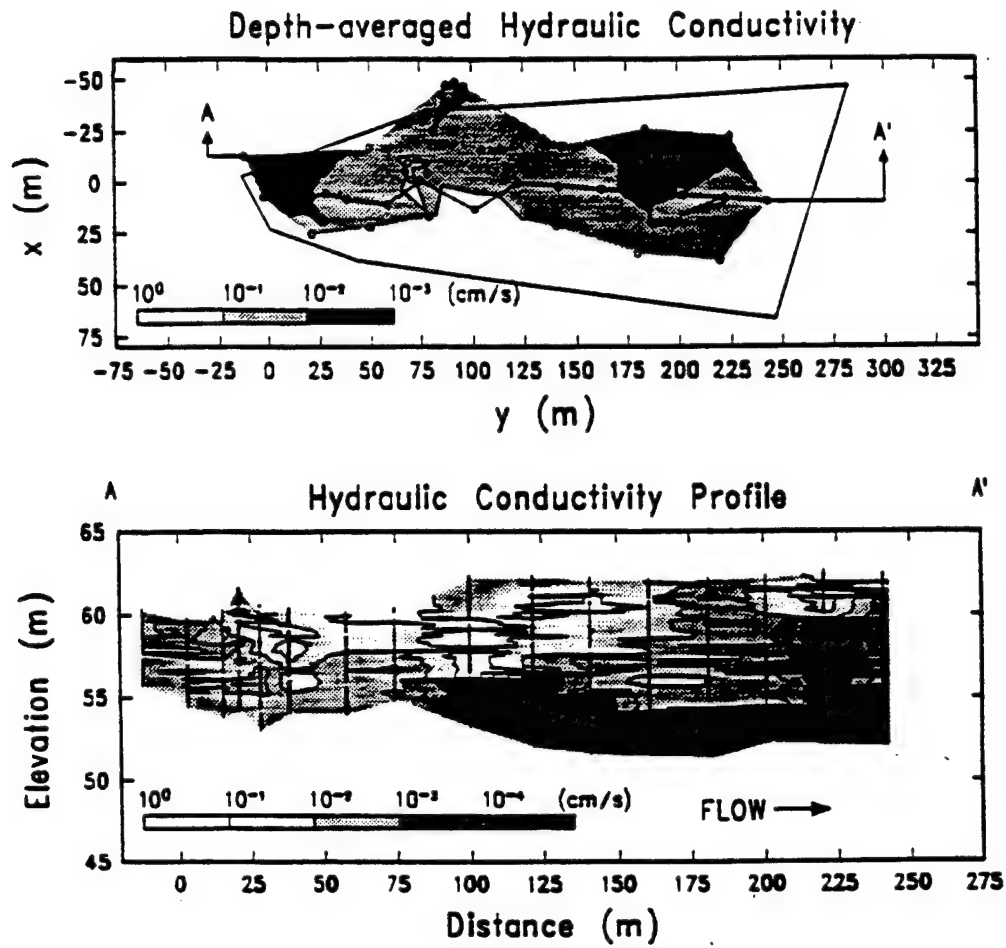


Figure 3. Vertically Averaged Hydraulic Conductivity and Conductivity Profile Along Section A-A. Source: Boggs et al. (1993).

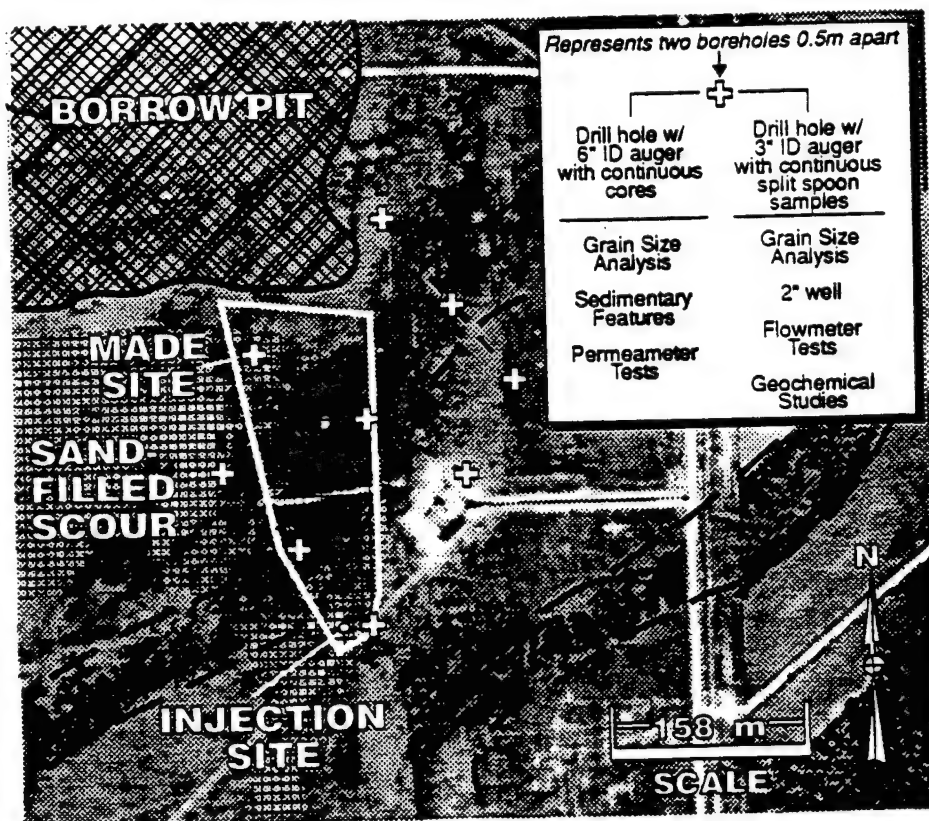


Figure 4. Aerial Photograph of MADE Site.

Laboratory permeameter tests of recompact soil samples raised questions of whether the measured hydraulic conductivity was representative of the in-situ conductivity due to the cohesionless nature of the highly sandy soils. Tests on minimally disturbed, trimmed samples from lined split core barrel samplers were similarly suspect. The solution was the design of a constant head permeability test which could be conducted without removing the soil from the sampling tube. Eighty-eight measurements were taken from nine core samples. The permeameter and borehole flowmeter measurements differed by up to three orders of magnitude in some areas. This discrepancy was attributed in part to the fact that the permeameter measures vertical conductivity whereas the borehole flowmeter measures horizontal values. A further reason is the difference in effective measurement volumes between the two instruments. An additional limitation of the permeameter data is that the nine core samples came from the same area and cannot characterize the entire site.

Slug tests, which consist of instantaneously adding a known volume of water to a well and recording the decline in pressure head over time, were conducted in 22 partially penetrating piezometers in order to measure hydraulic conductivity. Inconclusive results were obtained, as the underlying assumptions of the mathematical models were violated. The extreme heterogeneity of the aquifer compromised the tests significantly, as reported by Boggs et al. (1990).

The double-packer test consists of the injection of water into an isolated interval of the well under constant pressure or constant flow rate. The isolation is achieved by the inflation of packers located above and below the injection interval. The results of the packer tests gave horizontal hydraulic conductivities for discrete layers that were consistently higher than those measured with the borehole flowmeter method. Boggs et al. (1990) concluded that the disparity is due to artificial vertical movement of the injected water within the disturbed annulus of soil just outside of the well casing. Ample evidence points to the disturbance of sediments adjacent to the well, which may have increased the hydraulic conductivity compared to undisturbed sediments. The flowmeter method is less susceptible to annulus effects, because pumping of the fully screened well produces predominantly horizontal flow towards the well (Boggs et al., 1990).

The indirect calculations of hydraulic conductivity included grain-size analysis, direct-current resistivity, and surface geophysical surveys. The following discussion will be limited to the soil grain-size analysis as the others are beyond the scope of this report. Boggs et al. (1990) discussed the estimation of the hydraulic conductivity from empirical formulas using measurements of grain-size distributions. A total of 214 measurements were made on soil samples located sporadically around the site. The geometric mean of the hydraulic conductivity was much higher than found by the direct methods.

An additional study, conducted by Stauffer and Manoranjan (1994), proved by vertical kriging and segmented trend surfaces, the extent to which grain-size analysis can be useful. Core samples collected over the entire saturated length of the aquifer from 17 irregularly spaced locations were dried and sieved to determine particle size distributions. The empirical formula used in the preceding experiment by Boggs et al. (1990) was again employed to determine hydraulic conductivity. However, the data was not analyzed in two or three spatial dimensions to determine variability in the data. On contrary, the data was kriged in only one dimension, vertically, to obtain statistical insight into the trends in conductivity. They concluded that grain-size analysis can provide understanding of the general trend of hydraulic conductivity patterns which are comparable to those found with the borehole flowmeter.

## 2. Aquifer Tests

Two large-scale traditional aquifer tests, titled AT1 and AT2, were conducted at the site to estimate the average hydraulic conductivity and specific yield. The first, AT1, started in March, 1985, and lasted eight days. For three days drawdown was measured in twelve primary observation wells by pressure transducers and a data logging system. The observation wells were positioned in three radial lines leading from the pumping well, PW1, which lay outside the domain of the MADE-2 plumes, approximately 70 meters southeast of the injection wells. Thirteen additional wells within a 100-meter radius of PW1 were also monitored twice daily during the test in order to delineate the extent of the drawdown cone (Boggs et al., 1990).

The period of pumping was followed by 5 days of recovery measurements. The resultant plots of time versus drawdown were evaluated using the Neumann type-curve method for anisotropic confined aquifers. From the plots, the mean transmissivity and specific yield were calculated as  $1.8 \text{ cm}^2/\text{s}$  and 0.04, respectively. Assuming an average saturated thickness of 8.2 m, the mean hydraulic conductivity was  $0.002 \text{ cm/s}$ . In addition, the drawdown curves from each observation well were used to construct drawdown contours which were distorted ellipses, suggestive of horizontal heterogeneity or anisotropy.

AT2 was conducted within the MADE-2 experimental area, with pumping well PW2 located 65 meters north of the injection site. Observation wells were aligned along three radials extending from PW2. A total of 32 staged observation wells (20 primary and 12 secondary) were monitored for the 16 day test (8 days of pumping and 8 days of recovery). The different stages of the wells allowed analysis of the vertical anisotropy of conductivity. The drawdown data were plotted on log-log graphs to obtain transmissivity and specific yield values using the Neumann type-curve method. The average transmissivity value of the test was calculated by arithmetically averaging all values obtained from the pumping well-observation well pairs. The transmissivity value of  $20.1 \text{ cm}^2/\text{s}$  was divided by the average saturated thickness of 9.8 meters to obtain a hydraulic conductivity of  $0.02 \text{ cm/s}$ . These values are an order of magnitude larger than in AT1 because of the different location, which is more representative of the MADE-2 plume region. The mean specific yield in AT2 was determined to be 0.1.

Contour plots of the drawdown were elliptical as seen with AT1. It is debated whether heterogeneity or horizontal anisotropy is the cause. A value of 2.6 was computed for the horizontal anisotropy with the maximum principal axis oriented about  $35^\circ$  west of north. A vertical anisotropy ( $K_v/K_h$ ) was also calculated from the mean of the staged observation wells; the value was 0.18.

Table 2 summarizes the average hydraulic conductivity values obtained from each test. Calculations for the average conductivity in the aquifer tests only included the primary wells.



TABLE 2. SUMMARY OF HYDRAULIC CONDUCTIVITY MEASUREMENTS.

| Method              | No. of Measurements | Mean Conductivity cm/s |
|---------------------|---------------------|------------------------|
| Borehole Flowmeter  | 2187                | $5.52 \times 10^{-3}$  |
| Permeameter         | 88                  | $6.12 \times 10^{-5}$  |
| Slug Test           | 22                  | $1.65 \times 10^{-2}$  |
| Double-Packer       | 37                  | $4.20 \times 10^{-2}$  |
| Grain-Size Analysis | 214                 | $4.30 \times 10^{-2}$  |
| AT1                 | 11                  | $2.00 \times 10^{-3}$  |
| AT2                 | 15                  | $2.00 \times 10^{-2}$  |

### 3. Hydraulic Head Monitoring

Monitoring of the hydraulic (piezometric) head was conducted before and during the tracer experiment using single and multistage piezometers. Figure 5 shows the locations of the piezometers. The wells are designated with a 'P' and a number corresponding to the order in which they were placed. A suffix of 'A', 'B', or both follows the piezometer number, designating the level of screening of the well. An 'A' represents screening of the upper level; a 'B' denotes the lower level; the combination indicates multilevel screening. The actual screen levels varied; but lower stage was screened at an average elevation of 56.3 meters, and the upper at an average elevation of 61.1 meters. Forty-nine piezometers were monitored manually using an electric probe on a monthly basis. A total of 17 monthly surveys were taken, starting June 19, 1990, and ending on September 11, 1991. Moreover, eight pairs of staged piezometers were equipped with continuous water level recorders (piezometers P8AB, P27AB, P44AB, P53AB, P54AB, P55AB, P60AB, P61AB). Measurements taken from the continuously monitored piezometers matched the manual survey heads closely.

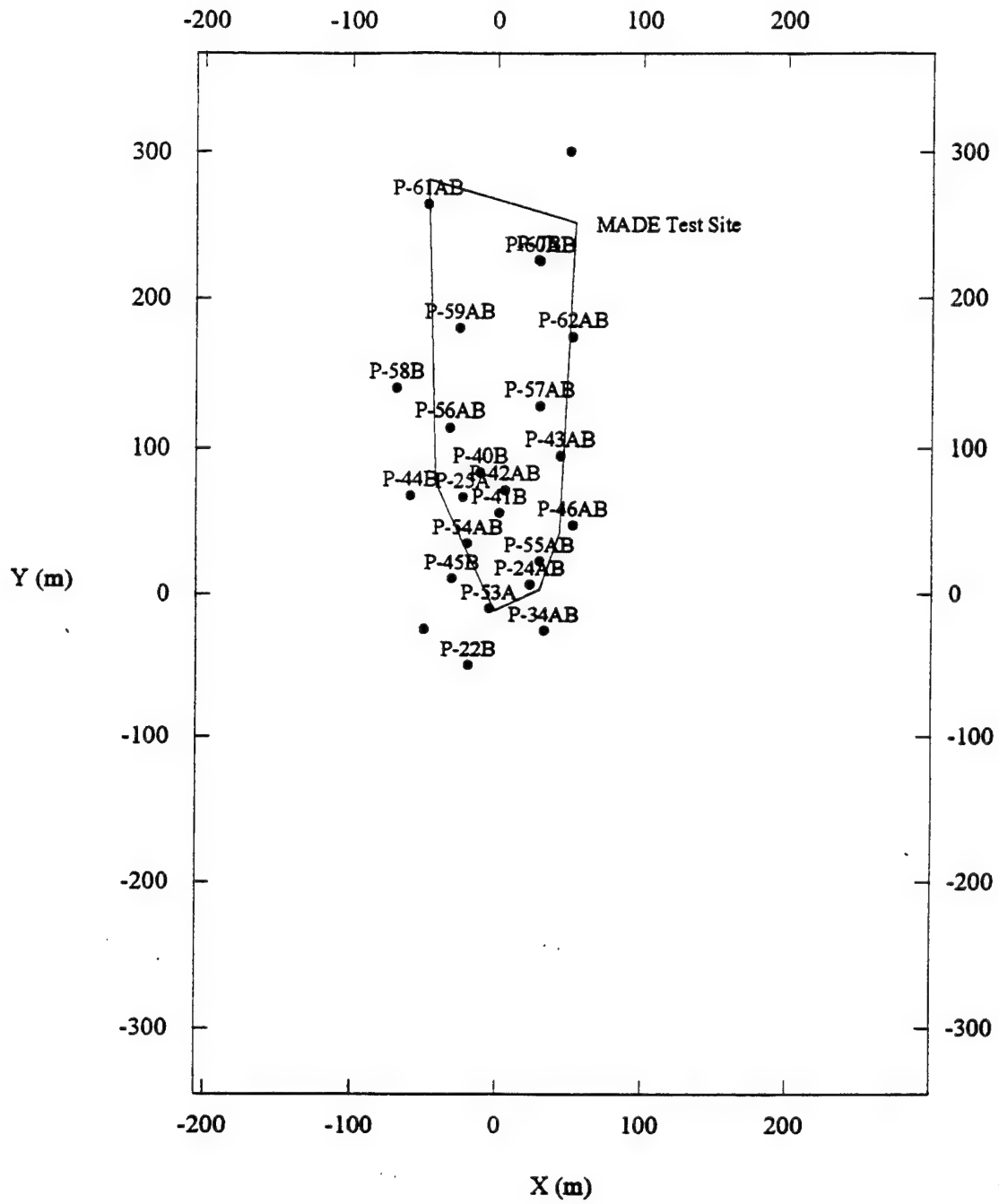
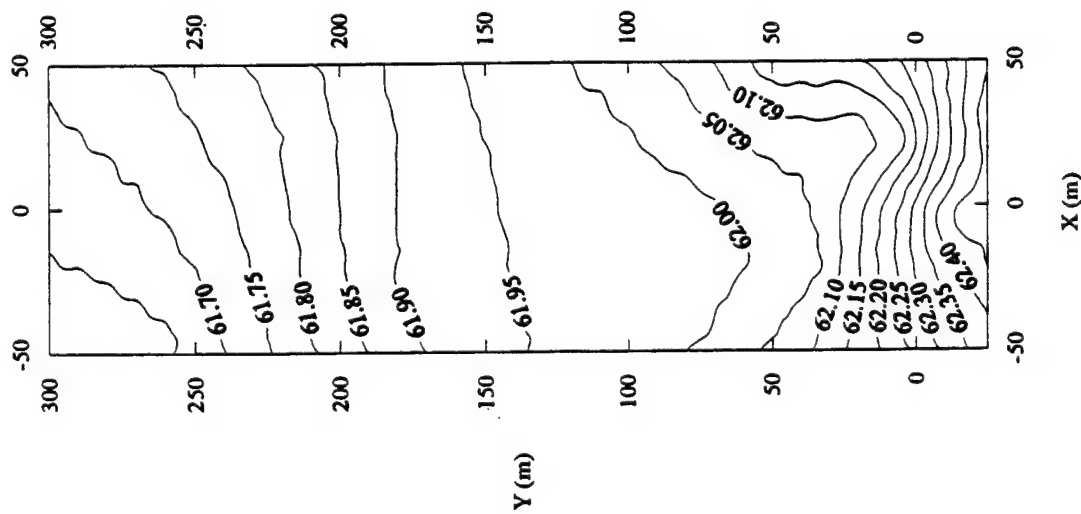


Figure 5. Piezometer Locations.

The groundwater table fluctuated seasonally over a range of 2-3 meters, resulting in an approximate 30 percent variation in saturated thickness of the aquifer (Boggs et al., 1993). The average horizontal hydraulic gradient of 0.0017, experienced seasonal periodicity corresponding to water table fluctuations (Stauffer et al., 1994). Figure 6 shows hydraulic heads from June 19, 1990, for both upper and lower screened piezometers. Heads were kriged using GEO-EAS and plotted using the contouring and surface mapping program SURFER 5.0 for Windows. The hydraulic heads dip towards the plan northwest. In the southern end the contours are closely packed, reflecting the lower values of transmissivity in the southern zone compared to the mid and far field where the head contours are more spread out.

Upper Screened Heads of June 19, 1990



Lower Screened Heads of June 19, 1990

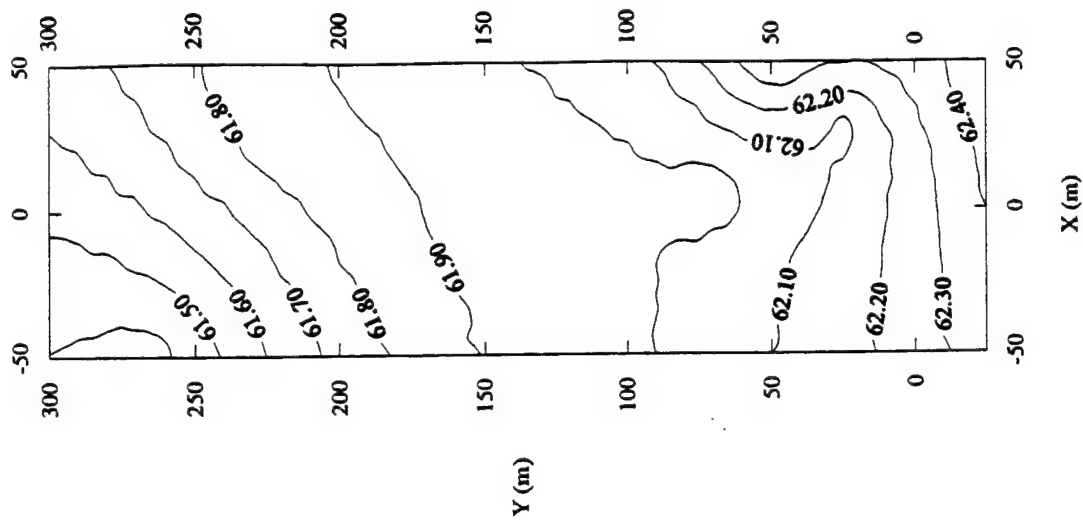


Figure 6. Heads at Upper and Lower Piezometers, June 19, 1990.

Hydrographs were produced with the data obtained from the continuously monitored piezometers showing head versus days since injection. The hydraulic heads were averaged over approximate monthly intervals for comparison with computer simulations described later in the paper. Figure 7 shows a plot of two averaged hydrographs from piezometers located approximately 50 meters apart. Well P53 is located in an area of low conductivity, 5 meters upgradient from the injection point. Well P54, located 20 meters downgradient from the injection site, is in an area of higher conductivity. There are about two orders of magnitude difference between the two locations. The cross-correlation, computed for the two data sets by the FORTRAN code CROSS, written by Dr. Wilson of West Virginia University, is presented in Figure 8. The figure shows a lag of 0 (zero) days, indicating a simultaneous rise in head. However, when the cross-correlation is computed for two piezometers separated by a distance of approximately 280 meters (piezometer P53 and piezometer P61, located 264 meters downgradient from injection), the lag is -1 days. The results imply that the rise in head in downgradient well P61 happens approximately one day earlier than in P53, decreasing the hydraulic gradient in times of higher recharge to the aquifer. A possible justification for this phenomenon is that P61 lies in an area of lower conductivity compared to P53. Recharge thus produces a small mounding effect in P61, before the groundwater level reaches an equilibrium. However, the lag has a minimal effect on the flow, and it appears that the water table tends to rise almost simultaneously over the entire domain.

### Hydrographs of P53A and P54A

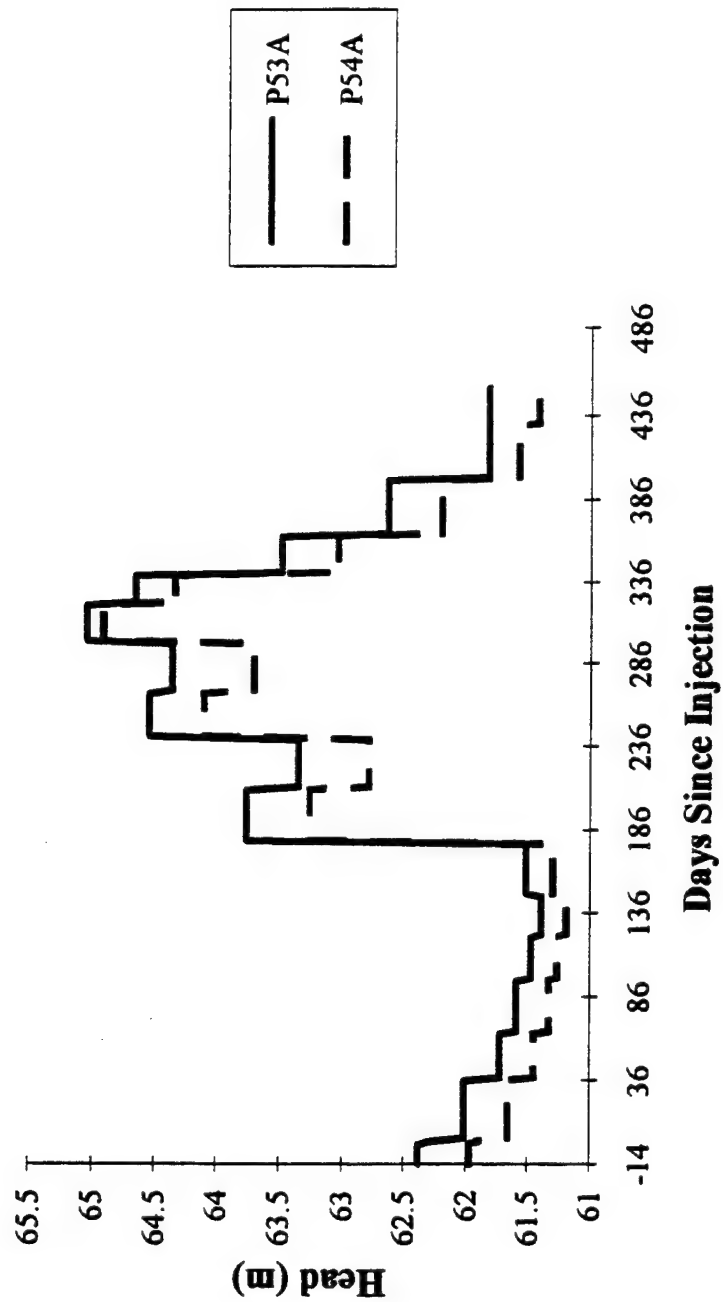


Figure 7. Averaged Hydrographs of Piezometers P53A and P54B.

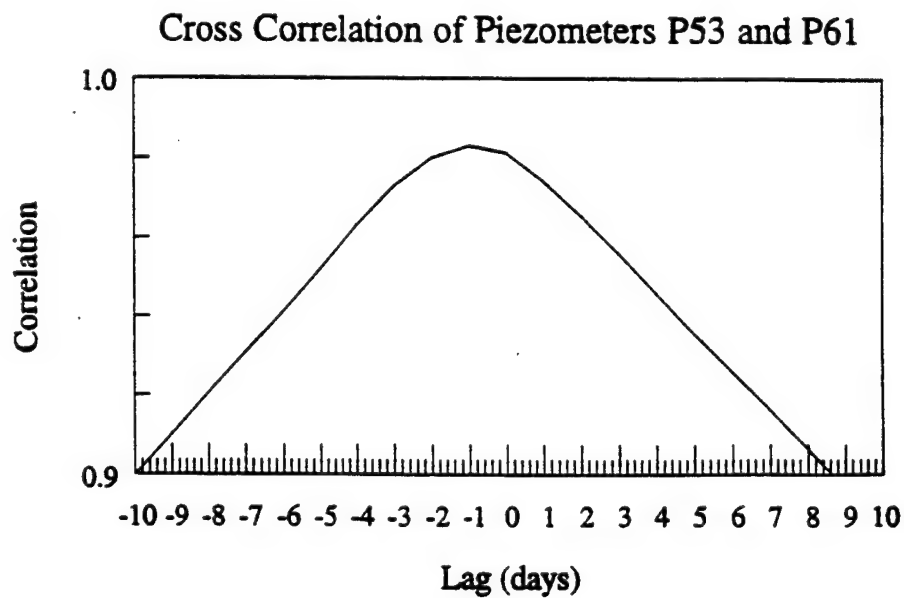
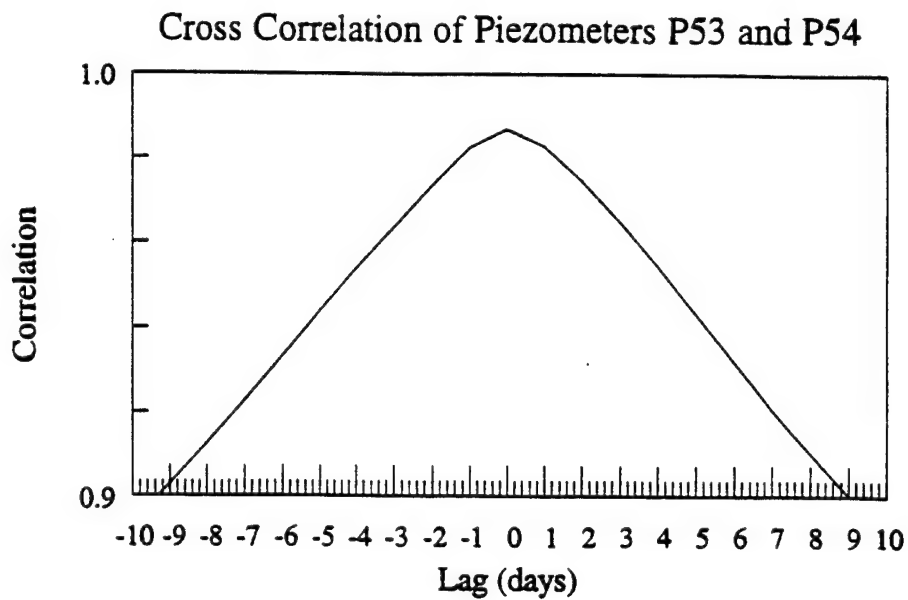


Figure 8. Cross-Correlation of Piezometers P53 and P54 (Upper) and Piezometers P53 and P61 (Lower).

#### 4. Other Aquifer Measurements

Aquifer porosity and bulk density were calculated from 84 minimally disturbed soil core samples collected from four separate core holes at the tracer test site (Boggs et al., 1992). The average porosity of the aquifer was calculated to be 0.31 with a standard deviation of 0.08. The trend in the porosity showed higher values as depth increased. The lower elevations, below about 56 meters MSL, exhibited values of 0.4 and greater, while the upper levels decreased to as low as 0.2. This is consistent with the soil types found in the respective elevations: sand-filled gravel with open or clay-filled pores in the upper layers and a higher sand content, averaging 70%, in the lower levels.

The dry bulk density was calculated from the same core samples as the porosity measurements. The volumes of the core samples were measured. The samples were then oven dried and sieved to find particle density. The bulk density was then estimated from the particle density and the measured volume. The average value for the bulk density was  $1.77 \text{ g/cm}^3$  with a standard deviation of  $0.18 \text{ g/cm}^3$ .

#### B. HYDROLOGY

Daily precipitation and temperature data were collected at the CAFB weather station, located less than 2 km away, to quantify the effects of recharge to the Columbus aquifer. Daily pan evaporation data were collected at Mississippi State University, approximately 35 km distant, and supplied by the State Climatologist, Dr. C. L. Wax. Based on the recommendation of Dr. Wax, a pan coefficient of 0.8 was used to estimate the evapotranspiration (Gray and Rucker, 1994). The net recharge was then calculated by subtracting an estimated evapotranspiration value from daily precipitation. Missing evaporation data were estimated from the daily maximum temperatures using the empirical equation of Pote and Wax.



A graph of the net recharge versus time (days since injection) is presented in Figure 9. Negative values in the graph depict days that had higher evapotranspiration than precipitation. These are more common during the summer months.

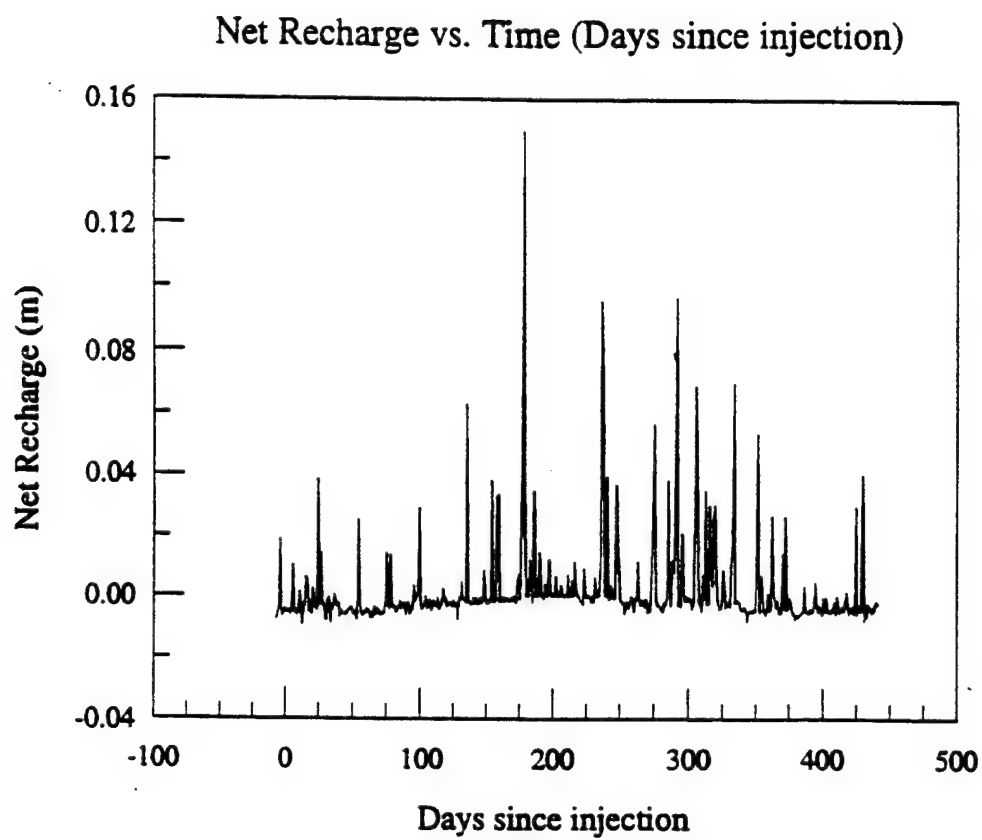


Figure 9. Net Recharge Vs. Time.

### SECTION III

#### TRACER MONITORING

The tracers for MADE-2 were tritiated water and four dissolved organic compounds (benzene, naphthalene, p-xylene, and o-dichlorobenzene). Tritium was used as a passive tracer since it does not undergo chemical reactions or sorption and has a half life much longer than the period of the experiment. The four organic compounds are common constituents of fuels and solvents. A small fraction of the p-xylene was labeled with radioactive  $^{14}\text{C}$  to study the biological or chemical transformation of p-xylene should it occur during the experiment. Table 3 lists the initial concentrations and total injected mass for each tracer.

The experiment began with the injection of  $9.7 \text{ m}^3$  of solution into five wells, spaced 1 meter apart in a linear array. The wells were screened from 57.5 to 58.1 meters MSL. The injection started on June 26, 1990, and lasted 48.5 hours. A constant injection rate of  $3.3 \text{ L/min}$  was maintained, raising the hydraulic head in the injection wells by 0.45 meters. The contaminant solution was prepared and stored on site using ambient groundwater from a well located upstream from the injection point. No non-aqueous phase contaminants were injected.

TABLE 3. INITIAL CONCENTRATIONS AND INJECTED MASS.

| Tracer                     | Mean Concentration | Mass Injected |
|----------------------------|--------------------|---------------|
| Tritium                    | 55610 pCi/mL       | 0.5387 Ci     |
| $^{14}\text{C}$ (p-xylene) | 2770 pCi/mL        | 0.0268 Ci     |
| benzene                    | 68.1 mg/L          | 659.7 g       |
| p-xylene                   | 41.4 mg/L          | 402.0 g       |
| naphthalene                | 7.23 mg/L          | 70.0 g        |
| o-dichlorobenzene          | 32.8 mg/L          | 317.7 g       |

The monitoring of the tracers was accomplished by withdrawing groundwater samples through multilevel samplers (MLS) and positive displacement (BarCad) samplers. Figure 10, adapted from Boggs et al. (1993), shows the placement of the MLS and BarCad samplers. A total of 328 MLS were placed in the study area in a complex spatial pattern. Each MLS

incorporated 20 to 30 sampling points spaced 0.38 meters apart in the vertical direction. A three dimensional representation of the plume was inferred from the MLS data.

A total of five MLS sampling episodes, or "snapshots" were conducted at approximate 100 day intervals, starting 27 days after injection. Snapshots 1-4 surveyed the entire plume; but Snapshot 5, starting 440 days after injection, was designed only to investigate the bounds of the organic plumes and did not encompass the more extensive tritium or  $^{14}\text{C}$  plumes.

Additional sampling of the contaminants was accomplished using BarCad positive displacement samplers, placed along two "fencelines" oriented normal to the flow. The fencelines were two parallel rows, approximately 6 and 16 meters downgradient from the injection site. Sampling took place every two weeks in the early stages of the experiment, eventually moving to 3-month intervals in the latter portion. Table 4 lists the tracer sampling dates of both snapshot and fenceline data with the total number of wells sampled at each time.

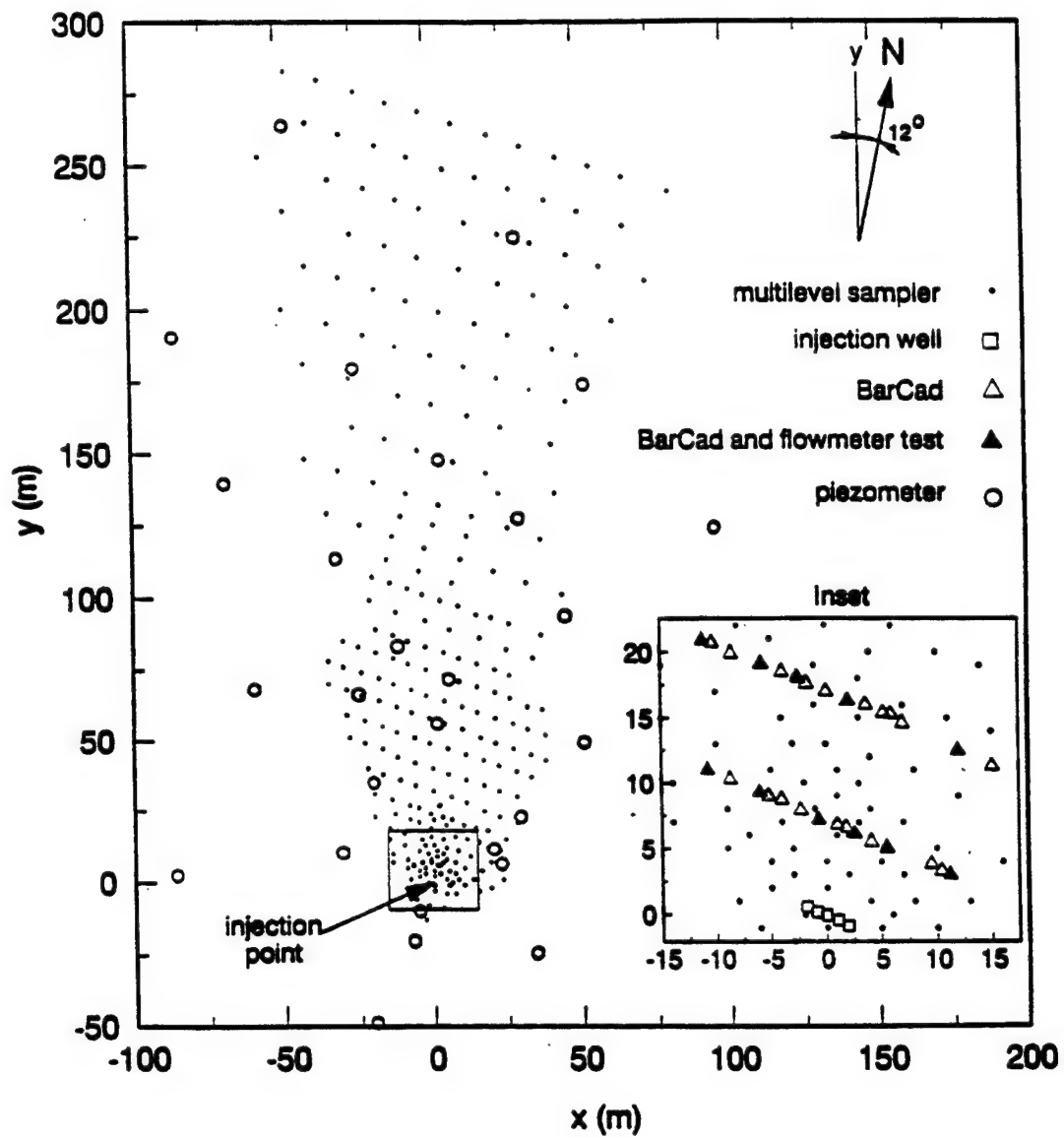


Figure 10. Sampling Well Network. Source: Boggs, et al (1993).

TABLE 4. SUMMARY OF TRACER SAMPLING.

| Sampling Event<br>(F=fenceline,<br>S=snapshot) | Date            | Time After Injection<br>(days) | No. of Wells Sampled |
|--|-----------------|--------------------------------|----------------------|
| F01  | Jul 9-11, 1990  | 13                             | 26                   |
| S21  | Jul 23-27, 1990 | 27                             | 99                   |
| F02  | Aug 13-17, 1990 | 48                             | 31                   |
| F03  | Sep 17-19, 1990 | 83                             | 53                   |
| F04  | Oct 5-17, 1990  | 111                            | 39                   |
| S22  | Nov 5-8, 1990   | 132                            | 111                  |
| F05  | Dec 3-4, 1990   | 160                            | 29                   |
| F06  | Jan 8-9, 1991   | 195                            | 25                   |
| S23  | Feb 5-7, 1991   | 224                            | 190                  |
| F07  | Apr 3-5, 1991   | 281                            | 42                   |
| S24  | May 21-23, 1991 | 328 *                          | 205                  |
| S25  | Sep 9-11, 1991  | 440                            | 79                   |

\* May 21, 1991, is actually 329 days since the start of injection. Boggs et al. (1993), MacIntyre et al. (1993), and Stauffer et al. (1994) all refer to May 21 as day 328. That convention is maintained in this report.

Analyses of tritium and  $^{14}\text{C}$  were conducted at the Water Resources Research Center at Mississippi State University. The field samples were measured with a liquid scintillation counter in dual-isotope mode. The background concentrations of tritium and  $^{14}\text{C}$  at the site established the sensitivity of the measurements and were found to be 2 and 3 pCi/mL, respectively.

Analytical measurements were performed on the organic tracers by the TVA Environmental Chemistry Laboratory. The extracted organic tracers were analyzed by gas chromatography (GC) using a flame ionization detector (FID) system. The sensitivity for the GC/FID method was 4  $\mu\text{g/L}$  for naphthalene, p-xylene, and o-DCB, and 50  $\mu\text{g/L}$  for benzene.

## SECTION IV

### MADE-2 DATABASE

The database for MADE-2, compiled by the Tennessee Valley Authority (TVA), is stored on three 3.5-inch disks. DISKA contains the concentration data for benzene, naphthalene, p-xylene, o-dichlorobenzene, tritium, and  $^{14}\text{C}$ . DISKB stores the piezometric head measurements, and DISKC stores hydraulic conductivity data from the borehole flowmeter tests. Additional information, including format and organization, can be found in the READ.ME files located on each disk.

The tracer concentration data are separated into two directories : \SNAPSHOT and \FENCE. Under \SNAPSHOT are located the five three-dimensional plume snapshots. Each snapshot is contained in individual files marked SNAP#.DAT, where # is the snapshot number. Table 5 is an example of the format used for the snapshot data.

**TABLE 5. EXAMPLE SNAPSHOT DATA.**

|           | Benzene | Naphthalene | p-Xylene | o-DCB  | Tritium  | Carbon-14 | X    | Y   | Z     | Sampling | Days Since |
|-----------|---------|-------------|----------|--------|----------|-----------|------|-----|-------|----------|------------|
| Sample ID | (ug/L)  | (ug/L)      | (ug/L)   | (ug/L) | (pCi/mL) | (pCi/mL)  | (m)  | (m) | (m)   | Date     | Injection  |
| S22D00606 | 660     | 63          | 550      | 720    | 1697     | 45.7      | -1.5 | 6.7 | 56.62 | 11/5/90  | 132        |
| S22D00608 | 1800    | 260         | 1800     | 1700   | 3464     | 140.9     | -1.5 | 6.7 | 57.12 | 11/5/90  | 132        |
| S22D00610 | 4500    | 480         | 4200     | 3100   | 7024     | 264       | -1.5 | 6.7 | 57.63 | 11/5/90  | 132        |
| S22D00614 | 2000    | 200         | 1800     | 1500   | 3277     | 129.7     | -1.5 | 6.7 | 58.65 | 11/5/90  | 132        |
| S22D00616 | 3800    | 400         | 3800     | 2700   | 4716     | 205.4     | -1.5 | 6.7 | 59.16 | 11/5/90  | 132        |
| S22D00618 | 2900    | 290         | 2600     | 2000   | 3715     | 158.1     | -1.5 | 6.7 | 59.66 | 11/5/90  | 132        |
| S22D00620 | 3000    | 320         | 2900     | 2200   | 4222     | 169.4     | -1.5 | 6.7 | 60.17 | 11/5/90  | 132        |
| S22D00622 | 1300    | 67          | 590      | 450    | 2714     | 98.8      | -1.5 | 6.7 | 61.08 | 11/5/90  | 132        |
| S22D00803 | 52      | < 4.0       | 9        | < 4.0  | 3        | 3.3       | 4.5  | 4.2 | 55.84 | 11/5/90  | 132        |
| S22D00805 | 88      | < 4.0       | 12       | 8      | 57       | 5.1       | 4.5  | 4.2 | 56.1  | 11/5/90  | 132        |
| S22D00807 | 63      | < 4.0       | 27       | 36     | 143      | 7.3       | 4.5  | 4.2 | 56.85 | 11/5/90  | 132        |
| S22D00809 | 81      | 5           | 61       | 64     | 41       | 5.9       | 4.5  | 4.2 | 57.36 | 11/5/90  | 132        |

Under the directory \ DISKA \ FENCE are located the tracer data associated with the fenceline samplers. The format is similar to the snapshot data and a separate file is designated for each data set.

The piezometer data on DISKB is divided into two subdirectories, \MONTHLY, and \RECORDER. The "monthly" surveys are found under \MONTHLY, and a separate file is provided for survey. Piezometer labels ending in "A" are screened in the upper level, and labels ending in "B" designate lower level screens. Table 6 gives an example of the piezometric data.

TABLE 6. EXAMPLE SURVEY PIEZOMETRIC HEAD DATA.

| well  | x<br>(meters) | y<br>(meters) | date   | elapsed time<br>(days) | water level elevation<br>(meters) |
|-------|---------------|---------------|--------|------------------------|-----------------------------------|
| P-3   | -86.1         | 2.56          | 1/8/91 | 196                    | 63.82                             |
| P-40  | -11.41        | 83.28         | 1/8/91 | 196                    | 63.47                             |
| P-41  | 1.62          | 56.17         | 1/8/91 | 196                    | 63.51                             |
| P-45  | -30.84        | 10.38         | 1/8/91 | 196                    | 63.77                             |
| P-52  | -85.85        | 190.51        | 1/8/91 | 196                    | 63.05                             |
| P-8A  | 95.13         | 123.75        | 1/8/91 | 196                    | 63.49                             |
| P-8B  | 95.13         | 123.74        | 1/8/91 | 196                    | 63.41                             |
| P-10A | 103.2         | 5.73          | 1/8/91 | 196                    | 65.43                             |
| P-10B | 101.69        | 6.15          | 1/8/91 | 196                    | 63.73                             |

The subdirectory \RECORDER of DISKB contains the continuously monitored piezometer data for 16 wells. An example of the data is provided in Table 7.

TABLE 7. EXAMPLE CONTINUOUS PIEZOMETRIC HEAD DATA.

| well  | x<br>(meters) | y<br>(meters) | elapsed time<br>(days) | year | Julian day | water level elevation<br>(meters) |
|-------|---------------|---------------|------------------------|------|------------|-----------------------------------|
| P-53a | -4.9          | -10.3         | -7                     | 90   | 170        | 62.44                             |
| P-53a | -4.9          | -10.3         | -6                     | 90   | 171        | 62.42                             |
| P-53a | -4.9          | -10.3         | -5                     | 90   | 172        | 62.4                              |
| P-53a | -4.9          | -10.3         | -4                     | 90   | 173        | 62.39                             |
| P-53a | -4.9          | -10.3         | -3                     | 90   | 174        | 62.36                             |
| P-53a | -4.9          | -10.3         | -2                     | 90   | 175        | 62.33                             |
| P-53a | -4.9          | -10.3         | -1                     | 90   | 176        | 62.31                             |



The hydraulic conductivity data for 67 of the wells tested with borehole flowmeters are on DISKC. Each well has a separate file designated by the well name. The remaining 10 profiles were measured after the conclusion of MADE-2, and the data are available from TVA on a separate disk. The authors have incorporated these new data on their own copies of DISKC. Table 8 is an example of a conductivity data file.

TABLE 8. EXAMPLE BOREHOLE FLOWMETER CONDUCTIVITY DATA.

FLOWMETER WELL K-14 HYDRAULIC CONDUCTIVITY - DEPTH PLOT DATA

WELL COORDINATES: X = 114.42 Y = 204.20

[A] DEPTH BELOW GRADE (M)

[B] DEPTH BELOW GRADE (FT)

[C] ELEVATION ABOVE MEAN SEA LEVEL (M)

[D] ELEVATION ABOVE MEAN SEA LEVEL (FT)

[E] HYDRAULIC CONDUCTIVITY (CM/SEC)

[F] HEAD IN THE AQUIFER (FT ABOVE SEA LEVEL)

| [A]   | [B]   | [C]    | [D]    | [E]      | [F]   |
|-------|-------|--------|--------|----------|-------|
| 4.654 | 15.27 | 60.67  | 199.05 | 8.30E-02 | 201.4 |
| 4.807 | 15.77 | 60.518 | 198.55 | 8.30E-02 | 201.4 |
| 4.807 | 15.77 | 60.518 | 198.55 | 3.23E-02 | 201.4 |
| 4.959 | 16.27 | 60.366 | 198.05 | 3.23E-02 | 201.4 |
| 4.959 | 16.27 | 60.366 | 198.05 | 3.32E-02 | 201.4 |
| 5.111 | 16.77 | 60.213 | 197.55 | 3.32E-02 | 201.4 |

The MADE-2 coordinate system (XY) has its origin at the center of the injection site with the longitudinal axis (Y-axis) aligned along the expected mean trajectory of the plume, 12° west of north. Since borehole flowmeter data were carried over from MADE-1, many of the wells are still located in the MADE-1 reference coordinate system (X'Y'). The MADE-2 origin is located at coordinates (X' = 85.2 meters, Y' = 188.4 meters) with the Y-axis rotated 25.68° counterclockwise from the Y'-axis of MADE-1. The transformation can be performed by applying the following formulas on wells K01 through K59:

$$X' = X\cos\theta - Y\sin\theta + h$$

$$Y' = Y\cos\theta - X\sin\theta + k$$

$$X = (X'-h)\cos\theta + (Y'-k)\sin\theta$$

$$Y = (Y'-k)\cos\theta + (X'-h)\sin\theta$$

where  $X'$  and  $Y'$  designate the MADE-1 coordinates,  $X$  and  $Y$  are the MADE-2 coordinates,  $h = 85.2$  meters,  $k = 188.4$  meters, and  $\theta = -25.68^\circ$  (Boggs et al., 1993).

## SECTION V

### FLOW MODELING

#### A. CODE SELECTION

A numerical code had to be chosen to model MADE-2. At the direction of the sponsor, only public domain codes available at Tyndall Air Force Base at the time of selection (June 1992) were considered. Table 9 is an inventory of the candidate groundwater codes (Gray, 1992).

All codes listed in Table 9 solve the groundwater flow equation and the advective-dispersive transport equation, except for MODFLOW, which requires an additional code (MT3D) to solve the transport problem. Only MODFLOW, HST3D, and SWICHA can solve the equations in all three spatial dimensions. Though limited to one-dimensional problems, SAMFT1D can predict the motion of up to three immiscible phases; but the others are single phase codes. The entry 'Unsat?' refers to the ability of the code to solve the flow equation in the unsaturated zone. This is a difficult task, since the hydraulic conductivity of the vadose zone is a function of the degree of saturation. SUTRA and SAMFT1D have this capability; the others are only valid in the saturated zone. Pre- and postprocessors (denoted as 'Pre?' and 'Post?') are available for some of the codes to allow the user to more easily manipulate data for preparation of input files and display of output files. While not strictly necessary, these programs are extremely useful.

**TABLE 9. AVAILABLE GROUNDWATER CODES IN JUNE 1992.**

| <b>Model, Version</b> | <b>Date</b> | <b>Flow</b> | <b>X-<br/>port</b> | <b>Dim</b> | <b>Unsat?</b> | <b>Pre?</b> | <b>Post?</b> | <b>Method</b> |
|-----------------------|-------------|-------------|--------------------|------------|---------------|-------------|--------------|---------------|
| MODFLOW, 4.2          | 11/91       | yes         | no *               | 3          | no            | yes         | yes          | FD            |
| HST3D, 1.5            | 2/92        | yes         | yes                | 3          | no            | no          | no           | FD            |
| SWICHA, 5.05          | 2/91        | yes         | yes                | 3          | no            | no          | no           | FE            |
| SUTRA, 0690-<br>2D    | 6/90        | yes         | yes                | 2          | partial       | yes         | yes          | FD/FE         |
| MOC, 3.0              | 11/89       | yes         | yes                | 2          | no            | yes         | no           | FD/MOC        |
| Random Walk           | 81          | yes         | yes                | 2          | no            | no          | no           | FD/RW         |
| SAMFT1D, 1.0          | 9/90        | yes         | yes                | 1          | yes           | ?           | ?            | FD/FE         |

FD = Finite-Difference, FE = Finite-Element, MOC = Method of Characteristics

RW = Random walk

\* Companion transport code (MT3D) now available.

In view of the extreme heterogeneity of the aquifer and the nature of the observed plume, it was obvious that a three-dimensional solver would be needed to produce realistic predictions (Gray, 1992). From the codes listed in Table 9, MODFLOW was chosen for its ease of use, excellent documentation, and wide acceptance.

MODFLOW (modular three-dimensional finite-difference flow model) was written by McDonald and Harbaugh (1988) of the U. S. Geological Survey. Originally, MODFLOW was coded in FORTRAN 66, but was upgraded to FORTRAN 77. MODFLOW has a modular structure, wherein similar program functions are grouped together, and specific computational and hydrologic options are independent of other options. Such structuring allows the addition and subtraction of new modules as the need arises without the disruption of the rest of the code. The major options can simulate the effects of wells, recharge, rivers, drains, evapotranspiration, streams, and general head boundaries. The solution methods, which solve the matrix equations established by the MODFLOW, are found in the strongly implicit module (SIP), the slice-

successive over relaxation module (SOR), and the preconditioned conjugate gradient module (PCG2), developed by Hill (1991).

The input structure of the program uses separate batch files. Format instructions stated within the batch file dictate the format for the input without modification to the program. The type of output may also be selected to fit a particular need. An output control module allows the results to be saved on disk or printed to the screen.

MODFLOW solves the groundwater flow equation (1) for the hydraulic head using a finite-difference approximation. Equation (1) assumes time-dependent, constant density groundwater flow in an anisotropic, heterogeneous, saturated medium.

$$\frac{\partial}{\partial x} \left( K_{xx} \frac{\partial h}{\partial x} \right) + \frac{\partial}{\partial y} \left( K_{yy} \frac{\partial h}{\partial y} \right) + \frac{\partial}{\partial z} \left( K_{zz} \frac{\partial h}{\partial z} \right) - W = S_s \frac{\partial h}{\partial t} \quad (1)$$

where:  $x, y, z$  are the principal coordinates.

$K_{xx}, K_{yy}, K_{zz}$  are the principal hydraulic conductivity values.

$h$  is the hydraulic (piezometric) head.

$W$  is the net volumetric inflow or outflow per volume of aquifer (sources / sinks).

$S_s$  is the specific storage.

Employing either head or flow boundary conditions and initial (starting) heads with Equation (1) constitutes a mathematical representation of a groundwater flow system (McDonald and Harbaugh, 1988). The solution gives head values as a function of space and time. Specific discharges are estimated by differencing the heads. The assumption of constant density implicit in Equation (1) means that buoyancy forces are neglected and decouples the transport equation from the flow equation. This permits one to solve the flow problem before considering the transport problem. The validity of this assumption will be discussed later.

## B. DISCRETIZATION

To implement a numerical model, a proper grid must be chosen. The MADE-2 site is an area of approximately 300 meters x 200 meters with about 2 meters of relief. The dimensions of the computational grid were reduced to 330 meters by 105 meters, using a uniform grid spacing of 5 meter x 5 meter cells. Grid convergence tests will be discussed later. MODFLOW can simulate flow using a variably-sized grid, however the uniformity allows simplification in the extraction of results and aquifer parameters (hydraulic head, permeability, specific yield, etc.). The saturated zone, whose thickness varied from 9 to 11 meters, was discretized into 9 layers, as described below. With 66 rows and 21 columns, the number of cells totaled 12 474.

In terms of MADE-2 coordinates, the domain stretched from -52.5 meters to 52.5 meters in the X direction and -27.5 meters to 302.5 meters in the Y direction, with the axes parallel to the MADE-2 coordinate system. Although the Y axis runs 12° west of true north, the positive Y direction is defined as plan north. The directions mentioned in later sections of this report are plan directions unless otherwise specified. The origin of the domain was the site of the central injection well. All five injection wells were contained in one cell (Row 61, Column 11). Figure 11 shows the grid used for the flow model, and later for the transport model.



MODFLOW uses a block-centered technique to evaluate the conductances between adjacent nodes. The original block-centered flow package (BCF1) can simulate both confined and unconfined aquifer systems. It allows cells to dry out as the water table falls, but cannot allow rewetting of cells as the water table rises. This limitation forced an earlier discretization of MADE-2 to use a thick top layer to insure that the top layer never went dry (Gray, 1993). In that grid, the bottom eight layers were 1 meter thick and the top, with a base at 59.0 meters MSL, was as much as 6 meters thick. A later version of the block-centered flow package (BCF2), developed by McDonald et al. (1991), permits rewetting as the water table rises above the bottom of a dry cell. This is an important feature for simulating the MADE-2 experiment, as the water table was seen to fluctuate between 2-3 meters.

The discretization employed in this work set the base of the top layer at 63.0 meters MSL, so that the saturated thickness of the top layer never exceeded 2.1 meters. The next seven layers were each 1 meter thick; and the bottom layer varied from 56.0 meters MSL at its top, to the impermeable bottom formed by the aquitard below. The thickness of the lower layer, averaging 3.31 meters, ranged from 0.49 meters at the thinnest point to 6.1 meters at the thickest. This is a large range, but the bottom layer is the least important to the overall flow. In terms of MODFLOW classification, layer 1 is unconfined, layers 2 through 7 are fully convertible, and layers 8 and 9 are confined (Gray and Rucker, 1994).

Temporal discretization divided the 468-day experiment into stress periods and time steps. Stress periods are defined in regard to MODFLOW as time intervals in which all external stresses (sources and boundary conditions) are constant (McDonald and Harbaugh, 1988). In turn the stress periods are divided into time steps. The stress periods for the MADE-2 experiment were centered on the 17 piezometric surveys and the injection period for a total of 18 stress periods. Each stress period was divided into 2-day time steps. Except for the injection period, the stress periods are roughly centered on the head survey dates. Table 10 lists the survey dates and stress period lengths used for the MADE-2 simulations. Simulation Day numbers are counted from the start of the simulation period with Simulation Day 1 being June 12, 1990. The injection took



place on Simulation Days 15 and 16. The reader should be aware that reports presenting field results are usually given in terms of days since the start of injection.

TABLE 10. STRESS PERIODS FOR MADE-2 SIMULATIONS.

| Stress Period | Starting Date | Starting Sim. Day Number | Stress Period Length (Days) | Head Survey Date | Head Survey Sim. Day Number |
|---------------|---------------|--------------------------|-----------------------------|------------------|-----------------------------|
| 1             | June 12, 1990 | 1                        | 14                          | June 19, 1990    | 8                           |
| 2 *           | June 26       | 15                       | 2                           | "                | "                           |
| 3             | June 28       | 17                       | 36                          | July 23          | 42                          |
| 4             | Aug. 3        | 53                       | 28                          | Aug. 13          | 63                          |
| 5             | Aug. 31       | 81                       | 32                          | Sept. 17         | 98                          |
| 6             | Oct. 2        | 113                      | 26                          | Oct. 15          | 126                         |
| 7             | Oct. 28       | 139                      | 24                          | Nov. 7           | 149                         |
| 8             | Nov. 21       | 163                      | 32                          | Dec. 5           | 177                         |
| 9             | Dec. 23       | 195                      | 32                          | Jan. 8, 1991     | 211                         |
| 10            | Jan. 24, 1991 | 227                      | 30                          | Feb. 8           | 242                         |
| 11            | Feb. 23       | 257                      | 28                          | March 8          | 270                         |
| 12            | March 23      | 285                      | 30                          | April 4          | 297                         |
| 13            | April 22      | 315                      | 24                          | May 10           | 333                         |
| 14            | May 16        | 339                      | 18                          | May 20           | 343                         |
| 15            | June 3        | 357                      | 24                          | June 13          | 367                         |
| 16            | June 27       | 381                      | 34                          | July 9           | 393                         |
| 17            | July 31       | 415                      | 32                          | Aug. 19          | 434                         |
| 18            | Sept. 1       | 447                      | 22                          | Sept. 11         | 457                         |
| Last day      | Sept. 22      | 468                      | -                           | -                | -                           |

\* injection period.

### C. INITIAL AND BOUNDARY CONDITIONS

The piezometric heads from the monthly surveys were used to establish the initial head at each node, as well as the head at each boundary node as a function of time (Gray and Rucker, 1994). Because piezometers were not placed at every node, the data were kriged to infer the needed values. Kriging is a geostatistical procedure by which a relatively small number of irregularly spaced data are used to estimate values at a large number of discrete points using a weighted moving average interpolation method. Kriging is the best linear unbiased estimator and

reproduces the measurements exactly. The kriged heads from the first survey were used to establish the initial heads, with the kriged results of the later surveys being used as boundary conditions in MODFLOW's General Head Boundary module. Earlier modeling by Gray (1993) assumed the hydraulic head did not vary as a function of depth and employed Surfer Version 4 to krig heads in two spatial dimensions. These were used as boundary and initial conditions for every layer. However Gray and Rucker (1994) recognized that the heads were a function of depth. They also used a new geostatistical program, Geo-EAS, which allowed more flexibility in the kriging process.

Geo-EAS Version 1.2.1, developed by Englund and Sparks (1991) for the EPA, is a menu driven geostatistical program which performs two-dimensional kriging. It allows the user to plot the variogram and change the variogram to fit the data. Currently, three variogram types can be used in Geo-EAS: linear, spherical, and exponential. Each incorporates a nugget and sill to properly reflect the data's variation. Surfer Version 4, used by Gray (1993), does not give the flexibility that Geo-EAS allows. The variogram only uses a linear model with the effects of the nugget and sill being overlooked. However, it does produce better contour plots of the results. Later versions of Surfer have removed many of the shortcomings mentioned above.

The commercial spreadsheet Quattro Pro was used to evaluate the distribution of the piezometer screen midpoints. The average elevations of the upper and lower piezometer screens were found to be 60.5 and 56.0 meters MSL, respectively. Based on the average screen elevation, the piezometers were divided into two groups. For example, the file GW010891 (groundwater head survey of January 8, 1991) was divided to create UP018091.DAT and LO010891.DAT. The program MADETIGE reformatted the files to Geo-EAS input requirements and eliminated piezometers which were far outside the computational domain or were not screened close to the average elevations. A total of 15 piezometers, whose midpoints ranged from 59.76 to 61.22 meters MSL, were used in the upper set of files. The lower set of 23 piezometers had midpoints which ranged from 55.51 to 56.71 meters MSL. The horizontal distribution of the upper and lower piezometers seen in Figure 12 shows sparse coverage towards the north end of the grid.

Geo-EAS was used to separately krig the upper and lower piezometer files for each survey date. Table 11 shows the parameters used in fitting models to the variograms, including model type, nugget, sill, and range. With a few exceptions, the linear model gave a good fit to the data. As anomalies were found in the data, piezometers were removed to allow a better fit. For example, the file UP081991.DAT had an odd point, with the piezometer P43A having a head of 58.78 meters MSL. This point was removed from the variogram. The result: a better looking variogram with the curve fitting more closely to the data. Figures 13 and 14 show contour maps of kriged monthly survey heads for June 19, 1990, and March 8, 1991. The contour maps for the remaining kriged head surveys can be found in Appendix A. In almost every survey, the heads dip towards the northwest. The contour plots were created by Surfer Version 5 for Windows. The program GEO2SRF reformatted the Geo-EAS output for input to Surfer.

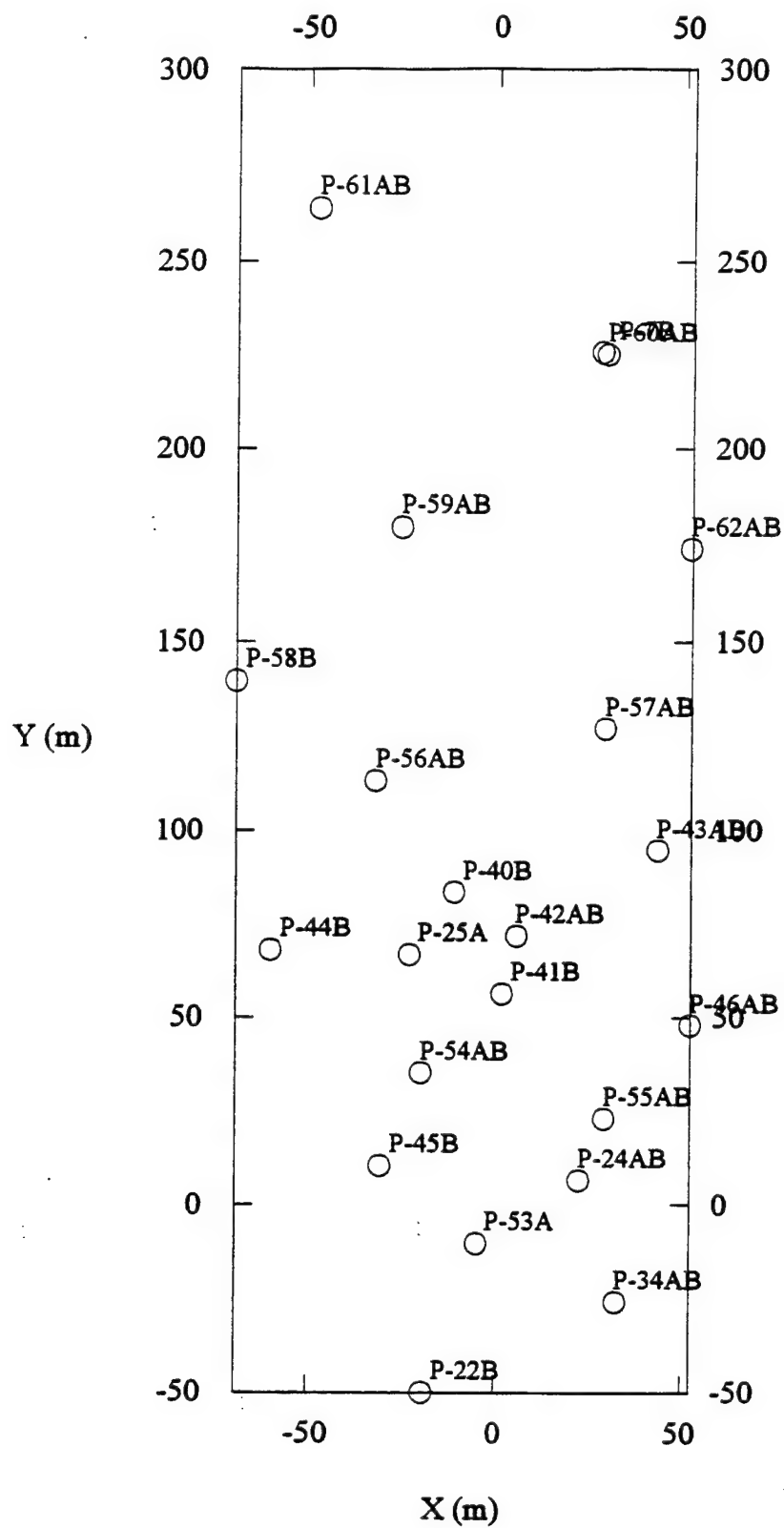
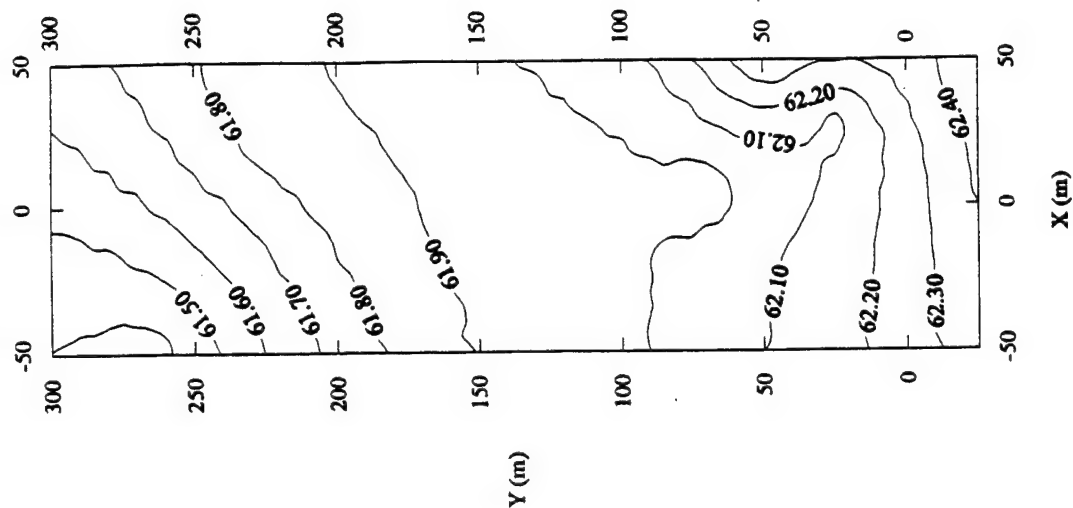


Figure 12. Piezometers Used for Kriging.

Lower Screened Heads of June 19, 1990



Upper Screened Heads of June 19, 1990

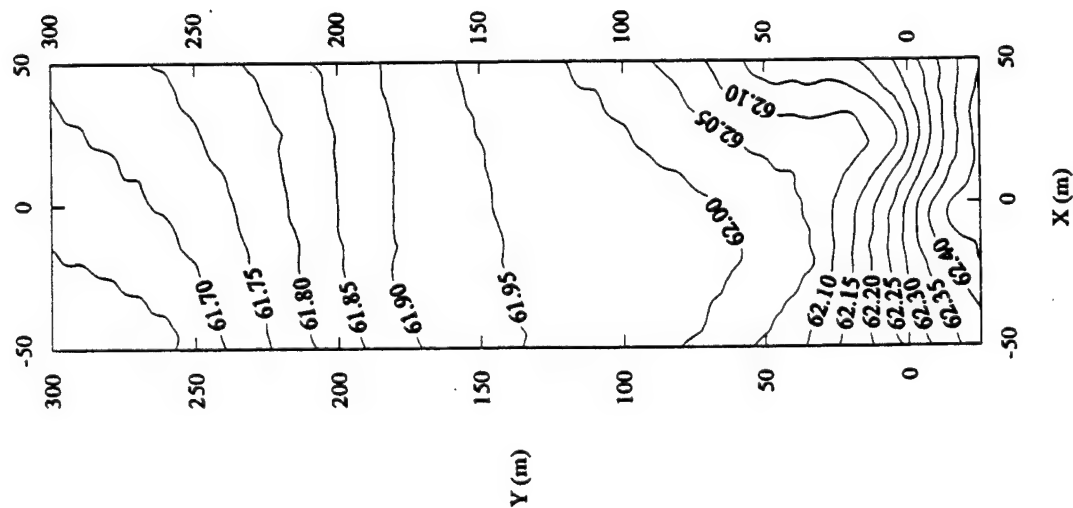
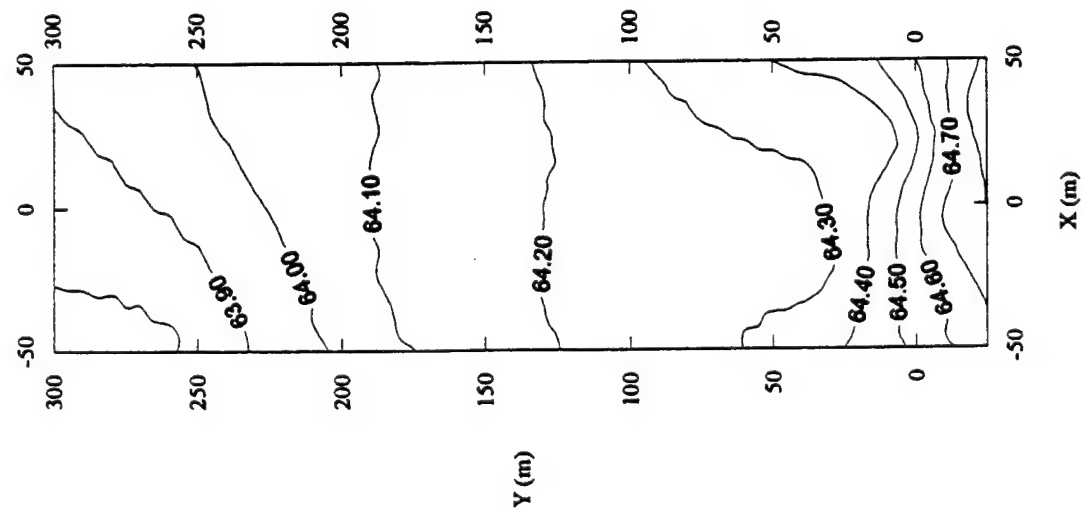


Figure 13. Upper and Lower Kriged Heads of June 19, 1990.

Upper Screened Heads of March 8, 1991



Lower Screened Heads of March 8, 1991

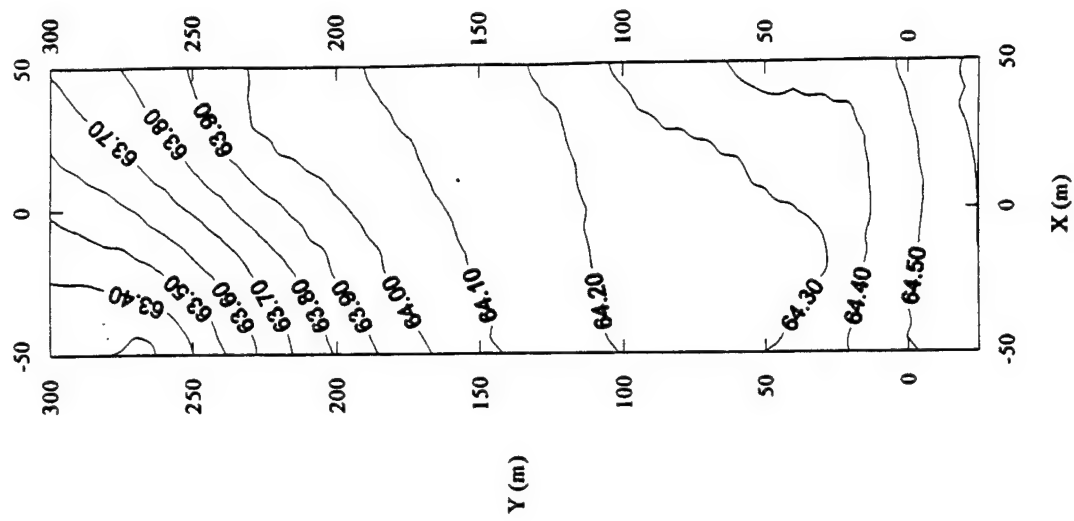


Figure 14. Upper and Lower Kriged Heads of March 8, 1991.

TABLE 11 (A). KRIGING PARAMETERS FOR THE UPPER LEVEL HEAD SURVEYS.

| Survey Date   | Type   | Nugget | Sill  | Range |
|---------------|--------|--------|-------|-------|
| June 19, 1990 | linear | 0      | 0.10  | 300   |
| July 23       | linear | 0      | 0.06  | 300   |
| Aug. 13       | linear | 0      | 0.05  | 300   |
| Sept. 17      | linear | 0      | 0.05  | 300   |
| Oct. 15       | linear | 0      | 0.03  | 300   |
| Nov. 7        | linear | 0      | 0.03  | 300   |
| Dec. 5        | linear | 0      | 0.012 | 300   |
| Jan. 8, 1991  | linear | 0      | 0.20  | 300   |
| Feb. 8        | linear | 0      | 0.15  | 300   |
| March 8       | linear | 0      | 0.15  | 300   |
| April 4       | linear | 0      | 0.15  | 300   |
| May 10        | linear | 0      | 0.15  | 300   |
| May 20        | linear | 0      | 0.15  | 300   |
| June 13       | linear | 0      | 0.10  | 300   |
| July 9        | linear | 0      | 0.15  | 300   |
| Aug. 19       | linear | 0      | 0.05  | 300   |
| Sept. 11      | linear | 0      | 0.05  | 300   |

TABLE 11 (B). KRIGING PARAMETERS FOR THE LOWER LEVEL HEAD SURVEYS.

| Survey Date   | Type   | Nugget | Sill | Range |
|---------------|--------|--------|------|-------|
| June 19, 1990 | linear | 0      | 0.12 | 300   |
| July 23       | linear | 0      | 0.12 | 300   |
| Aug. 13       | linear | 0      | 0.10 | 300   |
| Sept. 17      | linear | 0      | 0.05 | 300   |
| Oct. 15       | linear | 0      | 0.03 | 300   |
| Nov. 7        | linear | 0      | 0.05 | 300   |
| Dec. 5        | linear | 0      | 0.03 | 300   |
| Jan. 8, 1991  | linear | 0      | 0.15 | 300   |
| Feb. 8        | linear | 0      | 0.15 | 300   |
| March 8       | linear | 0      | 0.15 | 300   |
| April 4       | linear | 0      | 0.15 | 300   |
| May 10        | linear | 0      | 0.15 | 300   |
| May 20        | linear | 0      | 0.15 | 300   |
| June 13       | linear | 0      | 0.12 | 300   |
| July 9        | linear | 0      | 0.12 | 300   |
| Aug. 19       | linear | 0      | 0.08 | 300   |
| Sept. 11      | linear | 0      | 0.06 | 300   |

For input to MODFLOW the kriged heads of the upper piezometers were assigned to Layers 1 through 4. The kriged heads of the lower piezometers were assigned to Layers 8 and 9. Linear interpolation was used to assign heads to Layers 5, 6, and 7. Program BASMAKER was written as a preprocessor for MODFLOW in order to set up the 'basic' input data including grid dimensions, number of stress periods, hydrologic packages to be used, and initial head at each node. Vertical interpolation of the initial heads was performed within the program.

The boundary conditions for the model were established in the General Head Boundary package. This package served to specify heads (a Dirichlet boundary condition) at boundary nodes, and to change them for each stress period. The program GHBMaker created the input file necessary for MODFLOW execution using the remaining head surveys. The program extracts the heads only along the boundary and uses the vertical interpolation scheme described above to assign boundary heads to all the layers.

#### D. MODELING OF AQUIFER PARAMETERS

Aquifer parameters such as horizontal hydraulic conductivity, vertical conductance, and specific yield were modeled for input to the Block-Centered Flow package. Each is explained below.

##### 1. Hydraulic Conductivity and Vertical Leakance

Horizontal hydraulic conductivity was measured by the borehole flowmeter in 77 separate profiles, located around the MADE-2 site. The data were measured over successive 15-cm layers within the saturated zone of the aquifer. The profiles contained gaps caused by joints in the well screens which were filled in using values from immediately above and below the gap.

In order to combine the profiles to characterize the entire site it was important to note that the top elevations of the profiles varied from 57.62 meters to 62.68 meters MSL depending on the



local water table elevation on the date of measurement. One consequence was that the 15-cm layers differed from one profile to the next. KAVG94 was written to average the borehole flowmeter conductivities over the MODFLOW grid layers. The program extended the profiles up to 64.0 meters MSL by assuming a constant conductivity from the top of the well screen to the top of the aquifer. The lowest data varied from 51.88 meters to 56.22 meters; these values were extended down to the next lower integer elevation. The 15-cm intervals were arithmetically averaged over each MODFLOW layer to generate horizontal conductivities for all nine MODFLOW layers (Gray and Rucker, 1994). This process assumes horizontal isotropy.

Vertical conductivity between the layers was also calculated with KAVG94, assuming the aquifer material was locally isotropic. By harmonically averaging the conductivity between MODFLOW nodes, a vertical leakance was generated. Vertical leakance, called VCONT in MODFLOW, is the vertical conductivity divided by the thickness between adjacent nodes. MODFLOW uses VCONT to calculate vertical flow between successive layers. Because of the variable thickness of the lowest layer (9), the leakance between Layers 8 and 9 was based on the interval between 56.5 meters and 55.5 meters, except for three profiles (K-2, K-26, and K-28) which ended at 56.0 meters. For the lowest layer, VCONT is implicitly set to zero because the lower boundary of the domain is assumed impermeable. The general formula for VCONT is

$$VCONT_{i,j,k+1/2} = \frac{2}{\frac{\Delta v_k}{(K_z)_{i,j,k}} + \frac{\Delta v_{k+1}}{(K_z)_{i,j,k+1}}} \quad (2)$$

where:  $\Delta v_k$  and  $\Delta v_{k+1}$  are the thicknesses of layers  $k$  and  $k+1$ , respectively

$(K_z)_{i,j,k}$  and  $(K_z)_{i,j,k+1}$  are the vertical conductivities

A major disadvantage of VCONT, as seen in the MADE-2 experiment, happens in the top layers of the aquifer. When the top layer is unconfined its thickness fluctuates as the water table fluctuates. The average water table depth should be used to calculate VCONT between the water table layer and the one below it. However, VCONT is calculated by using the distance between nodes, since the water table elevation is not known a priori. If the vertical conductivity is not

homogeneous, then the equivalent conductivity between the nodes will be underestimated, because the upper layer is assumed thicker than it really is. This is not a problem for the top most layer (Layer 1) as it is always homogeneous (from extrapolation of the profiles to the top of the aquifer). But the problem arises in lower layers as the water table reaches them. The phenomena also affects horizontal conductance, which also is based on fully saturated conditions.

The output file for KAVG94 (KAVG94.OUT) contained 77 conductivity profiles, each averaged over the same nine grid layers. The well number, X and Y well coordinates, grid layer, horizontal conductivity (m/d), transmissivity ( $\text{m}^2/\text{d}$ ), vertical conductivity, and VCONT were all listed. KAVTOGE separated the output into layer files in Geo-EAS format. The file names were KLAY#.DAT, where # represented the MODFLOW layer number. The layer files contained only the well number, location, transmissivity (conductivity for Layer 1) and VCONT. In order to avoid unphysical negative values after kriging, and to respect the lognormal distribution of the conductivity, the data were log-transformed by the program KA2LOG to establish  $\ln(K)$  values. The data were presented in Geo-EAS format and named KLOG#.DAT. Spherical and exponential variograms were successfully fitted to the log transformed data.

The data for each layer were kriged horizontally to obtain natural log transmissivity and natural log VCONT values at every grid node. The data were then transformed back to unlogged values by the program DLOGFILE. The files were converted to Surfer format and contour plots were made for all nine layers. Figure 15 shows an example of the kriged transmissivity and VCONT for Layer 3. The figure shows a series of high conductivity regions trending from southwest to northeast in the zone from about Y = 40 meters to 200 meters. These may reflect the hypothesized river channel.

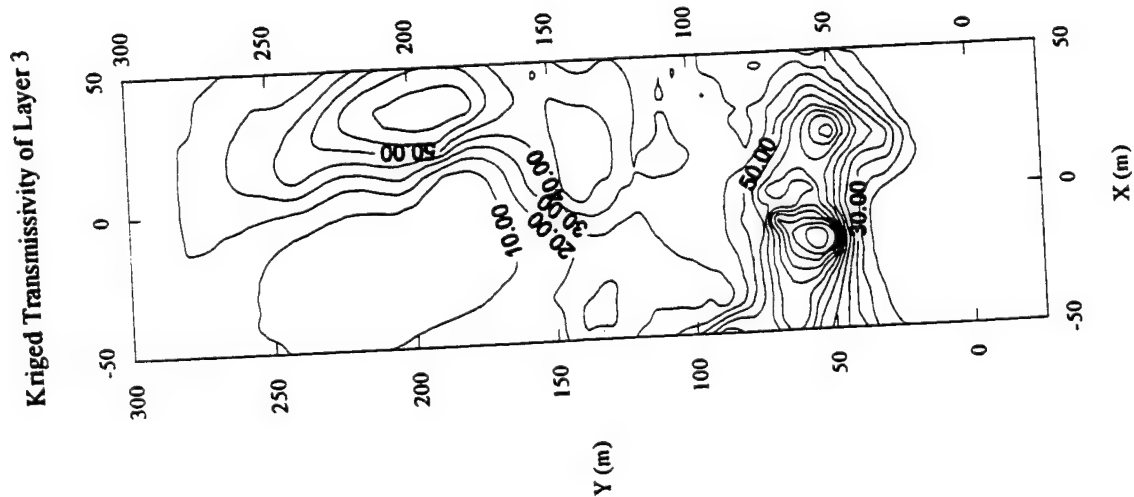
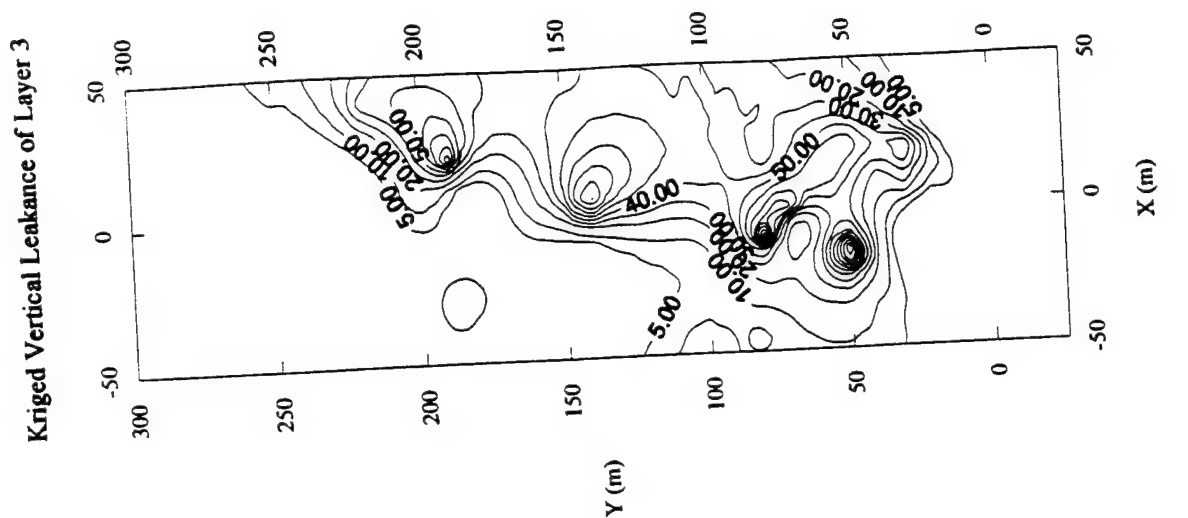


Figure 15. Kriged Transmissivity [m<sup>2</sup>/d] and Leakance [1/d] for M2-5.

The kriged conductivities were prepared for the MODFLOW input file of BCF2 by the program BCF2MAKR. This preprocessor is project-specific, i.e., designed for the explicit use of the MADE-2 project. The program also added the layer elevations, horizontal anisotropy values, and the specific yield (or storage coefficient for confined aquifers) to the input file.

## 2. Horizontal Anisotropy

A value for horizontal anisotropy can be introduced in the MODFLOW input file. Defined as a column to row ratio, the value multiplies the conductance between nodes along rows to obtain conductance between nodes along a column. In the standard version of MODFLOW only one value can be entered for each layer, although this was later modified, as described later. As a starting point, the aquifer was assumed to be horizontally isotropic; a value of 1.0 was used in all nine layers for the initial simulations.

## 3. Storage Parameters

In a steady-state simulation, the right hand side (R.H.S.) of Equation (1) is zero ( $\partial h / \partial t = 0$ ) and specific yield is not needed. As discussed, the experiment underwent temporal changes in the hydrological features, requiring a transient simulation. Thus, specific yield values were needed to properly solve the groundwater flow equation. The specific yield was chosen based on the pumping test, AT2. The base value of 0.1 was assigned to all unconfined layers (including the convertible layers as they changed from confined to unconfined). No measurements were made for specific storage, so a confined storage coefficient base value of 0.0001 was assumed, based on the textbook values for specific storage in sand and sandy gravel given by Anderson and Woessner (1992). This value was assigned to all the nodes in each layer.

## E. HYDROLOGIC STRESSES

The remaining stresses to the flow system include recharge and injection well flow rates. Since the site was covered primarily by weeds and brush and no surface water was observed, the MODFLOW surface water packages were not used.

### 1. Recharge

The daily net recharge values were incorporated into the flow model using the Recharge package. Since pan evaporation, used to account for evapotranspiration, was subtracted from the daily precipitation, a negative value of recharge indicated a net loss of water. Thus the Evapotranspiration package was not used. The daily net recharge values were arithmetically averaged over each stress period giving the values seen in Table 12.

TABLE 12. AVERAGE NET RECHARGE.

| Stress Period | Recharge (m/d) | Stress Period | Recharge (m/d) |
|---------------|----------------|---------------|----------------|
| 1             | -0.00313       | 10            | 0.00809        |
| 2             | -0.00478       | 11            | 0.00114        |
| 3             | -0.00148       | 12            | 0.00794        |
| 4             | -0.00409       | 13            | 0.01022        |
| 5             | -0.00286       | 14            | 0.00357        |
| 6             | -0.00107       | 15            | 0.00046        |
| 7             | 0.00071        | 16            | -0.00273       |
| 8             | 0.00942        | 17            | -0.00159       |
| 9             | 0.00387        | 18            | -0.00384       |

### 2. Well Simulation

The simulation of a well was required during the second stress period, in which the injection of tracers in the aqueous phase raised the hydraulic head approximately 0.45 meters.

The injection occurred at a rate of 4.85 m<sup>3</sup>/d on Simulation Days 15 and 16 at Row 61, Column 11, and Layer 7. These data were input to the Well package.

## F. SOLUTION METHOD

MODFLOW solves the partial differential equation of groundwater flow using a finite-difference technique. Several methods to solve the resulting system of algebraic equations are available, including the strongly implicit method (SIP), slice successive over relaxation method (SOR), and the preconditioned conjugate gradient method (PCG). For the present study, the PCG2 (Hill, 1990) package was chosen because it is efficient and because it requires approximately one-fourth the storage needed by the SIP package.

The PCG2 module solves the set of linear difference equations iteratively. The equations are produced from the finite-difference model, and can be expressed in matrix notation as

$$\underline{\underline{A}} * \underline{x} = \underline{b} \quad (3)$$

where  $\underline{\underline{A}}$  is the coefficient matrix,  $\underline{x}$  is the vector of hydraulic heads, and  $\underline{b}$  is the vector of defined flows. In an iterative solver, it is assumed that the solution has converged when some residual (difference in results between successive iterations) is less than a user-specified convergence criterion (Hill, 1990). For the problem at hand, and for most other problems, the convergence criterion was chosen to be of the same order of magnitude as the measurement uncertainty. Hence, a value of 0.01 meters was used since hydraulic head measurements were reported to 2 decimal places (for example, 62.75 meters).

A relaxation parameter (RELAX) is also specified as input in the PCG2 package. Hill (1990) suggested that a value of 1.0 to be used. A smaller value, such as 0.99 or 0.98 may reduce the number of iterations needed for the solution to converge. Initially, the relaxation was set at 0.98.

## G. COMPUTER SIMULATIONS

After all the parameters were established and the input files were written for each module, MODFLOW was run numerous times. The first MADE-2 simulations, conducted during the summer of 1992, simplified the model to steady state (Gray, 1992). The first transient simulations were conducted in the summer of 1993 (Gray, 1993). Many of the techniques for manipulation of data to a usable form described above were established at that time. The 1993 simulations included a homogeneous hydraulic conductivity field, based on the findings of the AT-2 pump test, as well as a more realistic heterogeneous field. The early vertical discretization of the aquifer described above refers to the 1993 simulations.

The present study is a direct continuation of work performed in the summer of 1994 (Gray and Rucker, 1994). Five cases (M2-5-1 through M2-5-5) were run during the summer of 1994 and are described in Table 13. Simulations M2-5-1 through M2-5-5 do not include conductivity profiles K-72 through K-81 as they were not measured until spring 1995. Computations were performed on a Sun Sparc 2 workstation.

TABLE 13. SUMMARY OF MODFLOW CASES M2-5-1 THROUGH M2-5-5.

| Case | RELAX | WETDRY<br>(meters) | Specific<br>Yield | Confined<br>Storage Coef. | Run Time<br>(min) | Final Volume<br>Error |
|------|-------|--------------------|-------------------|---------------------------|-------------------|-----------------------|
| 1    | 0.98  | -0.1               | 0.1               | 0.0001                    | 60                | -0.25%                |
| 2    | 1.00  | -0.1               | 0.1               | 0.0001                    | NA                | -0.24%                |
| 3    | 0.98  | -0.01              | 0.1               | 0.0001                    | 72                | -0.25%                |
| 4    | 0.98  | -0.1               | 0.2               | 0.0005                    | 94                | -1.52%                |
| 5    | 0.98  | -0.1               | 0.05              | 0.00005                   | 58                | -0.23%                |

Simulations were conducted prior to Case 1 (M2-5-1), however this was the first one to converge. Case 2 tested the relaxation parameter in the PCG2 solver package. Though the relaxation parameter did little to change the results, it is believed to have slowed convergence. Case 3 examined the change in the WETDRY parameter in the BCF2 package. This parameter controls the rewetting of dry cells. A negative sign indicates the head of the cell in question

depends solely on the head of the cell below it. The absolute value of WETDRY is the excess head required to rewet the cell, calculated as the head in the cell below minus the bottom elevation of the cell in question. For example, if the head of a cell in Layer 2 increased to a value of the absolute value of WETDRY above the bottom of an overlying dry cell in Layer 1, the cell in Layer 1 would rewet. A positive sign for WETDRY requires that the head in the four adjacent cells in the same layer must be WETDRY above their bottoms for rewetting to occur. This method is unstable when there are fixed heads in the grid, as demonstrated by unsuccessful simulations.

Cases 4 and 5 investigated the effects of uniformly changing the aquifer storage parameters. Increasing storage increased run time and final volume error. The volume error is the percent relative discrepancy between inflow and outflow and is accumulated throughout the simulation. Errors below 1% are excellent; acceptable errors range up to 10%.

Figure 16 compares the Case 1 head contours for Layer 4 with the upper observed heads for Simulation Day 270. Figure 17 gives the corresponding results for Layer 9 and the lower observed heads. The agreement is good. The pattern progresses from a high gradient in the southern portion of the domain (near field) to a gradual dipping in the northeast (far field). The wider spacing in the mid field is a result of the higher conductivity values.

To more accurately check the results of the simulation, a quantitative approach was used in which the heads of a continuously monitored piezometer were compared to simulated heads in the equivalent location. Program WELLGRPH extracted the head as a function of time at a specific location from the MODFLOW output file. The model boundary conditions changed only 16 times in a 468-day simulation so the model cannot possibly predict the erratic day to day variations seen in the measured hydrographs. Therefore, for comparison the program HYDROGRA(ph) averaged the observed heads over each stress period and compared the result to the unaveraged simulated heads (Gray and Rucker, 1994). Figure 18 shows the resultant hydrograph of piezometer P53A for Case 1.



Upper Screened Heads of March 8, 1991

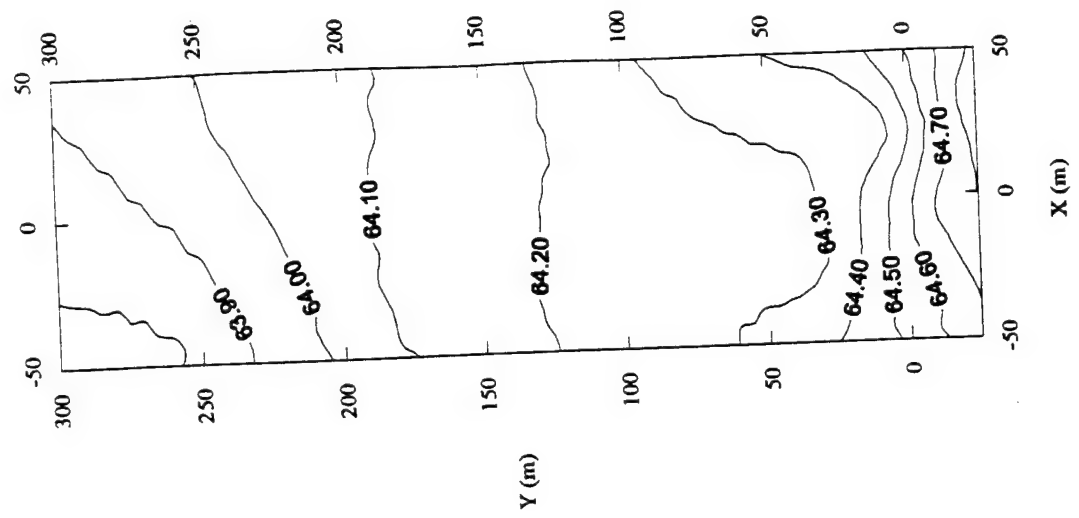
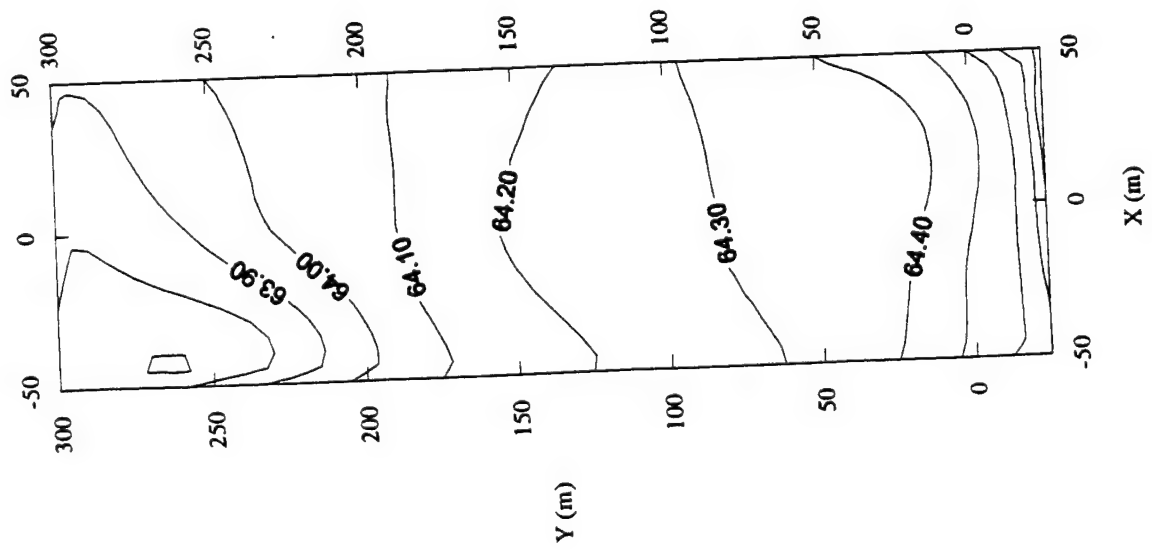
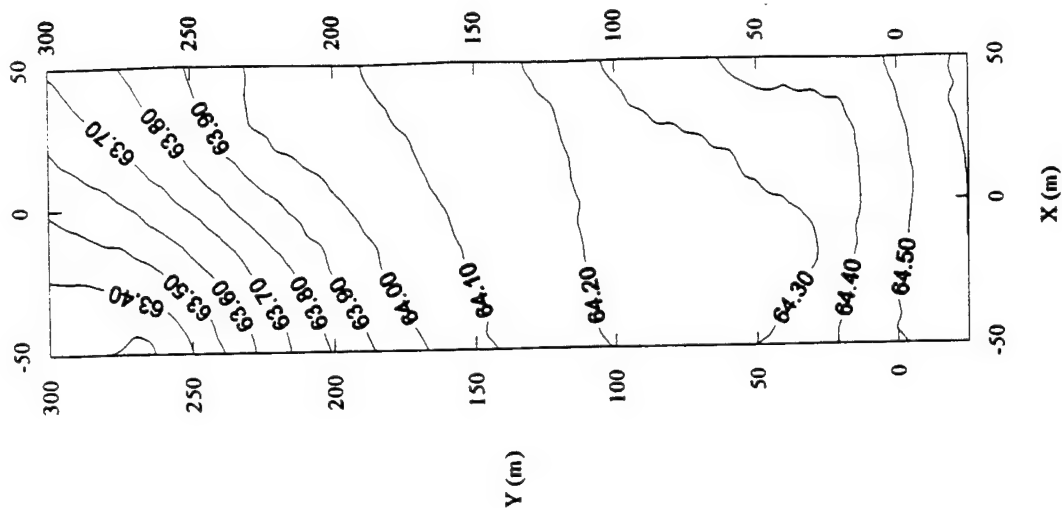


Figure 16. Left: M2-5-1, Day 270, Layer 4 Heads. Right: Upper Kriged Heads of March 8, 1991.

Lower Screened Heads of March 8, 1991



Heads c7 Layer 9, Day 270, Run M2-5-1

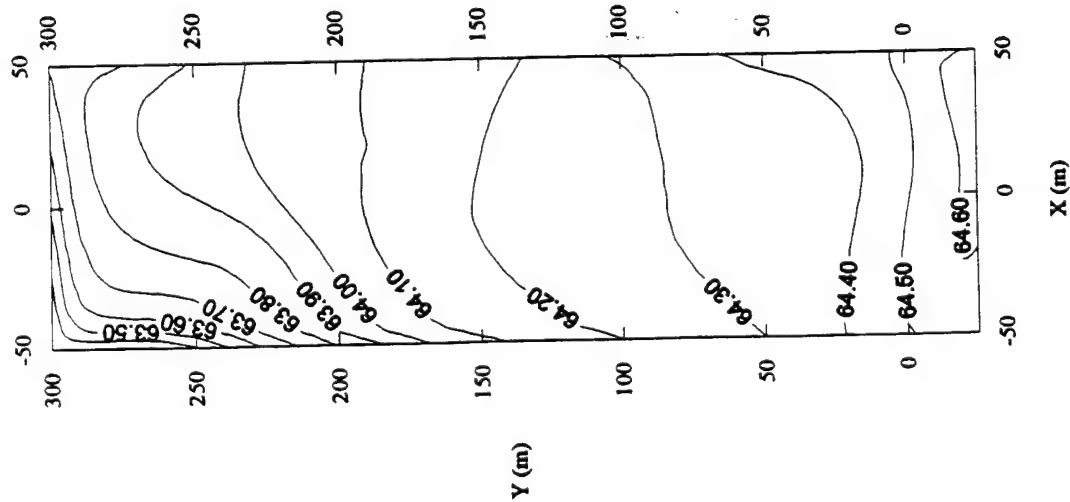


Figure 17. Left: M2-5-1, Day 270, Layer 9 Heads. Right: Lower Krige Heads of March 8, 1991.

# Piezometer P53A

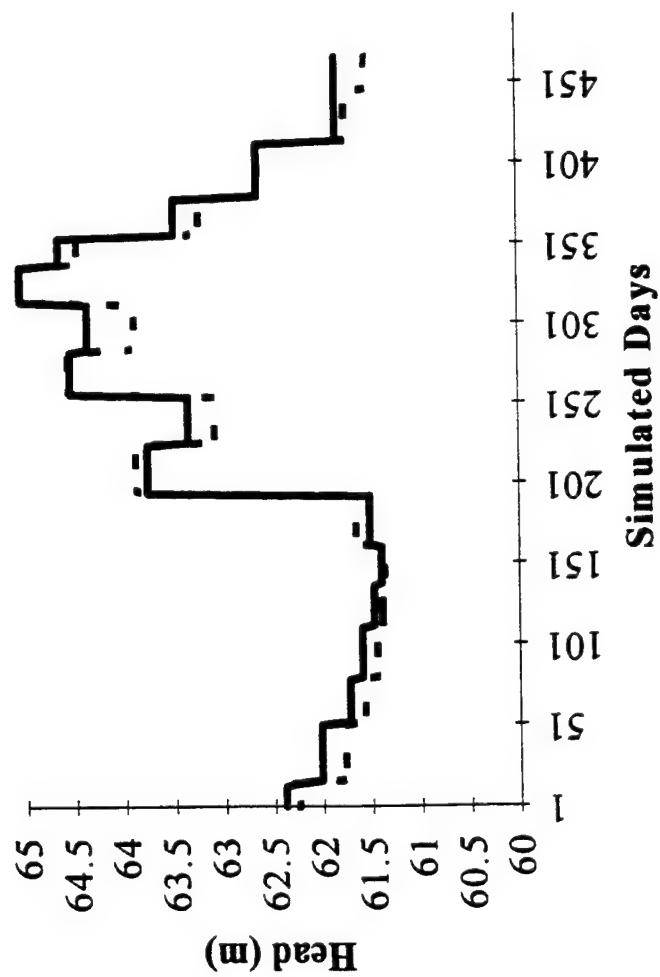


Figure 18. Observed and Simulation M2-5-1 Hydrographs of P53A.

In addition HYDROGRA calculated the minimum, maximum, and root mean square (RMS) differences between the time averaged observed head and simulated head. These calculations are summarized in Table 14 for Cases 1, 4, and 5. Cases 2 and 3 showed poorer results. Case 5, with the smallest storage coefficients, gave the best agreement as indicated by the RMS error.

The remainder of this section concerns work supported by the present contract. In the fall of 1995, Case 5 was rerun at West Virginia University on a 90 MHz Pentium personal computer (PC). Slight differences were encountered, especially in run time and percent discrepancy. The PC took approximately one-fourth the time (15 minutes) to converge compared to the Sun Sparcstation 2. However, the PC had a -1.40 % cumulative volumetric error compared to the Sun's 0.23% . These differences were considered insignificant.

With the addition of ten new conductivity wells (K72 through K81) in the spring of 1995, the transmissivity and vertical leakance fields were re-kriged with Geo-EAS using the procedure described previously. These revised conductivities were the basis of the M2-8 series of simulations. Table 15 lists the parameters used to create the variogram models for the nine layers, including model type, nugget, sill, and range. The table also lists some important statistical parameters, such as mean and variance of the natural logarithms.

TABLE 14. OBSERVED HEADS MINUS MODFLOW HEADS FOR M2-5-1,4,5.

|         | Min.<br>(m) | Min.<br>(m) | Min.<br>(m) | Max.<br>(m) | Max.<br>(m) | Max.<br>(m) | RMS<br>(m) | RMS<br>(m) | RMS<br>(m) |
|---------|-------------|-------------|-------------|-------------|-------------|-------------|------------|------------|------------|
| Well    | Case1       | Case4       | Case5       | Case1       | Case4       | Case5       | Case1      | Case4      | Case5      |
| P53A    | -0.65       | -1.32       | -0.57       | 0.74        | 0.51        | 0.14        | 0.329      | 0.228      | 0.194      |
| P54A    | -0.53       | -0.84       | -0.37       | 0.39        | 0.58        | 0.30        | 0.143      | 0.165      | 0.136      |
| P54B    | -0.42       | -0.78       | -0.17       | 0.43        | 0.52        | 0.43        | 0.147      | 0.159      | 0.143      |
| P55A    | -0.53       | -0.80       | -0.37       | 0.44        | 0.50        | 0.44        | 0.199      | 0.204      | 0.199      |
| P55B    | -0.12       | -0.44       | +0.01       | 1.01        | 1.01        | 1.01        | 0.374      | 0.374      | 0.374      |
| P60A    | -0.51       | -0.51       | -1.51       | 0.30        | 0.38        | 0.30        | 0.188      | 0.188      | 0.188      |
| P61A    | -0.40       | -0.40       | -0.40       | 0.36        | 0.36        | 0.36        | 0.188      | 0.188      | 0.188      |
| P61B    | -0.39       | -0.39       | -0.39       | 0.23        | 0.23        | 0.23        | 0.154      | 0.154      | 0.154      |
| Average | -0.44       | -0.69       | -0.35       | 0.49        | 0.51        | 0.40        | 0.215      | 0.208      | 0.197      |

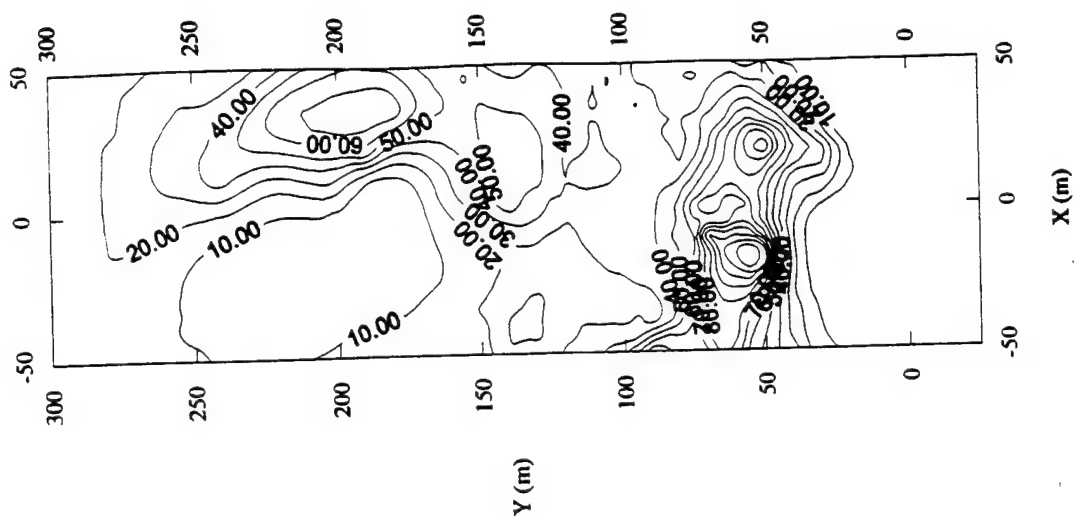
TABLE 15. KRIGING PARAMETERS FOR TRANSMISSIVITY AND LEAKANCE.

| Parameter | Layer | Type | Nugget | Sill | Range | Mean | $\sigma^2$ |
|-----------|-------|------|--------|------|-------|------|------------|
| Trans.    | 1     | Exp. | 1.5    | 4.0  | 100   | 1.43 | 5.06       |
|           | 2     | Sph. | 1.0    | 4.7  | 100   | 1.55 | 4.93       |
|           | 3     | Sph. | 1.5    | 4.7  | 100   | 1.84 | 5.32       |
|           | 4     | Exp. | 1.0    | 6.5  | 200   | 1.83 | 5.36       |
|           | 5     | Sph. | 1.0    | 5.0  | 80    | 1.53 | 5.13       |
|           | 6     | Exp. | 1.0    | 5.0  | 80    | 1.24 | 4.68       |
|           | 7     | Exp. | 0.5    | 4.0  | 120   | 1.05 | 3.51       |
|           | 8     | Exp. | 0.5    | 2.5  | 100   | 0.89 | 2.35       |
|           | 9     | Sph. | 0.0    | 2.25 | 60    | 1.76 | 2.19       |
| VCONT     | 1     | Exp. | 1.5    | 4.0  | 100   | 1.43 | 5.06       |
|           | 2     | Sph. | 1.0    | 4.3  | 100   | 1.39 | 4.33       |
|           | 3     | Sph. | 1.5    | 4.5  | 90    | 1.32 | 4.89       |
|           | 4     | Exp. | 1.0    | 7.0  | 160   | 0.96 | 5.59       |
|           | 5     | Sph. | 1.0    | 5.0  | 70    | 0.71 | 5.07       |
|           | 6     | Exp. | 1.0    | 4.0  | 70    | 0.31 | 3.75       |
|           | 7     | Exp. | 0.5    | 3.0  | 100   | 0.18 | 2.87       |
|           | 8     | Exp. | 0.5    | 3.0  | 90    | 0.02 | 2.99       |

where Trans. = Transmissivity, Exp. = Exponential, Sph. = Spherical, and  $\sigma^2$  = variance

Figure 19 compares the kriged conductivities of layer 3 for the cases of M2-5 and M2-8. The difference in the mid field demonstrates the importance of a more exhaustive data set. The remaining transmissivity and VCONT contours for the M2-8 simulations can be found in Appendix B.

Transmissivity of Layer 3, Run M2-5



Transmissivity of Layer 3, Run M2-8

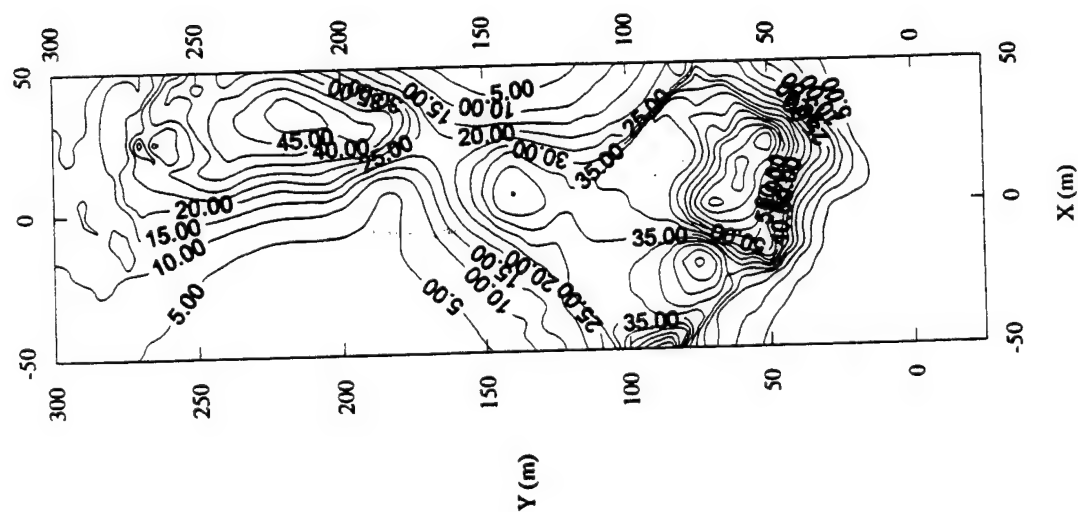


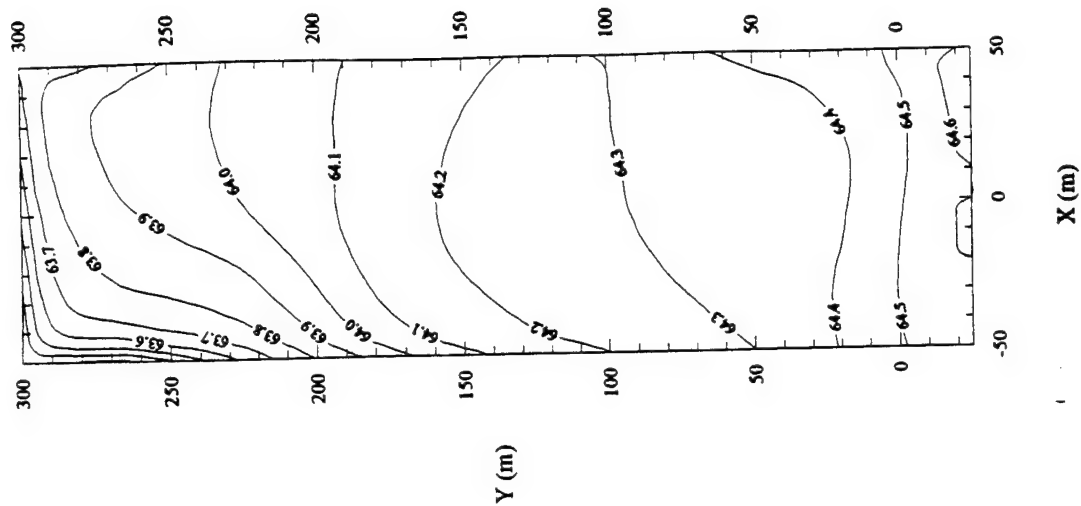
Figure 19. Layer 3 Transmissivity [m/d] of M2-8 (Left) and M2-5 (Right).

Simulation M2-8-1 used the same parameters as M2-5-1, except for the new set of conductivity data in the former. M2-8-1 took approximately 45 minutes to converge on a 486 PC with a speed of 33 MHz. The Layer 4 and 8 head contours (Figure 20) of day 270 show good agreement with the observations in Figure 14. The Layer 4 results are quite similar to those of M2-5-1 in Figure 16. However, the average RMS error compared to the recording piezometers was 0.207 meters (as calculated by HYDROGRA) compared to 0.215 meters in M2-5-1. Simulation M2-8-2 changed the storage coefficients to those used in M2-5-5. The model was rerun on the 486, converging after 45 minutes. The head contours were virtually unchanged. The average RMS error for M2-8-2 was 0.205 meters, better than M2-8-1, yet not as good as M2-5-5 (0.197 meters). Simulation M2-8-2 was taken as the new base case, as it included all updated information. Table 16 lists the summary of the head differences for the two cases of M2-8-1 and M2-8-2.

TABLE 16. SUMMARY STATISTICS FOR M2-8.

|         | Min.<br>(m) | Min.<br>(m) | Max.<br>(m) | Max.<br>(m) | RMS<br>(m) | RMS<br>(m) |
|---------|-------------|-------------|-------------|-------------|------------|------------|
| Well    | M2-8-1      | M2-8-2      | M2-8-1      | M2-8-2      | M2-8-1     | M2-8-2     |
| P53A    | -0.98       | -0.67       | 0.35        | 0.36        | 0.204      | 0.198      |
| P54A    | -0.64       | -0.38       | 0.51        | 0.51        | 0.154      | 0.149      |
| P54B    | -0.47       | -0.47       | 0.40        | 0.35        | 0.177      | 0.176      |
| P55A    | -0.57       | -0.53       | 0.45        | 0.45        | 0.202      | 0.202      |
| P55B    | -0.17       | +0.01       | 1.02        | 1.02        | 0.381      | 0.381      |
| P60A    | -0.51       | -0.51       | 0.35        | 0.35        | 0.192      | 0.194      |
| P61A    | -0.40       | -0.40       | 0.36        | 0.36        | 0.188      | 0.188      |
| P61B    | -0.39       | -0.39       | 0.23        | 0.23        | 0.155      | 0.155      |
| Average | -0.52       | -0.42       | 0.46        | 0.45        | 0.207      | 0.205      |

Head of Layer 9, Day 270, Run M2-8-1



Head of Layer 4, Day 270, Run M2-8-1

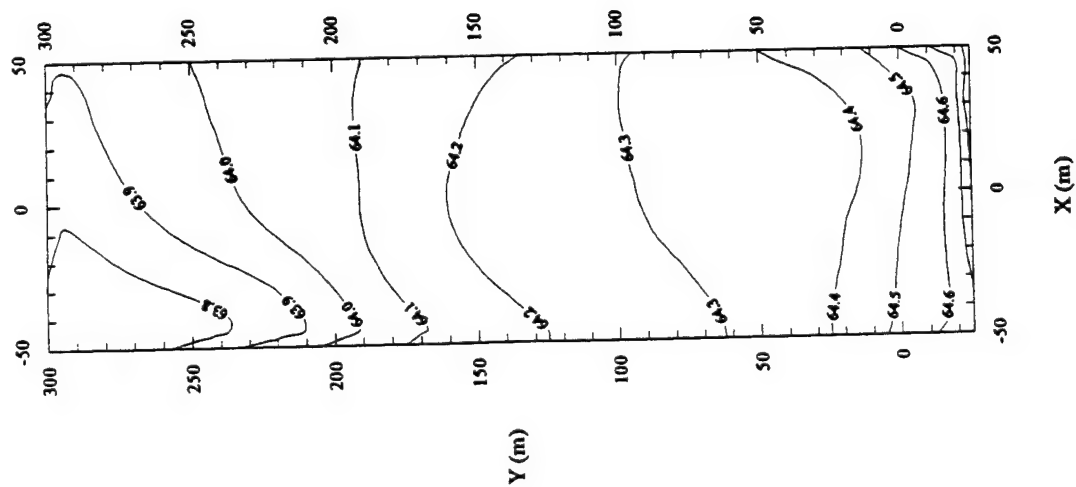


Figure 20. M2-8-1, Day 270. Left: Layer 4, Right: Layer 9.



Other experimental simulations, such as those of M2-6, which studied a two-dimensional version of M2-5, and M2-7, which studied the effects of differential temporal discretization, were no help in understanding the flow phenomena at the MADE-2 site. These cases merely tried to simplify the model for solving the transport problem, discussed later.

Following a suggestion of Dr. C. Zheng, simulations M2-9 tried an approach different than kriging to estimate the conductivity field. The polygonal method, in which a polygon of influence is assigned to each measurement, produces a step-like conductivity array. Program NGP (nearest grid point) tested the conductivity data of the 77 profiles for each layer and produced a blocky conductivity field in which each node is assigned the value of the nearest conductivity measurement. Figure 21 shows a conductivity layer which is representative of all the layers, since each profile extends vertically downward in the same horizontal location. Simulation M2-9-1, using the same storage coefficients as M2-5-5, took approximately 15 minutes on a 90 MHz Pentium PC to converge. Figure 22 shows Layers 4 and 9 on day 270, equivalent to the observed upper and lower staged piezometers of March 8, 1991, in Figure 14. The major discrepancy occurs in the near field where the contours are spread out too much, indicating a higher transmissivity than expected. The averaged RMS error was also higher than previous simulations with a value of 0.232 m. No additional simulations were conducted using the polygonal method.

The output of the flow model was used as input for the transport model, MT3D. A linking package called LKMT18, written by Zheng (the author of MT3D), produced an output file which contained the heads, velocities, and cell-by-cell flow terms needed to solve the three-dimensional transport equation. The next section describes the process by which the transport equation was solved.

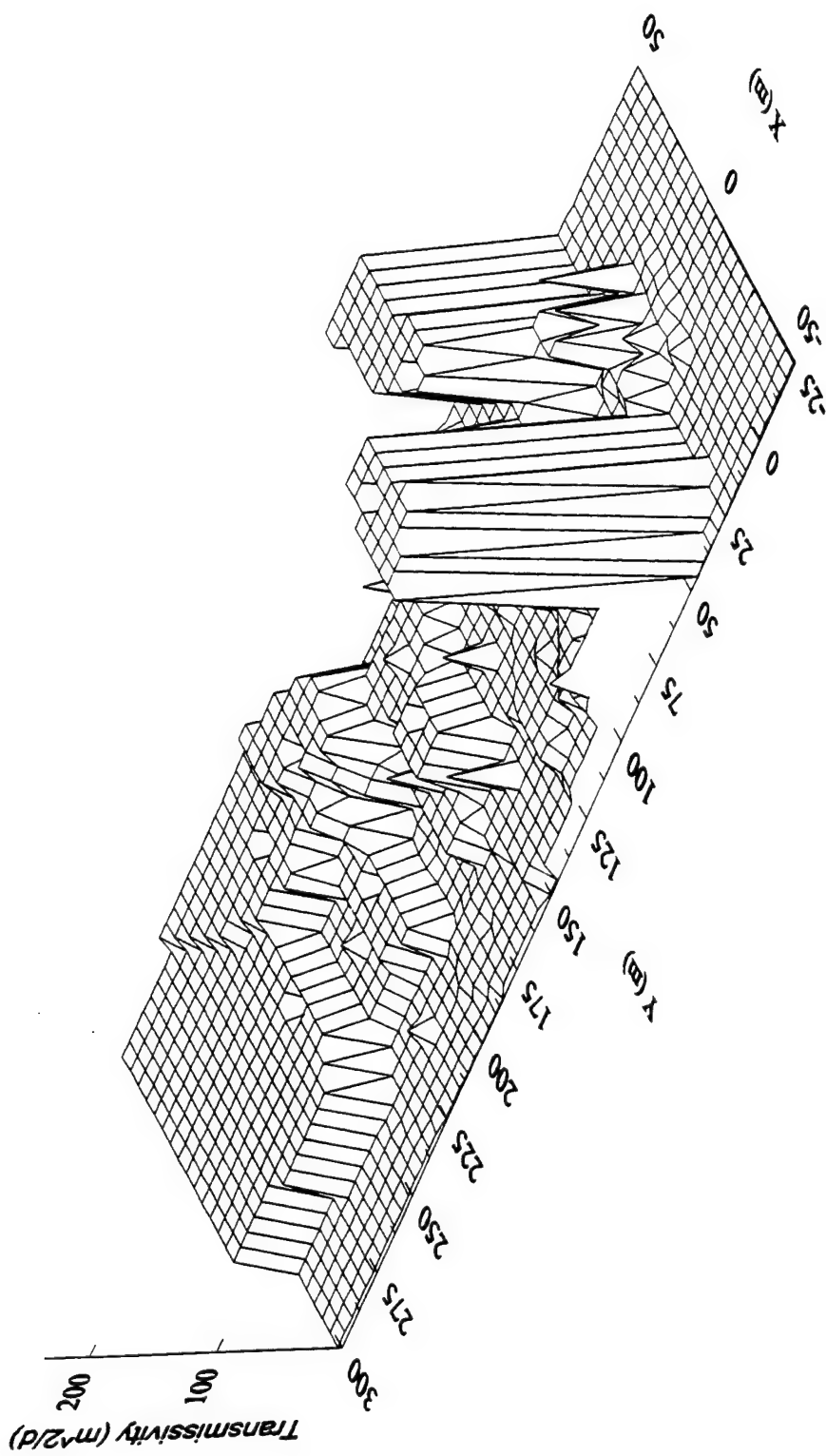
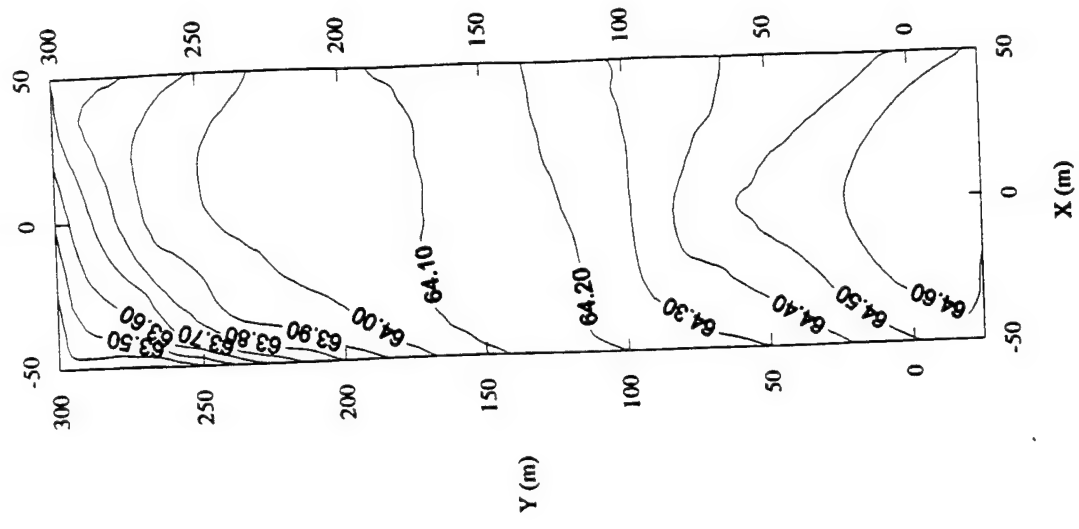


Figure 21. Nearest Grid Point Transmissivity Distribution for Layer 9.

Heads of Layer 4, Day 270, Run M2-9-1



Heads of Layer 4, Day 270, Run M2-9-1

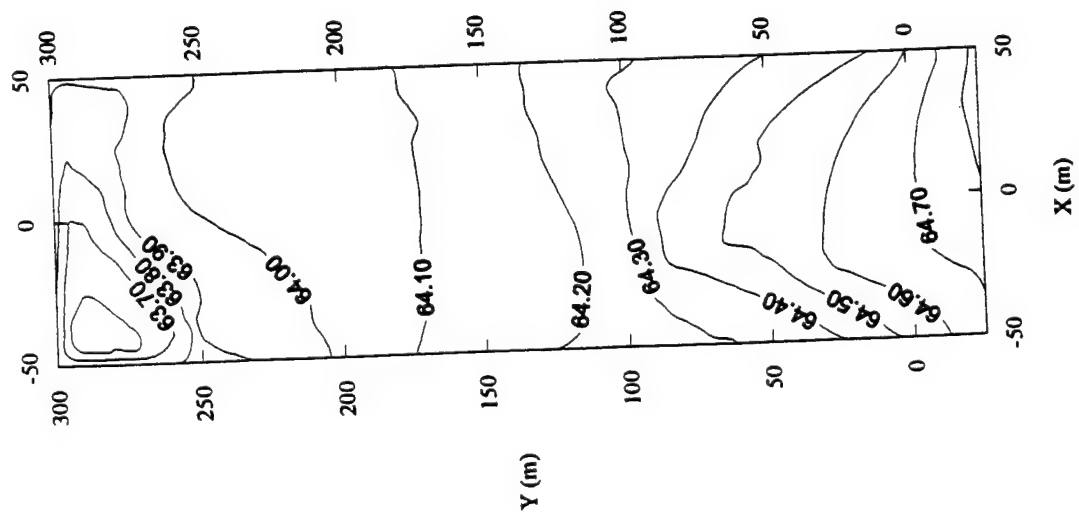


Figure 22. M2-9-1 Heads for Day 270. Left: Layer 4; Right: Layer 9.

## SECTION VI

### TRANSPORT MODELING

#### A. THEORY

The transport equation was solved separately using MT3D, a modular three-dimensional transport model (Zheng, 1990). Decoupling the flow problem from the transport problem is permissible if density variations are negligible. However, if density varies significantly due to concentration or temperature variations, the two problems must be solved simultaneously; groundwater velocities can be affected by buoyancy forces. The validity of this assumption is discussed further in a later section.

MT3D can only model only one contaminant at a time. Even though several species were injected in MADE-2, they do not react with each other. Therefore, MT3D was used to simulate the migration of each contaminant independently.

The transport equation that MT3D solves incorporates the terms representing advection, dispersion, reactions, and any sinks and sources. Equation (4) is the partial differential equation governing three dimensional transport of contaminants in groundwater:

$$\frac{\partial C}{\partial t} = - \frac{\partial}{\partial x_i} (v_i C) + \frac{\partial}{\partial x_i} \left( D_{ij} \frac{\partial C}{\partial x_j} \right) + \sum_{k=1}^N R_k + \frac{q_s}{\theta} C, \quad (4)$$

where:  $x_i$  refers to the Cartesian coordinate axes

$C$  is concentration

$t$  is time

$D_{ij}$  is the hydrodynamic dispersion (dispersion and diffusion) tensor

$v_i$  is the seepage velocity

$q_s$  is volumetric flux of water per unit volume of aquifer representing sinks/sources

$C_s$  is the contaminant concentration of the water added by sinks/sources

$\theta$  is the porosity

$\sum R_k$  is the chemical reaction term

## 1. Advection

Advection is the migration of miscible contaminants at the groundwater seepage velocity. MT3D solves the advective-dispersive-reactive equation using a mixed Eulerian-Lagrangian scheme. In the Eulerian approach, the transport equation is solved using fixed nodes, as in the finite-difference method. This method is advantageous in dispersion or reaction dominated flow. However, if advection explains most of the contaminant migration, the Eulerian approach is susceptible to large numerical dispersion and oscillation in the solution and may require small grid spacing and time steps (Zheng, 1990). Numerical dispersion causes a smearing of concentration fronts which should have a sharp appearance. Therefore, the Lagrangian approach is often used for the advection dominated flows which exist in many field conditions. The Lagrangian method tracks moving particles and provides an efficient solution to problems with sharp concentration fronts.

The second term in the transport equation  $\left( \frac{\partial}{\partial x_i} (v_i C) \right)$  describes advection and can be modeled by the Lagrangian approach in MT3D using either the method of characteristics (MOC), the modified method of characteristics (MMOC), or a combination of the two called the hybrid method of characteristics (HMOC). A fourth approach uses the Eulerian Upstream Finite Differencing (UD). Each Lagrangian method uses a particle tracking technique, which decreases the amount of numerical dispersion and oscillation in the solution.

The MOC method uses forward tracking of particles, in which a set number of particles are introduced in each computational cell of the domain and are assigned a position and concentration. The particles are tracked using a very small time step and the average particle concentration for the cell is calculated at the end of each time increment. The concentrations of

each particle are also updated to reflect changes due to dispersion and chemical reactions. The major advantage to the MOC method is that it is virtually free of numerical dispersion. However, the method is computationally difficult and requires large amounts of computer memory to store particle locations. It can also lead to large mass balance discrepancies, as it is independent of the principle of conservation of mass.

The MMOC method also tracks particles, but does so by placing only one particle at the node of each cell and tracking it backwards in time to find its position at the old time level. Since only one particle per cell is used in the MMOC method, it is much faster than the MOC method where many particles are sometimes in a cell. Moreover, the MMOC method places a new particle at the node in the beginning of each new time level, thereby eliminating the need to store the location of the particle. The method is virtually free of numerical dispersion, except at sharp concentration fronts, and is intended for use where sharp fronts do not occur.

The third method of particle tracking incorporates the advantages of both methods above. Near sharp fronts the MOC method distributes the required number of particles around each front. Elsewhere, the MMOC method is employed to reduce the total number of particles needed. The solution automatically adapts to either method as concentration fronts dissipate by dispersion or chemical reactions. A user-specified criterion controls the switching between MOC and MMOC. In certain circumstances the HMOC method may not give the optimal solution, in which case the MOC or MMOC may be chosen (Zheng, 1990).

Lastly, an upstream finite differencing option for the advection term is also included. The UD method may lead to large numerical dispersion for problems having sharp fronts, but is more efficient, computationally. The method also conserves mass, and may reduce the mass balance discrepancy at every step.

## 2. Dispersion

Dispersion in porous media refers to the spreading of contaminants over a greater region than would be predicted solely from the Darcy velocity vectors. Hydrodynamic dispersion incorporates both mechanical dispersion due to deviations from the average groundwater velocity within a representative elementary volume and molecular diffusion due to concentration variations. The third term of Equation (4),  $\frac{\partial}{\partial x_i} \left( D_{ij} \frac{\partial C}{\partial x_j} \right)$ , represents dispersion with  $D_{ij}$  being the hydrodynamic dispersion tensor. A fully explicit, block-centered finite-difference method is used to approximate this term. The limitation associated with an explicit solver is the small time stepping criteria needed to ensure numerical stability. However, due to the large memory requirement for the particle tracking, an implicit solver would more than likely exceed memory availability on smaller personal computers.

## 3. Chemical Reactions

The fourth term in Equation (4) represents reactions associated with contaminant migration such as equilibrium controlled linear or nonlinear sorption and first order, irreversible rate reactions. The chemical reaction term is expressed as (Zheng, 1990):

$$\sum_{k=1}^N R_k = \frac{\rho_b}{\theta} \frac{\partial \bar{C}}{\partial t} - \lambda \left( C + \frac{\rho_b}{\theta} \bar{C} \right) \quad (5)$$

where:  $\rho_b$  is the bulk density of the aquifer material

$\bar{C}$  is the concentration of the sorbed species per unit mass of porous media

$\lambda$  is the rate constant of the first order rate reactions

The reaction term allows for sorption, the mass transfer process between the contaminants dissolved in the groundwater and the solid contaminants sorbed on the porous media. It is

assumed that the two-phase interaction between solid and solution is in equilibrium and that the reaction is fast enough to be considered instantaneous. The relationship between the sorbed and the dissolved concentration is called an isotherm. MT3D can simulate both linear and nonlinear isotherms. The nonlinear isotherms available are the Freundlich and the Langmuir.

Biodegradation and radioactive decay can be simulated as first-order rate reactions. The rate constant,  $\lambda$ , is usually given as the half-life, which is the time needed to decrease the concentration to one-half its initial value.

#### 4. Sink and Sources

The fifth term of the governing equation,  $\frac{q_i}{\theta} C_i$ , represents any sinks or sources of solute mass that may leave or enter the domain. They can be of either point or areal type. Point sources include wells, rivers and drains; areally distributed sinks or sources include recharge and evapotranspiration. The concentration must be given for any source term. On the other hand, it is not necessary to specify the concentration for any sink, since it is assumed that it is equivalent to the ambient groundwater concentration. The only exception is evapotranspiration, in which pure water is taken from the aquifer (Zheng, 1990). In reality, however, volatile contaminants, including tritiated water, may leave through evapotranspiration. This is a definite limitation in simulating MADE-2.

#### B. DISCRETIZATION

MT3D is designed to allow use of the same grid as MODFLOW, and this feature was exploited in the present study. Thus the MT3D domain was divided into 66 rows, 21 columns, and 9 layers. The block centered formulation places a node at the center of each cell, where MODFLOW calculates head and MT3D calculates concentration. The hydraulic and chemical parameters such as hydraulic conductivity and dispersivity are assumed to be uniform over the entire cell (Zheng, 1990).



The temporal discretization is also identical to MODFLOW's with the stress periods and time steps given in Table 10. However, the time step used in the implicit solution of the head values by the flow model may be too large for the explicit transport model, which places restrictions on the time increments. Therefore, the MODFLOW time steps are automatically divided by MT3D into transport steps, smaller increments of time in which heads are kept constant as the change in concentration is calculated.

### C. INITIAL AND BOUNDARY CONDITIONS

Because the experiment requires a transient simulation, initial conditions are necessary to solve the transport equation. For the MADE-2 model, time began 14 days prior to any injection of contaminants. Hence, all concentration values at the beginning of the transport simulation were set to zero. The boundary conditions for all time were that on the lateral boundaries the concentration of entering water was set to zero whereas outflowing water carried the concentration of the upstream node out of the domain. It was implicitly assumed that there is no loss of contaminant through the water table, an assumption which is unlikely to be precisely correct.

### D. TRANSPORT PARAMETERS

The following additional parameters were needed for transport modeling: soil porosity, dispersivity, chemical reaction constants, and contaminant source strengths.

#### 1. Porosity

The porosity of the aquifer is needed to convert the specific discharge or Darcy velocity calculated by the flow model to seepage velocity for the solution of the transport equation. Porosity was measured for 84 samples taken from only four coreholes. Based on these 84

measurements, an average porosity of 0.32 was calculated. Lacking adequate data to infer the expected spatial variation in porosity, this value was used for every cell in the domain.

## 2. Dispersivity

Boggs et al. (1993) describe two cases in which dispersivity was calculated from the first and second spatial moments of the observed MADE-2 tritium plume, a base case and an extrapolated case. The base case was calculated solely from the observations; the extrapolated case included a model for the portions of the plume which had spread beyond the sampling domain. Longitudinal dispersivities of 19.6 meters and 9.5 meters were calculated for the base case and extrapolated case, respectively. A horizontal transverse dispersivity of 2.2 meters was calculated in only the base case. This may be an overestimate due to the theory of the transport model used in calculating this number. Transverse dispersivities are usually taken to be approximately 10% of the longitudinal (Freeze and Cherry; 1979). In this work, vertical transverse and lateral transverse dispersivities were 10% of the longitudinal value.

The molecular diffusion coefficient of tritium in water was estimated using the Wilke-Chang method. This value was multiplied by an assumed tortuosity of 0.25 to yield  $2.16 \times 10^{-4} \text{ m}^2 / \text{day}$ , for the molecular diffusion coefficient of tritium in a saturated porous media. The same value was used for the other contaminants. This cannot be justified, but its effect on the results is probably negligible. (A later recalculation gave a value of  $0.475 \times 10^{-4} \text{ m}^2 / \text{day}$  for the molecular diffusion coefficient of tritium in a saturated porous media. Again, the effect of the error is probably negligible.)

## 3. Chemical Reactions

Tritium in the form of tritiated water is nonreactive in the groundwater environment, but it undergoes radioactive decay with a 12.26 year half-life. Sorption of tritiated water does not occur, however the hydrocarbon contaminants do experience sorption. MT3D simulates the effects of sorption in the Chemical Reaction module through the use of a retardation factor (R).

A retardation factor of 5 implies the contaminant moves 5 times slower than the groundwater seepage velocity. A linear equilibrium isotherm was assumed and the retardation factor was calculated as:

$$R_{i,j,k} = 1 + \frac{\rho_b}{\theta_{i,j,k}} K_d \quad (6)$$

where:  $K_d$  is the distribution coefficient.

$\rho_b$  is the bulk density of the dry soil

$\theta_{i,j,k}$  is the porosity of cell  $i,j,k$

Although Boggs et al. (1993) obtained estimates for  $R$  from field and laboratory data, these could not be entered directly to MT3D. Instead, Equation (6) was solved for  $K_d$  and  $K_d$ ,  $\theta$ , and  $\rho_b$  were entered, allowing the program to calculate  $R$  internally. Table 17 shows the values used to simulate sorption.

TABLE 17. PARAMETERS FOR ORGANIC TRANSPORT SIMULATIONS.

| Organic     | $\theta$ | Bulk Density<br>$\times 10^6$ ( $g/m^3$ ) | Retardation Factor | $K_d \times 10^8$<br>( $m^3/g$ ) | RC1<br>( $day^{-1}$ ) | Initial Concentration<br>( $g/m^3$ ) |
|-------------|----------|---|--------------------|----------------------------------|-----------------------|--------------------------------------|
| Benzene     | 0.32     | 1.77                                      | 1.30               | 5.42                             | 0.0070                | 68.01                                |
| Naphthalene | 0.32     | 1.77                                      | 1.42               | 7.59                             | 0.0064                | 7.216                                |
| o-DCB       | 0.32     | 1.77                                      | 1.32               | 5.78                             | 0.0046                | 32.75                                |
| p-Xylene    | 0.32     | 1.77                                      | 1.24               | 4.33                             | 0.0107                | 41.44                                |

Biodegradation was simulated by using experimentally determined rate constants obtained from MacIntyre et al. (1993). Degradation kinetics were calculated from field data and were approximately first order. The rate constant RC1 in Table 17 was entered directly into the transport model.

The last column of Table 17 lists the initial concentrations used for the transport simulations. These values were calculated by dividing the injected mass for each organic by the total volume of solution ( $9.7 \text{ m}^3$ ). The initial concentration is also entered directly in the transport model. The initial tritium concentration (not listed) was  $0.0555 \text{ Ci/m}^3$ .

#### 4. Contaminant Sources

The source of contaminants was a line of five injection wells spaced 1 meter apart. In the model these were consolidated into one well located at Row 61, Column 11, and Layer 7. MT3D allows the user to specify the concentration of injected contaminants for every stress period. For the MADE-2 experiment, injection started on Simulation Day 14 and lasted until Day 16, corresponding to Stress Period 2. There was no well flow in any other stress period.

#### E. MT3D OUTPUT

MT3D allows the user to create up to five output files including a generic output file, an unformatted concentration file, a mass balance file, a point observation file, and a configuration file. The generic output file contains all relevant information about the simulation. It reproduces the input data as well as the results. At the end of each time step, the generic output file summarizes the mass budget.

The unformatted concentration file and the configuration file are created for post-processing of the output data. Program POSTMT3D, created by Zheng, is used to prepare output in a format for Surfer to contour. The unformatted concentration file is a binary file containing only concentration values for every layer at user specified times. The configuration file contains model discretization data needed by the postprocessor for graphical presentation. The generic output, concentration, and configuration files are automatically created by MT3D.

The mass balance and observation files are only created when the option is invoked by the user in the Basic Transport module (BTN). The mass balance file lists the mass in, mass out,

difference between mass in and out, and relative percent difference between the two at every transport step throughout simulation. The observation file lists the concentration at any user-designated cell at every transport step.

## F. COMPUTER SIMULATIONS

The initial MADE-2 modeling efforts of Gray (1992) did not include transport modeling. Gray (1993) used MT3D with the parameters given above to simulate the tritium plume only, but MT3D ran so slowly compared to MODFLOW that it was not practical to simulate the entire experiment. Eighty days were simulated but only the first 52 days gave meaningful results. For the homogeneous conductivity case the transport simulation took approximately 6.4 hours to run on the Sun Sparc 2. However, the heterogeneous case took almost three times longer to simulate the same time period. The homogeneous case simulated advective flow using the HMOC solver, whereas the heterogeneous simulation used the MOC option. Gray concluded that heterogeneous conductivity produced more realistic results than a simplified homogeneous conductivity solution.

The transport modeling of Gray and Rucker (1994), summarized in Table 18, was a little more successful. The head solution from MODFLOW case M2-5-1 was used as input to MT3D running on a Sun Sparc 2.

In Table 18 the 'Disp.' column identifies which simulations used dispersion. Not all runs included dispersion, as it was thought to be the cause of the model not completing. The 'Long. Disp. (m)' column gives the longitudinal dispersivity used in each simulation. Transverse lateral and transverse vertical components of dispersivity were taken to be one-tenth this value. The 'Last Sim. Day' indicates the number of the last simulation day before the simulation stopped because of an overflow error or user termination. The overflow errors occurred in the mass balance file. FORTRAN has a non-zero minimum and a maximum number it can interpret, usually  $10^{-31}$  and  $10^{+31}$ , respectively. When these bounds are exceeded, an underflow or overflow error occurs. For the simulations of Table 18, extreme mass accretion in the mass balance file caused most simulations to terminate. Neither the mass balance calculation itself nor the cause of the

accumulation of mass is fully understood by the authors. The 'Mass Discrep.' column denotes the discrepancy between mass in and out of the domain. The 'Plume Characteristics' column describes the general features of the tritium plume. Many of the simulations had some negative concentrations. This non physical result is caused by numerical oscillation in the solution, and occurred most frequently with the HMOC or UD methods. In general, the lower dispersion coefficients caused fewer concentration values to be negative and resulted in faster run times.

TABLE 18. MT3D SIMULATIONS BY GRAY AND RUCKER (1994).

| Run | Advection Method | Disp. | Long. Disp. (m) | Last Sim. Day | Run Time (hours) | Mass Discrep. % | Plume Characteristics |
|-----|------------------|-------|-----------------|---------------|------------------|-----------------|-----------------------|
| 1   | HMOC             | yes   | 10.0            | 30.2*         | 15.75            | +7.93           | wide spread, some<0   |
| 2   | MMOC             | yes   | 10.0            | 5.0*          | 1.75             | N/A.            | injection not started |
| 3   | MMOC             | no    | N/A.            | 129.4         | 10.4             | +82             | wide spread           |
| 4   | HMOC             | no    | N/A.            | 20.4*         | 0.72             | +19.2           | not recorded          |
| 5   | MOC              | no    | N/A.            | 62.1*         | 3.5              | -13.1           | confined to 7 cells   |
| 6   | HMOC             | no    | N/A.            | 140.9         | 17.38            | +17.2           | confined to 8 cells   |
| 7   | HMOC             | yes   | 10.0            | 44.6*         | 47.05            | +4.55           | wide spread, lots<0   |
| 8   | UD               | yes   | 10.0            | 61.2          | 16.6             | ~0              | wide spread, lots<0   |
| 9   | UD               | yes   | 4.0             | 90.4          | <21.4            | ~0              | wide spread, lots<0   |
| 11  | UD**             | yes   | 4.0             | 90.4          | <29              | ~0              | identical to case 9   |
| 12  | UD               | yes   | 1.0             | 128           | <5.37            | ~0              | realistic, lots<0     |
| 13  | UD               | yes   | 0.0             | 138.3         | <8               | ~0              | realistic, few<0      |
| 14  | HMOC             | yes   | 1.0             | 105.9*        | <12.6            | +12.3           | realistic, lots<0     |

\* run terminated by user

\*\* double precision

The extension of the summer of 1994 work began with simulations exploring different dispersion values using a 90 MHz Pentium personal computer. However, no run extended beyond Simulation Day 226. The code was investigated thoroughly to find errors which would cause the mass accumulation. The exact source of error was not found, but it was theorized that it was related to the rewetting capability of MODFLOW. Before Stress Period 6 the water table was in a steady decline. Then a large positive recharge caused the water table to rise abruptly approximately 2 meters in Stress Period 7. In the belief that the abrupt rise in the water table was

at fault, a new flow simulation, designated as M2-6, divided the previous seventh stress period of 24 days into 6 separate stress periods with 4 days each to give a more gradual rise in head. Again, overflow errors caused the transport simulation to end after only 219 days.

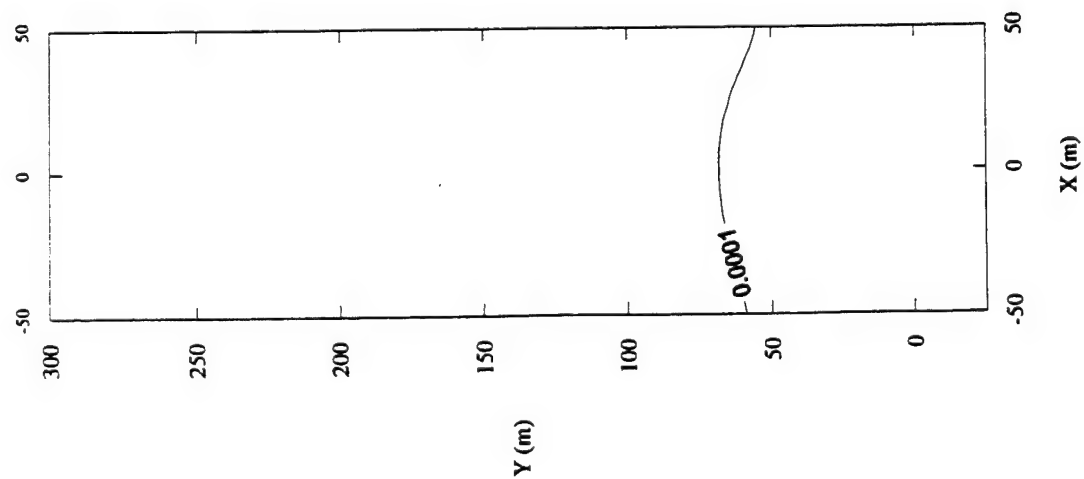
In order to reduce the complexity of the model, the grid was reduced to two dimensions by using one layer to represent the vertical discretization. This was the first simulation to model the entire 468-day experiment. Three separate simulations were run to test the effects of dispersivity and the different advection solvers. Table 19 summarizes the values used.

TABLE 19. SUMMARY OF 2-D TRANSPORT SIMULATIONS (M2-6).

| Run | # of Dim. | Days Simulated | Run Time | $D_L, D_V, D_T$ (m) | Conductivity of Layer |
|-----|-----------|----------------|----------|---------------------|-----------------------|
| 1   | 2         | 468            | 1 hr     | 5, 0.5, 0.5         | 1                     |
| 2   | 2         | 468            | 1 hr     | 10, 1, 1            | 1                     |
| 3   | 2         | 468            | 1 hr     | 10, 1, 1            | 4                     |

Figures 23 and 24 show Runs 1 and 2 at Simulation Days 148 and 344, respectively. All concentration values were normalized by the injected concentration. These runs used the hydraulic conductivity values of Layer 1 of the nine-layer, three-dimensional grid. These results do not compare well with the observed contours of Figure 25. The longitudinal spread of the simulated plume is not as far as the observed, only going to a maximum of 75 meters on Day 468 (not shown). In addition, the lateral spread is excessive. The conductivity was thought to be the hindrance. Therefore Run 3 used the conductivity of Layer 4. Figure 26 shows the Run 3 normalized tritium concentration on Days 148 and 344. There is very little improvement.

Tritium Plume of Day 148, Run 1



Tritium Plume of Day 344, Run 1

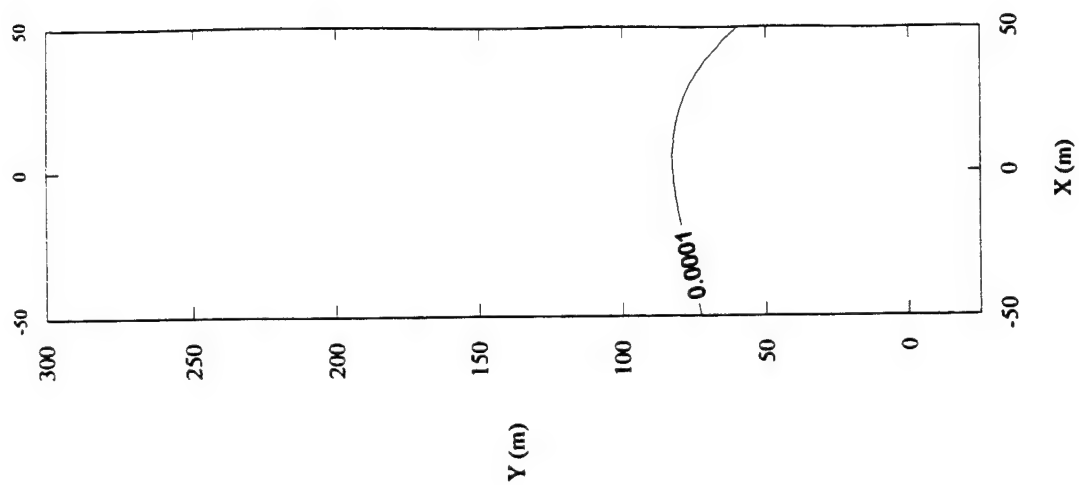
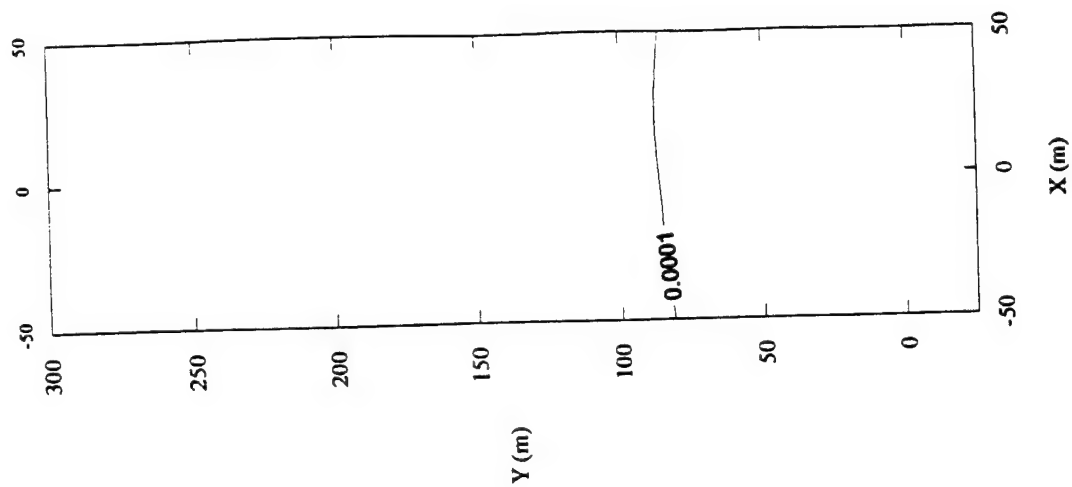


Figure 23. Two Dimensional Tritium Relative Concentration, Run M2-6-1. Left: Day 148; Right: Day 344.



Tritium Plume of Day 344, Run 2



Tritium Plume of Day 148, Run 2

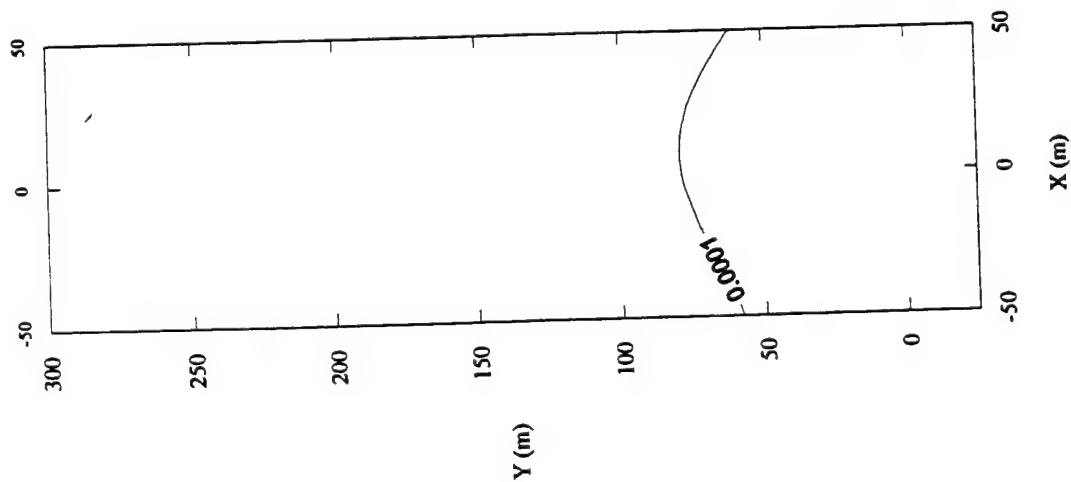


Figure 24. Two Dimensional Tritium Relative Concentration, Run M2-6-2. Left: Day 148; Right: Day 344.

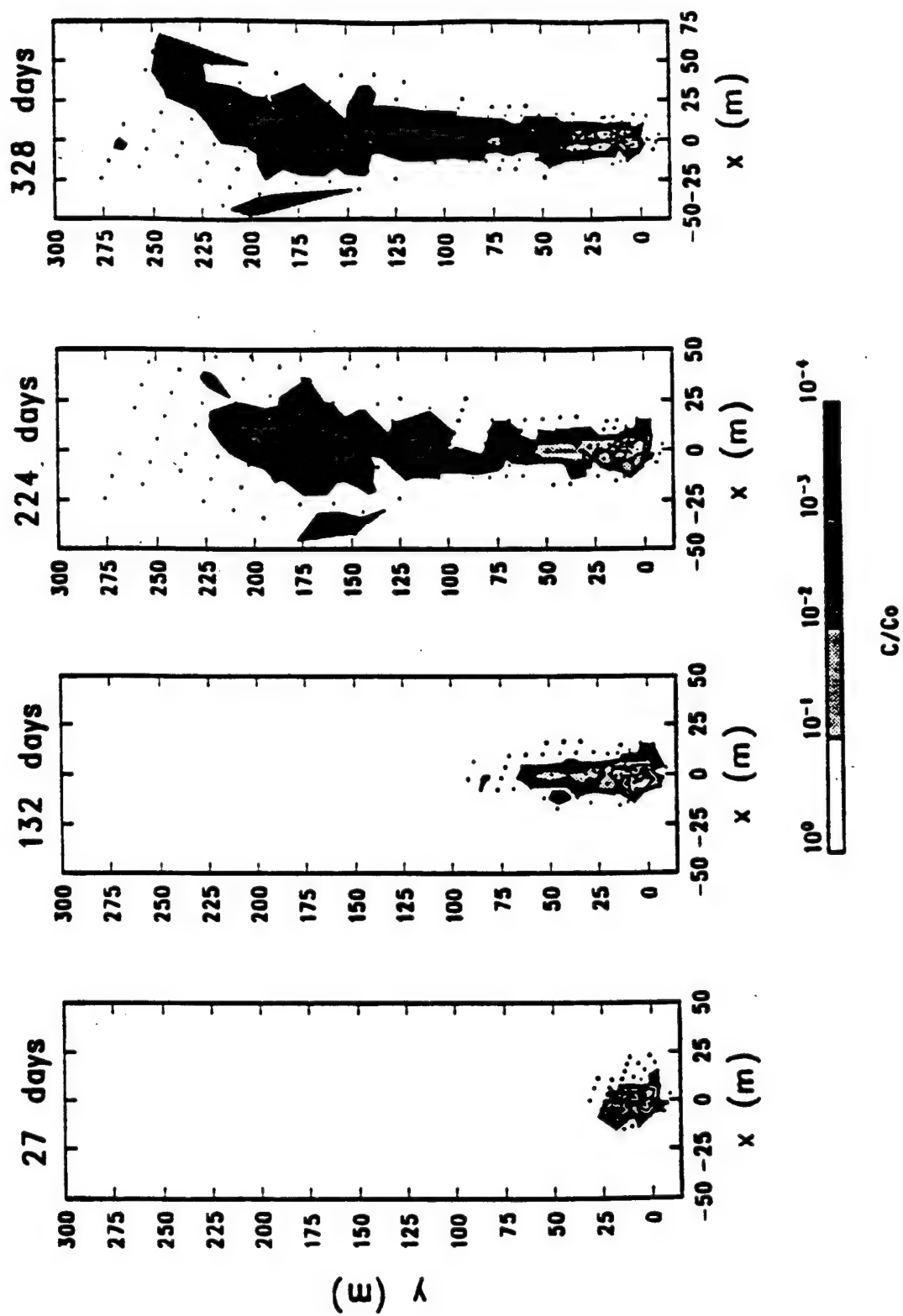
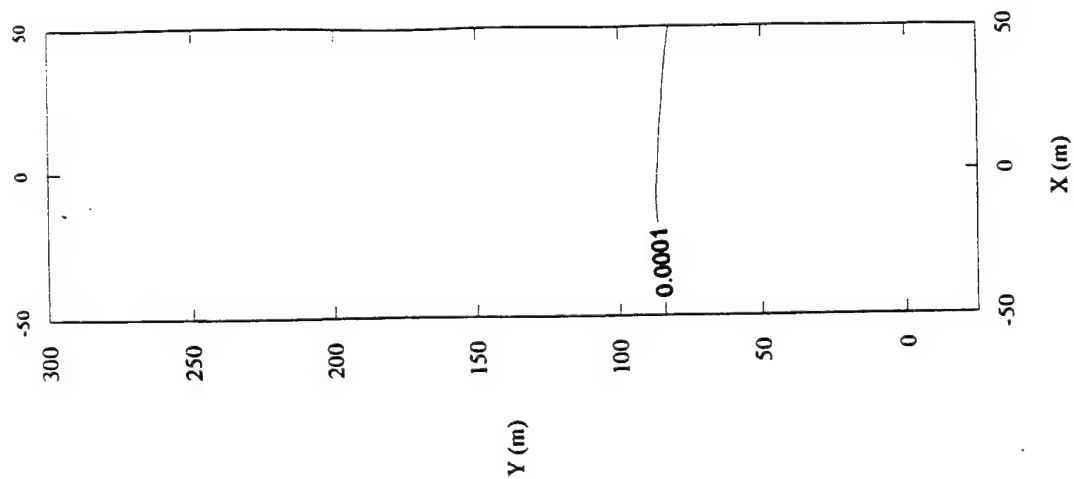


Figure 25. Observed Tritium Relative Concentration at 59.5 meters MSL. Source: Boggs et al (1993).

Tritium Plume of Day 344, Run 3



Tritium Plume of Day 148, Run 3

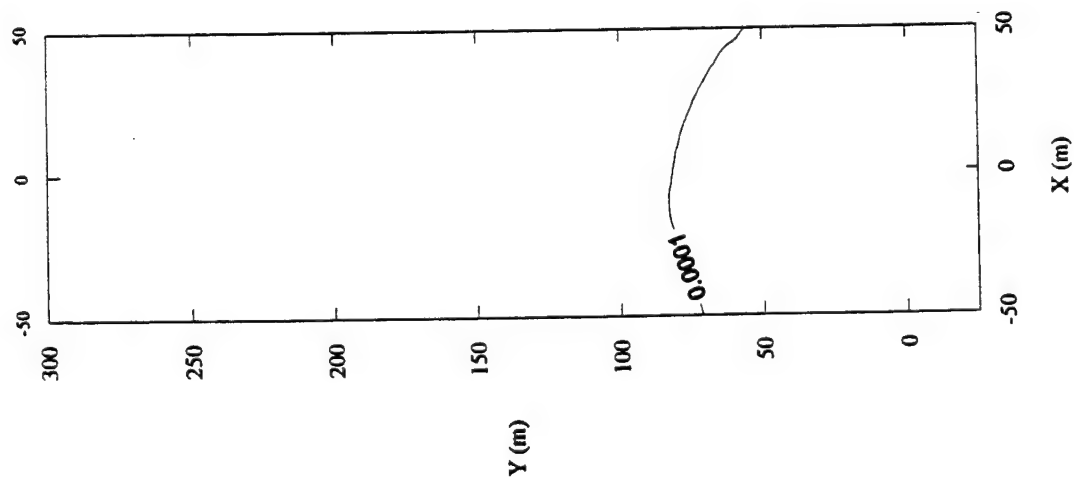


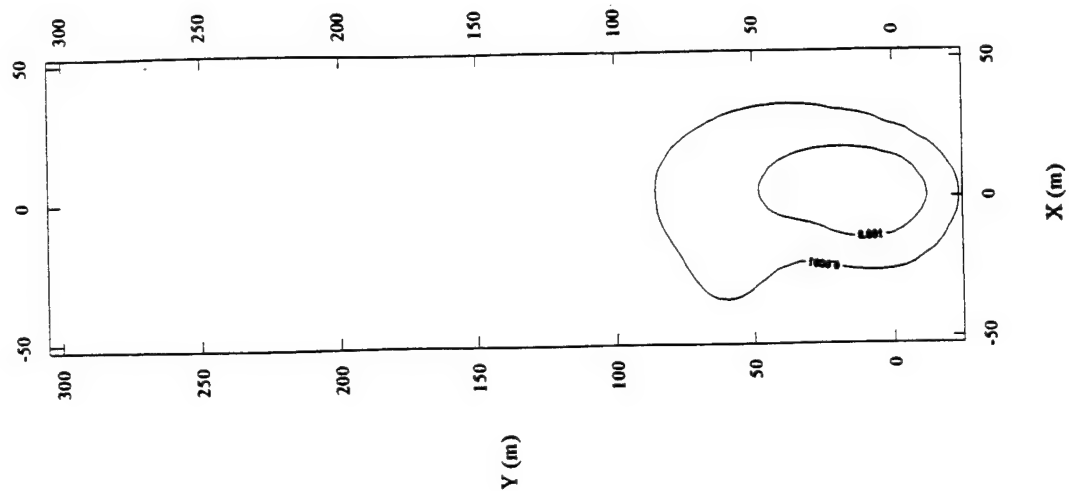
Figure 26. Two Dimensional Tritium Relative Concentration, Run M2-6-3. Left: Day 148; Right: Day 344.

Dr. Zheng, the author of MT3D, suggested reducing the value of the Percel variable, read from the Advection module input file. Percel is the Courant number, the maximum number of cells any particle is allowed to move in one transport step. The Courant number establishes the maximum time step allowed in order to maintain stability in the numerical procedure. In the manual for MT3D, it is suggested that Percel lie between 0.5 and 1.0. However, Dr. Zheng suggested using about 0.01. The first successful three-dimensional transport simulation, using a Percel of 0.01, took approximately 7 days on a 90 MHz Pentium PC. It quit on Day 446 (17 stress periods), due to an error in an input file for the last stress period. The simulation used the UD method for solving the advection term and had a longitudinal dispersion coefficient of 5.0 meters. The flow simulation of M2-5-5 was used as input for the seepage velocities. Figure 27 shows the normalized tritium contour of Simulation Day 344. This corresponds to the observed day of 328 since the simulation started 14 days prior to the injection. Although the simulated plume did not migrate as far as the observed plume in Figure 25, it looked much more reasonable than previous attempts. More simulations were performed to increase the migration, as summarized in Table 20.

TABLE 20. SUCCESSFUL HORIZONTALLY ISOTROPIC TRANSPORT SIMULATIONS.

| Run | # of<br>Dim. | Days<br>Simulated | Run<br>Time | Advection<br>Solver | $D_L, D_T, D_V$<br>(m) | Percel | DT0   | $\theta$ |
|-----|--------------|-------------------|-------------|---------------------|------------------------|--------|-------|----------|
| 1   | 3            | 446               | 7 days      | UD                  | 5, 0.5, 0.5            | 0.01   | 0.001 | 0.32     |
| 2   | 3            | 226               | 13 days     | MOC                 | 10.0, 0.1, 0.1         | 0.01   | 0.001 | 0.32     |
| 3   | 3            | 302               | 7 days      | MOC                 | 2.0, 0.2, 0.2          | 0.1    | 0.01  | 0.29     |
| 4   | 3            | 468               | 4 days      | UD                  | 2.0, 0.2, 0.2          | 0.1    | 0.01  | 0.29     |

Tritium Plume of Layer 4, Day 344, Run 1



Tritium Plume of Layer 4, Day 148, Run 1

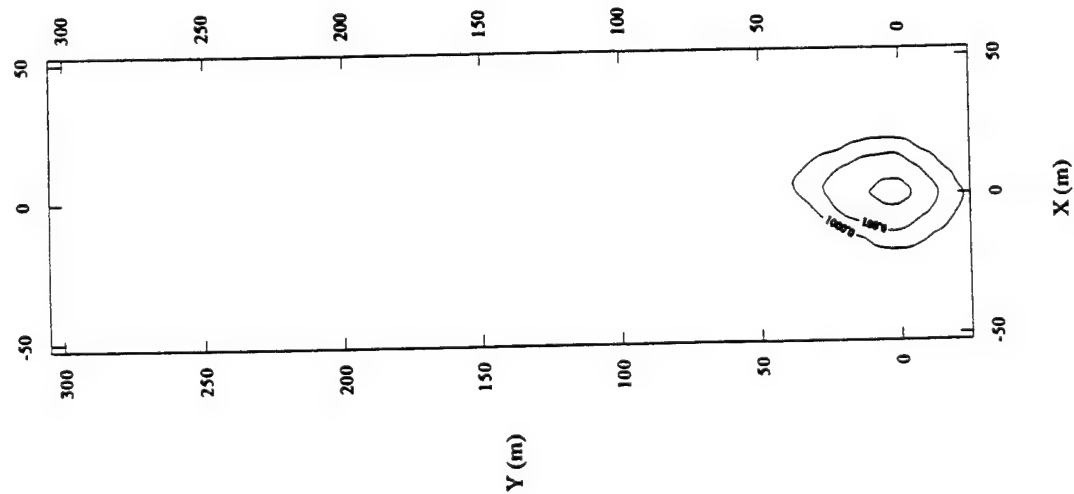


Figure 27. Normalized Tritium Concentration, M2-5-5, Run 1, Layer 4. Left: Day 148; Right: Day 344.

Runs 2 and 3 used the MOC advection solver, but did not produce desirable results. Many concentration values were less than zero, indicating large numerical oscillations. The MOC solver produced high numerical dispersion in the far field at sharp concentration fronts. Plots after Simulation Day 148 show increasing instability as the plume migrates farther downstream. The MOC option also took much longer than the UD to simulate a given period. Only runs using the UD option generated concentration values that were always positive. The DT0 value, specified by the user, is the largest transport step the simulation can use. As the dispersivity decreased, so did the Courant number and the maximum transport step to ensure stability.

The last column of Table 20 lists the porosity ( $\theta$ ) used in the simulation. As porosity decreases, seepage velocity increases. The porosity, while remaining within the range of the measurements, was decreased in the last two simulations to try to push the plume beyond the 75 meter distance obtained with the original porosity. Though not shown here, the normalized tritium plume of Run 4, with a porosity of 0.29, did not migrate as far as the previous simulation due to the decreased dispersion. However, it did produce a skinnier plume, much more realistic than its predecessor.

All above simulations used the flow model of M2-5-5. The M2-8 flow simulations, which included the latest conductivity data, were conducted after the above transport simulations.

The simulation of the tritium plume was also attempted using the M2-9-1 flow model, based on the nearest grid point hydraulic conductivity field. The simulation lasted approximately 4 days on a 90 MHz Pentium and used a longitudinal dispersivity of 1.0 meters. The upstream finite-differencing method was used to solve the advection term, and the Courant number was set to 0.01. Figure 28 shows the normalized tritium plume for Day 344. The plume only reached approximately 25 meters downgradient from the source. Obviously, the contaminant was stuck in a very low conductivity block and did not reach areas of higher conductivity.

Normalized Tritium Plume of Layer 4, Day 344, Run M2-9-1

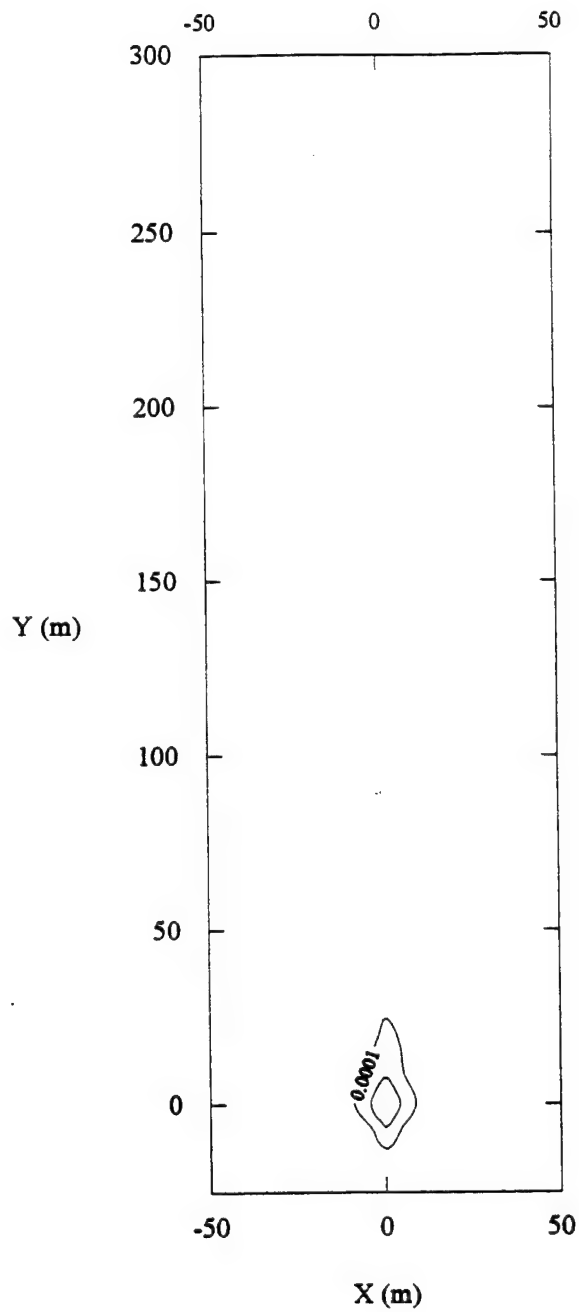


Figure 28. Normalized Tritium Concentration, M2-9-1, Layer 4, Day 344.

## SECTION VII

### EFFECTS OF HORIZONTAL ANISOTROPY

As described in the previous section, several problems hampered attempts to simulate the MADE-2 tritium plume. First, MT3D Version 1.80 ran excessively slowly, up to 3 weeks in some simulations. This was personally frustrating as well as computationally expensive. Second, the MT3D particle tracking methods produced excessive numerical dispersion. Even with low to zero hydrodynamic dispersion, the concentration of cells located far downstream often increased above the injected concentration with the MOC method. Last, the simulations failed to accurately match the observed plume for runs that did complete the 468-day experiment. The simulated plume did not spread far enough in the longitudinal direction. The dipping of the calculated heads to the northwest in the far field also seemed to contradict the observed plume behavior, which migrated to the northeastern corner of the domain. All these issues had to be dealt with if a successful simulation was to be completed.

#### A. MT3D CODING MODIFICATIONS

The excessive run time of the transport code MT3D seemed related to the rewetting capability of the MODFLOW flow code. Before the Courant number was pushed to a very low number, decreasing the time stepping factor, MT3D usually stopped around Day 226. However, unrealistic mass accretion started around Day 162 when an influx of recharge started to raise the water table and rewet dry cells in the upper layers. The subdivision of original Stress Period 7 into shorter stress periods in order to smooth the abrupt increase in head, failed to enable the code to run any longer.

Koch (1994) reported finding a dimension error, which essentially acted as a virus, in the advection package of MT3D. But after modifying MT3D, Version 1.1, his simulations still only ran to about 140 days, crashing as a result of overflow errors. Further investigation by Koch (1994) identified an additional problem: the artificially small time step criterion for the sink/source terms at the water table (Equations 4.29 through 4.32 of Zheng, 1990). The MODFLOW flow



model was set up in such a way that prior to Day 130, a negative recharge (indicating evaporation) was used. After this time, an abrupt addition of positive recharge lead to the rise of the water table, rewetting previously dry cells. This is when the problem of small time steps occurred. Koch (1994) described the difficulty, and fixed the problem for the particle tracking MOC, MMOC, and HMOC options. Koch's modified MT3D, referred to as Version 1.1, was essential in the following simulations. Even though Koch's corrections allowed MT3D to run in a reasonable time frame, his tritium plumes only extended to approximately 75 meters after 224 Simulation Days, compared to the observed 225 meters (Koch, 1994).

Zheng (1995) produced results in which the tritium plume extended to about 120 meters downgradient. However, his simulations were for an "averaged" steady-state condition in which the time stepping-problem did not occur. Modeling only the tritium plume, he tested various dispersivity values as well as different conductivity variations. He concluded that the simulated plume is more sensitive to the way the hydraulic conductivity field is generated than to the dispersivity values used, and recommended using the nearest grid point method instead of kriging the conductivities in order to reduce smoothing.

## B. HORIZONTAL ANISOTROPY

All previous modeling attempts had failed to accurately match the observed plume. The simulated plume never extended farther than 120 meters downgradient, whereas the observed plume extended to about 225 meters. Recalling the results of pump tests AT-1 and AT-2, horizontal anisotropy was applied to the conductivity field to increase longitudinal advection.

### 1. Flow Modeling with Horizontal Anisotropy

MODFLOW allows the user to specify horizontal anisotropy in the Block-Centered Flow package as long as the principal axes of hydraulic conductivity are aligned with the coordinate axes and the anisotropy is constant in each layer. The horizontal anisotropy factor, TRPY, is the ratio of column transmissivity (or hydraulic conductivity) to row transmissivity. One value of

TRPY may be given for each layer. A value of 1.0 produces horizontally isotropic conditions. A value greater than 1.0 increases the column transmissivities while leaving the row transmissivities unchanged.

The horizontally anisotropic simulations were based on the conductivity field of the M2-8 simulations which incorporated the new conductivity readings from wells K72 - K81. Several values of TRPY were tested in order to increase longitudinal velocities and plume advection. Table 21 lists the results of the uniformly horizontally anisotropic flow simulations.

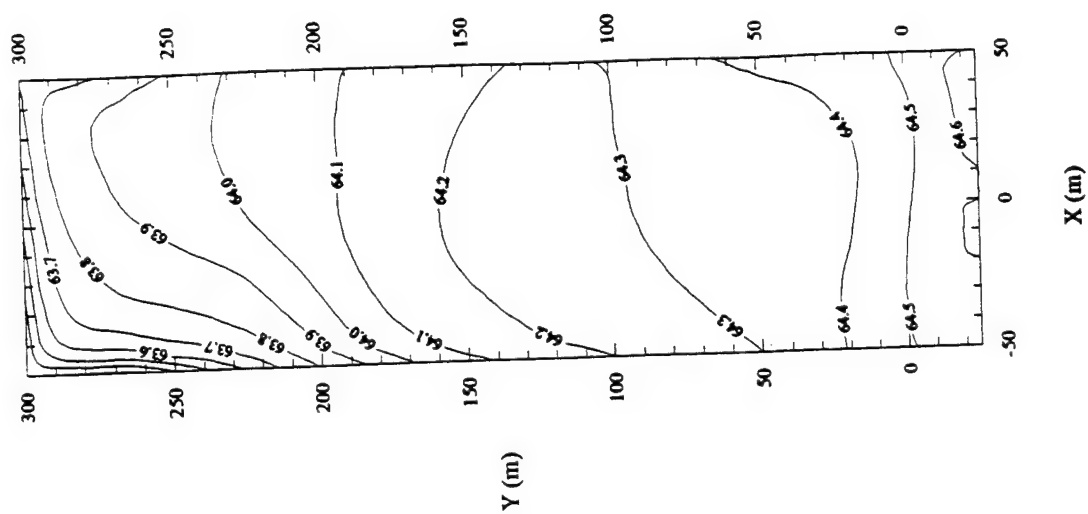
TABLE 21. UNIFORMLY HORIZONTALLY ANISOTROPIC FLOW SIMULATIONS.

| Simulation      | M2-8-2 | M2-8-3 | M2-8-4 | M2-8-5 | M2-8-6 |
|-----------------|--------|--------|--------|--------|--------|
| TRPY            | 1.0    | 2.0    | 10.0   | 50.0   | 100.0  |
| RMS of P53A (m) | 0.1985 | 0.1991 | 0.2036 | 0.2082 | 0.2112 |
| RMS of P54A (m) | 0.1487 | 0.1427 | 0.1377 | 0.1457 | 0.1518 |
| RMS of P54B (m) | 0.1760 | 0.1752 | 0.1841 | 0.2096 | 0.2016 |
| RMS of P55A (m) | 0.2030 | 0.1993 | 0.1998 | 0.2091 | 0.2160 |
| RMS of P55B (m) | 0.3815 | 0.3685 | 0.3514 | 0.3567 | 0.3671 |
| RMS of P60A (m) | 0.1943 | 0.1906 | 0.1849 | 0.1846 | 0.1869 |
| RMS of P61A (m) | 0.1883 | 0.1883 | 0.1883 | 0.1883 | 0.1883 |
| RMS of P61B (m) | 0.1550 | 0.1550 | 0.1550 | 0.1550 | 0.1550 |
|                 |        |        |        |        |        |
| Average RMS (m) | 0.2056 | 0.2023 | 0.2000 | 0.2071 | 0.2097 |
| % Discrepancy   | 3.84   | 3.70   | 2.90   | 1.40   | 0.84   |

Five uniformly anisotropic flow simulations were conducted, with anisotropy (TRPY) ranging from 1 to 100. The last two values of 50 and 100 were used only to observe the head-gradient changes noticed from the high Darcy velocities. To date, no study has been found to indicate that such extreme conditions exist anywhere in the world; therefore no physical meaning can be attached to the higher numbers (Rucker, 1995). Although the highest horizontal anisotropic value found in the literature was only 3.5, at a site in Dawsonville, Georgia (Maslia and Randolph, 1987), a model value of 10.0 gave the best averaged RMS error. The RMS error is the root mean square difference between the averaged observed head and the simulated head.

These flow simulations were conducted on a 33 MHz 486 PC, and took approximately 45 minutes to complete. Figures 29 through 33 show heads for simulations M2-8-2 through M2-8-6 for Layers 4 and 9 at Day 270, corresponding to the upper and lower kriged observed heads of March 8, 1991, which are shown in Figure 14. The head contours look reasonably accurate except for the later simulations of M2-8-5 and M2-8-6 which had unrealistically high anisotropy. The most noticeable problem is with the contour of 64.20 meters MSL. The conductivities for this region show high variability through a lateral cross-section.

Head of Layer 9, Day 270, Run M2-8-2



Head of Layer 4, Day 270, Run M2-8-2

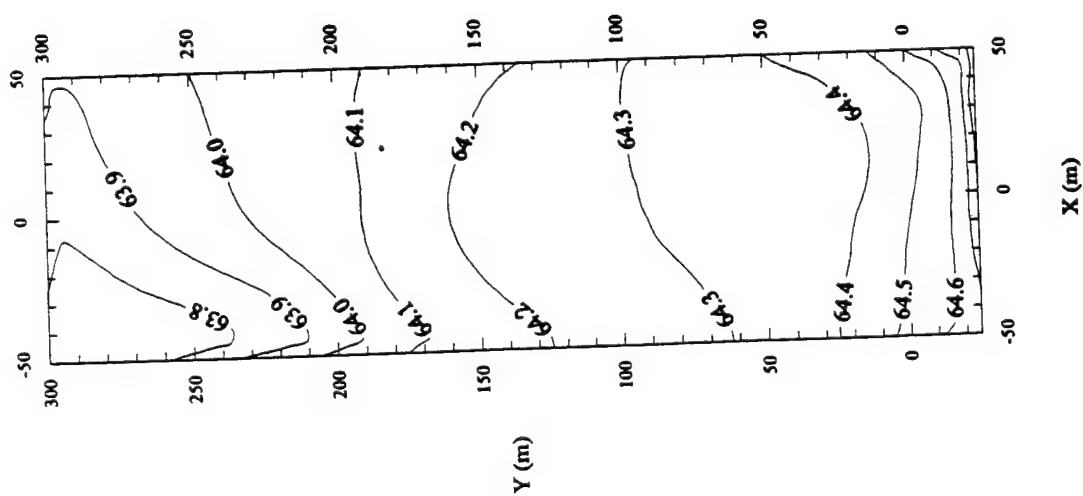
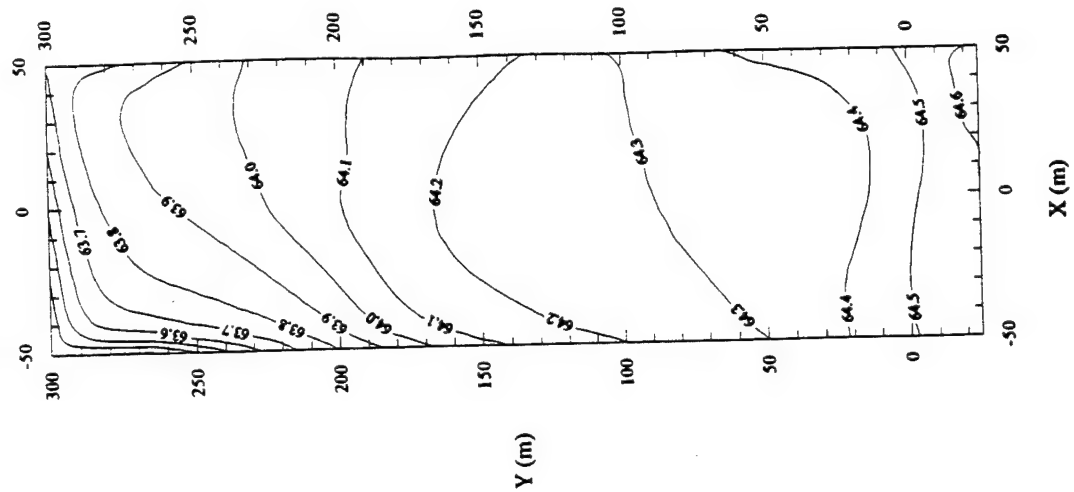


Figure 29. Heads of M2-8-2, Day 270. Left: Layer 4; Right: Layer 9.

Heads of Layer 9, Day 270, Run M2-8-3



Heads of Layer 4, Day 270, Run M2-8-3

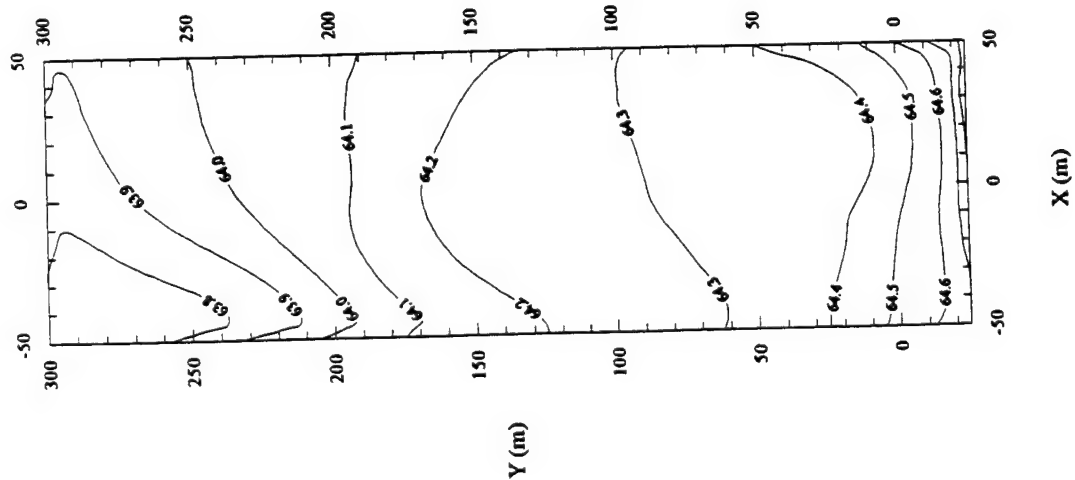
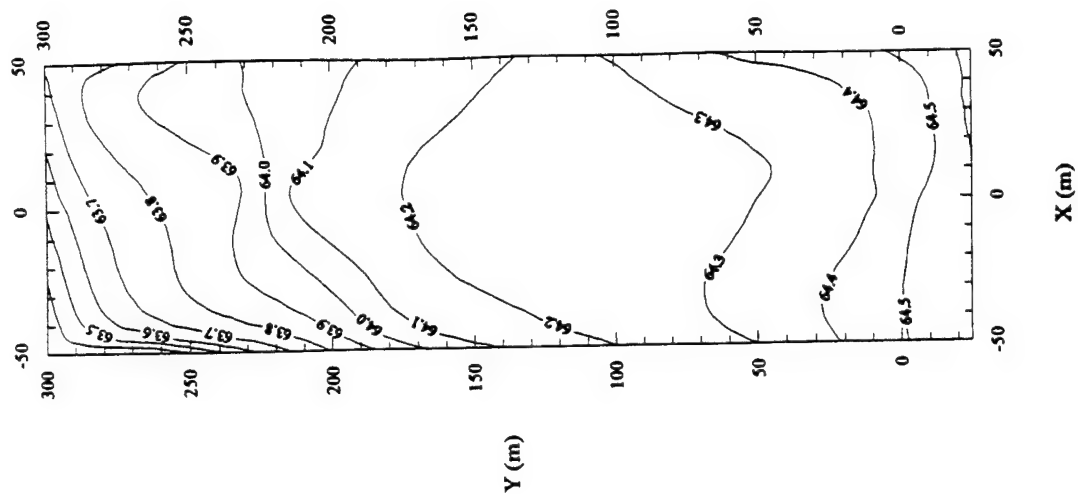


Figure 30. Heads of M2-8-3, Day 270. Left: Layer 4; Right: Layer 9.

Heads of Layer 9, Day 270, Run M2-8-4



Heads of Layer 4, Day 270, Run M2-8-4

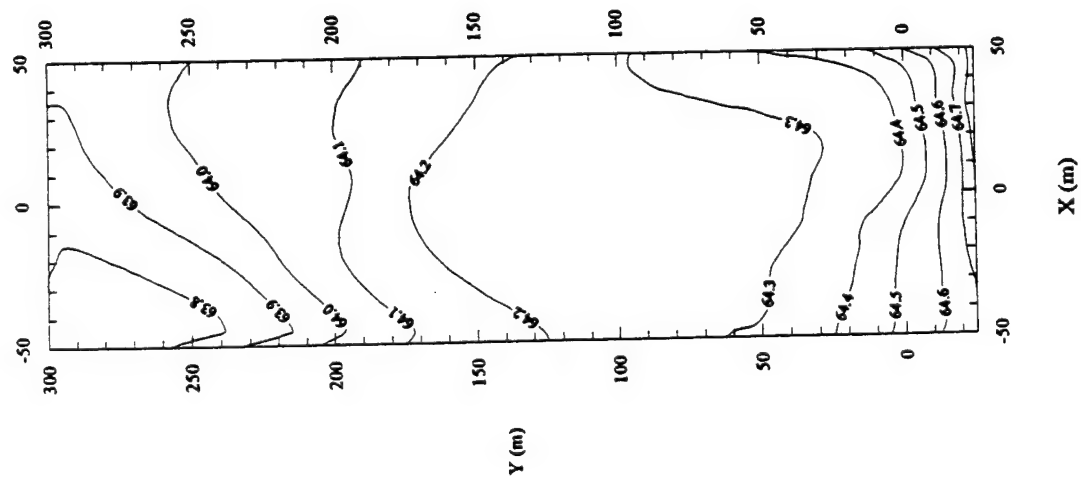
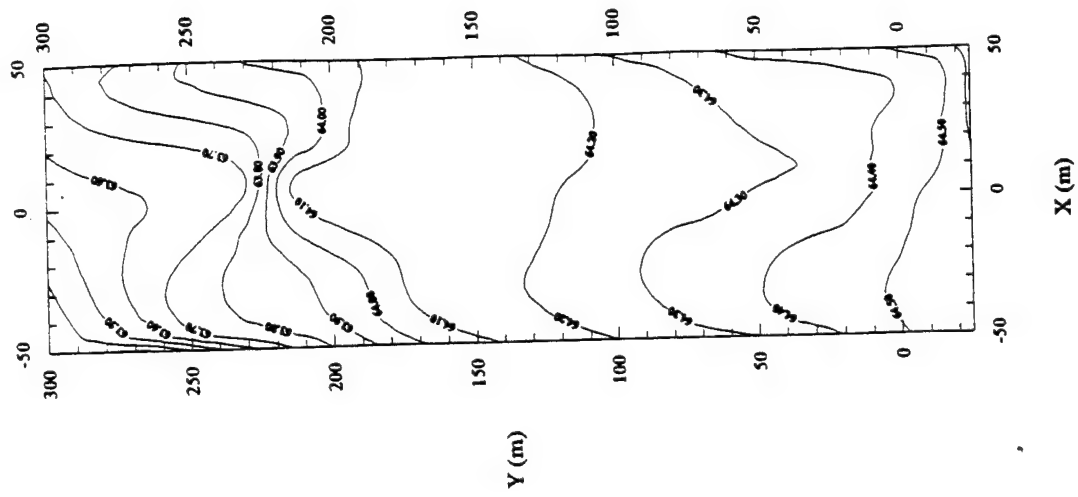


Figure 31. Heads of M2-8-4, Day 270. Left: Layer 4; Right: Layer 9.



Heads of Layer 9, Day 270, Run M2-8-6



Heads of Layer 4, Day 270, Run M2-8-6

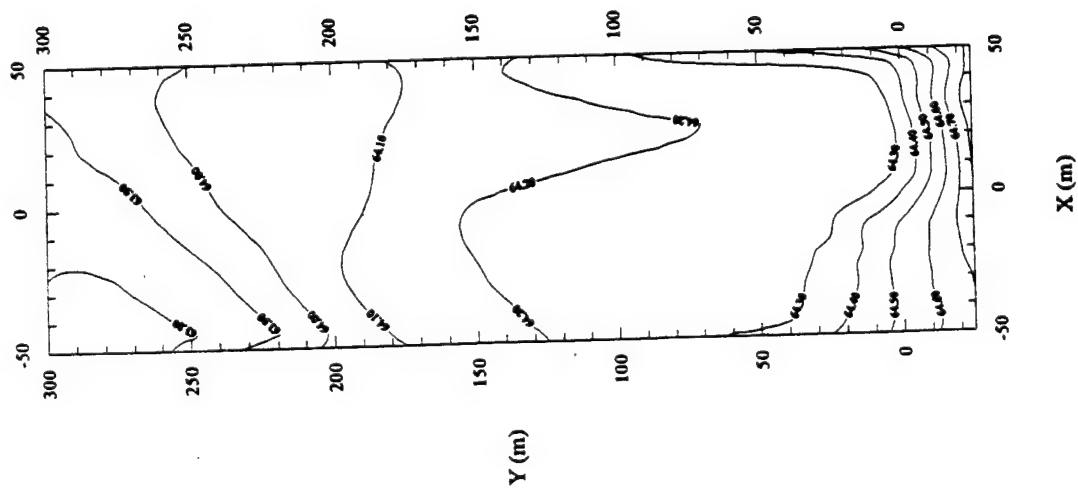


Figure 33. Heads of M2-8-6, Day 270. Left: Layer 4; Right: Layer 9.



Through careful examination of individual RMS error values for each simulation, it was noticed that every piezometer had a different "optimum" TRPY value. For example, piezometer P53A had a smaller difference in head when anisotropy was equal to 1, whereas piezometer P60A was optimized at a value of 10. This prompted an additional simulation with anisotropy varying, not only by layer, but also by column and row. Minor adjustments were made to the original MODFLOW source code to read the TRPY value from a two-dimensional array reader, with one array for each layer. This allows each cell to have a different TRPY value. The modified version of MODFLOW was saved as MF95. MF95 was demonstrated to be correct by reproducing previous simulations. The coding changes can be found in Appendix C.

The new simulation, M2-8-7, used a smoothly varying anisotropy factor (TRPY) array for each of the nine layers, produced by kriging optimum values of anisotropy at the eight specified piezometer locations. The kriged values ranged from 1.0 to 50.0, and the resulting TRPY isopleths can be seen in Figure 34. An upper kriged TRPY, taken from piezometers designated by "A" was assigned to Layers 1 through 4. The lower kriged TRPY, taken from piezometers designated as "B" was assigned to Layers 5 through 9. The flow simulation took approximately 45 minutes to complete on the 486 PC. Figure 35 shows the heads of Layers 4 and 9 at Simulation Day 270. The contours compare well with the observed heads in Figure 14.

M2-8-7 produced the best averaged RMS error to date, with a slightly lower value of 0.1944 meters. However, the real advance was the increased velocity field. Program VELCOMP compared the Darcy velocity arrays of the isotropic simulation (M2-8-2) to that of the variably anisotropic simulation (M2-8-7) and computed a percent relative increase at all nodes. An average increase of 231% was calculated for the longitudinal velocities.

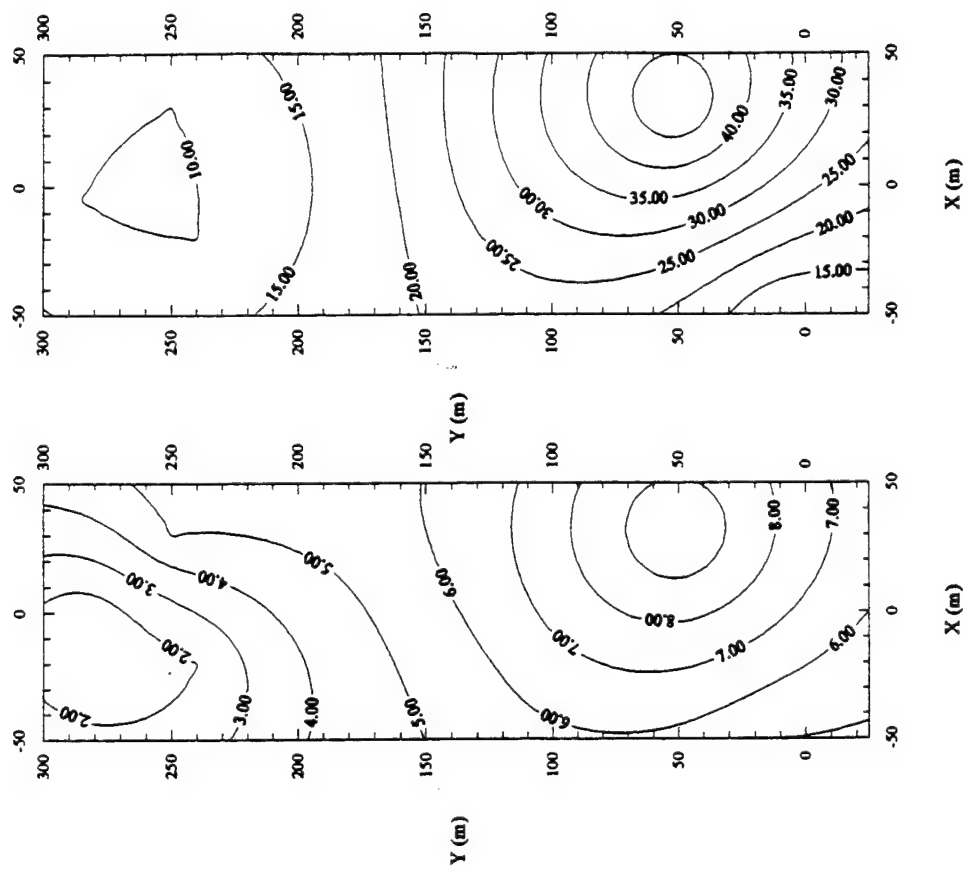
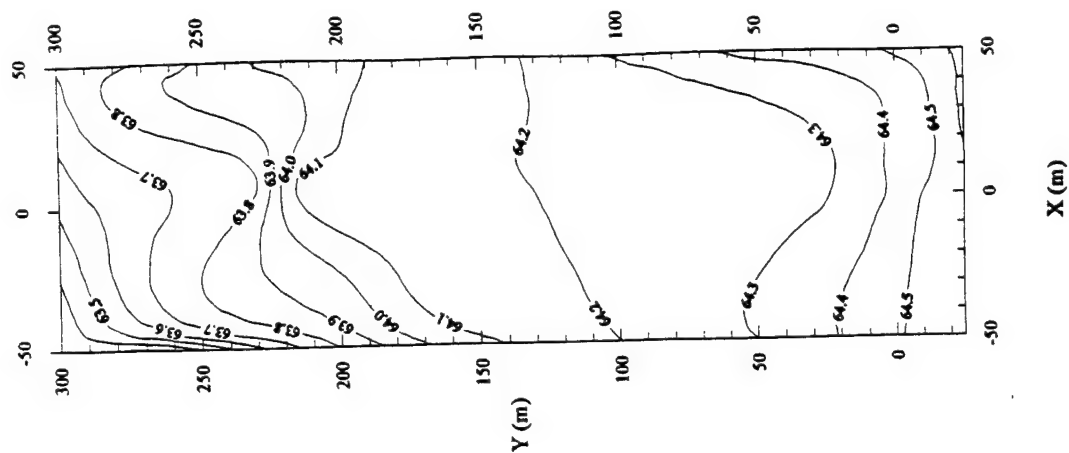


Figure 34. Kriged TRPY for M2-8-7. Left: Upper Levels; Right: Lower Levels.

Head of Layer 9, Day 270, Run M2-8-7



Head of Layer 4, Day 270, Run M2-8-7

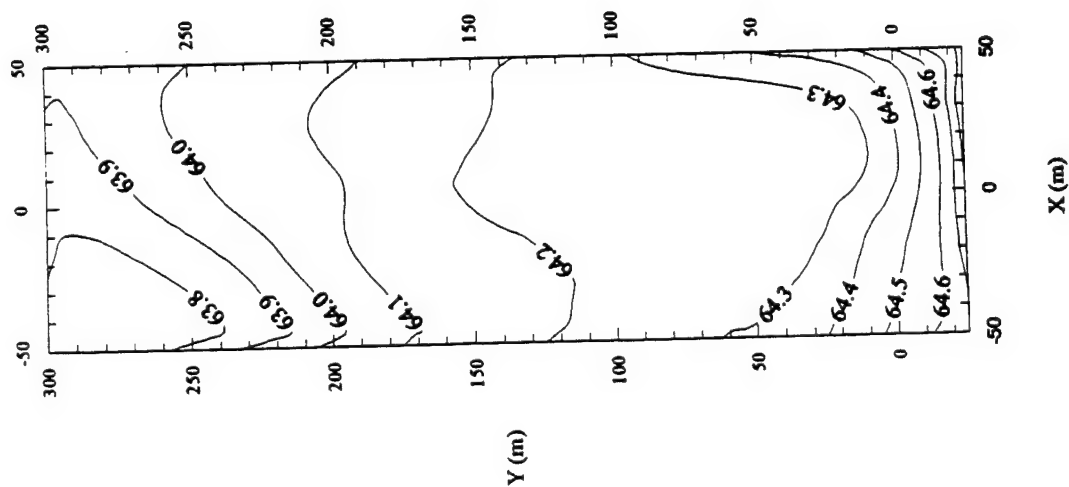


Figure 35. Heads of M2-8-7, Day 270. Left: Layer 4; Right: Layer 9.

## 2. Transport Modeling of M2-8-7

MT3D Version 1.1, modified by Koch, was used to solve the transport equation for the variably horizontally anisotropic flow field of M2-8-7. An additional change suggested by Koch to speed the simulations was to skip the transport calculations during the first 10 days of the flow simulation because there were no contaminants present before Day 14. The first simulations considered the tritium plume. Virtually all parameters remained the same as before, including porosity, diffusivity, and decay coefficient. The only major change was the increase of the initial tritium concentration from  $0.0555 \text{ Ci/m}^3$  to  $1000 \text{ Ci/m}^3$  to avoid underflow errors. As long as all terms used in calculating the change in concentrations are linear, the above increase is acceptable, because the calculated concentrations are divided by the initial concentration to obtain a normalized tritium concentration. A longitudinal dispersivity of 0.5 meters and transverse and vertical dispersivities of 0.01 meters were used on the advice of Koch. The MOC option was used to solve the advective portion of the transport equation because Koch (1994) reported that the other particle trackers gave rise to numerical dispersion and smaller time stepping at sharp concentration fronts, and the upstream finite-difference option had not been corrected.

The first transport simulation in this series took approximately 7 hours to complete on a Sun Sparcstation 10. Figure 36 shows the contours for normalized tritium concentration at approximately 100-day intervals. The exact days were chosen to match the snapshots. The last day, Day 456, does not have a corresponding snapshot, but is shown to demonstrate the migration of tritium at the end of the experiment. It was obvious that the predicted tritium plume was still a poor fit to the observed data shown in Figure 25 because the center of mass migrated away from the injection zone. In reality the contaminant remained primarily in the low conductivity zone near the injection site while a tail of low concentrations extended to the mid and far field regions.

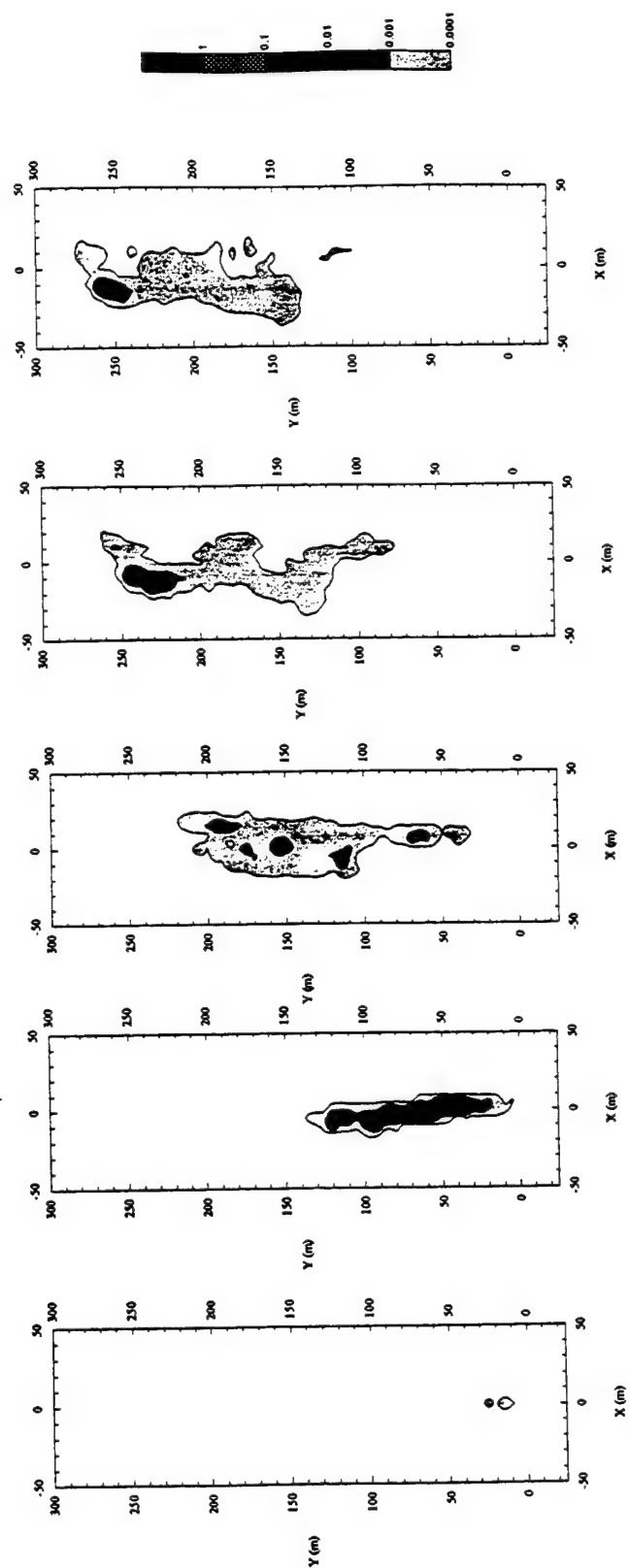


Figure 36. Normalized Tritium Concentration, M2-8-7, Layer 4, Days 44, 148, 240, 344, and 456.

### C. ANISOTROPY VARYING BY CONDUCTIVITY

Based on geologic considerations, Young (1994) had proposed a geological history of the area around the MADE-2 site, which posited braided streams giving rise to a metastable meandering river channel. Boggs et al. (1992) had concluded that the MADE-2 site contained lenses of extreme heterogeneity. The deposit characteristics of a meandering river as described by Freeze and Cherry (1979) almost identically match the characteristics of the MADE-2 site, including coarse sand and gravel along point bars and large amounts of clay and silt from channel fill deposits. From these considerations Young (1994) concluded that a channel may have existed through the site and that sediments were deposited in such a way that permeability is higher in the longitudinal direction of the channel than in the lateral direction. Figure 5 shows an aerial photograph of the site with the channel axis cutting through the site at about 30° east of north.

With insight gained from the previous set of calculations, a new MODFLOW simulation, M2-8-8, was performed. Rehfeldt et al. (1992) had suggested that the presence of the hypothesized channel in the mid field may be in the regions of  $K_h > 10^{-2}$  cm/s (~8.6 m/d). Therefore, to emulate the effects of the channel, a high anisotropy value was assigned to the higher conductivity cells, and low anisotropy factor to lower conductivity cells for run M2-8-8. Program TRPY tested the conductivity arrays for each layer and wrote the new anisotropy arrays to the Block Centered Flow package input file. After several tests, it was concluded that cells whose horizontal conductivity was above 3.0 m/d ( $\sim 3.5 \times 10^{-3}$  cm/s), should have TRPY set to 15, and cells with lower conductivity should have TRPY equal to 1. Figure 37 shows two typical layers with the high anisotropy cells shaded in gray.

The flow model was rerun to obtain new head and Darcy velocity values for the transport simulation. The calculated averaged RMS head discrepancy for the simulation was 0.1958 meters, slightly higher than M2-8-7, yet still better than simulation M2-5-5 of Gray and Rucker (1994). The predicted head contours of Figure 38 are a reasonable facsimile to the observed ones in Figure 14.

Again, tritium was the first contaminant to be tested for solute migration. All other parameters described above were adopted for this simulation as well. The resultant plume contours of Figure 39 show very good agreement with the observed (Figure 25). The contaminant moves slowly in the near field, increasing speed as it enters the mid regions of the domain. The last days show a long tail trailing off to the northeast, just as observed.

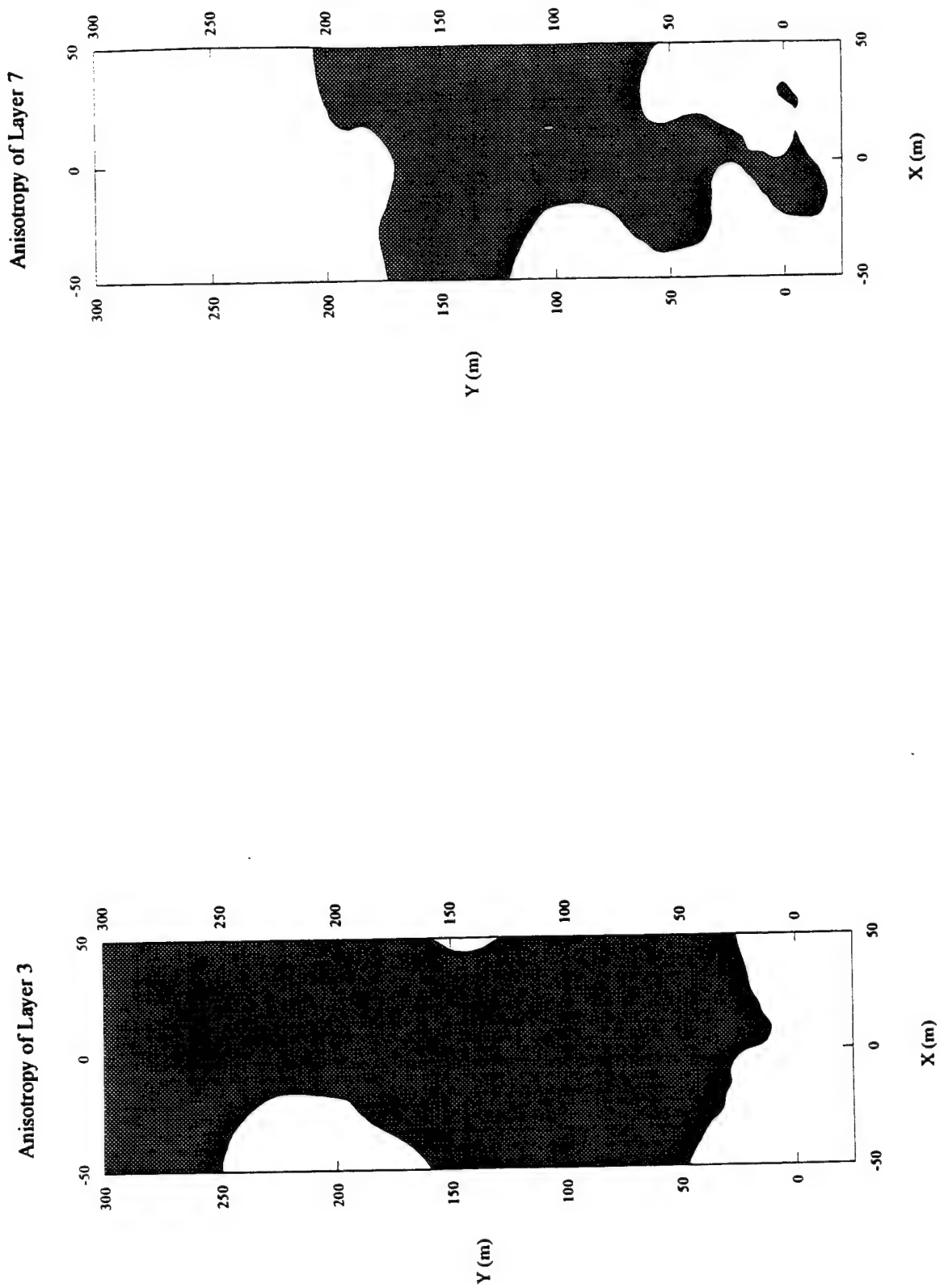
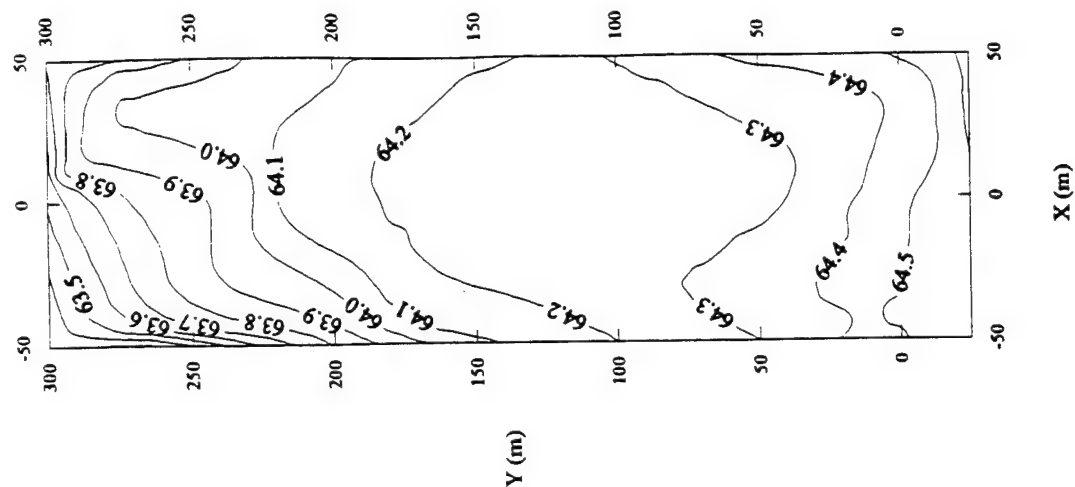


Figure 37. Regions of  $TRPY = 15$  Indicated By Shading. Left: Layer 3; Right: Layer 7.



Heads of Layer 9, Day 270, Run M2-8-8



Heads of Layer 4, Day 270, Run M2-8-8

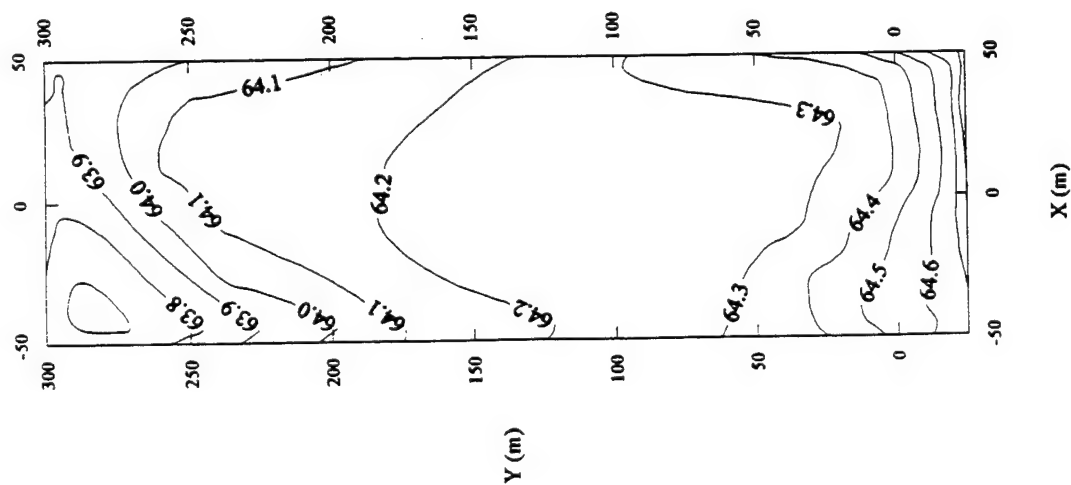


Figure 38. Heads of M2-8-8, Day 270. Left: Layer 4; Right: Layer 9.

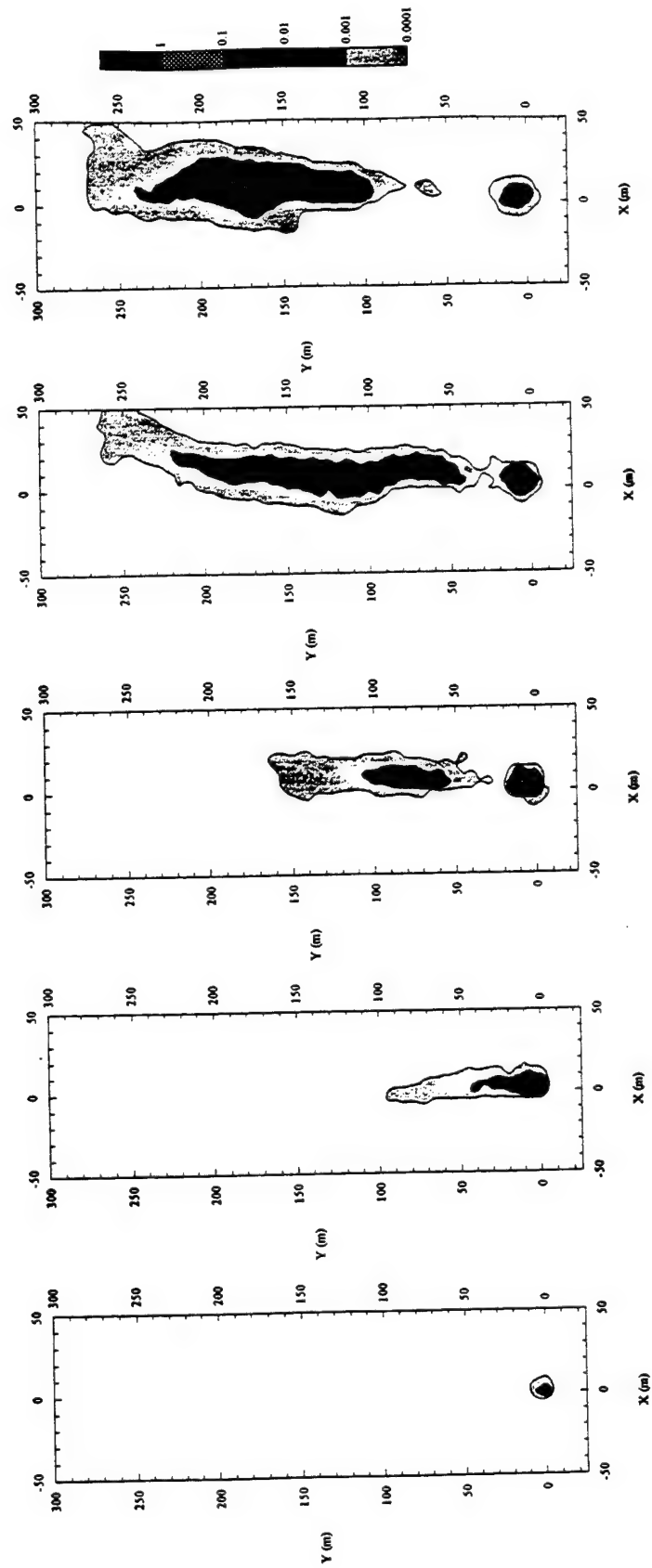


Figure 39. Normalized Tritium Concentration, M2-8-8, Layer 4, Days 44, 148, 240, 344, and 456.

The transport of the four organics were also tested with the new flow model. All parameters of the above simulation were used for these simulations with the exception of the sorption and biodegradation coefficients. Table 17 shows the values used to calculate the retardation factors and the initial concentrations for each of the four organic contaminants. The table does not include any information about  $^{14}\text{C}$ . This contaminant was not modeled, since much of the information needed for simulations was not found in any of the literature. The coefficient of molecular diffusion in a saturated porous medium was set to the value for tritium for all of the organics. This is incorrect but the resulting errors are probably small.

Each dissolved organic transport simulation took between 4 to 7 hours to complete on a Sun Sparcstation 10. Figures 40 through 44 show the normalized concentrations on a vertical profile through the longitudinal midsection of the domain for Days 44, 148, 240, 344, and 456. A YZ profile through column 11 was used to present the contours to compare to the snapshot data of Boggs et al. (1993) presented in Figures 45 through 49.

Again, there is good agreement between observed and simulated plumes. The migration of each simulated plume seems to follow the path of its corresponding observed plume. Early in the simulation, on Day 44, the contaminants stay in the near field; however the simulated plumes are more concentrated in the lower portion of the domain. Since the injection took place in Layer 7 (57.5 meters MSL) and the water table decreased for the first 130 days of simulation, it seems logical that the simulated contaminant does not rise to around 60 meters MSL, as compared to the observed plume. The positive net recharge in the seventh stress period (Day 148), which raised the water table, also pulled the bulk of the contaminant to the upper portion of the domain. This affected the tritium plume the most, allowing a better fit to the observed tritium plume of Figure 46. The positive recharge throughout much of the remainder of the simulation kept the majority of each plume around 60 meters MSL.

The simulated longitudinal spread of each contaminant did not match the observations perfectly, but did reproduce the gross patterns of transport. The simulated tritium plume, for example, migrated to about 105 meters downgradient from the injection point on Day 148 (Figure

41). Its observed counterpart only migrated to about 65 meters (Figure 46). The next snapshot shows the observed tritium plume (Figure 47) to spread out to about 200 meters, with the simulated plume moving only out to 150 meters. This discrepancy probably results from the hydraulic conductivity field used in simulating the flow and transport of the chemicals. Although kriging allows the modeler to acquire the best estimate of the variability, without having a completely exhaustive data set an exact match is impossible.

The dispersivity values in the transport calculations are the only other major source of uncertainty in the modeling. Dispersivity accounts for spreading due to heterogeneity which causes variations in the flow velocities and paths. However, the dispersivities assumed for these simulations seemed adequate. Just as in Zheng (1994), it is concluded that the simulated plumes are more sensitive to the treatment of hydraulic conductivity than to the dispersivity values used.

Figures 50 through 54 present areal displays of the dissolved organic plumes for Layer 4 for Simulation Days 44, 148, 240, 344, and 456. These figures do not have corresponding observation plots, but they show how the contaminants are transported.

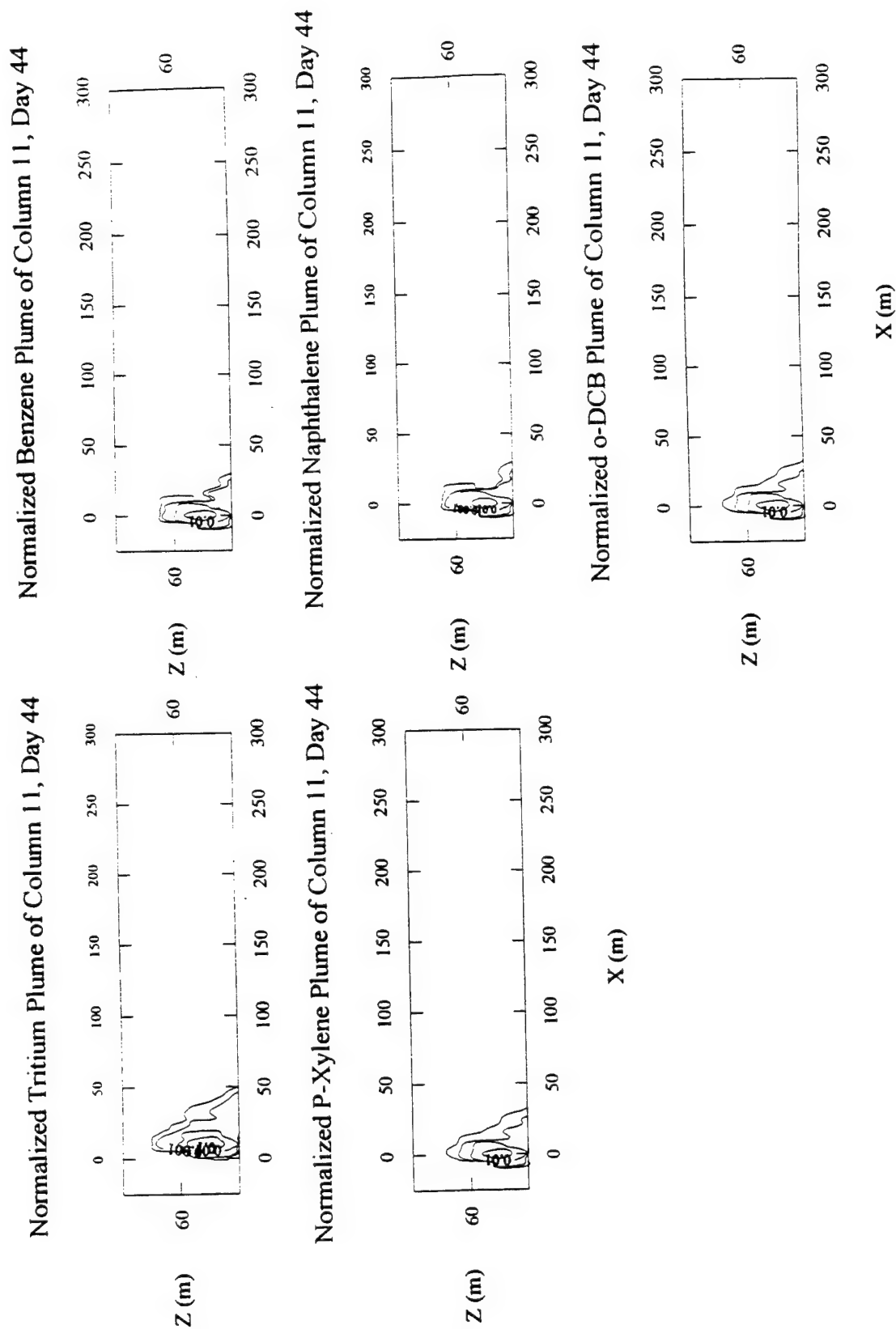


**Figure 40. M2-8-8 Normalized Concentration Profiles Along Column 11, Day 44.**  
Isopleths Presented at 0.1, 0.01, 0.001, and 0.0001.

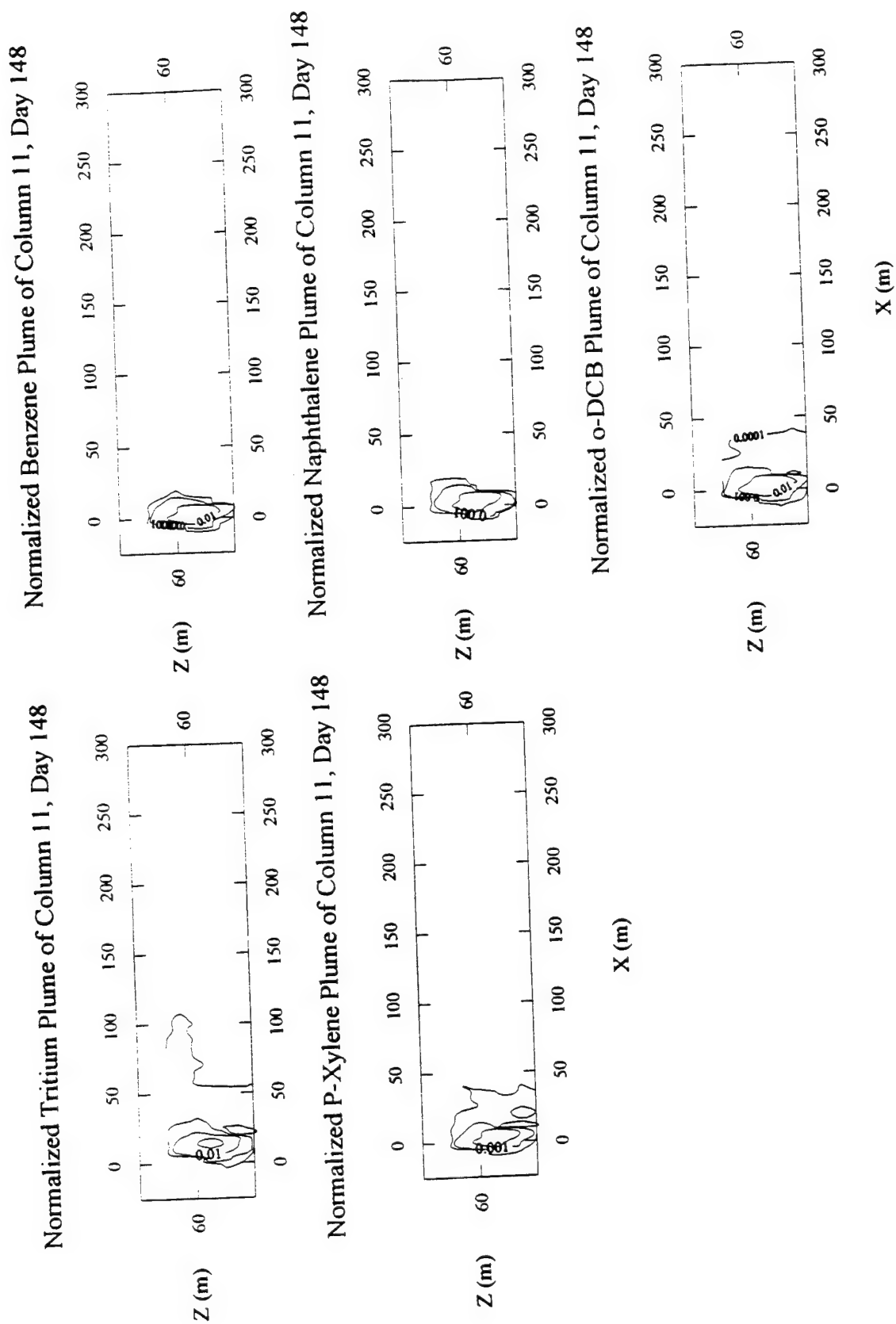
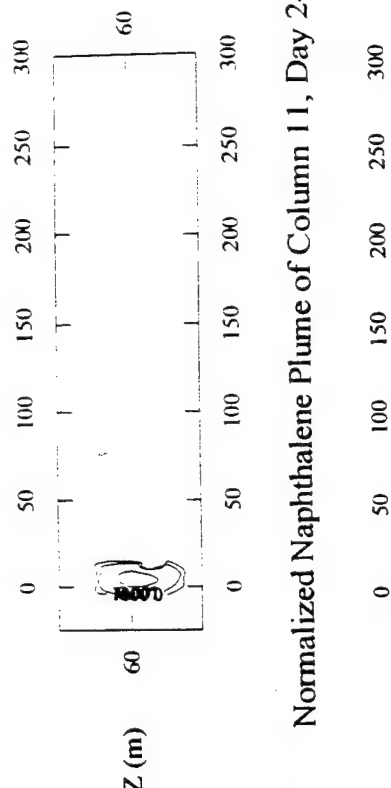
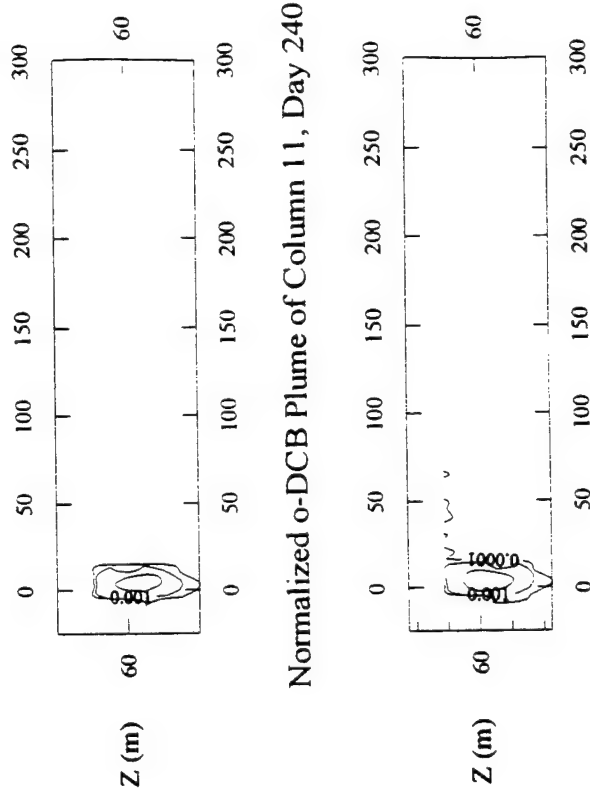


Figure 41. M2-8-8 Normalized Concentration Profiles Along Column 11, Day 148. Isopleths Presented at 0.1, 0.01, 0.001, and 0.0001.

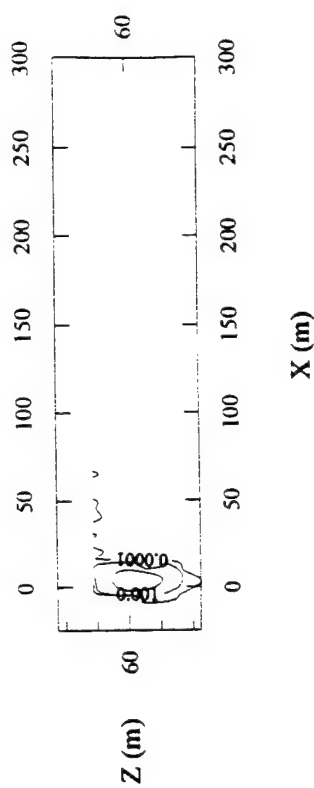
Normalized Benzene Plume of Column 11, Day 240



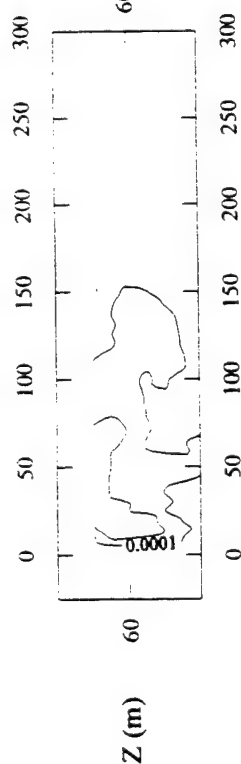
Normalized Naphthalene Plume of Column 11, Day 240



Normalized o-DCB Plume of Column 11, Day 240



Normalized Tritium Plume of Column 11, Day 240



Normalized P-Xylene Plume of Column 11, Day 240

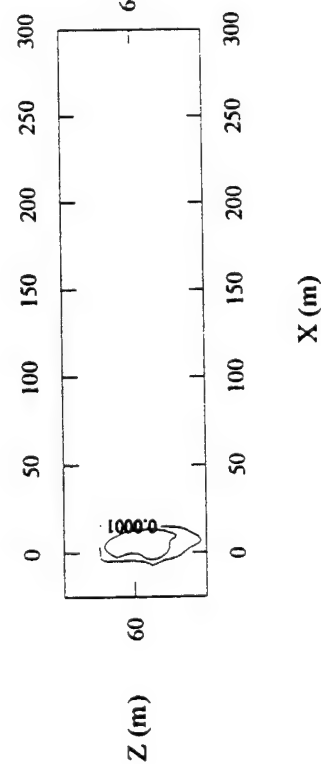


Figure 42. M2-8-8 Normalized Concentration Profiles Along Column 11, Day 240.  
Isopleths Presented at 0.1, 0.01, 0.001, and 0.0001.

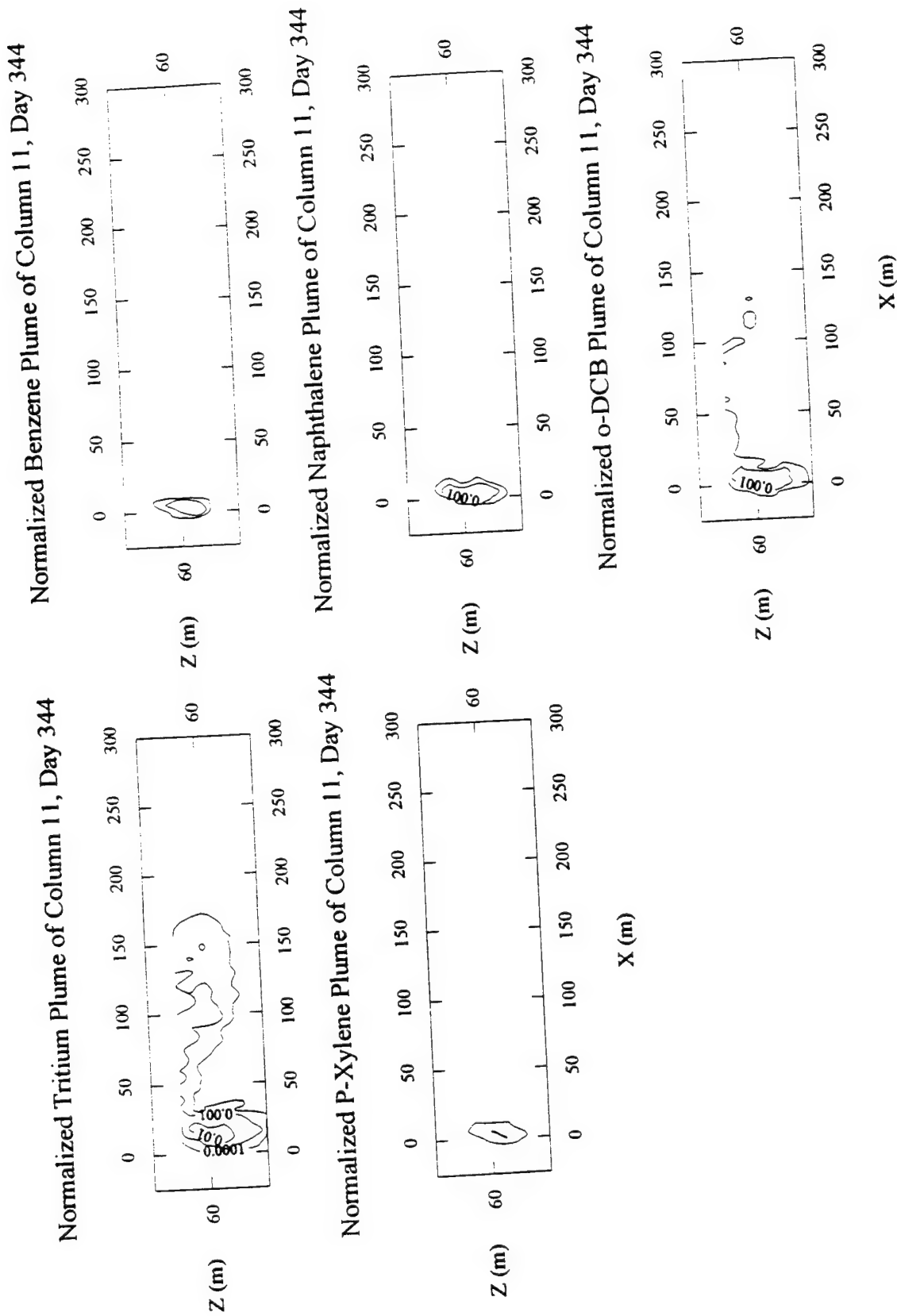


Figure 43. M2-8-8 Normalized Concentration Profiles Along Column 11, Day 344. Isopleths Presented at 0.1, 0.01, 0.001, and 0.0001.



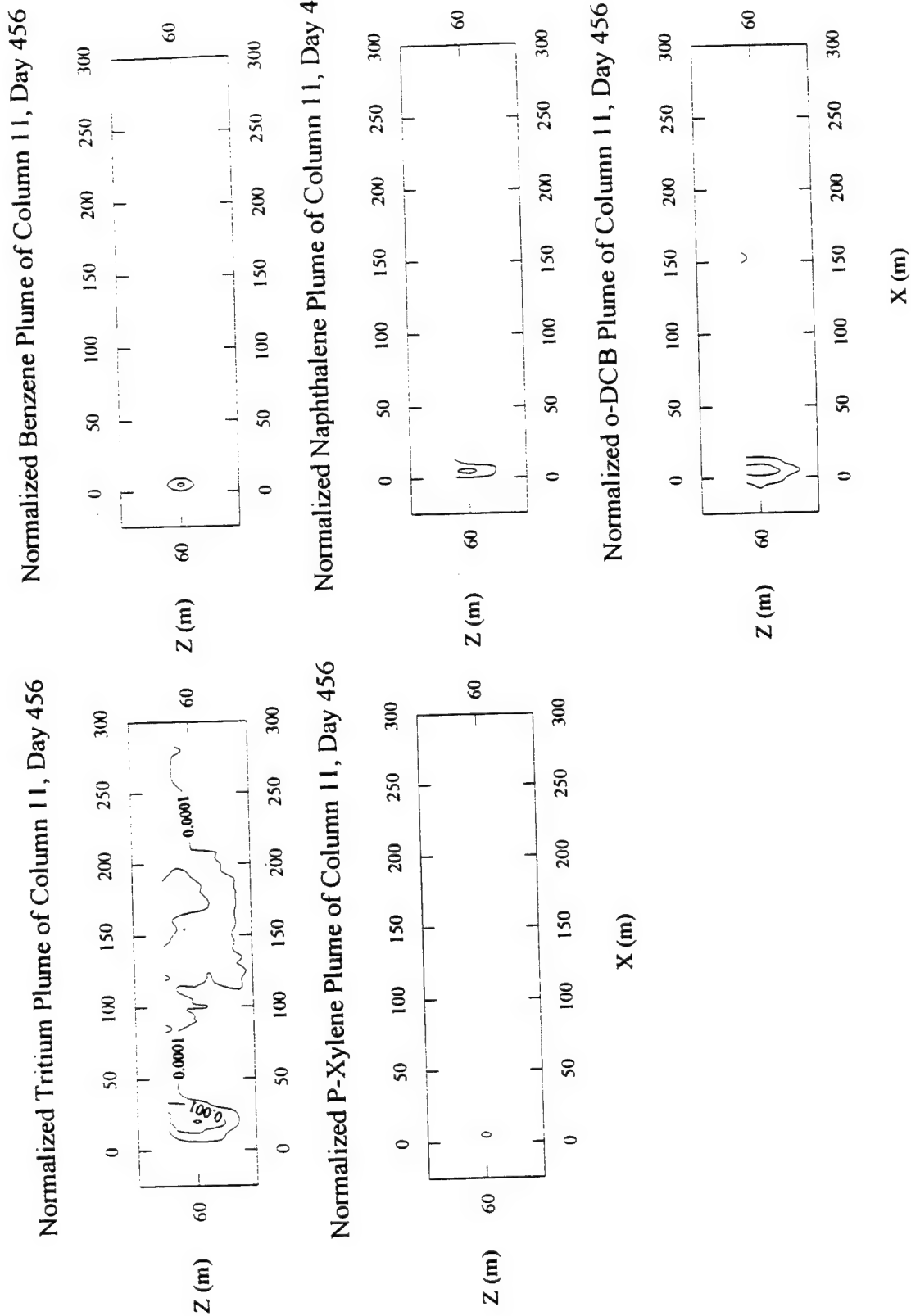


Figure 44. M2-8-8 Normalized Concentration Profiles Along Column 11, Day 456. Isopleths Presented at 0.1, 0.01, 0.001, and 0.0001.

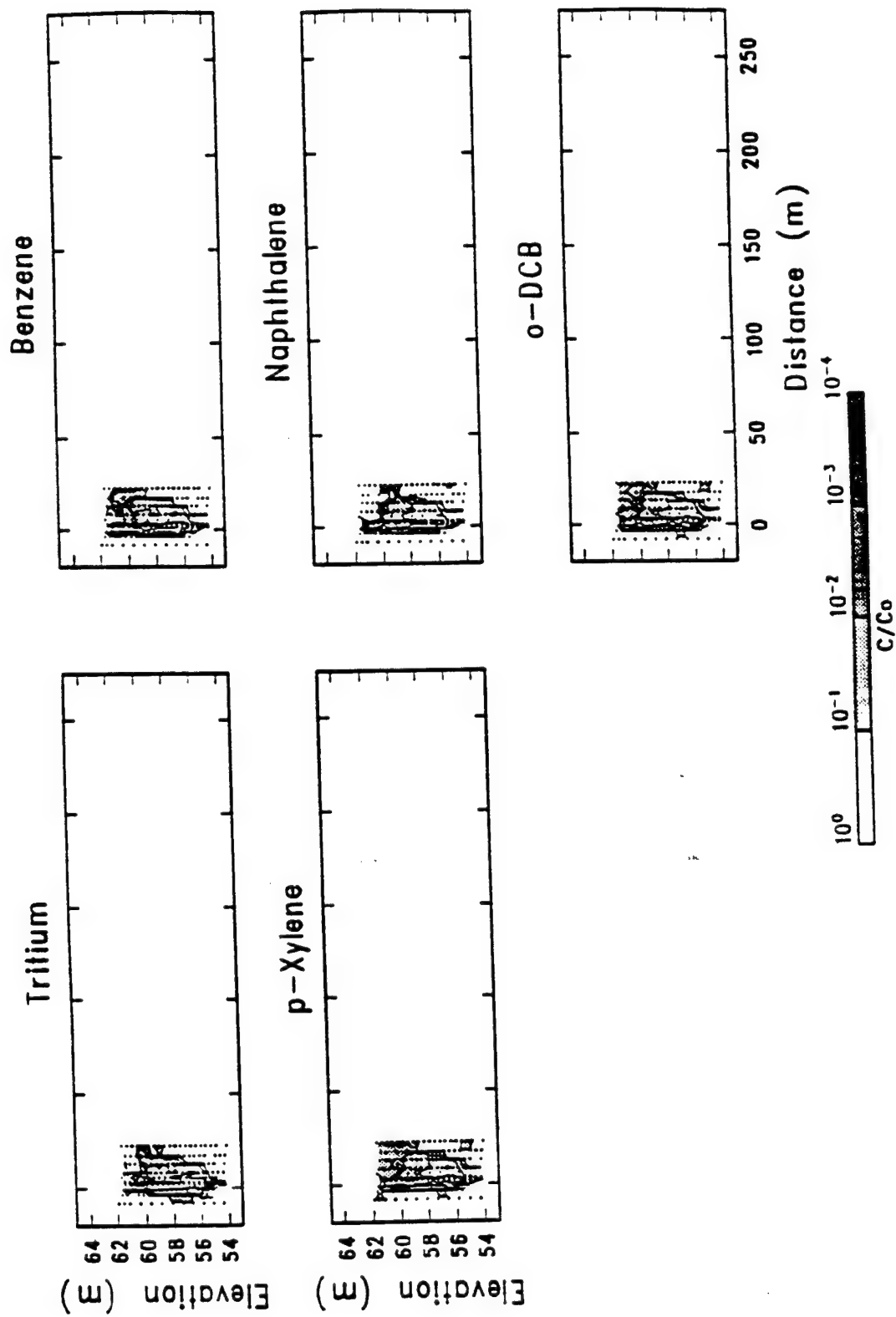


Figure 45. Observed Normalized Concentration Profiles, Day 44. Source: Boggs et al. (1993).

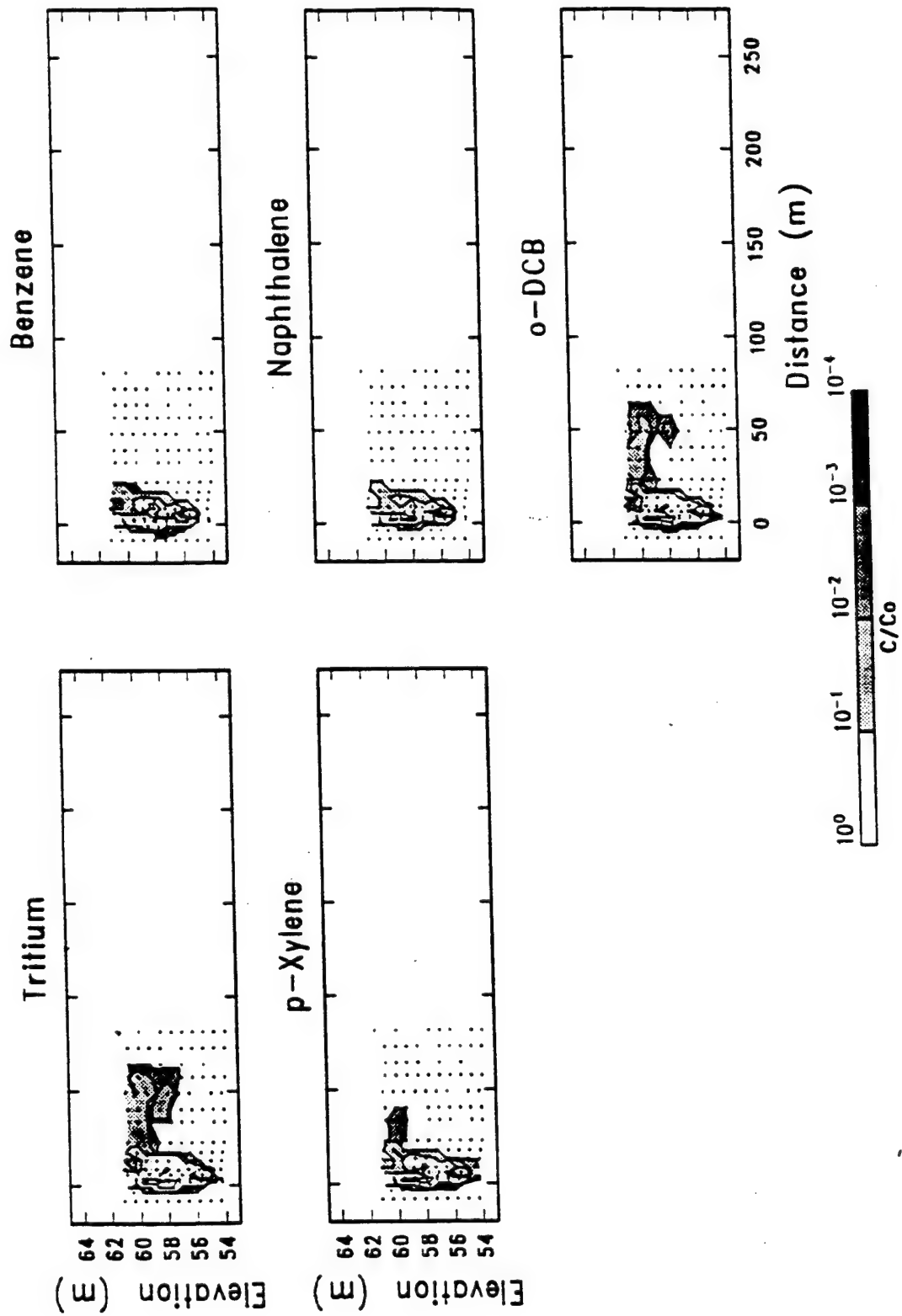


Figure 46. Observed Normalized Concentration Profiles, Day 148. Source: Boggs et al. (1993).

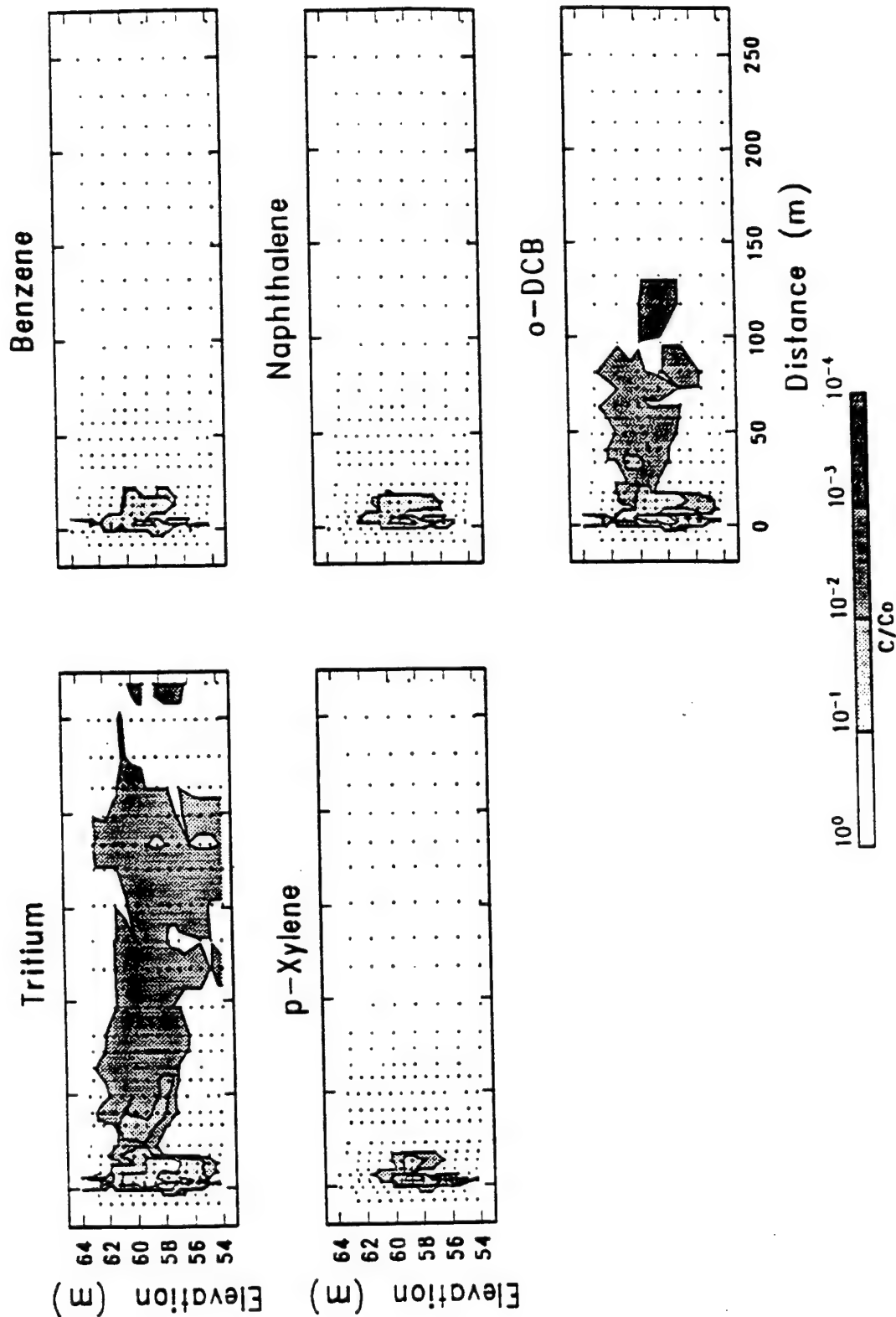


Figure 47. Observed Normalized Concentration Profiles, Day 240. Source: Boggs et al. (1993).

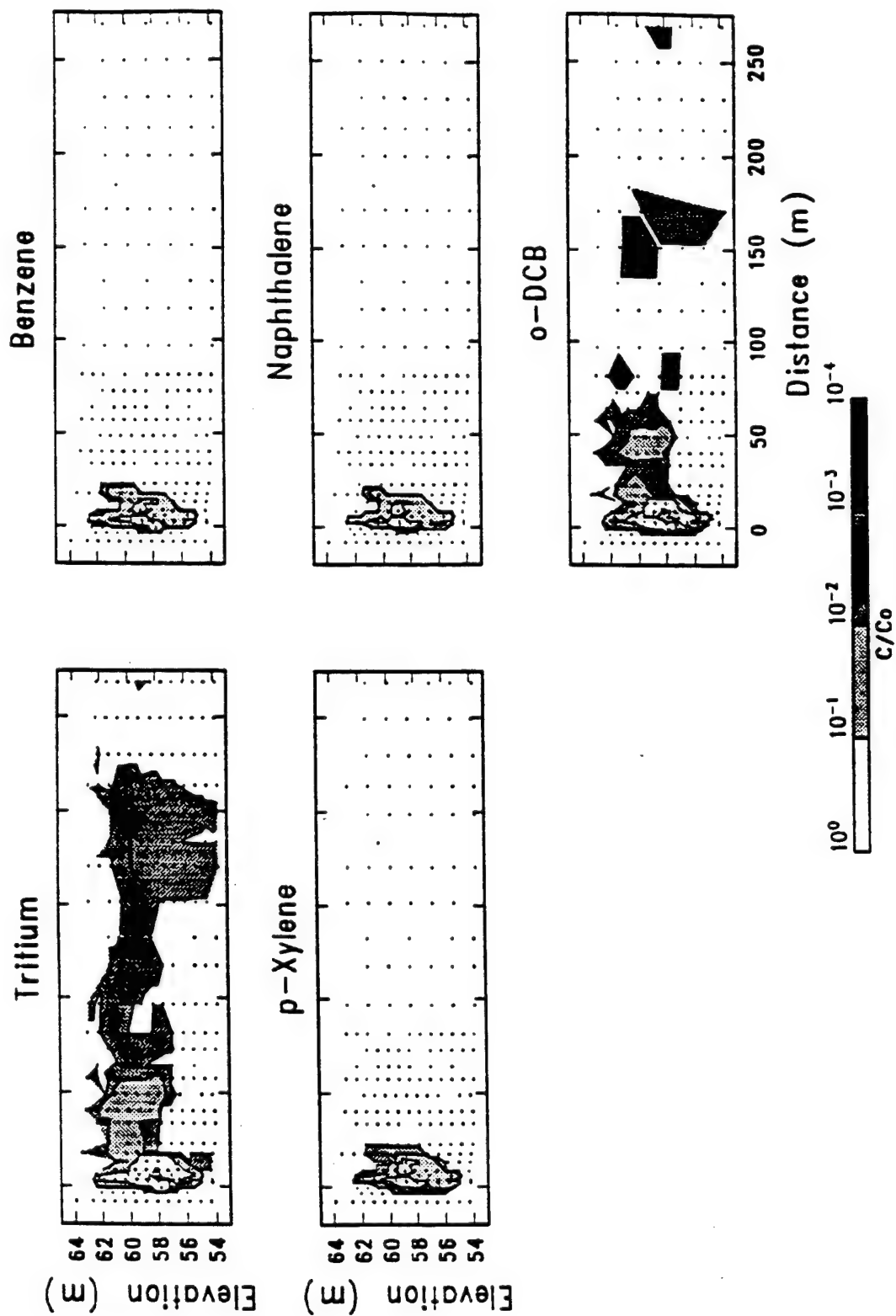


Figure 48. Observed Normalized Concentration Profiles, Day 344. Source: Boggs et al. (1993).

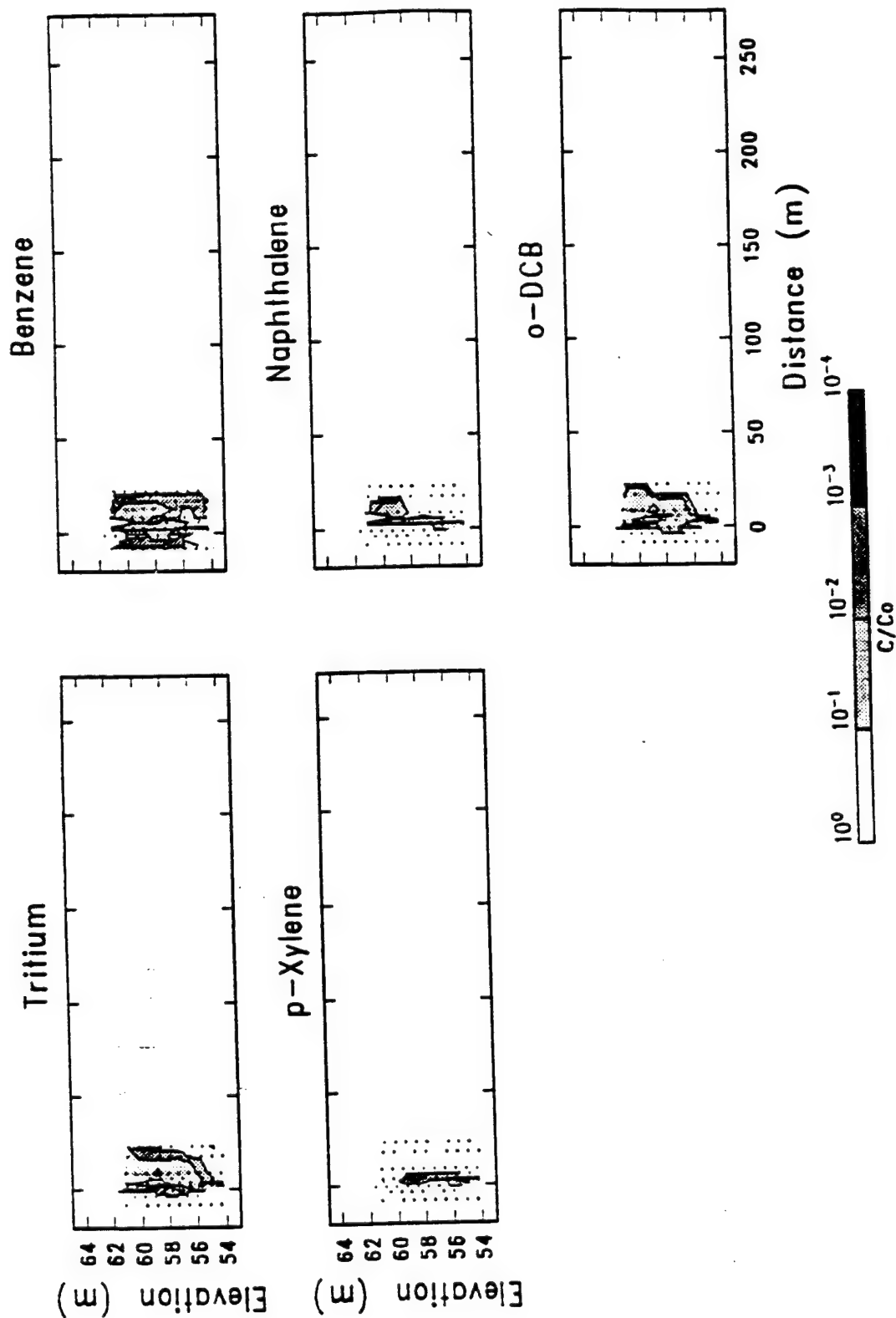


Figure 49. Observed Normalized Concentration Profiles, Day 456. Source: Boggs et al. (1993).

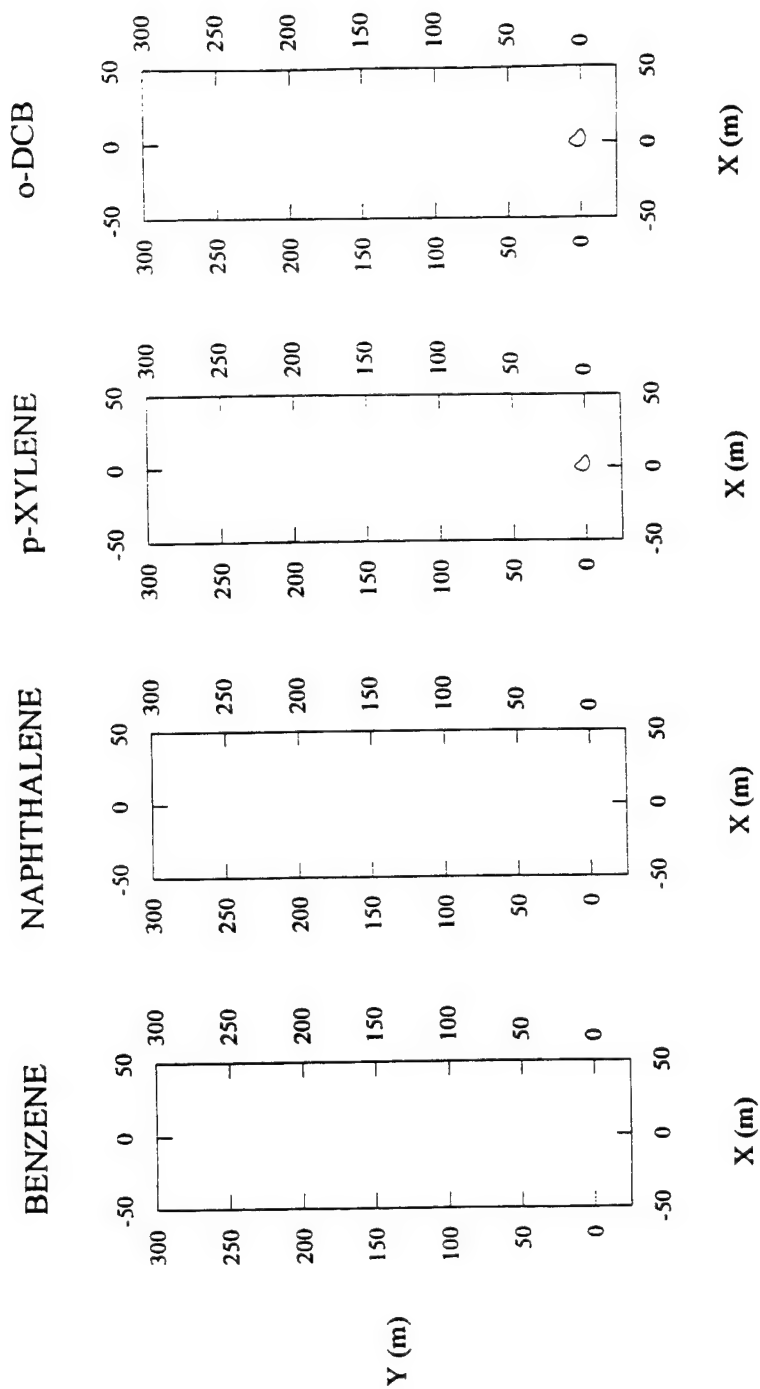


Figure 50. M2-8-8 Normalized Organic Concentrations in Layer 4, Day 44.  
Isopleths Presented at 0.0001.

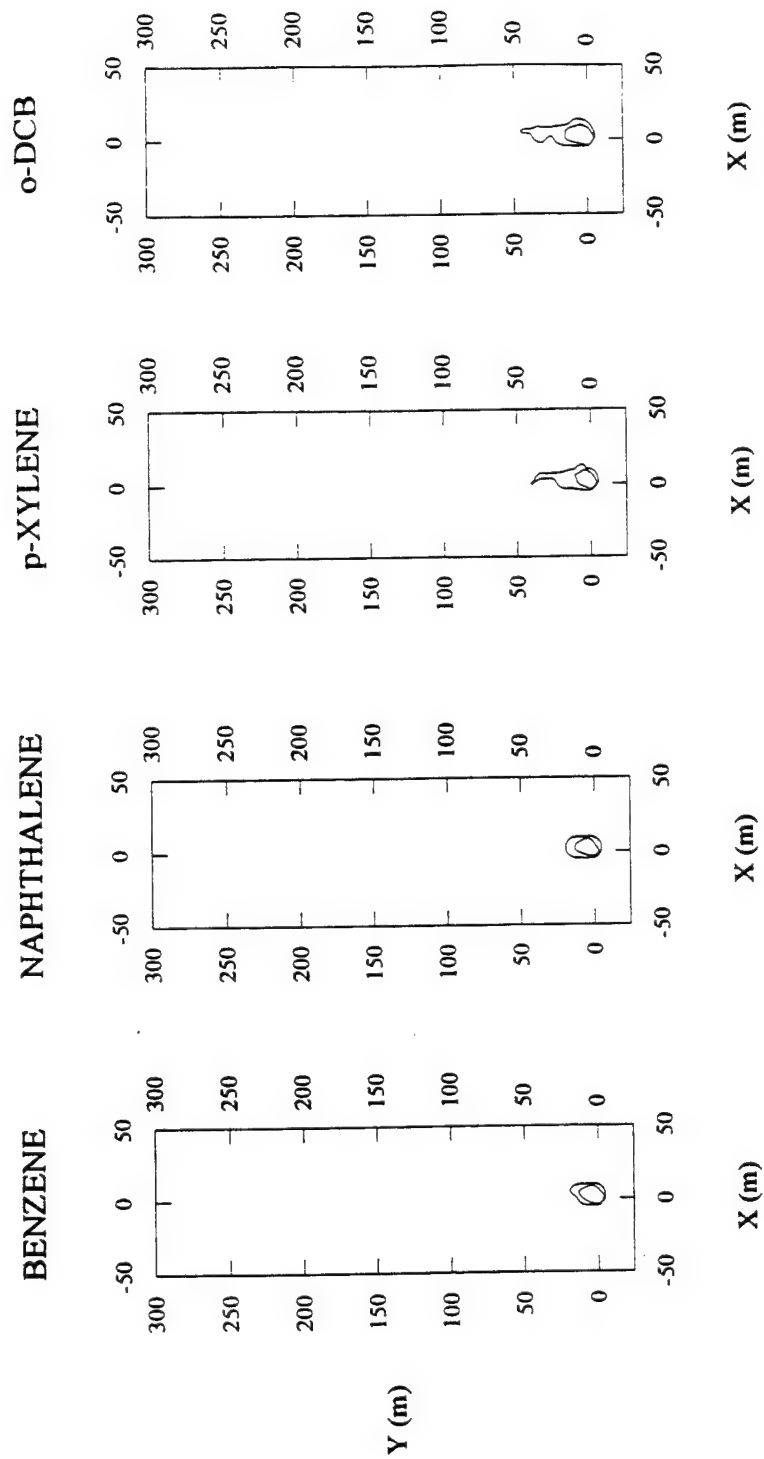


Figure 51. M2-8-8 Normalized Organic Concentrations in Layer 4, Day 148.  
Isopleths Presented at 0.001 and 0.0001.



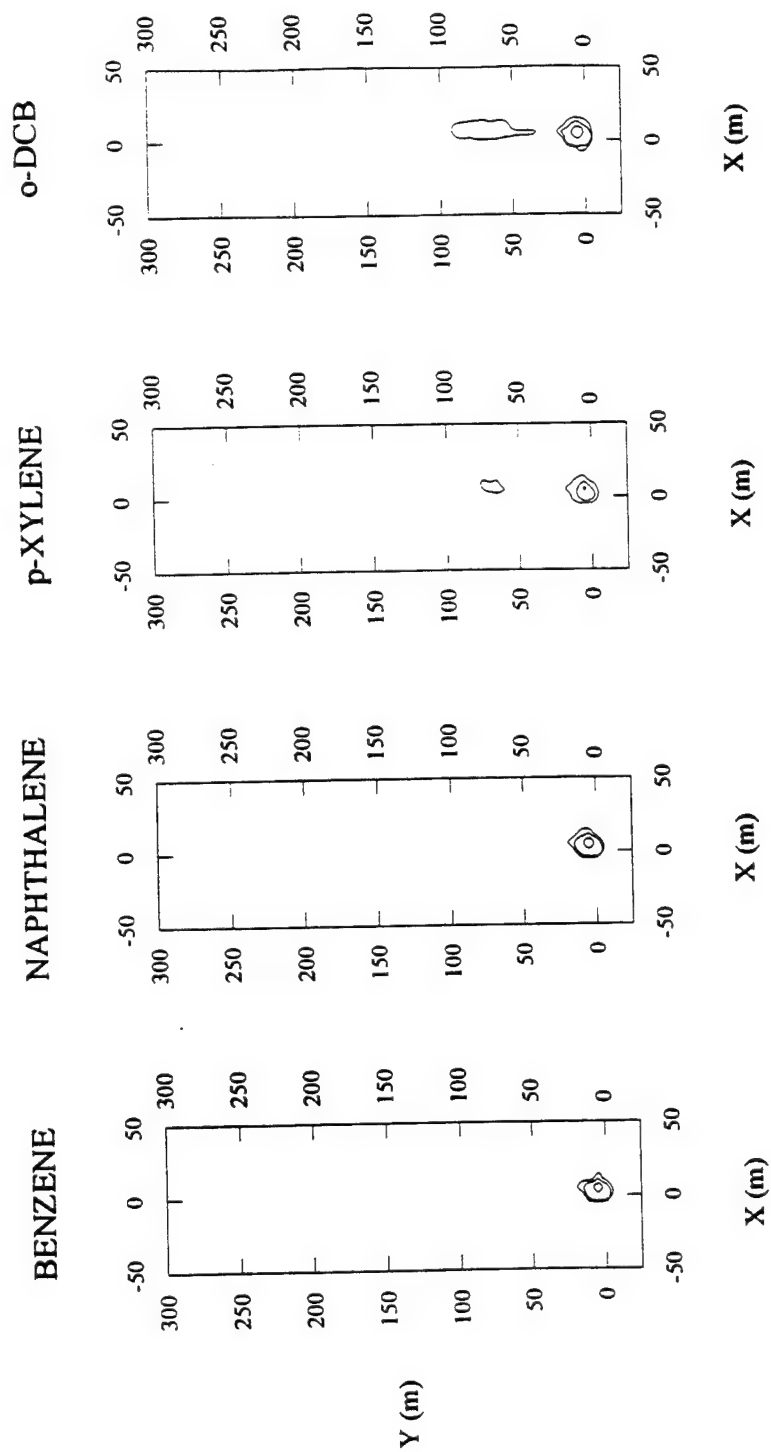


Figure 52. M2-8-8 Normalized Organic Concentrations in Layer 4, Day 240. Isopleths Presented at 0.01, 0.001, and 0.0001.

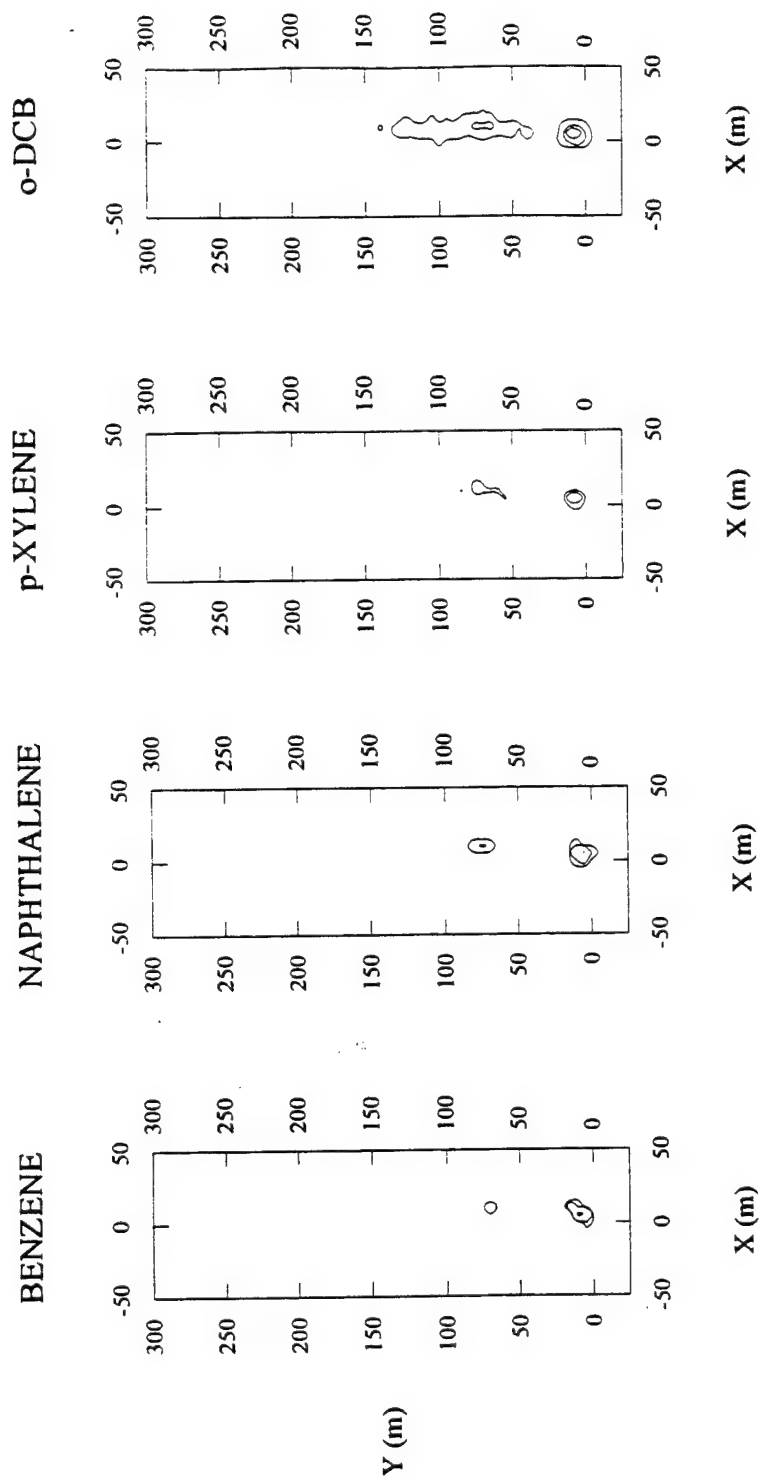


Figure 53. M2-8-8 Normalized Organic Concentrations in Layer 4, Day 344. Isopleths Presented at 0.1, 0.01, 0.001, and 0.0001.

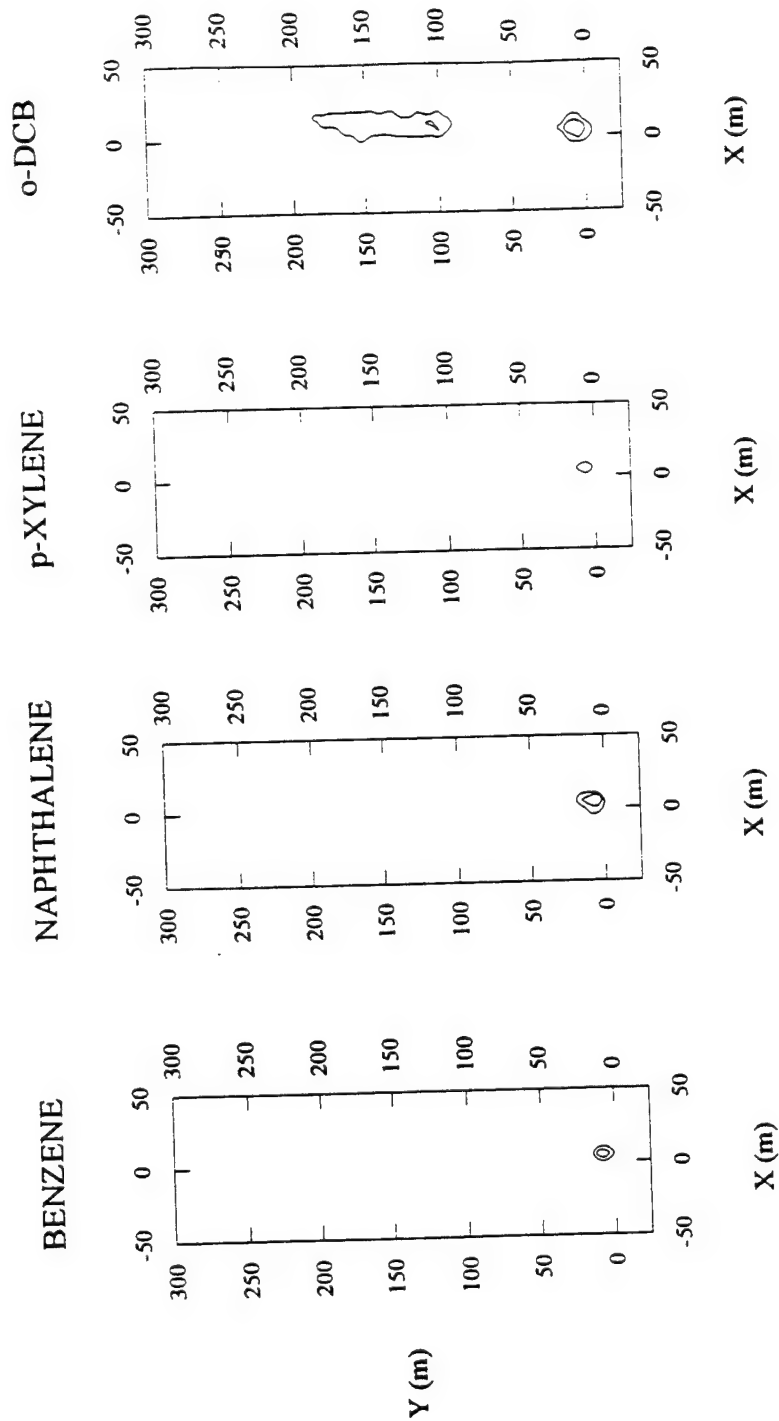


Figure 54. M2-8-8 Normalized Organic Concentrations in Layer 4, Day 456.  
Isopleths Presented at 0.01, 0.001, and 0.0001.

Program MASSCALC was written to calculate the zeroth, first, and second spatial moments of the concentration, and to find the total mass, center of mass, and variance of the contaminant plumes. Corresponding moment calculations on field data (Boggs et al., 1993) used three-dimensional numerical integration to account for the variation of concentration between sampling points. However, in a finite-difference calculation, the concentration is assumed constant over the entire cell. Therefore, MASSCALC calculated the moments by summation. Tables 22(a) through 22(e) list the results of MASSCALC from simulation M2-8-8.

TABLE 22 (A). TRITIUM PLUME CHARACTERISTICS FROM SIMULATION M2-8-8.

| Day:                              | 44    |  | 148   |  | 240   |  | 344   |  | 456    |
|-----------------------------------|-------|--|-------|--|-------|--|-------|--|--------|
| M/M <sub>0</sub>                  | .9931 |  | .9982 |  | .9818 |  | 1.443 |  | .9306  |
| X <sub>c</sub> (m)                | 1.06  |  | 1.97  |  | 4.88  |  | 9.367 |  | 13.25  |
| Y <sub>c</sub> (m)                | 1.61  |  | 6.17  |  | 27.06 |  | 93.38 |  | 159.51 |
| Z <sub>c</sub> (m)                | 57.12 |  | 58.36 |  | 59.42 |  | 59.61 |  | 58.85  |
| $\sigma_{xx}^2$ (m <sup>2</sup> ) | 4.73  |  | 7.61  |  | 23.90 |  | 68.94 |  | 178.25 |
| $\sigma_{yy}^2$ (m <sup>2</sup> ) | 16.93 |  | 92.61 |  | 1584  |  | 4081  |  | 3775   |
| $\sigma_{zz}^2$ (m <sup>2</sup> ) | .579  |  | 1.09  |  | 1.33  |  | 1.57  |  | 1.62   |

TABLE 22 (B). BENZENE PLUME CHARACTERISTICS FROM SIMULATION M2-8-8.

| Day:                              | 44    |  | 148   |  | 240   |  | 344   |  | 456   |
|-----------------------------------|-------|--|-------|--|-------|--|-------|--|-------|
| M/M <sub>0</sub>                  | 1.02  |  | .477  |  | .257  |  | .150  |  | .0369 |
| X <sub>c</sub> (m)                | 1.11  |  | 1.64  |  | 2.22  |  | 7.04  |  | 6.62  |
| Y <sub>c</sub> (m)                | 0.9   |  | 3.95  |  | 8.26  |  | 30.6  |  | 64.1  |
| Z <sub>c</sub> (m)                | 57.09 |  | 57.81 |  | 59.60 |  | 60.77 |  | 59.44 |
| $\sigma_{xx}^2$ (m <sup>2</sup> ) | 4.69  |  | 6.34  |  | 9.19  |  | 15.1  |  | 21.4  |
| $\sigma_{yy}^2$ (m <sup>2</sup> ) | 8.15  |  | 30.6  |  | 219   |  | 1490  |  | 4170  |
| $\sigma_{zz}^2$ (m <sup>2</sup> ) | .45   |  | .852  |  | 1.15  |  | 1.24  |  | .499  |

TABLE 22 (C). NAPHTHALENE CHARACTERISTICS FROM SIMULATION M2-8-8.

|                                   |       |  |       |  |       |  |        |  |       |
|-----------------------------------|-------|--|-------|--|-------|--|--------|--|-------|
| Day:                              | 44    |  | 148   |  | 240   |  | 344    |  | 456   |
| M/M <sub>0</sub>                  | .977  |  | .502  |  | .309  |  | .158   |  | .0422 |
| X <sub>c</sub> (m)                | 1.09  |  | 1.50  |  | 2.79  |  | 4.56   |  | 3.67  |
| Y <sub>c</sub> (m)                | .867  |  | 3.19  |  | 4.93  |  | 13.9   |  | 7.64  |
| Z <sub>c</sub> (m)                | 57.04 |  | 57.84 |  | 58.84 |  | 59.43  |  | 59.53 |
| $\sigma_{xx}^2$ (m <sup>2</sup> ) | 4.57  |  | 5.61  |  | 6.91  |  | 7.49   |  | 4.85  |
| $\sigma_{yy}^2$ (m <sup>2</sup> ) | 5.88  |  | 9.12  |  | 12.02 |  | 331.04 |  | 10.43 |
| $\sigma_{zz}^2$ (m <sup>2</sup> ) | .411  |  | .651  |  | 1.19  |  | 1.27   |  | .335  |

TABLE 22 (D). P-XYLENE PLUME CHARACTERISTICS FROM SIMULATION M2-8-8.

|                                   |       |  |       |  |       |  |       |  |       |
|-----------------------------------|-------|--|-------|--|-------|--|-------|--|-------|
| Day:                              | 44    |  | 148   |  | 240   |  | 344   |  | 456   |
| M/M <sub>0</sub>                  | .78   |  | .264  |  | .095  |  | .036  |  | .006  |
| X <sub>c</sub> (m)                | 1.17  |  | 1.75  |  | 3.37  |  | 5.18  |  | 4.11  |
| Y <sub>c</sub> (m)                | 1.03  |  | 3.82  |  | 8.00  |  | 20.76 |  | 6.09  |
| Z <sub>c</sub> (m)                | 57.11 |  | 57.97 |  | 59.10 |  | 59.76 |  | 59.64 |
| $\sigma_{xx}^2$ (m <sup>2</sup> ) | 4.86  |  | 6.46  |  | 7.43  |  | 10.70 |  | 3.65  |
| $\sigma_{yy}^2$ (m <sup>2</sup> ) | 9.10  |  | 25.56 |  | 133.3 |  | 564.8 |  | 4.27  |
| $\sigma_{zz}^2$ (m <sup>2</sup> ) | .4767 |  | .859  |  | 1.31  |  | 1.29  |  | .229  |

TABLE 22 (E). O-DCB PLUME CHARACTERISTICS FROM SIMULATION M2-8-8.

|                                   |       |  |       |  |       |  |       |  |       |
|-----------------------------------|-------|--|-------|--|-------|--|-------|--|-------|
| Day:                              | 44    |  | 148   |  | 240   |  | 344   |  | 456   |
| M/M <sub>0</sub>                  | 1.12  |  | .648  |  | .1378 |  | .0528 |  | .0087 |
| X <sub>c</sub> (m)                | 1.17  |  | 1.63  |  | 3.37  |  | 5.18  |  | 4.11  |
| Y <sub>c</sub> (m)                | 1.03  |  | 3.85  |  | 8.00  |  | 20.76 |  | 6.09  |
| Z <sub>c</sub> (m)                | 57.11 |  | 57.91 |  | 59.10 |  | 59.76 |  | 59.64 |
| $\sigma_{xx}^2$ (m <sup>2</sup> ) | 4.86  |  | 6.25  |  | 7.43  |  | 10.70 |  | 3.65  |
| $\sigma_{yy}^2$ (m <sup>2</sup> ) | 9.10  |  | 26.54 |  | 133.3 |  | 564.8 |  | 4.27  |
| $\sigma_{zz}^2$ (m <sup>2</sup> ) | .4767 |  | .799  |  | 1.31  |  | 1.29  |  | .229  |

M/M<sub>0</sub> is total mass to injected mass, X<sub>c</sub>, Y<sub>c</sub>, and Z<sub>c</sub> are the plumes' centroids in the respective directions, and  $\sigma_{xx}^2$ ,  $\sigma_{yy}^2$ , and  $\sigma_{zz}^2$  are the principal second moments.

The results in Table 22 generally compare reasonably well to the observed plume parameters from Boggs et al (1993), seen in Table 23.

TABLE 23 (A). OBSERVED TRITIUM PLUME CHARACTERISTICS.

| Day:                              | 44    |  | 148   |  | 240   |  | 344   |  | 456 |
|-----------------------------------|-------|--|-------|--|-------|--|-------|--|-----|
| M/M <sub>0</sub>                  | 1.52  |  | 1.05  |  | 0.98  |  | 0.77  |  | -   |
| X <sub>c</sub> (m)                | 0.0   |  | -0.9  |  | 0.2   |  | 2.1   |  | -   |
| Y <sub>c</sub> (m)                | 3.9   |  | 8.1   |  | 46.5  |  | 76.8  |  | -   |
| Z <sub>c</sub> (m)                | 58.22 |  | 58.68 |  | 58.80 |  | 58.48 |  | -   |
| $\sigma_{yy}^2$ (m <sup>2</sup> ) | 10.3  |  | 94.4  |  | 4380  |  | 6560  |  | -   |
| $\sigma_{xx}^2$ (m <sup>2</sup> ) | 8.6   |  | 7.9   |  | 52.5  |  | 107   |  | -   |
| $\sigma_{zz}^2$ (m <sup>2</sup> ) | 2.0   |  | 1.3   |  | 2.5   |  | 2.9   |  | -   |

TABLE 23 (B). OBSERVED BENZENE PLUME CHARACTERISTICS.

| Day:                              | 44    |  | 148   |  | 240   |  | 344   |  | 456   |
|-----------------------------------|-------|--|-------|--|-------|--|-------|--|-------|
| M/M <sub>0</sub>                  | 0.92  |  | 0.43  |  | 0.23  |  | 0.07  |  | 0.06  |
| X <sub>c</sub> (m)                | -0.2  |  | -1.1  |  | -0.8  |  | -1.0  |  | -1.1  |
| Y <sub>c</sub> (m)                | 3.8   |  | 6.3   |  | 12.4  |  | 7.7   |  | 7.9   |
| Z <sub>c</sub> (m)                | 58.13 |  | 58.68 |  | 59.24 |  | 58.90 |  | 58.67 |
| $\sigma_{yy}^2$ (m <sup>2</sup> ) | 9.2   |  | 38.4  |  | 826   |  | 24.7  |  | 21.4  |
| $\sigma_{xx}^2$ (m <sup>2</sup> ) | 7.9   |  | 6.9   |  | 6.1   |  | 8.4   |  | 10.7  |
| $\sigma_{zz}^2$ (m <sup>2</sup> ) | 1.9   |  | 1.1   |  | 1.2   |  | 1.2   |  | 1.3   |

TABLE 23 (C). OBSERVED NAPHTHALENE PLUME CHARACTERISTICS.

| Day:                              | 44    |  | 148   |  | 240   |  | 344   |  | 456   |
|-----------------------------------|-------|--|-------|--|-------|--|-------|--|-------|
| M/M <sub>0</sub>                  | 0.58  |  | 0.45  |  | 0.25  |  | 0.08  |  | 0.06  |
| X <sub>c</sub> (m)                | -.3   |  | -1.2  |  | -1.4  |  | -1.0  |  | -1.8  |
| Y <sub>c</sub> (m)                | 3.5   |  | 5.8   |  | 6.6   |  | 7.2   |  | 7.3   |
| Z <sub>c</sub> (m)                | 58.05 |  | 58.54 |  | 59.03 |  | 58.71 |  | 58.62 |
| $\sigma_{yy}^2$ (m <sup>2</sup> ) | 8.5   |  | 19.2  |  | 14.7  |  | 16.2  |  | 12.8  |
| $\sigma_{xx}^2$ (m <sup>2</sup> ) | 7.3   |  | 6.7   |  | 6.1   |  | 4.8   |  | 4.7   |
| $\sigma_{zz}^2$ (m <sup>2</sup> ) | 1.6   |  | 1.4   |  | 1.3   |  | 1.0   |  | 1.3   |

TABLE 23 (D). OBSERVED P-XYLENE PLUME CHARACTERISTICS.

|                                   |       |  |       |  |       |  |       |  |       |
|-----------------------------------|-------|--|-------|--|-------|--|-------|--|-------|
| Day:                              | 44    |  | 148   |  | 240   |  | 344   |  | 456   |
| M/M <sub>0</sub>                  | 0.77  |  | 0.58  |  | 0.23  |  | 0.03  |  | 0.01  |
| X <sub>c</sub> (m)                | -2    |  | -1.0  |  | -1.2  |  | -1.1  |  | -1.3  |
| Y <sub>c</sub> (m)                | 3.6   |  | 6.1   |  | 6.4   |  | 10.5  |  | 6.4   |
| Z <sub>c</sub> (m)                | 58.04 |  | 58.60 |  | 58.93 |  | 58.66 |  | 57.93 |
| $\sigma_{yy}^2$ (m <sup>2</sup> ) | 9.1   |  | 22.8  |  | 16.3  |  | 213   |  | 11.8  |
| $\sigma_{xx}^2$ (m <sup>2</sup> ) | 7.2   |  | 5.8   |  | 6.4   |  | 4.6   |  | 4.0   |
| $\sigma_{zz}^2$ (m <sup>2</sup> ) | 1.9   |  | 1.1   |  | 1.3   |  | 1.0   |  | 1.3   |

TABLE 23 (E). OBSERVED O-DCB PLUME CHARACTERISTICS.

|                                   |       |  |       |  |       |  |       |  |       |
|-----------------------------------|-------|--|-------|--|-------|--|-------|--|-------|
| Day:                              | 44    |  | 148   |  | 240   |  | 344   |  | 456   |
| M/M <sub>0</sub>                  | 0.81  |  | 0.80  |  | 0.60  |  | 0.21  |  | 0.13  |
| X <sub>c</sub> (m)                | 0.0   |  | -1.0  |  | 0.0   |  | -0.2  |  | -1.5  |
| Y <sub>c</sub> (m)                | 3.9   |  | 7.4   |  | 34.7  |  | 22.1  |  | 8.1   |
| Z <sub>c</sub> (m)                | 58.09 |  | 58.57 |  | 58.93 |  | 58.90 |  | 58.68 |
| $\sigma_{yy}^2$ (m <sup>2</sup> ) | 11.3  |  | 64.4  |  | 3540  |  | 1180  |  | 21.9  |
| $\sigma_{xx}^2$ (m <sup>2</sup> ) | 7.9   |  | 7.8   |  | 25.2  |  | 22.4  |  | 7.1   |
| $\sigma_{zz}^2$ (m <sup>2</sup> ) | 2.1   |  | 1.4   |  | 2.0   |  | 1.6   |  | 1.8   |

The relative mass balance (M/M<sub>0</sub>) for each contaminant, computed by MASSCALC, was plotted with the observed relative mass balance versus Simulation Day in Figures 55 through 59. All showed good agreement between the two with the exception of tritium. Since tritium does not undergo substantial decay, the mass balance should be approximately 1.0 (or 100%). However, Figure 55 shows errors in both observation and simulation. The observations gave a 152% overestimate at Day 44 which Boggs et al. (1993) attributed to preferential sampling in relatively high conductivity zones. The 23% underestimate at Day 344 of the observed data was due to truncation of the leading edge of the plume. The simulated tritium plume gave excellent results except for a 44% overestimate on Day 344. This simulation was repeated many times; however, the number persisted in every calculation. It is not known what caused this error. A

potential cause is the use of the MOC option, which does not inherently conserve mass. But in view of the anomalous nature of this discrepancy, this explanation seems unlikely.



### Relative Mass Balance for Tritium

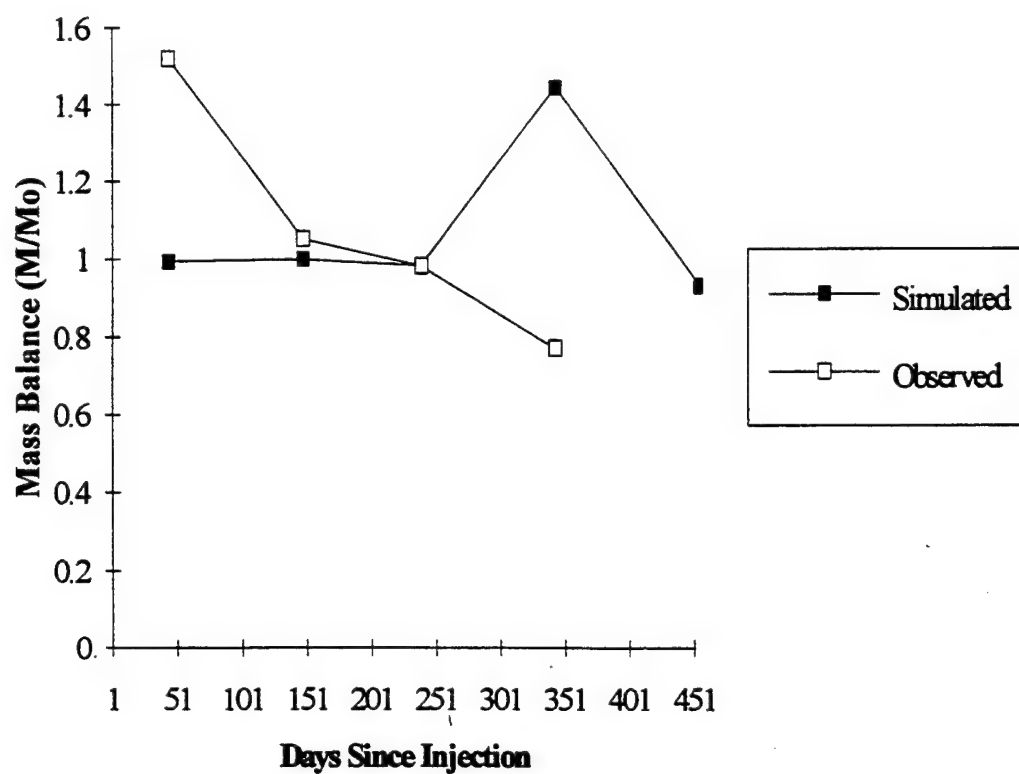
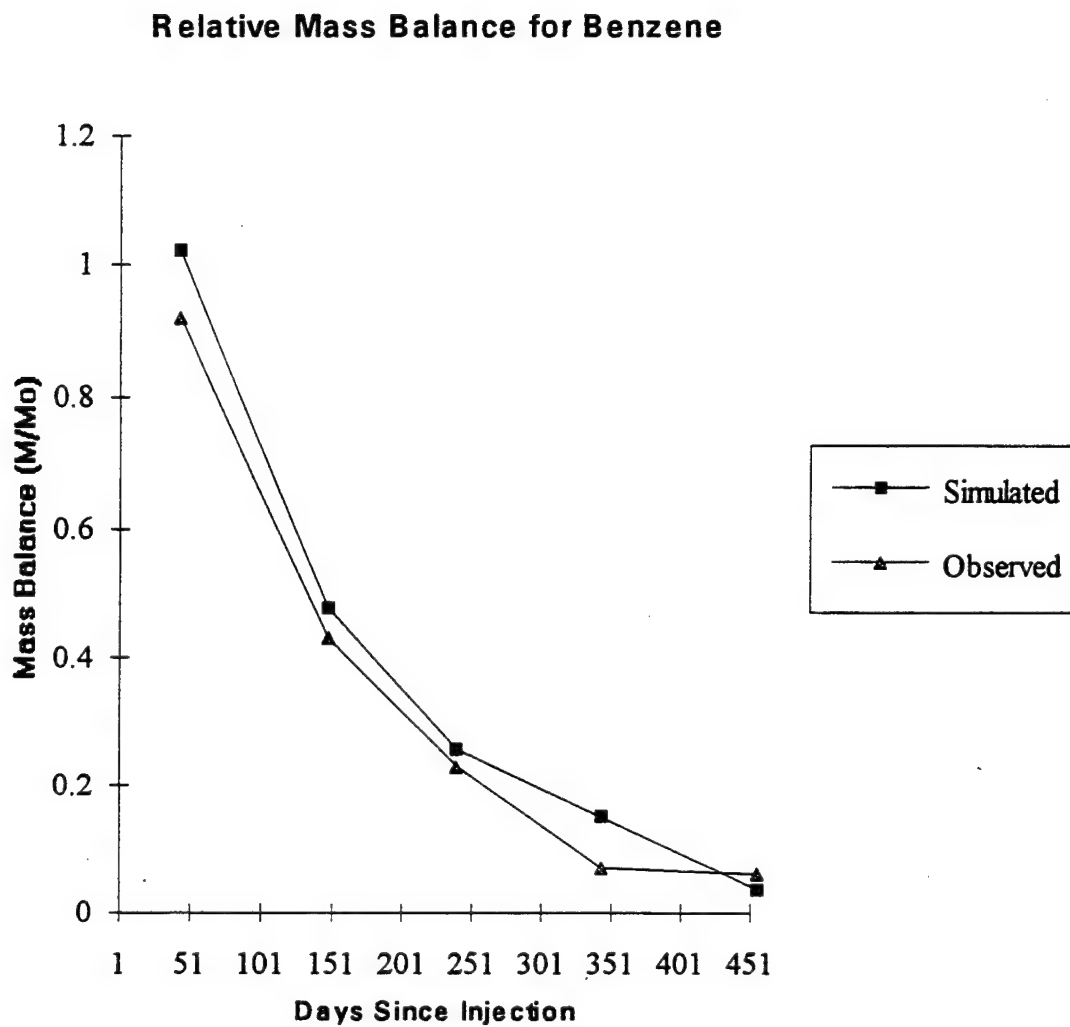
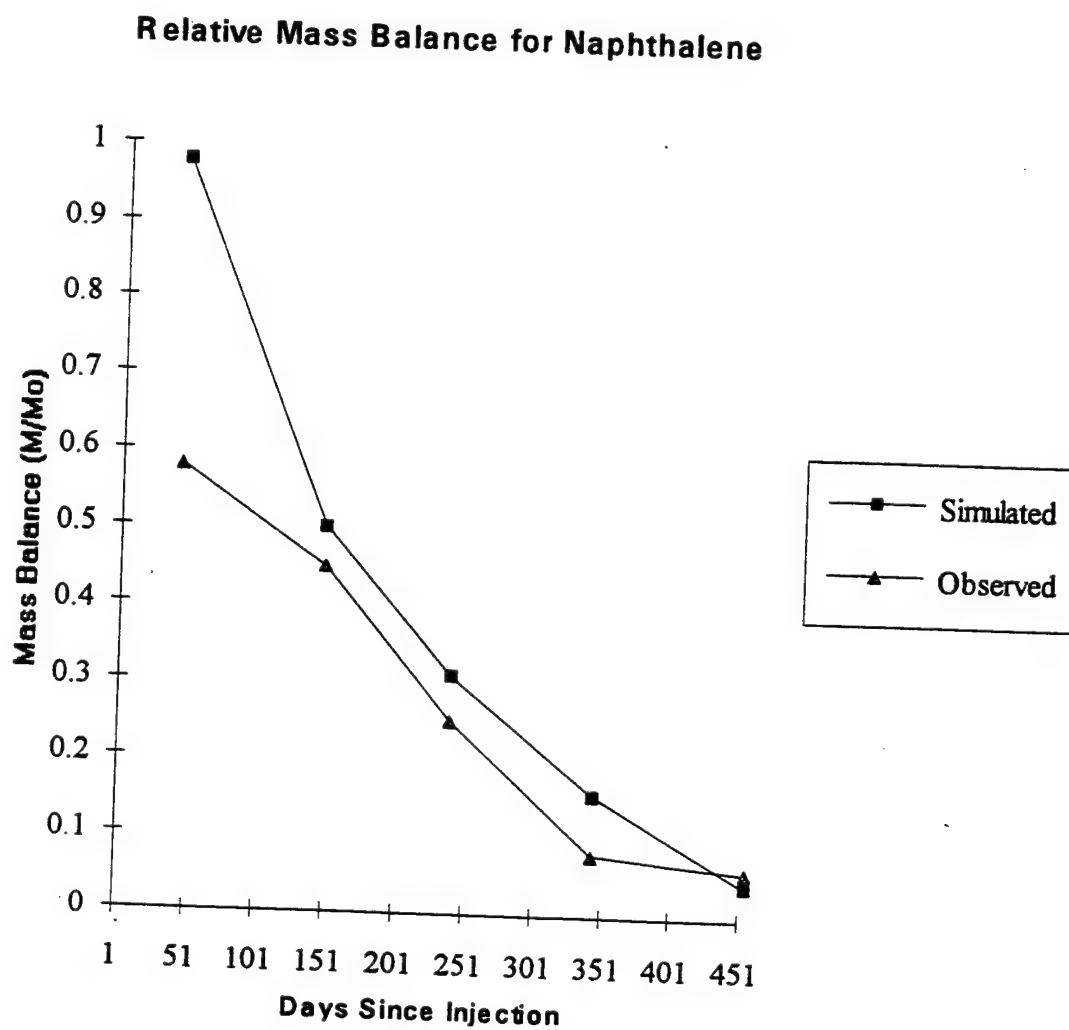


Figure 55. Observed and M2-8-8 Mass Ratio for Tritium.



**Figure 56. Observed and M2-8-8 Mass Ratio for Benzene.**



**Figure 57. Observed and M2-8-8 Mass Ratio for Naphthalene.**

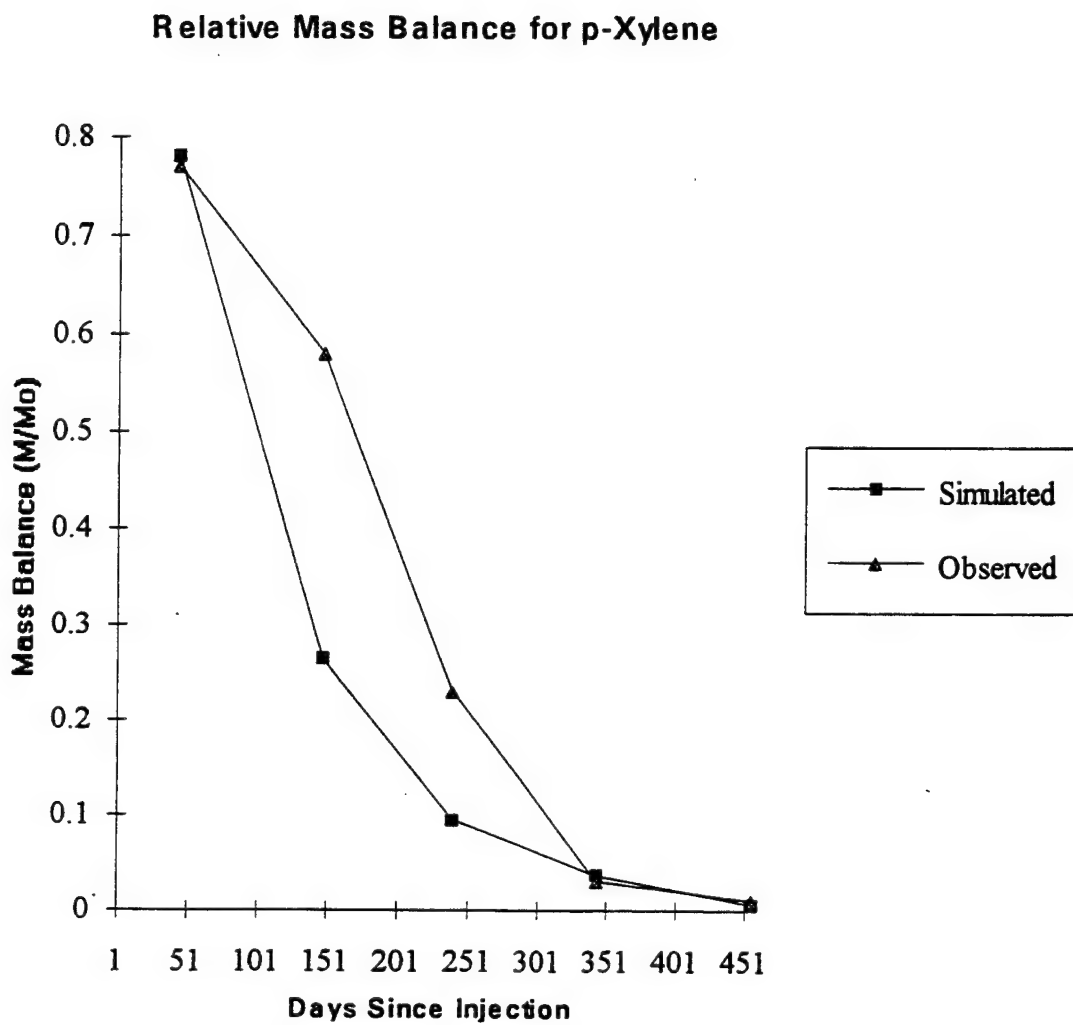


**Figure 58. Observed and M2-8-8 Mass Ratio for p-Xylene.**

### Relative Mass Balance for o-DCB

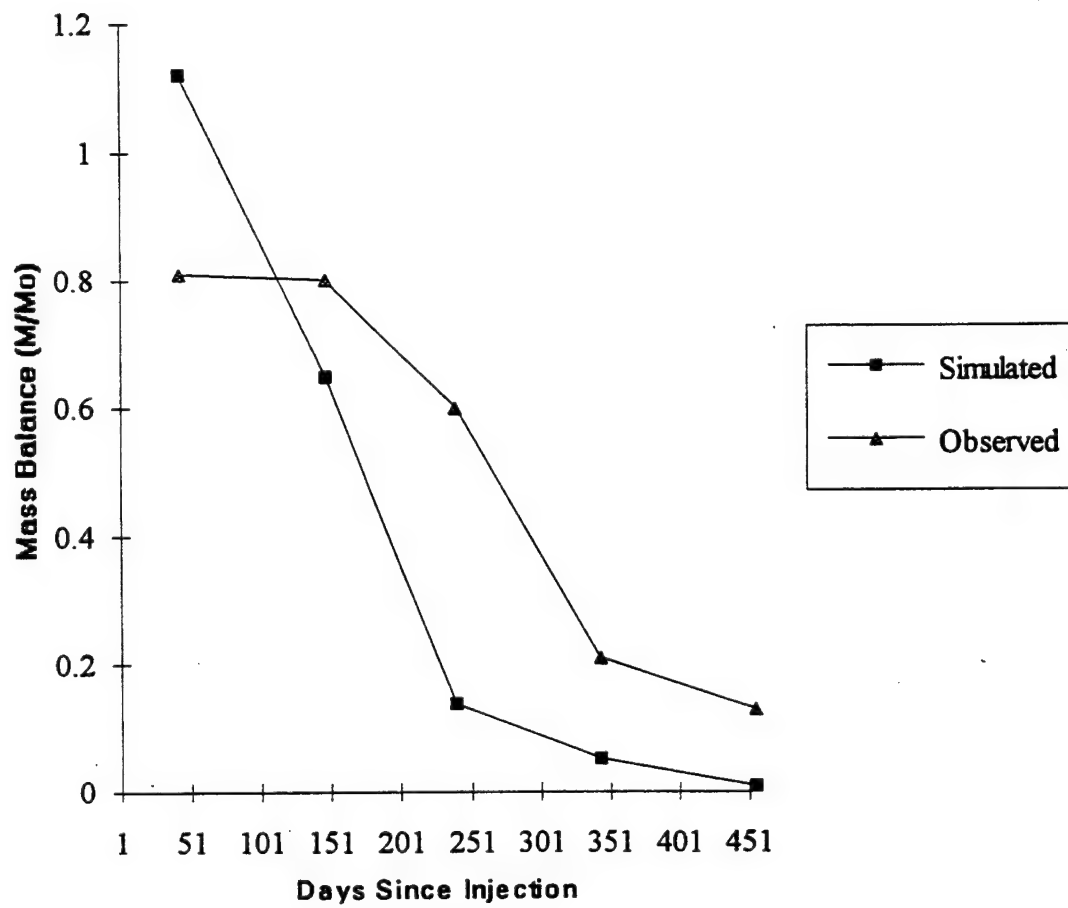


Figure 59. Observed and M2-8-8 Mass Ratio for o-DCB.

Finally, the center of mass trajectories for each contaminant were plotted to show differences between the observed and simulated plumes. Figures 60 through 64 show these trajectories projected on the XY plane. In reality, the center of mass moves vertically between 57 and 61 meters MSL. The numbers on the plots represent the following code:

- 1 = injection period, simulation day 16
- 2 = simulation day 44
- 3 = simulation day 148
- 4 = simulation day 240
- 5 = simulation day 344
- 6 = simulation day 456

Each simulated center of mass is generally close to the observed, although the simulated plumes deviate systematically to the east. The effects of biodegradation are seen in the upgradient motion of the center of mass in the later simulated plumes of naphthalene, p-xylene, and o-DCB. Similar behavior was noted in the later observed plumes of benzene, p-xylene, and o-DCB. The reasons for the lack of upgradient center of mass motion in the predicted benzene and observed naphthalene plumes are unclear. The case of benzene is particularly puzzling because of the excellent mass balance agreement shown in Figure 56.

The simulated center of mass trajectories veer east, as opposed to the observed trajectories, which deviate slightly to the west. The maximum discrepancy can be seen in tritium with an approximate 10 meter shift to the east.

### Center of Mass Trajectory for Tritium

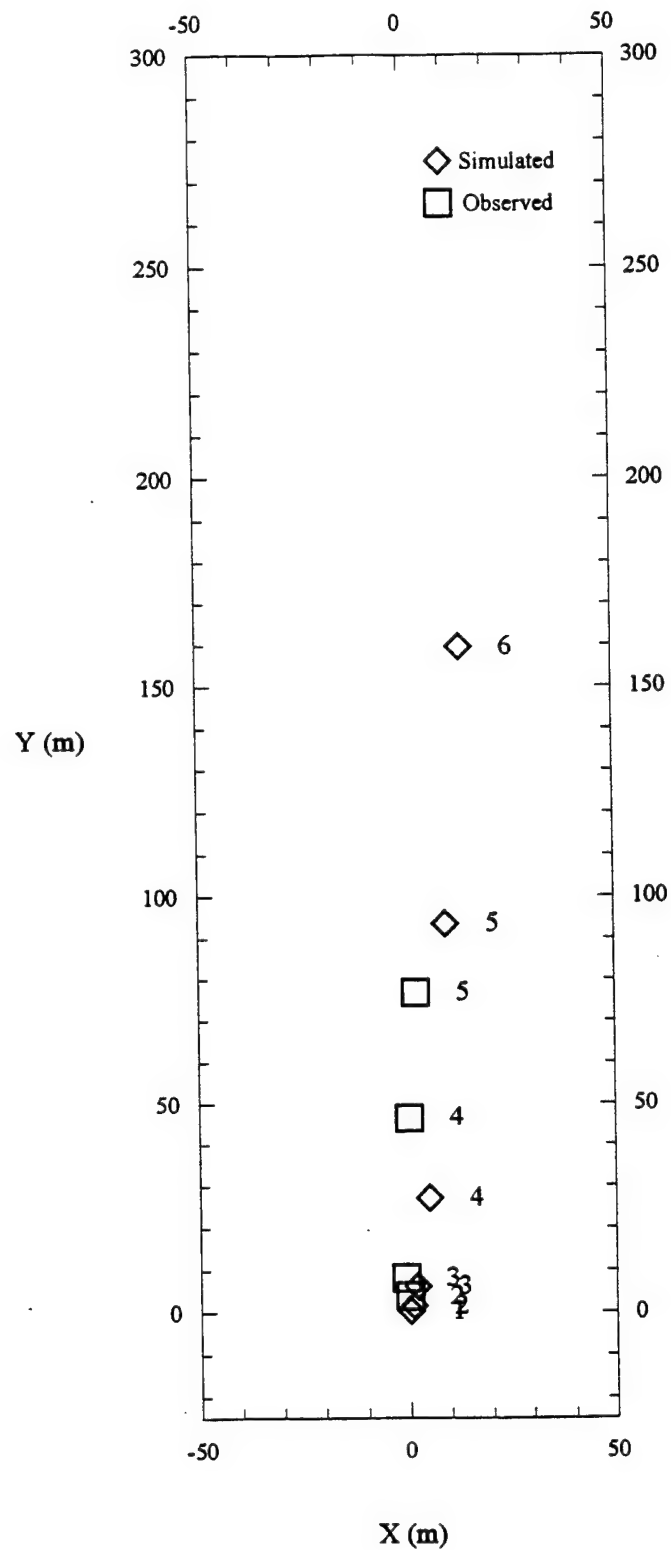


Figure 60. Observed and M2-8-8 Center of Mass Trajectory for Tritium.

# Center of Mass Trajectory for Benzene

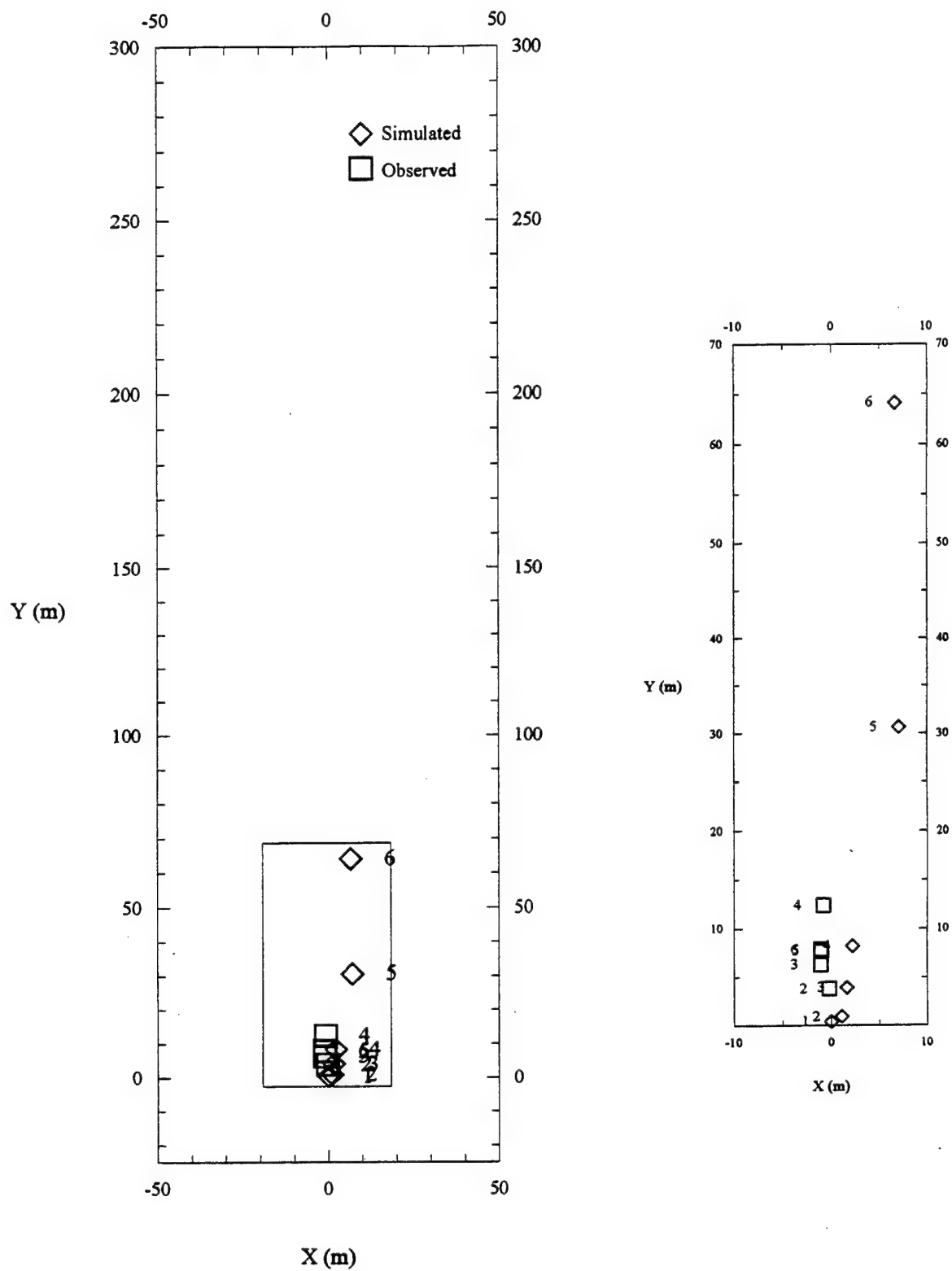


Figure 61. Observed and M2-8-8 Center of Mass Trajectory for Benzene.



# Center of Mass Trajectory for Naphthalene

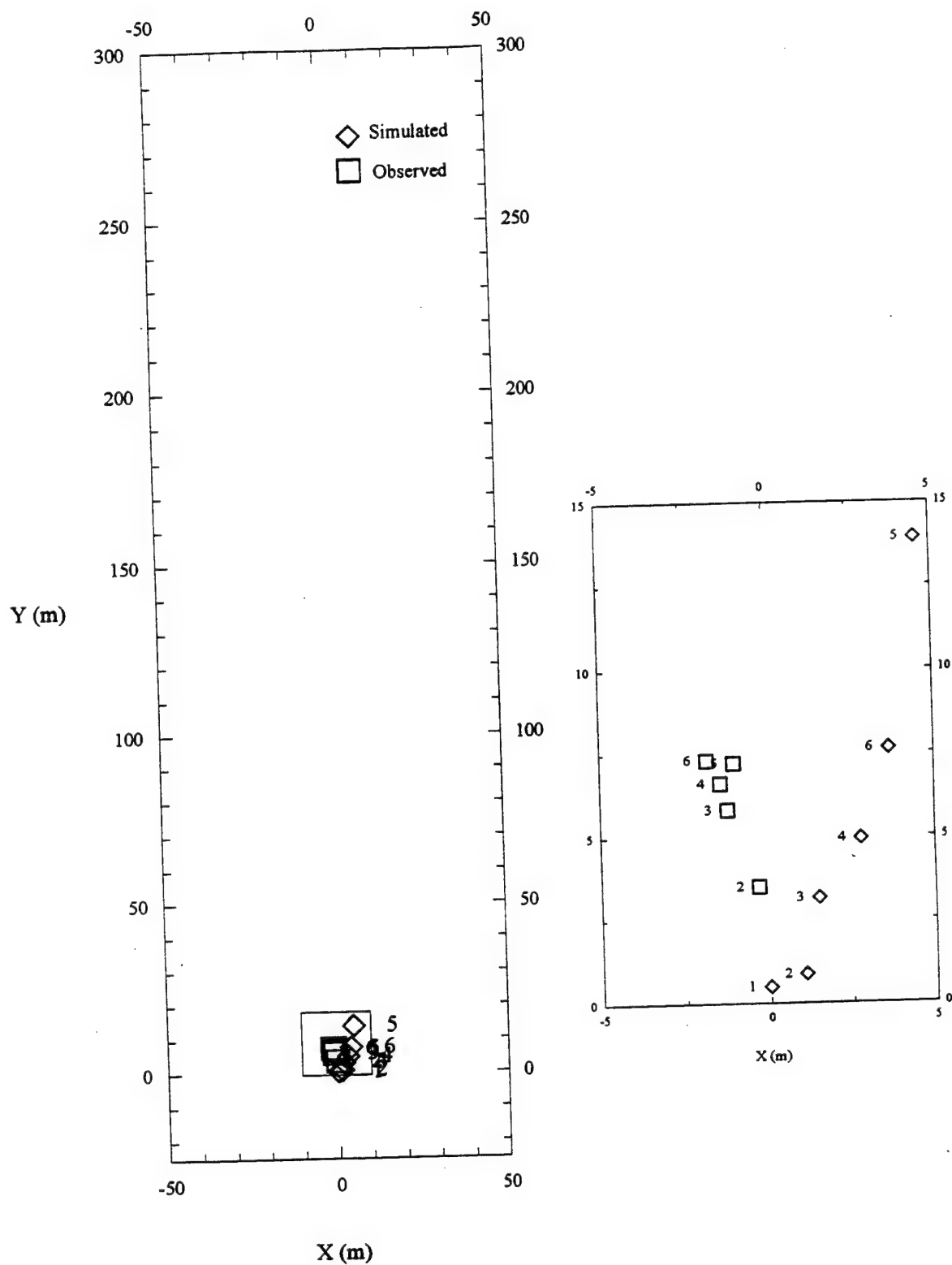


Figure 62. Observed and M2-8-8 Center of Mass Trajectory for Naphthalene.

# Center of Mass Trajectory for p-Xylene

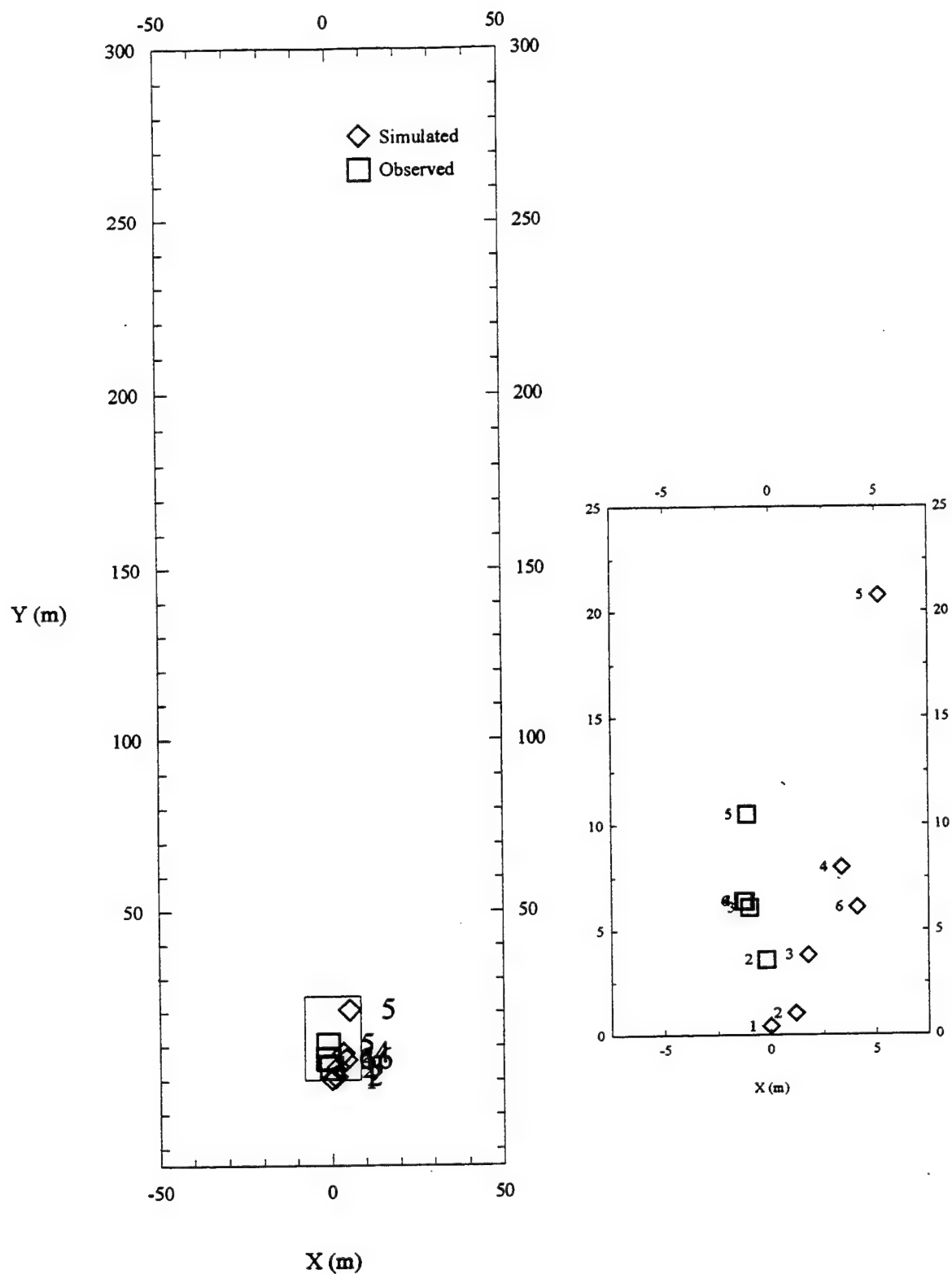


Figure 63. Observed and M2-8-8 Center of Mass Trajectory for p-Xylene.

# Center of Mass Trajectory for o-DCB

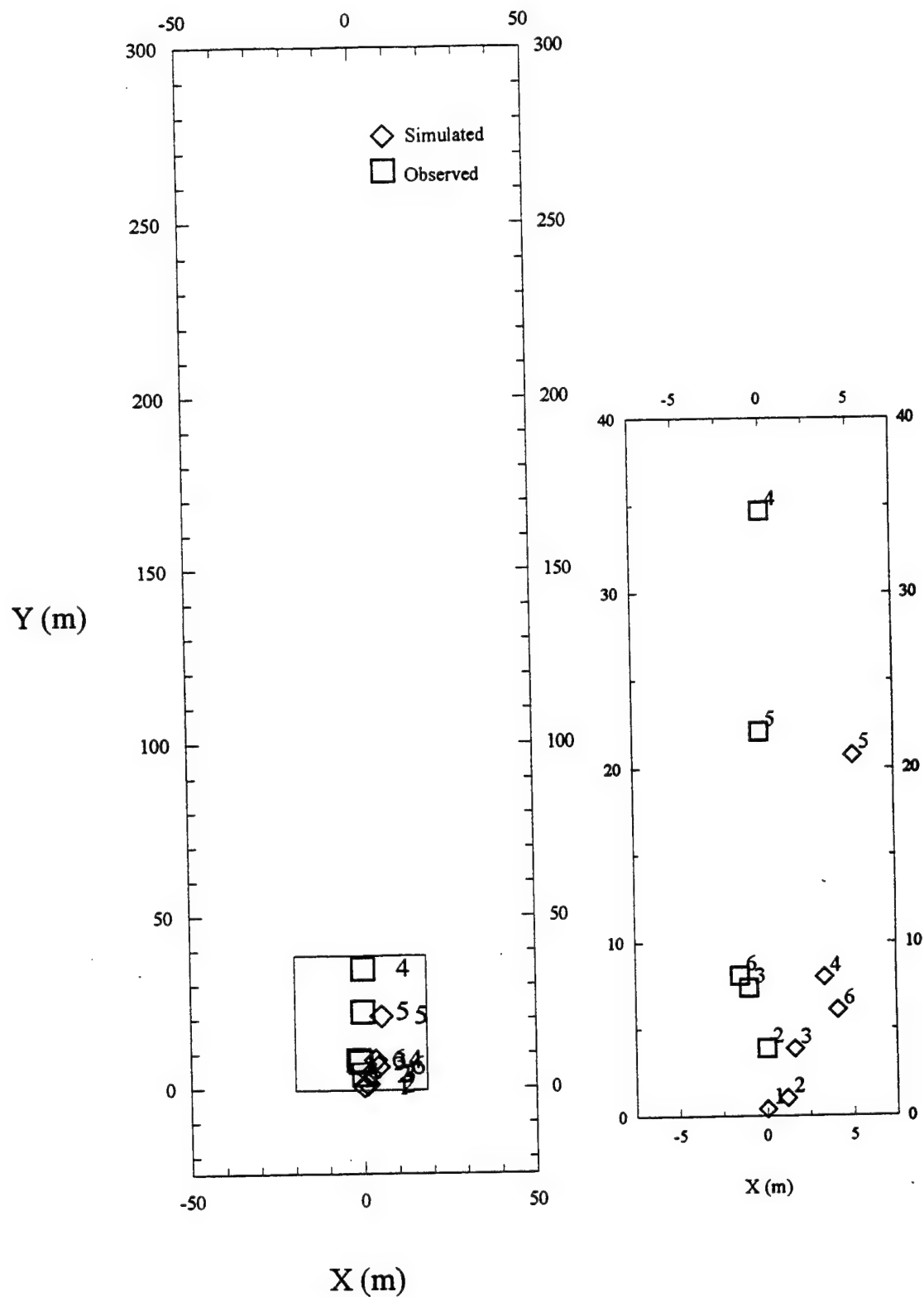


Figure 64. Observed and M2-8-8 Center of Mass Trajectory for o-DCB.

#### D. FURTHER CONSIDERATION OF ANISOTROPY

Although the use of horizontal anisotropy varying with conductivity gave plumes which compared well with observations, the justification for this procedure remained weak. The assumed maximum principal axis was in the Y direction, 12° west of north. This does not agree with the results of AT-2 (35° west of north) or with the hypothesized channel axis (30° east of north). Indeed, there is every reason to believe that the principal directions will be different in the channel zone than elsewhere.

Another question related to the magnitude of the anisotropy. The horizontal anisotropy factor used to increase velocities in the longitudinal direction was 5.8 times higher than estimated from pump test AT-2. This discrepancy was a major concern, and additional research was conducted in order to justify the value used.

Hantush (1966) describes the effects of a fully penetrating well in an infinite nonleaky horizontally anisotropic aquifer. The equal drawdown contours are ellipses, with their major axes oriented along the maximum principal direction of conductivity. Furthermore, he concludes that the usual methods for obtaining aquifer parameters for isotropic conditions are not valid for anisotropic conditions. The effective isotropic values are related to the actual principal values as follows:

$$\text{Transmissivity} = T = \sqrt{T_x T_y} \quad (7)$$

$$\text{Storativity} = S = \frac{4ut}{r^2} \sqrt{T_x T_y} \quad (8)$$

where  $T_x$  and  $T_y$  are the principal transmissivities in the X and Y directions, respectively

u is equal to  $\frac{r^2 S}{4Tt}$

r is the radius to the observation well

t is drawdown time

The effective isotropic transmissivity is the square root of the product of the two principal transmissivities. Applying these principles to the flow model is a difficult task, since the borehole flowmeter hydraulic conductivity values are somehow averaged in all horizontal directions. MODFLOW uses the conductivity values to calculate the conductance between adjacent cells. In MODFLOW the conductance is the product of hydraulic conductivity and cross sectional area of flow divided by the distance between the adjacent nodes. The conductance equation incorporates anisotropy by multiplying the column transmissivity by TRPY to get the row transmissivity. When a TRPY value greater than one was entered in the previous simulations, the overall effective conductivity was increased.

In an attempt to correct this problem, MODFLOW was modified to maintain the observed effective conductivity by automatically reducing the conductivity in the X direction to compensate for the increased conductivity along the Y direction. The column conductance was multiplied by the square root of TRPY and the row conductance was divided by the square root of TRPY. Assuming  $CR_{i,j+1/2,k}$  is the conductance between nodes  $i,j,k$  and  $i,j+1,k$  and  $CC_{i+1/2,j,k}$  is the conductance between nodes  $i,j,k$  and  $i+1,j,k$  leads to:

$$CR_{i,j+1/2,k} = 2 \text{ DELC}_i \times \frac{TR_{i,j,k} \cdot TR_{i,j+1,k}}{TR_{i,j,k} \text{ DELR}_{j+1} + TR_{i,j+1,k} \text{ DELR}_j} \quad (9)$$

$$CC_{i+1/2,j,k} = 2 \text{ DELR}_j \times \frac{TC_{i,j,k} \cdot TC_{i+1,j,k}}{TC_{i,j,k} \text{ DELC}_{i+1} + TC_{i+1,j,k} \text{ DELC}_i} \quad (10)$$

where  $\text{DELR}_j$  and  $\text{DELC}_i$  are the row and column widths of cell  $i,j,k$ , respectively

$TR_{i,j,k}$  and  $TC_{i,j,k}$  are the row and column transmissivities of cell  $i,j,k$ , respectively

If the domain is divided into a square cells, as in the MADE-2 model, then  $\text{DELR} = \text{DELC}$ , and the above two equations reduce to the harmonic mean of the transmissivities between two adjacent cells:

$$CR_{i,j+\frac{1}{2},k} = 2 \times \frac{TR_{i,j,k} TR_{i,j+1,k}}{TR_{i,j,k} + TR_{i,j+1,k}} \quad (11)$$

$$CC_{i+\frac{1}{2},j,k} = 2 \times \frac{TC_{i,j,k} TC_{i+1,j,k}}{TC_{i,j,k} + TC_{i+1,j,k}} \quad (12)$$

As mentioned, MODFLOW multiplies the column transmissivity by the anisotropy factor to obtain the row transmissivity. Hence,

$$TR_{i,j,k} = TRPY \times TC_{i,j,k} \quad (13)$$

and Equations (11) and (12) become

$$CR_{i,j+\frac{1}{2},k} = 2 \times TRPY \times \frac{T_{i,j,k} T_{i,j+1,k}}{T_{i,j,k} + T_{i,j+1,k}} \quad (14)$$

$$CC_{i+\frac{1}{2},j,k} = 2 \times \frac{T_{i,j,k} T_{i+1,j,k}}{T_{i,j,k} + T_{i+1,j,k}} \quad (15)$$

where  $T_{i,j,k}$  is the average transmissivity of cell  $i,j,k$ .

Because Hantush (1966) showed that the average transmissivity in an horizontally anisotropic media is the square root of the product of the conductivities along the principal axes, Equation (7) is rewritten as:

$$T_{i,j,k} = \sqrt{TR_{i,j,k} TC_{i,j,k}} \quad (16)$$

Substituting Equation (13) into (16) yields:

$$T_{i,j,k} = \sqrt{TRPY \times TC_{i,j,k} \times TC_{i,j,k}} \quad (17)$$

$$T_{i,j,k} = TC_{i,j,k} \sqrt{TRPY} \quad (18)$$

$$TC_{i,j,k} = T_{i,j,k} \times \frac{1}{\sqrt{TRPY}} \quad (19)$$

Similarly, the inverse of Equation (13) can be substituted into Equation (16) yielding:

$$TC_{i,j,k} = TR_{i,j,k} \times \frac{1}{TRPY} \quad (20)$$

$$T_{i,j,k} = \sqrt{TR_{i,j,k} \times TR_{i,j,k} \times \frac{1}{TRPY}} \quad (21)$$

$$T_{i,j,k} = TR_{i,j,k} \sqrt{\frac{1}{TRPY}} \quad (22)$$

$$TR_{i,j,k} = T_{i,j,k} \sqrt{TRPY} \quad (23)$$

The transmissivities of Equations (23) and (19) are substituted into Equations (11) and (12) to obtain the new conductances.

$$CR_{i,j+\frac{1}{2},k} = 2 \times \frac{T_{i,j,k} \sqrt{TRPY} \times T_{i,j+1,k} \sqrt{TRPY}}{T_{i,j,k} \sqrt{TRPY} + T_{i,j+1,k} \sqrt{TRPY}} \quad (24)$$

$$CR_{i,j+\frac{1}{2},k} = 2 \times \sqrt{TRPY} \times \frac{T_{i,j,k} T_{i,j+1,k}}{T_{i,j,k} + T_{i,j+1,k}} \quad (25)$$

$$CC_{i+\frac{1}{2},j,k} = 2 \times \frac{T_{i,j,k} \frac{1}{\sqrt{TRPY}} \times T_{i+1,j,k} \frac{1}{\sqrt{TRPY}}}{T_{i,j,k} \frac{1}{\sqrt{TRPY}} + T_{i+1,j,k} \frac{1}{\sqrt{TRPY}}} \quad (26)$$

$$CC_{i+\frac{1}{2},j,k} = 2 \times \frac{1}{\sqrt{TRPY}} \times \frac{T_{i,j,k} T_{i+1,j,k}}{T_{i,j,k} + T_{i+1,j,k}} \quad (27)$$

Equations (25) and (27) were incorporated into MODFLOW and several values of TRPY were applied to the flow model to test the new changes. The first run tested the old value of 15 with the same conditions as M2-8-8, which worked quite well in simulating the plumes. The flow

simulation took approximately 15 minutes to complete on a 90 MHz Pentium PC. The heads matched fairly well to the observed, with an average RMS of 0.2127 meters. However, the simulation of tritium migration was unsatisfactory. On Simulation Day 344 the tritium plume (Figure 65) only reached 75 meters, much less than the observed 225 meters in Figure 25. The reason for the shortcoming was due to the reduced Y conductivities. A factor of 15 was used in the original M2-8-8 simulations, but this simulation used the square root of 15 to calculate the conductances between rows (CR). This obviously did not produce the longitudinal velocities needed to push the plume outward. Also, the effect of reducing the conductance between columns (CC) by the square root of TRPY had virtually no influence on the longitudinal spreading. It only kept the plume from spreading in the lateral direction.

Other TRPY values were applied to the flow model to increase velocities to better match the observed tritium plume. Table 24 lists the corrected transmissivity simulations. The square root of the TRPY is provided to show the actual value that was multiplied and divided into observed values to give the row and column conductances, respectively.

**TABLE 24. SIMULATIONS OF M2-8-9 (CORRECTED ANISOTROPIC TRANSMISSIVITY).**

| <b>Run</b> | <b>TRPY</b> | <b><math>\sqrt{\text{TRPY}}</math></b> | <b>Averaged<br/>RMS (m)</b> | <b>Longitudinal Spread of Tritium Plume on<br/>Simulation Day 344</b> |
|------------|-------------|--|-----------------------------|---|
| 1          | 15          | 3.87                                   | 0.2127                      | 75 m  |
| 2          | 75          | 8.66                                   | 0.2216                      | 100 m   |
| 3          | 150         | 12.24                                  | 0.2235                      | 130 m   |
| 4          | 225         | 15                                     | 0.2243                      | crashed   |
| 5          | 300         | 17.32                                  | 0.2245                      | crashed   |



Tritium Plume of Layer 4, Day 344, Run 1 of M2-8-9

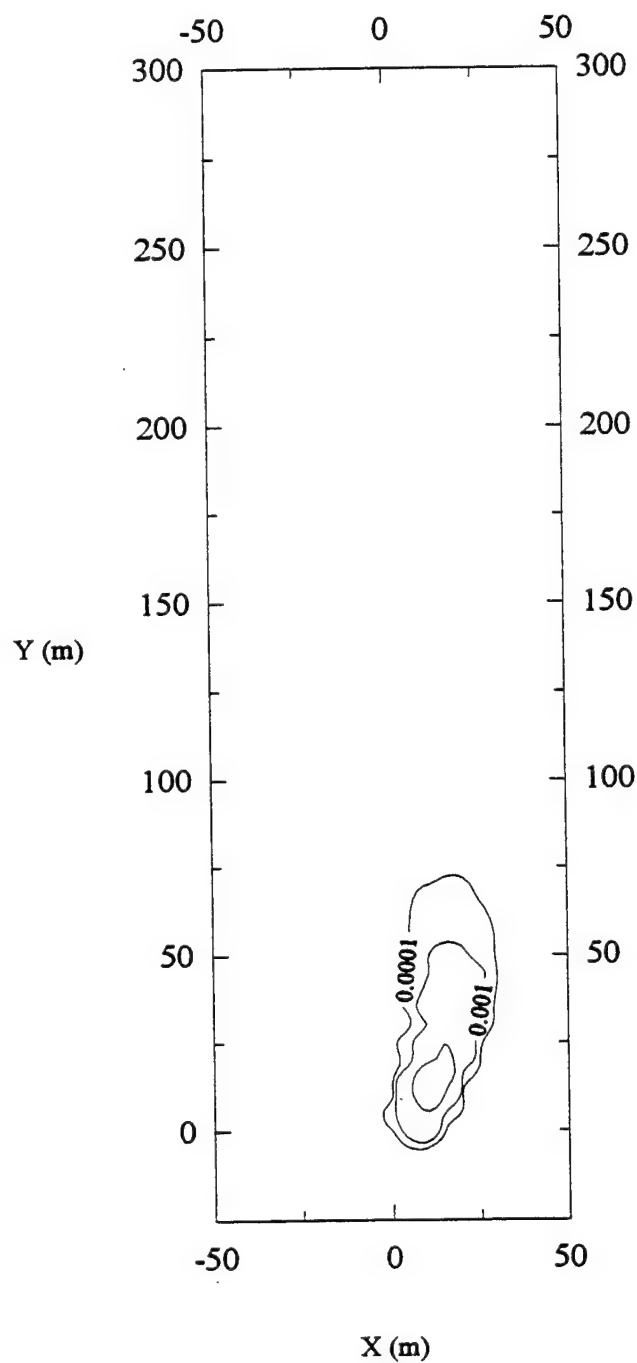


Figure 65. Normalized Tritium Concentration for Layer 4, Day 344, M2-8-9, Run 1.

The flow models for the M2-8-9 simulations became progressively worse as TRPY increased. The higher TRPY factors increased the longitudinal velocities, yet decreased the lateral velocities enough to skew the flow directions. Figures 66 through 70 show the heads of each run for Layer 4 and Day 298, centered on survey date April 4, 1991 (Figure 71). The velocity vectors are overlain on the plot to show the flow direction. The vectors were calculated by the program VECTOR, which extracted the seepage velocity vectors in the X and Y directions from the MODFLOW output file and computed a magnitude and direction for every cell. The velocities are actually computed in MODFLOW at each cell face, but were plotted at the cell center. Figure 72 shows the same layer and day for simulation M2-8-8 for comparison with Figures 66 through 70. Even though the simulations of M2-8-9 preserve the same hydraulic gradient over the entire domain as M2-8-8, the individual contours do not match. For example, the isopleth representing the hydraulic head of 63.60 meters for each M2-8-9 simulation extends into the far field, around 200 meters downgradient from the injection. The corresponding contour for M2-8-8 remains in the near field. The shape of the contour was also a major concern. The higher TRPY factors produced "humps" in the isopleths. These are obvious artifacts due to the treatment of transmissivity and are not seen in the kriged observed heads of Figure 71 (April 4, 1991).

# Heads of Layer 4, Day 298, Run 1 of M2-8-9

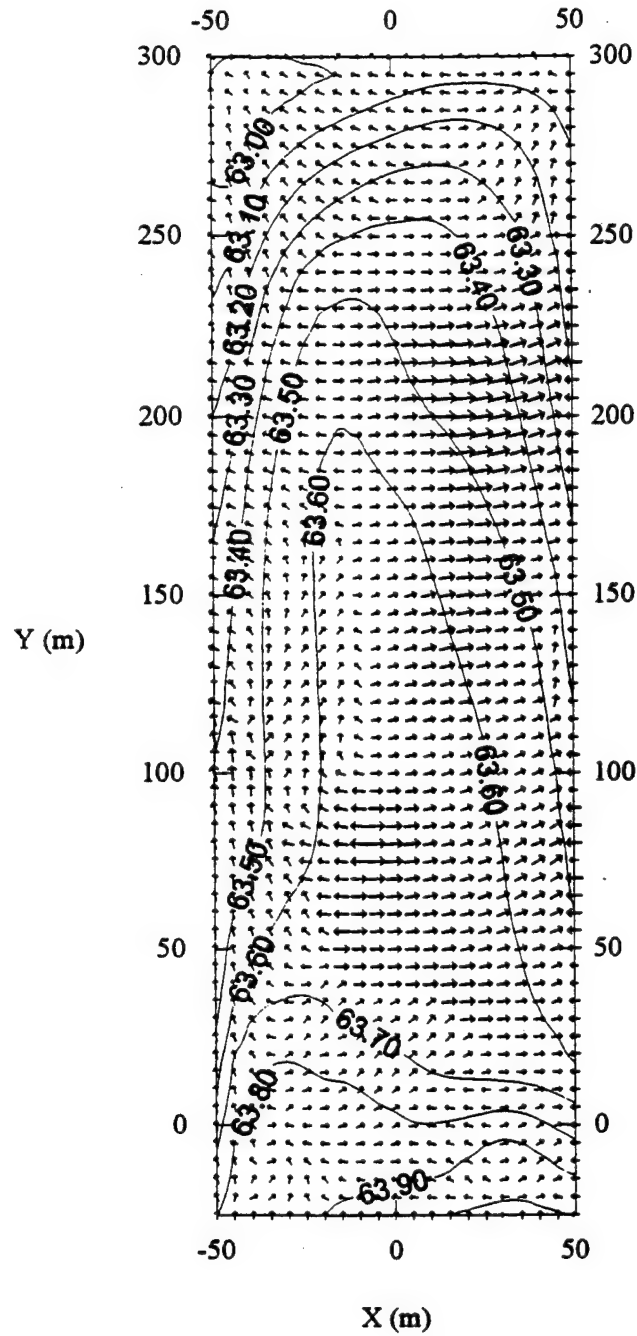


Figure 66. Head and Seepage Velocity in Layer 4, Day 298, M2-8-9, Run 1.

# Heads of Layer 4, Day 298, Run 2 of M2-8-9

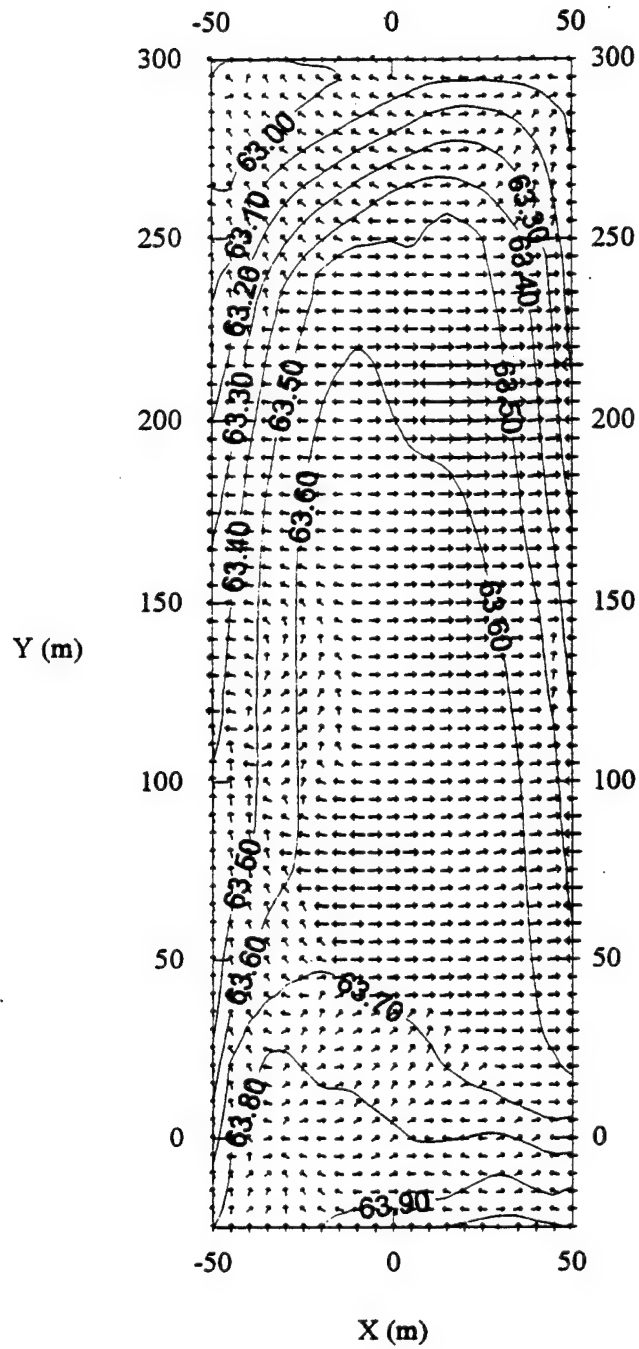
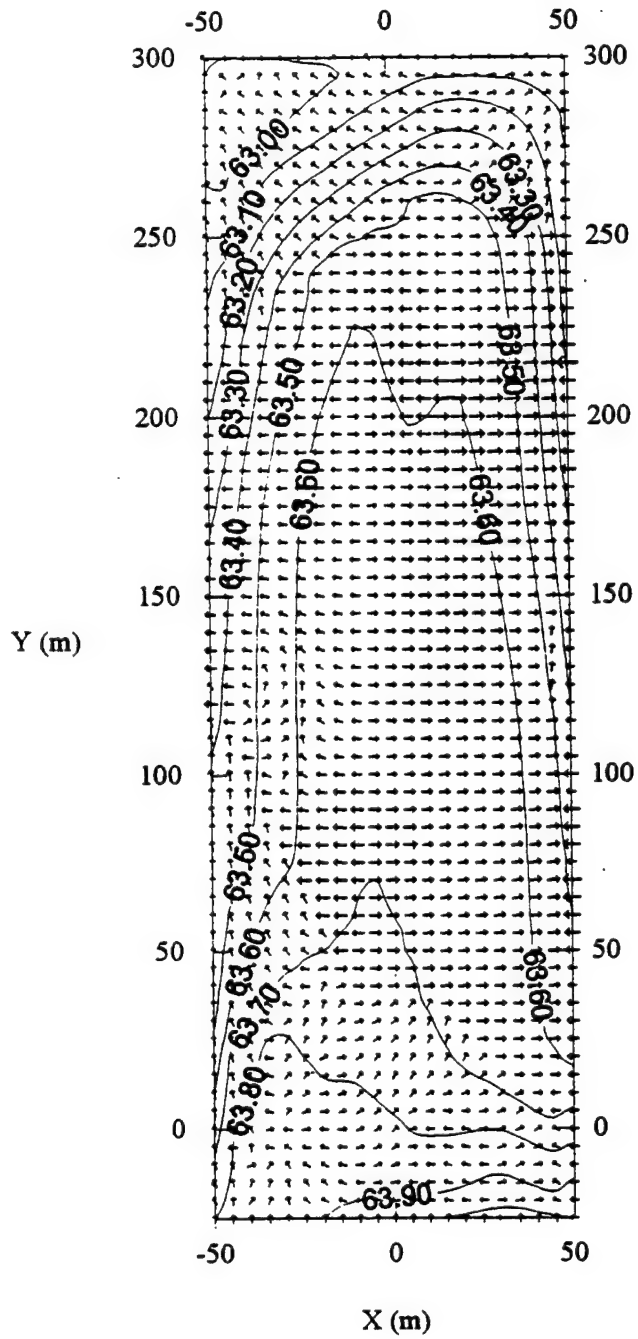


Figure 67. Head and Seepage Velocity in Layer 4, Day 298, M2-8-9, Run 2.

## Heads of Layer 4, Day 298, Run 3 of M2-8-9



**Figure 68. Head and Seepage Velocity in Layer 4, Day 298, M2-8-9, Run 3.**

## Hheads of Layer 4, Day 298, Run 4 of M2-8-9

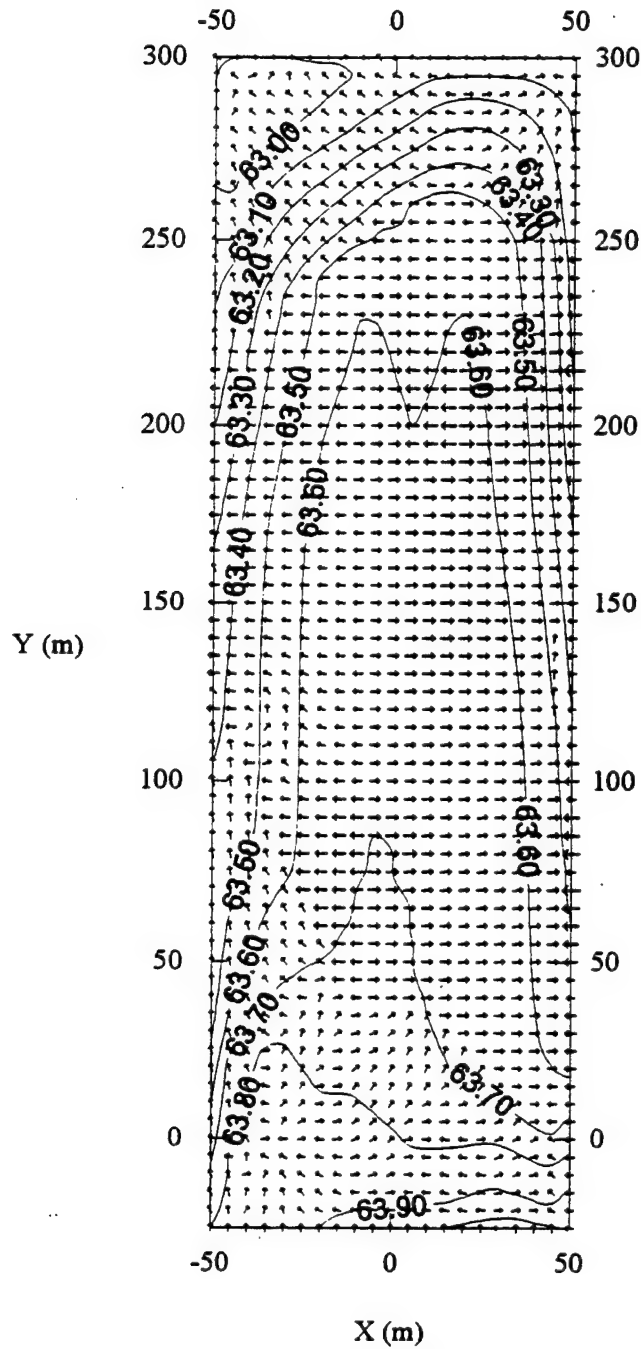
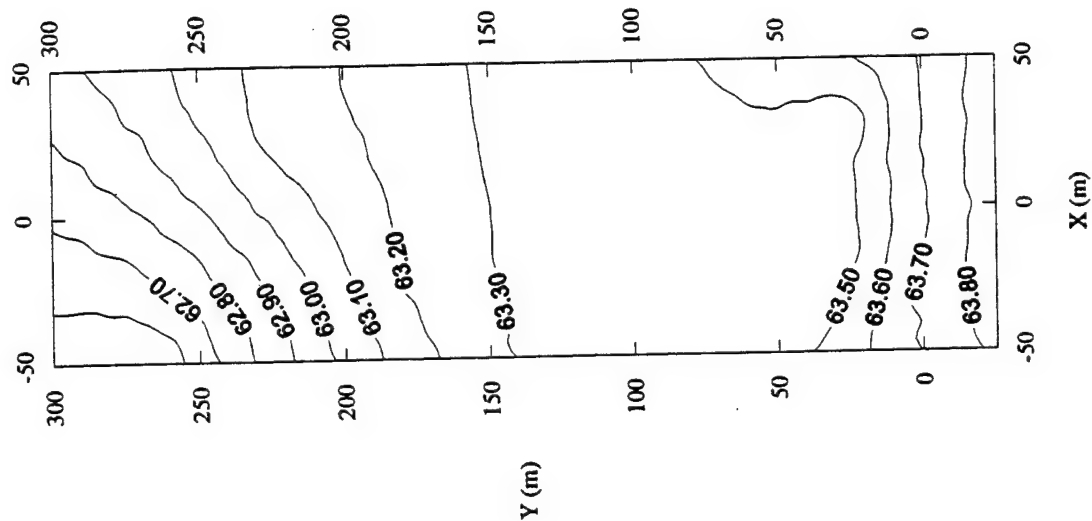


**Figure 69. Head and Seepage Velocity in Layer 4, Day 298, M2-8-9, Run 4.**

153

Lower Screened Heads of April 4, 1991



Upper Screened Heads of April 4, 1991

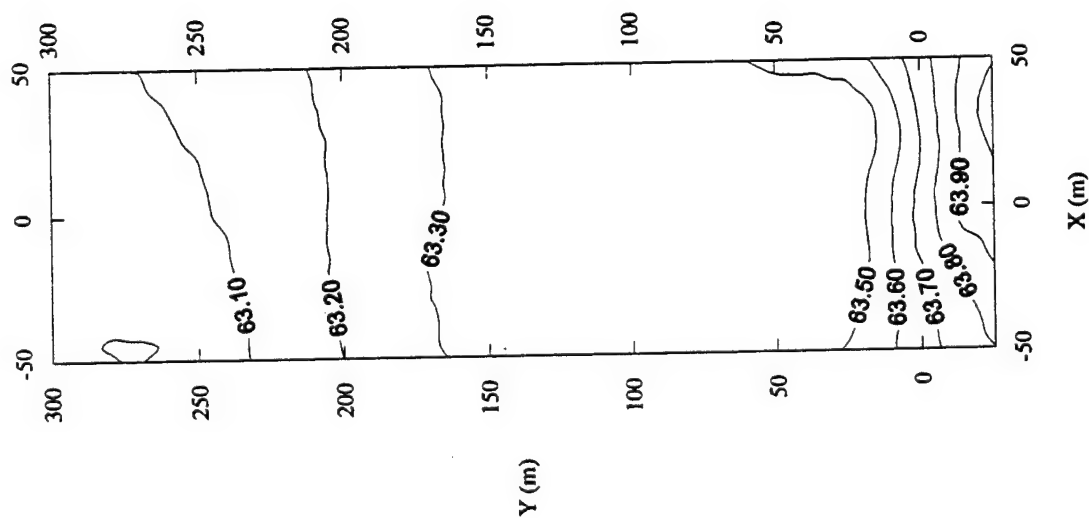


Figure 71. Kriged Observed Heads of April 4, 1991. Left: Upper Level; Right: Lower Level.



# Heads of Layer 4, Day 298, Run M2-8-8

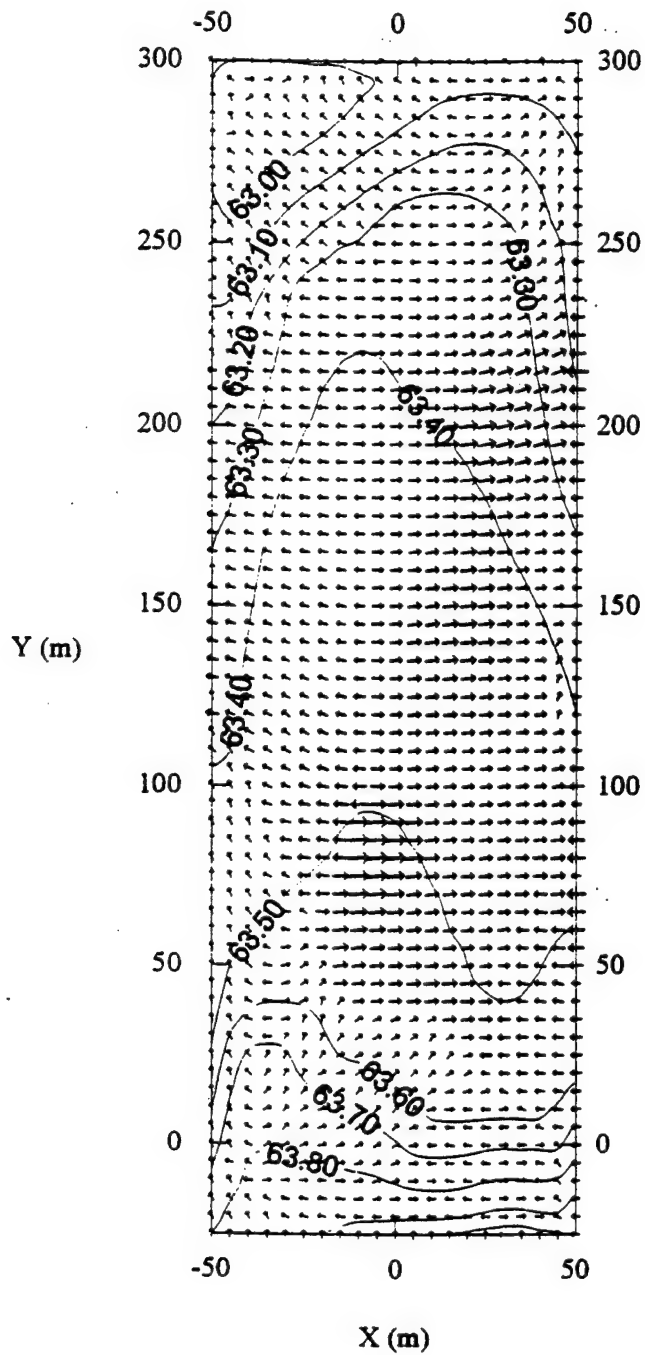


Figure 72. Head and Seepage Velocity in Layer 4, Day 298, M2-8-8.

The transport model was also run for all 5 simulations of M2-8-9 to test the tritium migration against the successful M2-8-8 simulations. The last column of Table 24 indicates how far the plume extended on Day 344. This value is based on the longitudinal spread of the normalized contour of 0.0001. In general as the TRPY factor increased, the plume migrated farther downgradient. However, there was a limit to the value of the anisotropy factor which could be used. The fourth run was the first to see the ill effects of an increasing anisotropy. The simulation became very unstable in the early days and by Day 344 (Figure 73) the errors propagated throughout the entire domain. Intense investigation of the output file created by MT3D shows the errors starting around Day 148, which is in the seventh stress period. Note from Table 12 that the transition from negative to positive net recharge began in Stress Period 7. The combination of skewed conductivities with the reversal of net recharge may have rendered the solution unstable.

The fifth run of simulation M2-8-9 also crashed around Day 148. However, errors of the last two runs began in two separate locations of the domain. Run 4 started to corrupt in Column 21, Row 58, whereas Run 5 started in Column 1, Row 57. Both cells began increasing in concentration faster than their neighbors, essentially creating mass from nothing. Both cells were also on the boundary. Hantush (1966) warns against applying the inverse of Equation (7) to some flow fields. The transformation to an isotropic media may produce an erroneous solution when the transformation of conductivity adversely affects the statement of boundary conditions (Hantush, 1966). Further research is needed in order to properly model the effects of horizontal anisotropy.

Tritium Plume of Layer 4, Day 344, Run 4 of M2-8-9

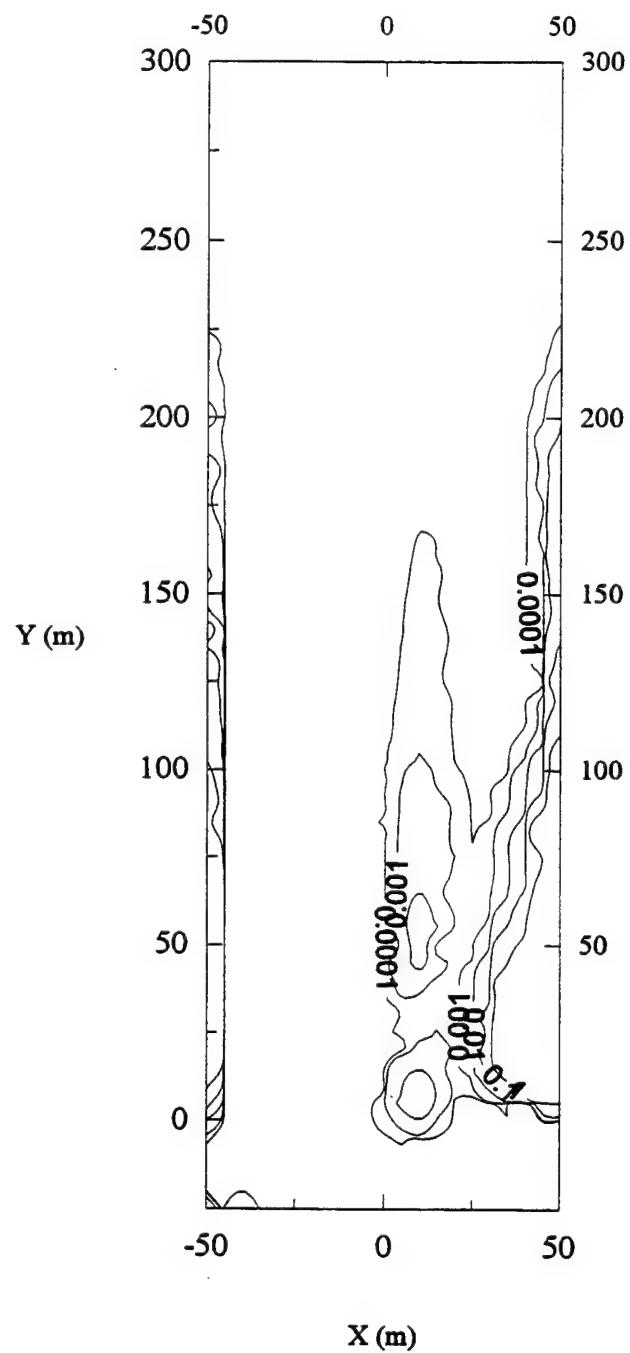


Figure 73. Normalized Tritium Concentration in Layer 4, Day 344, M2-8-9, Run 4.

## SECTION VIII

### DISCUSSIONS

#### A. BUOYANCY EFFECTS

Istok and Humphrey (1995) investigated the possibility of buoyancy-induced flow at small concentrations in a two-well lab experiment. Their study was the first to observe that relatively low density differences ( $\Delta\rho/\rho = 7.5 \times 10^{-5}$ ) may cause significant plume sinking. The test used bromide (Br<sup>-</sup>) with a wide range of injected concentrations (50, 250, 500, 750, and 1000 mg/L). The centroid of each plume sank due to negative buoyancy. The implications may have great significance for numerical modeling, especially for the MADE-2 project since the software used assumes the densities of the tracer solution and the ambient groundwater are equal.

The experiment by Istok and Humphrey (1995) was conducted in a steady-state, homogeneous flow field. The test conditions were designed to ensure horizontal flow with no vertical gradients. The effects of buoyancy-induced flow can be seen more easily in this experiment as ideal conditions were maintained. For the MADE-2 experiment the effects are less obvious. The large-scale heterogeneities combined with the fluctuating water table may mask the buoyancy effects.

The relative densities for the five contaminants were calculated (Table 25), but none separately fell within the range of investigation by Istok and Humphrey (1995). Their combined total of  $1.5 \times 10^{-4}$  does exceed the  $7.5 \times 10^{-5}$  relative density found to cause sinking. Calculations using a coupled flow and transport model are needed to determine whether buoyancy effects were significant in MADE-2. MODFLOW and MT3D are incapable of doing such calculations, but programs like HST3D and SUTRA are.

TABLE 25. RELATIVE DENSITIES OF CONTAMINANTS.

| Contaminant | Relative Density ( $\Delta\rho/\rho$ ) |
|-------------|--|
| Benzene     | $6.8 \times 10^{-5}$                   |
| Naphthalene | $7.2 \times 10^{-6}$                   |
| p-Xylene    | $4.1 \times 10^{-5}$                   |
| o-DCB       | $3.3 \times 10^{-5}$                   |
| Tritium     | $3.8 \times 10^{-12}$                  |
| Total       | $1.5 \times 10^{-4}$                   |

## B. GRID CONVERGENCE

A grid refinement study was attempted in order to determine if the MODFLOW results were independent of horizontal cell size. Based on the general theory of Richardson extrapolation, grid refinement studies are generally accepted in the CFD (Computational Fluid Dynamics) community as a tool to verify the accuracy and solution order of a numerical solution. However, Roache (1993) states that the theory behind the method can be independent of the equations being used and the dimensionality of the problem. One can easily apply the concept to any numerical model as a postprocessor to solutions on two grids with no reference to the codes, algorithms, or governing equations which produced the solutions (Roache, 1993). Therefore it was proposed to study the groundwater flow solution obtained by the MODFLOW code with two or more grid sizes.

Roache (1993) proposes a grid convergence index (GCI) to account for the solution's gridding as well as its order. The idea behind the GCI is to approximately relate the error obtained by an arbitrary grid refinement study to the error that would be obtained by a grid refinement study of the same problem with the same base grid by a second order method ( $p = 2$ )

and grid doubling ( $r = 2$ ). The grid refinement ratio,  $r$ , is the ratio of the coarse grid spacing ( $h_2$ ) to the fine grid spacing ( $h_1$ ):  $r = h_2/h_1$ .

The GCI was derived by calculating the estimated fractional error for the fine grid solution ( $f_1$ ), that would approximately have the same error with  $p = 2$  and  $r = 2$ . The fractional error in Equation (29) is expressed as  $E_1$ .

$$E_1 = \frac{\varepsilon}{r^p - 1} \quad (29)$$

where  $\varepsilon = \frac{(f_2 - f_1)}{f_1}$  (30)

and  $f_2$  is the coarse grid solution. The GCI for the fine grid solution is expressed as

$$GCI_1 = \frac{3 |\varepsilon|}{(r^p - 1)} \quad (31)$$

Notice that when the grid is doubled for a second order problem, the  $GCI = |\varepsilon|$ .

The error estimator of Equation (29) does not indicate whether a good estimate of the solution has been achieved. The error usually sought is one that gives confidence in the solution, or a bound on the error to show if the solution is too high or too low.  $E_1$  does not provide such a confidence interval. However, based on cumulative experience in the CFD community, at least a marginal confidence level exists for the error of Equation (30), obtained by a second order accurate solution and grid doubling. Therefore, GCI relates any grid refinement study to one of  $p = 2$  and  $r = 2$ .

Equation (31) may be evaluated using point-by-point values or solution functionals, such as the integrated Darcy velocity. However, the grid sizes must lie within the asymptotic range (as assumed in the Taylor series expansion on which the Richardson extrapolation is based). This can easily be tested in a fairly straightforward manner, as long as the solution order,  $p$ , is uniform.

If the exact solution model problem is known, then  $p$  can be monitored by

$$E_p = \text{error} / h^p \quad (32)$$

as  $h$  is refined. The consistency of  $E_p$  will verify the order and indicate that the asymptotic range has been achieved. Since this is rarely the case, three grid solutions must be performed and two GCI calculated from the solutions. Equation 33 equates the GCI of the coarse-intermediate calculation to the fine-intermediate calculation and indicates that the asymptotic range has been achieved.

$$GCI_{23} \approx r^p GCI_{12} \quad (33)$$

where  $GCI_{23}$  is the grid convergence index between an intermediate grid solution and a coarse solution

$GCI_{12}$  is the grid convergence index between a fine grid solution and an intermediate solution

The technique was applied to several MODFLOW simulations by using different grid spacings. The standard flow simulations used a grid spacing of 5 x 5 meter cells in the XY plane. The solution of a finer grid using a 3 x 3 meter cell would not converge, so only coarser grid spacings were used. Additional simulations were conducted by increasing the grid size to a 10 x 10 and 15 x 15 meter cells. Vertical discretization was not coarsened; the MODFLOW layers were based on stratigraphy of the site and were left intact for the grid refinement study (as suggested in conversation with Dr. Roache). To test the GCI of each simulation, the heads were extracted for piezometers P54A, P55A, and P55B at day 270. Table 26 lists the heads from each grid.

TABLE 26. EXTRACTED HEADS FOR VARIOUS GRID SIZES.

| Well              | P54A     | P55A     | P55B     | Average RMS |
|-------------------|----------|----------|----------|-------------|
| $\Delta x = 5$ m  | 64.285 m | 64.204 m | 64.379 m | 0.20561     |
| $\Delta x = 10$ m | 64.34 m  | 64.36 m  | 64.36 m  | 0.20817     |
| $\Delta x = 15$ m | 64.35 m  | 64.38 m  | 64.39 m  | 0.23136     |

The averaged RMS differences of heads were also tested for overall grid convergence. The GCIs were calculated in EXCEL and Table 27 lists the results.

TABLE 27. GCI VALUES.

|                         | <b>P54A</b> | <b>P55A</b> | <b>P55B</b> | <b>Average RMS</b> |
|-------------------------|-------------|-------------|-------------|--------------------|
| <b>GCI<sub>12</sub></b> | 0.00342     | 0.0097      | 0.00118     | 0.0498             |
| <b>GCI<sub>23</sub></b> | 0.00037     | 0.0007      | 0.00112     | 0.2673             |

Only piezometer P55B lies in the asymptotic range. The other GCI calculations show a difference of at least 1000% (ten times greater), thus indicating that the solutions do not lie in the asymptotic range. Therefore the GCI calculations are meaningless at these sites. The GCI calculations for P55B on the other hand indicates a 0.118% difference between the fine and intermediate grids and a 0.112% difference between the intermediate and coarse grids. This implies that the difference in head due to using the different grid spacings is negligible at the location of piezometer P55B. The GCI was only calculated for head differences, therefore nothing can be inferred about the convergence of other calculated parameters such as velocities.

Several errors could contribute to the results at the locations where the GCI did not lie in the asymptotic range. First, Roache (1993) mentioned using geostatistical methods to generate grid-block property variations with specified statistical parameters, and the question of whether the property fields should change as a result of a changing grid structure, or be fixed. These head solutions assumed changes in the geological variables as the grid became coarser. The hydraulic conductivity, for example, was re-kriged for every changing grid size. This method was much easier to simulate, but probably contributed to the different head solutions being out of the asymptotic range. Secondly, the numerical convergence criterion in the flow model was constant for all three solutions. This may cause over-confidence in the coarser grid solution. Lastly, machine precision may have caused errors to propagate throughout the simulations. Future simulations should use double precision in the modeling to reduce machine-related errors.



Since none of the solutions were in the asymptotic range, an error based on the grid spacing calculations could not be computed. The calculated GCIs were virtually meaningless. Future simulations should use fixed geological property fields, especially hydraulic conductivity.

## SECTION IX

### CONCLUSION

A numerical model of the MADE-2 experiment was created to simulate groundwater flow and contaminant transport using the public domain programs MODFLOW and MT3D. The following conclusions were reached.

1. The use of public domain software on a Pentium-class personal computer to model an experiment such as MADE-2 is very practical. MODFLOW, which solved the groundwater flow equation for the hydraulic heads, did a good job in matching the observed phenomena. The maximum average RMS difference for any simulation was 0.23 meters. This translates to an average 23 cm difference overall between heads of the observed and simulated within a 33000 m<sup>2</sup> domain.

The contaminant transport model, solved by MT3D, was less successful. The final agreement of the model with the observations was good, but the necessary assumptions concerning horizontal anisotropy have not been justified. Of course the simulated plume of any contaminant does not match exactly with the observed. Small scale heterogeneities in the field are impossible to reproduce using geostatistical techniques with a finite data set. Additional hydraulic conductivity measurements, however, would probably not change the results dramatically.

2. To accurately model the transport of tritium, a horizontal anisotropy factor which varied by position had to be introduced. Earlier modeling efforts, which assumed isotropic conditions, did not allow the plume to migrate as far as the observed plume. Pump test AT-2 suggested horizontal anisotropy with the major principal axis 35° west of north. In Boggs et al (1992), Young (1995), and other papers, a meandering abandoned stream channel was hypothesized, which cut through the MADE-2 site at approximately 30° east of north. Realistic plume predictions were achieved only by assuming the channel did in fact exist and was located as predicted. However, the assumed principal axes were not aligned with the channel axis or with

the AT-2 drawdown ellipses. The assumed major principal axis was aligned with the Y axis, 12° west of north. In addition, the assumed anisotropy factor implied higher conductivities than were measured with the borehole flow meter, and was higher than any found in the literature. In short, the horizontal anisotropy needed to match the observed plumes is not fully supported by the field data.

3. Knowing the plumes, *a priori*, was essential in accurately modeling the experiment. Without such knowledge it would have been impossible to estimate the values of dispersion or anisotropy needed to push the plume's tail into the far field. This is very discouraging, as the purpose was to predict the plume's movement, and not to just reproduce it. Future experiments at the MADE site will at least know something about the values of dispersion or anisotropy. However, modelers of other extremely heterogeneous sites will not be so fortunate. The tools used in this study do not provide a true predictive capability.

## REFERENCES

- M.P. Anderson and W.W. Woessner, 1992. Applied Groundwater Modeling, Academic Press, New York, p. 2.
- J. Bear, 1972. Dynamics of Fluids in Porous Media, Dover Publications, New York, p.123-124
- P.B. Bedient, H.S. Rifai, C.J. Newell, 1994. Ground Water Contamination, Prentice Hall, New Jersey, p.175.
- J.M. Boggs, S.C. Young, D.J. Benton, and Y.C. Chung, 1990. Hydrological Characterization of the MADE Site, EPRI Topical Report EN-6915, Electric Power Research Institute, Palo Alto, California
- J.M. Boggs, S.C. Young, L. Beard, L.W. Gelhar, K.H. Rehfeldt, and E.E. Adams, 1992. "Field Study of Dispersion in a Heterogeneous Aquifer 1. Overview and Site Description", Water Resources Research, 28, 3281-3291.
- J.M. Boggs, L.M. Beard, S.E. Long, W.G. MacIntyre, C.P. Antworth, and T.B. Stauffer, 1993. Database for the Second Macrodispersion Experiment (MADE-2), Electric Power Research Institute, TR-102072.
- J.M. Boggs, L.M. Beard, W.R. Waldrop, T.B. Stauffer, W.G. MacIntyre, and C.P. Antworth, 1993. Transport of tritium and Four Organic Compounds During a Natural-Gradient Experiment (MADE-2), EPRI Final Report TR-101998.
- E. Englund and A. Sparcs, 1991. Geo-EAS 1.2.1 Geostatistical Environmental Software User's Guide, U.S. EPA 600/8-91/008.
- R.A. Freeze and J.A. Cherry, 1979. Groundwater, Prentice Hall, New Jersey, p.147.
- D.D. Gray, 1992. Preliminary Numerical Model of Groundwater Flow and Transport at the MADE-2 Site, U.S. Air Force Summer Faculty Research Program (SFRP) Reports, Volume 6, pp. 11-1 through 11-19, Air Force Office of Scientific Research, Bolling AFB, Washington, DC.
- D.D. Gray, 1993. Numerical Model of Groundwater Flow and Transport at the MADE-2 Site, U.S. Air Force Summer Faculty Research Program (SFRP) Reports, Volume 2, pp. 21-1 through 21-19, Air Force Office of Scientific Research, Bolling AFB, Washington, DC. NTIS ADA 278 693
- D.D. Gray and D.F. Rucker, 1994. Improved Numerical Modeling of Groundwater Flow and Transport at the MADE-2 Site, U.S. Air Force SFRP Reports, Volume 7, pp. 16-1 through 16-20, Air Force Office of Scientific Research, Bolling AFB, Washington, DC.

M.S. Hantush, 1966. "Wells in Homogeneous Anisotropic Aquifers", Water Resources Research, 2, 273-279.

M.C. Hill, 1990. Preconditioned Conjugate Gradient 2 (PCG2), A Computer Program for Solving Groundwater Flow Equations, U.S. Geological Survey, Water-Resources Investigations Report 90-4048.

E.H. Issaaks and R.M. Srivastava, 1989. An Introduction to Applied Geostatistics, Oxford University Press, New York.

J.D. Istock and M.D. Humphrey, 1995. "Laboratory Investigation of Buoyancy-Induced Flow (Plume Sinking) During Two-Well Tracer Tests", Ground Water, 33, 597-604

M. Koch, 1994. Application of the MT3D Solute transport Model to the MADE-2 Site, U.S. Air Force SFRP Reports, Volume 2, pp. 22-1 through 22-20, Air Force Office of Scientific Research, Bolling AFB, Washington, DC.

D.R. LeBlanc, S.P. Garabedian, K.M. Hess, L.W. Gelhar, R.D. Quadri, K.G. Stollenwerk, and W.W. Wood, 1991. "Large-scale Natural Gradient Tracer Test in Sand and Gravel, Cape Cod, Massachusetts, 1, Experimental Design and Observed Tracer Movement", Water Resources Research, 27 (5), 895-910.

M.L. Maslia and R.B. Randolph, 1987. Methods and Computer Program Documentation for Determining Anisotropic Transmissivity Tensor Components of Two-Dimensional Groundwater Flow, U.S. Geological Survey Water-Supply Paper 2308.

M.G. McDonald and A.W. Harbaugh, 1988. Techniques of Water-Resources Investigations of the U.S. Geological Survey, Chapter A1, A Modular Three-Dimensional Finite-Difference Groundwater Flow Model, U.S. Government Printing Office, Washington DC.

M.G. McDonald, A.W. Harbaugh, B.R. Orr, and D.J. Ackerman, 1991. A Method for Converting No-Flow Cells to Variable Head Cells for the U.S. Geological Survey Modular Finite-Difference Groundwater Flow Model, U.S. Geological Survey Open File Report 91-536.

W.G. MacIntyre, J.M. Boggs, C.P. Antworth, and T.B. Stauffer, 1993. "Degradation Kinetics of Aromatic Organic Solutes Introduced Into a Heterogeneous Aquifer", Water Resources Research, 29, 4045-4051.

D.W. Pollock, 1989. Documentation of Computer Programs to Compute and Display Pathlines from the U. S. Geological Survey Modular Three-Dimensional Finite-Difference Groundwater Flow Model, Open File Report 89-381, U. S. Geological Survey, Reston Virginia.

K.R. Rehfeldt, P. Hufschmied, L.W. Gelhar, M. E. Schaefer, 1989. Measuring Hydraulic Conductivity with the Borehole Flowmeter, EPRI Topical Report EN 6911.

K.R. Rehfeldt, J.M. Boggs, and L.W. Gelhar, 1992. "Field Study of Dispersion in a Heterogeneous Aquifer 3. Geostatistical Analysis of Hydraulic Conductivity", Water Resources Research, 28, 3309-3324.

P.J. Roach, 1993. "A Method for Uniform Reporting of Grid Refinement Studies", FED-Vol. 158, Quantification of Uncertainty in Computational Fluid Dynamics, ASME, 109-120

D.F. Rucker, 1995. An Anisotropic Modeling Study of the MADE-2 Site, Air Force Summer Faculty Research Program (SFRP) Reports, in press.

T.B. Stauffer, C.P. Antworth, R.G. Young, W.G. MacIntyre, J.M. Boggs, and L.M. Beard, 1994. Degradation of Aromatic Hydrocarbons in an Aquifer During a Field Experiment Demonstrating the Feasibility of Remediation by Natural Attenuation, U. S. Air Force, Armstrong Laboratory, AL/EQ-TR-1993-0007.

E.A. Sudicky, 1986. "A Natural Gradient Experiment on Solute Transport in a Sand Aquifer: Spatial Variability of Hydraulic Conductivity and Its Role in the Dispersion Process", Water Resources Research, 24 (4), 566-578.

S.C. Young, 1994. "The Use of a Depositional Model for Interpreting Pumping Tests in a Heterogeneous Unconfined Aquifer. Part I: Multi-Well Aquifer Tests", in press.

S.C. Young, 1995. "Characterization of High-K Pathways by Borehole Flowmeter and Tracer Tests", Water Resources Research, 33, 311-318.

S.C. Young and H.S. Pearson, 1995. "The Electromagnetic Borehole Flowmeter: Description and Application", Ground Water Monitoring Review, Fall 1995, 138-147.

C. Zheng, 1990. MT3D, A Modular Three-Dimensional Transport Model for Simulation of Advection, Dispersion, and Chemical Reactions of Contaminants in Groundwater Systems, prepared for U.S. EPA Robert S. Kerr Environmental Research Laboratory, Ada, Oklahoma, by S.S. Papadopoulos & Associates, Inc., Rockville, Maryland.

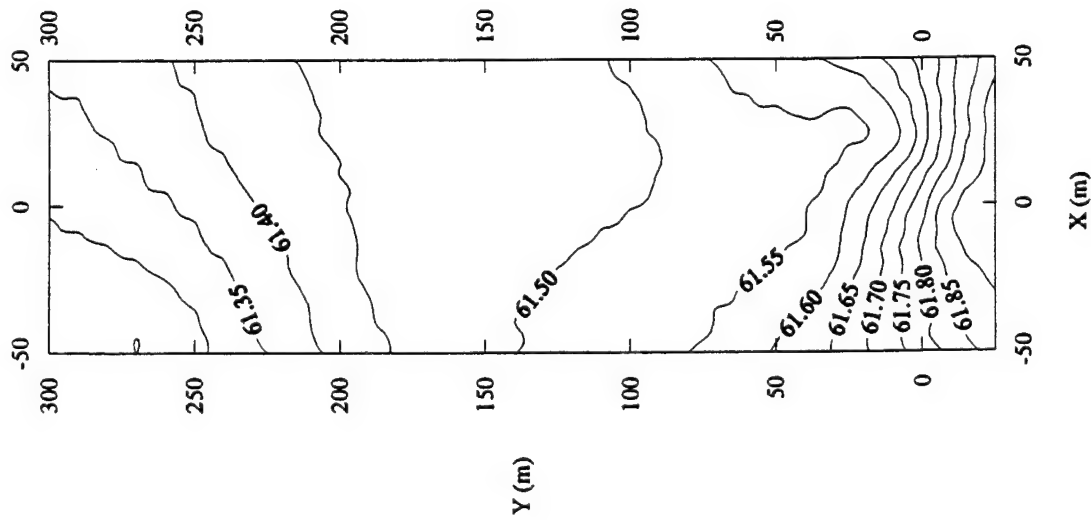
C. Zheng, J. Jiao, and C. J. Neville, 1994. "Numerical Simulation of a Large-Scale Tracer Test in a Strongly Heterogeneous Aquifer", Invited Presentation, American Geophysical Union, 1994 Annual Meeting.

**APPENDIX A**

**KRIGED OBSERVED HEAD SURVEYS**

(See Figure 13 for June 19, 1990, and Figure 14 for March 18, 1991.)

Upper Screened Heads of July 23, 1990



Lower Screened Heads of July 23, 1990

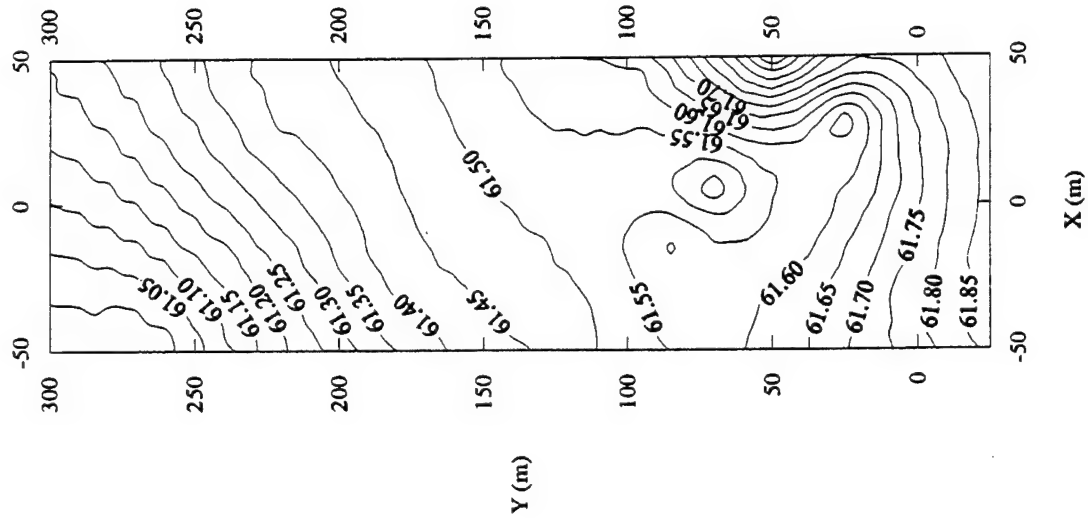
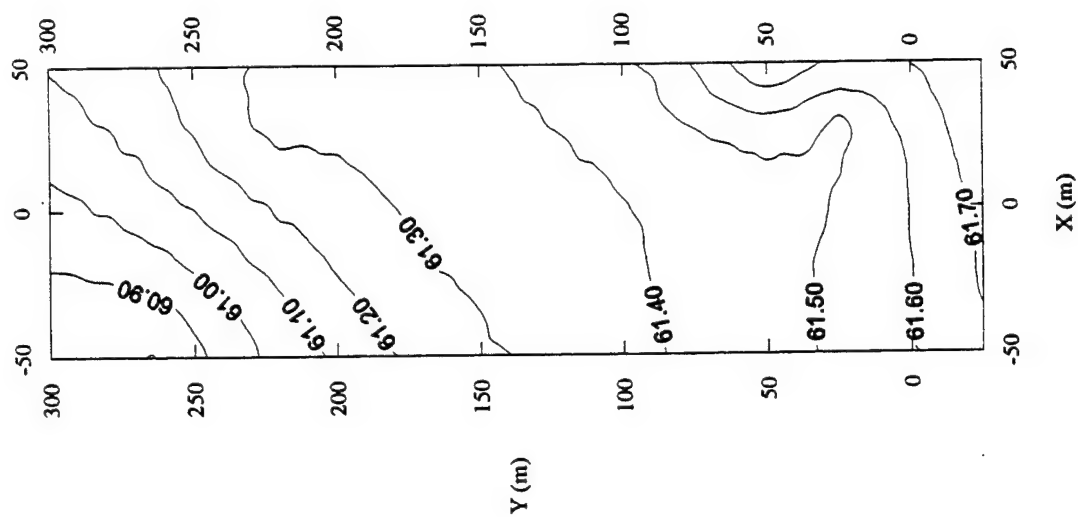


Figure A-1. Upper and Lower Krige Heads of July 23, 1990.



Lower Screened Heads of August 13, 1990



Upper Screened Heads of August 13, 1990

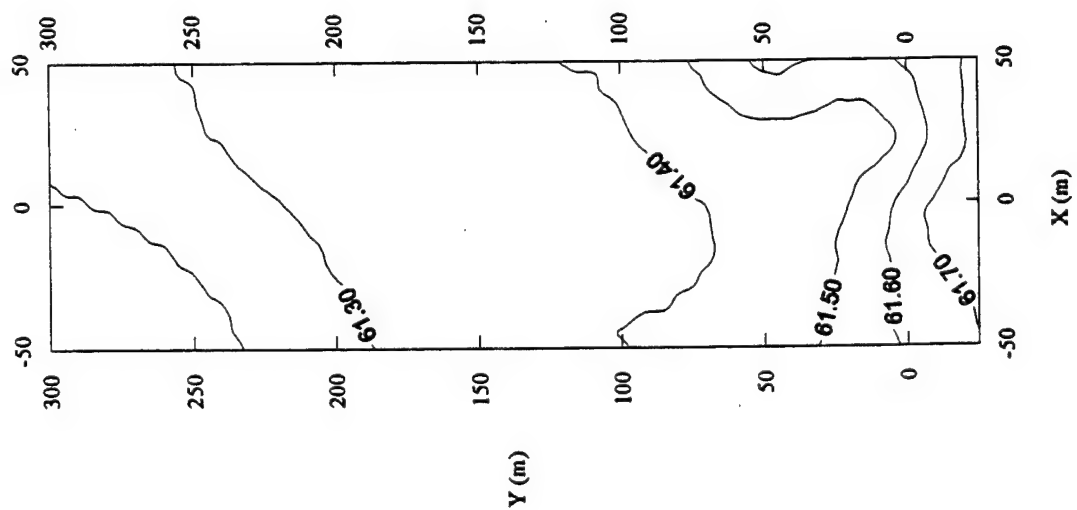
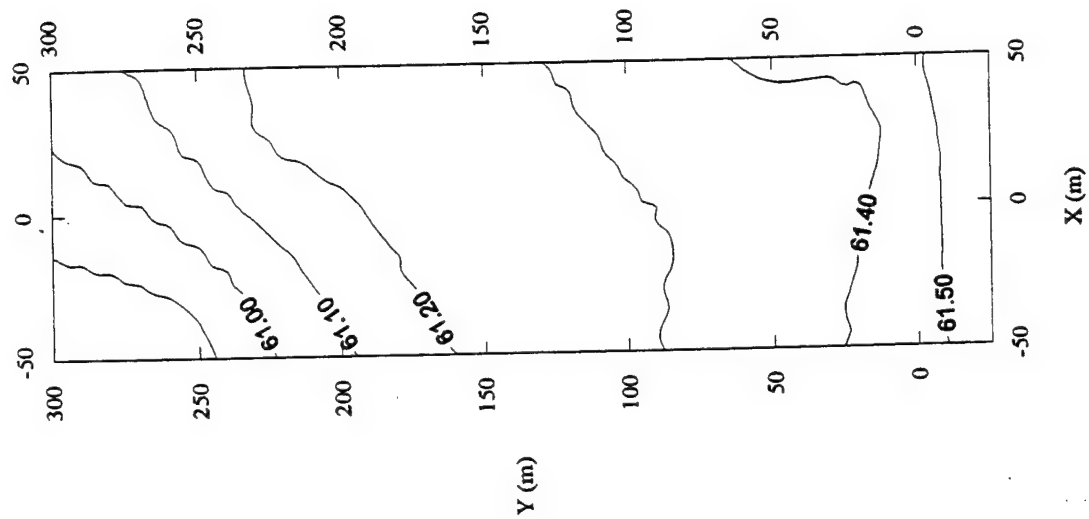


Figure A-2. Upper and Lower Kriged Heads of August 13, 1990.

Lower Screened Heads of September 17, 90



Upper Screened Heads of September 17, 1990

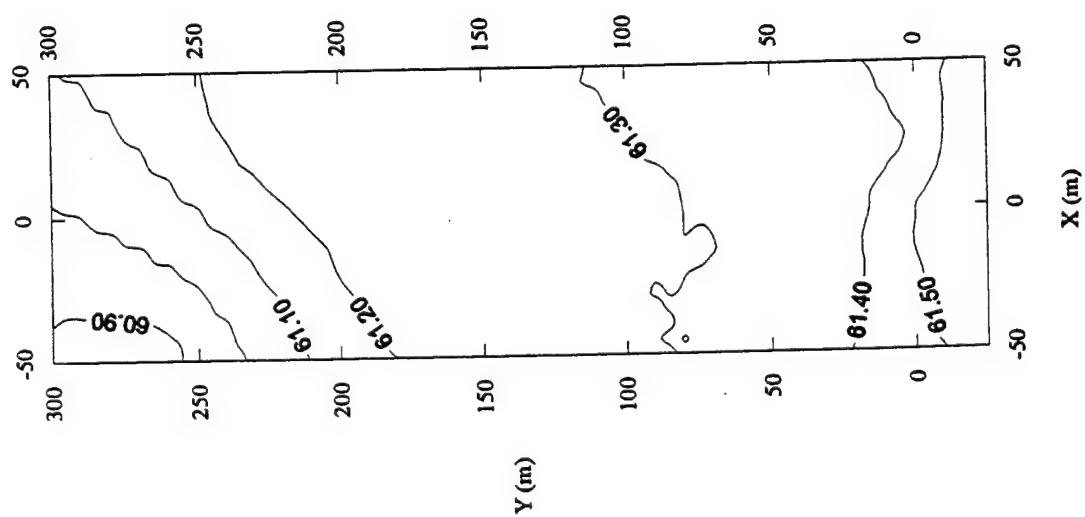
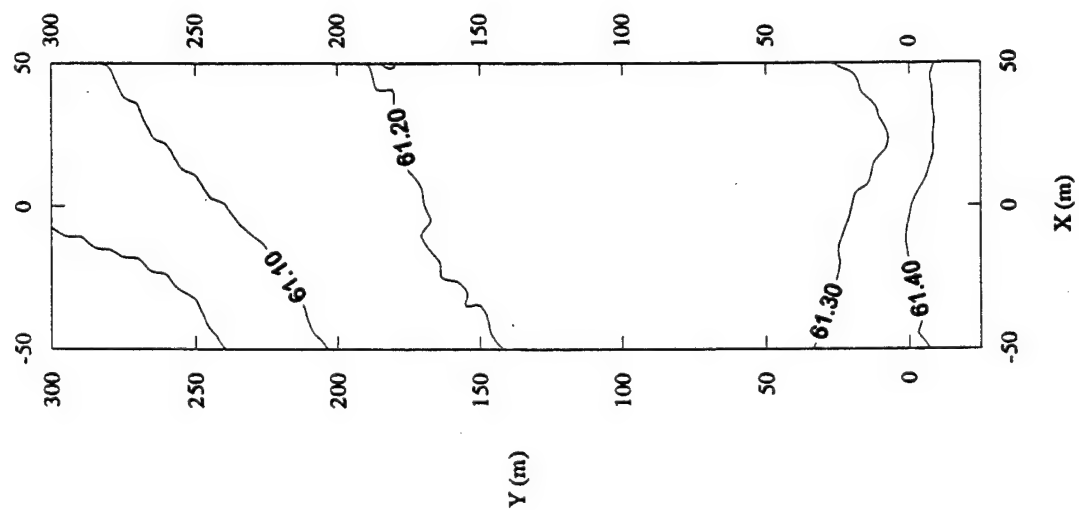


Figure A-3. Upper and Lower Kriged Heads of September 17, 1990.

Upper Screened Heads of October 15, 1990



Lower Screened Heads of October 15, 1990

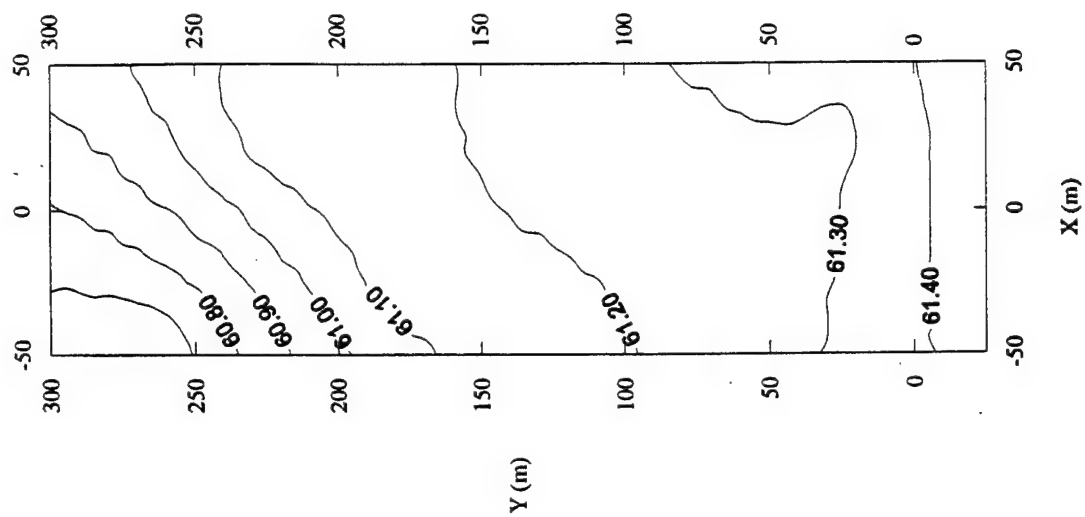
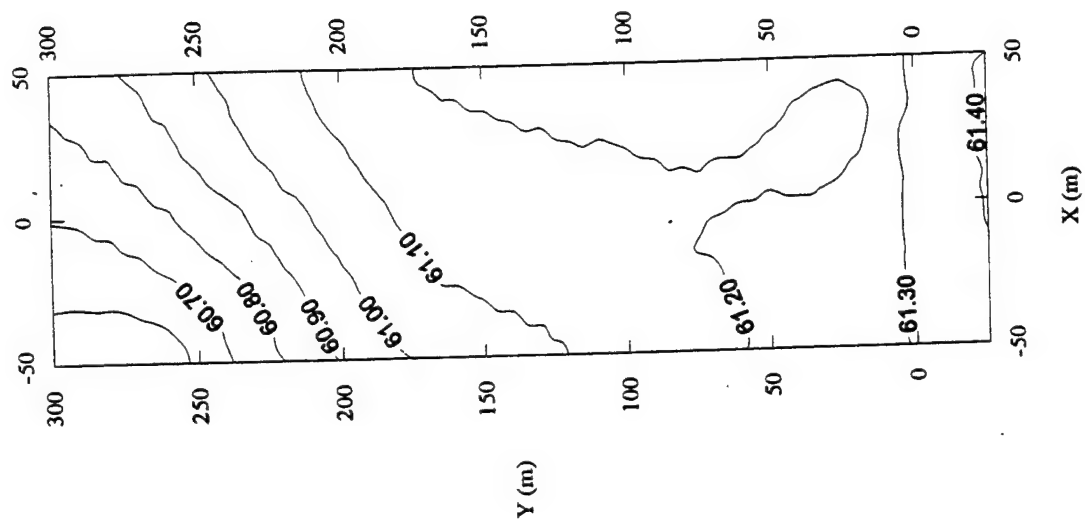


Figure A-4. Upper and Lower Kriged Heads of October 15, 1990.

Lower Screened Heads of November 7, 1990



Lower Screened Heads of November 7, 1990

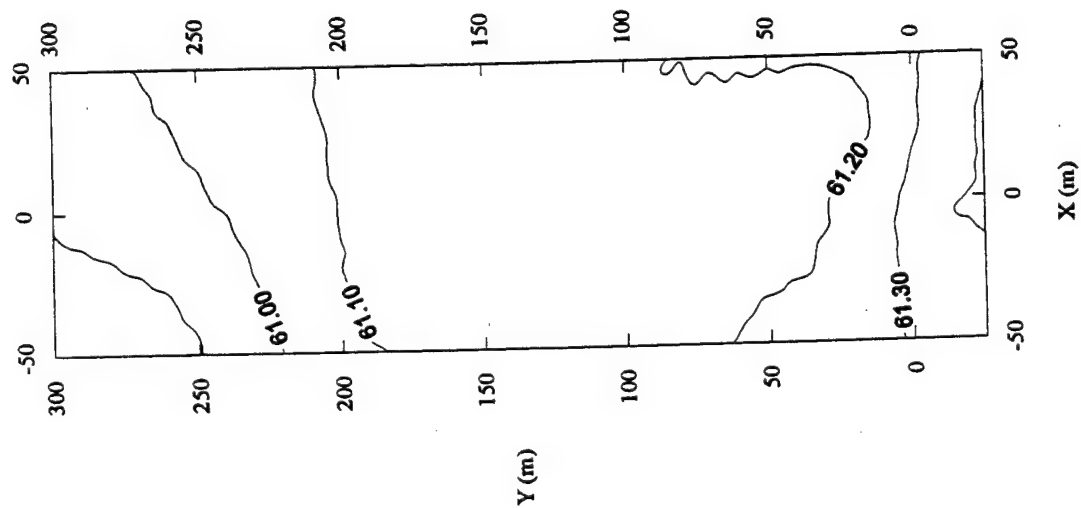
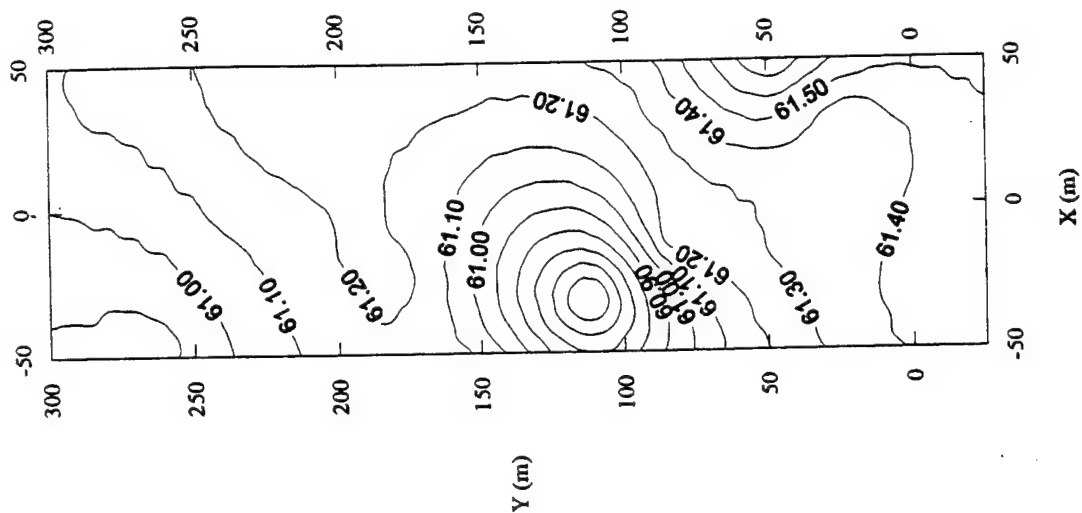


Figure A-5. Upper and Lower Kriged Heads of November 7, 1990.

Lower Screened Heads of December 5, 1990



Upper Screened Heads of December 5, 1990

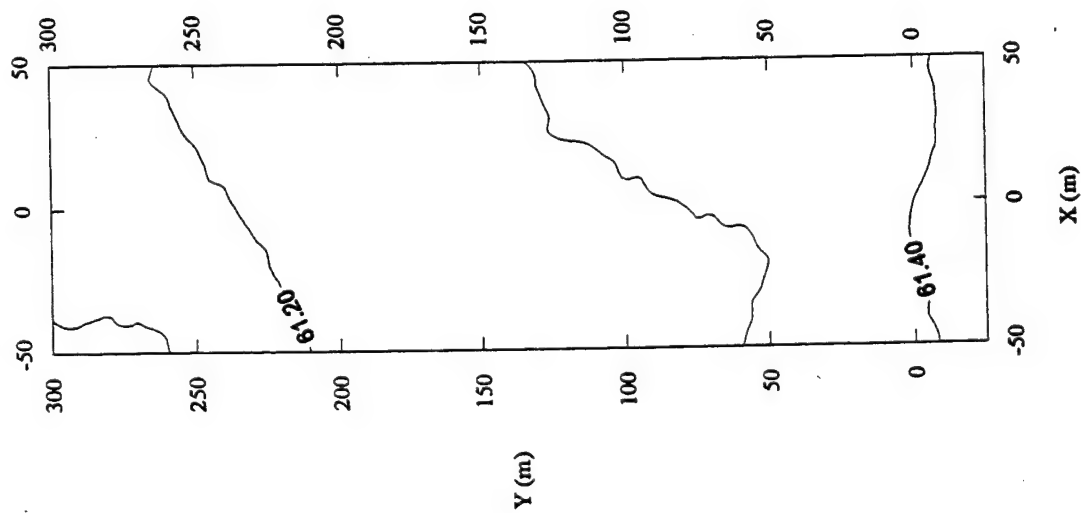
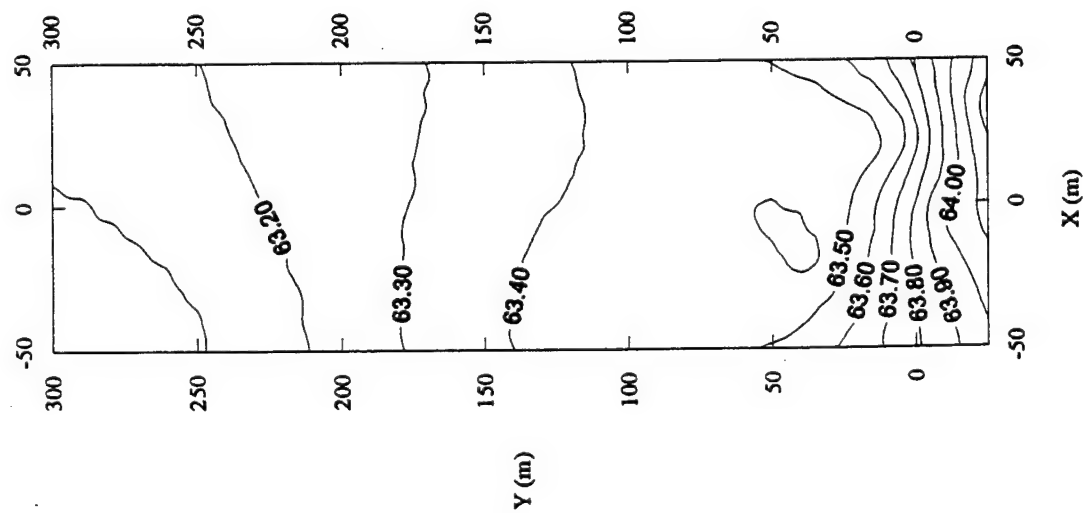


Figure A-6. Upper and Lower Kriged Heads of December 5, 1990.

Upper Screened Heads of January 8, 1991



Lower Screened Heads of January 8, 1991

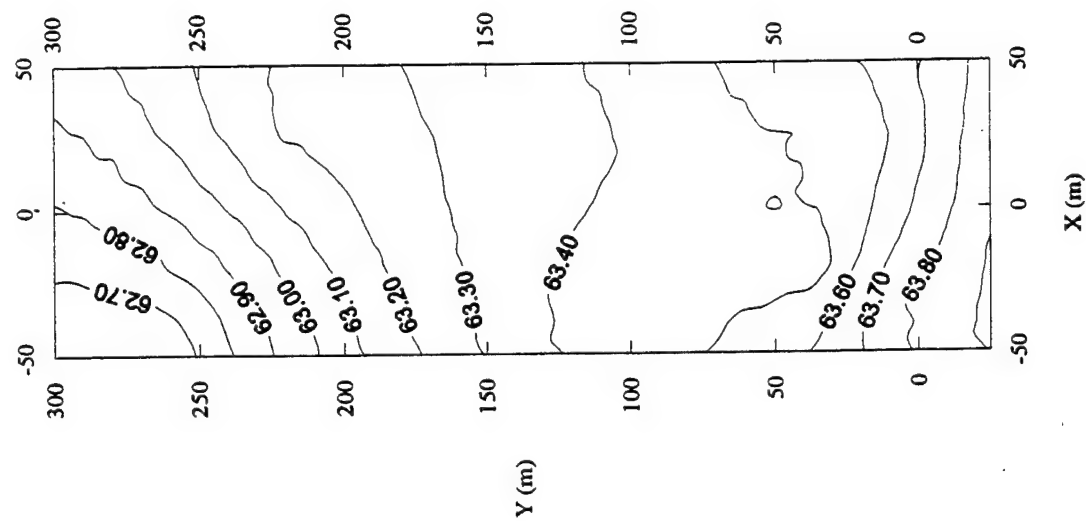
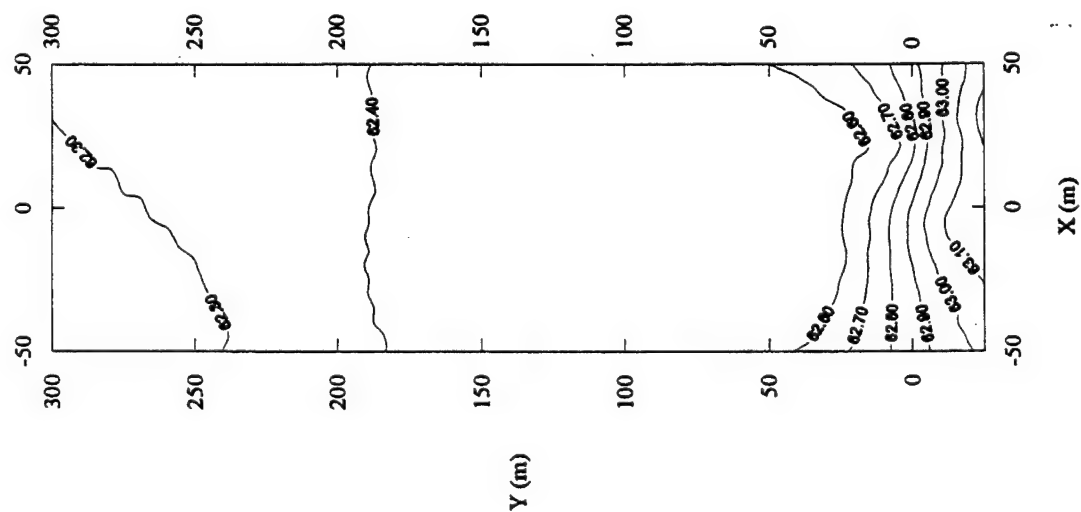


Figure A-7. Upper and Lower Kriged Heads of January 8, 1991.

Upper Screened Heads of February 8, 1991



Lower Screened Heads of February 8, 1991

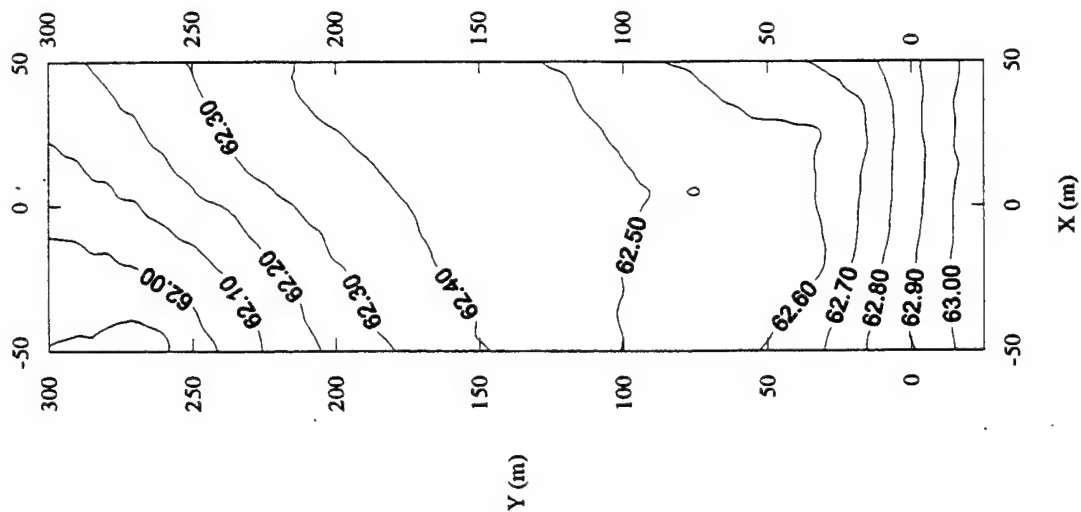
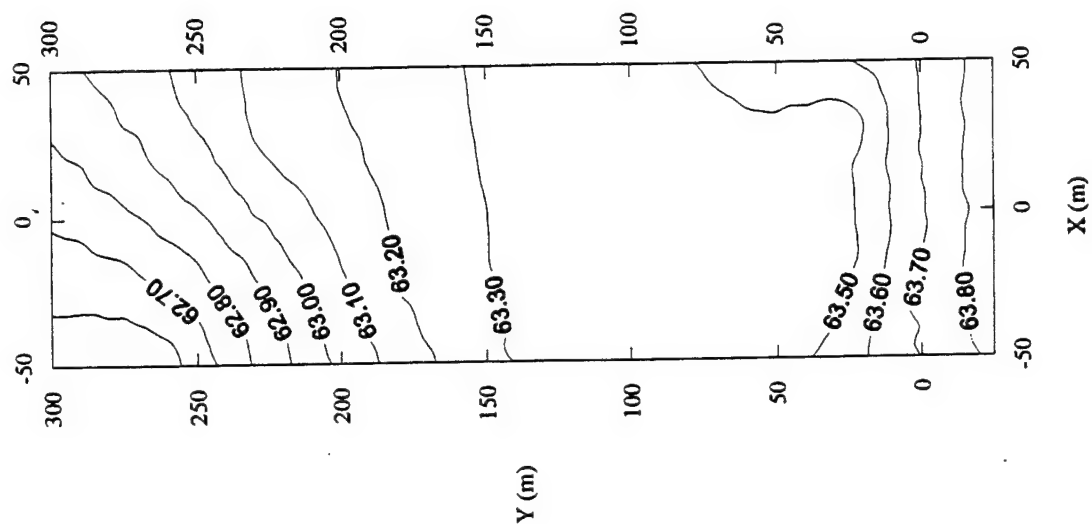


Figure A-8. Upper and Lower Kriged Heads of February 8, 1991.

Lower Screened Heads of April 4, 1991



Upper Screened Heads of April 4, 1991

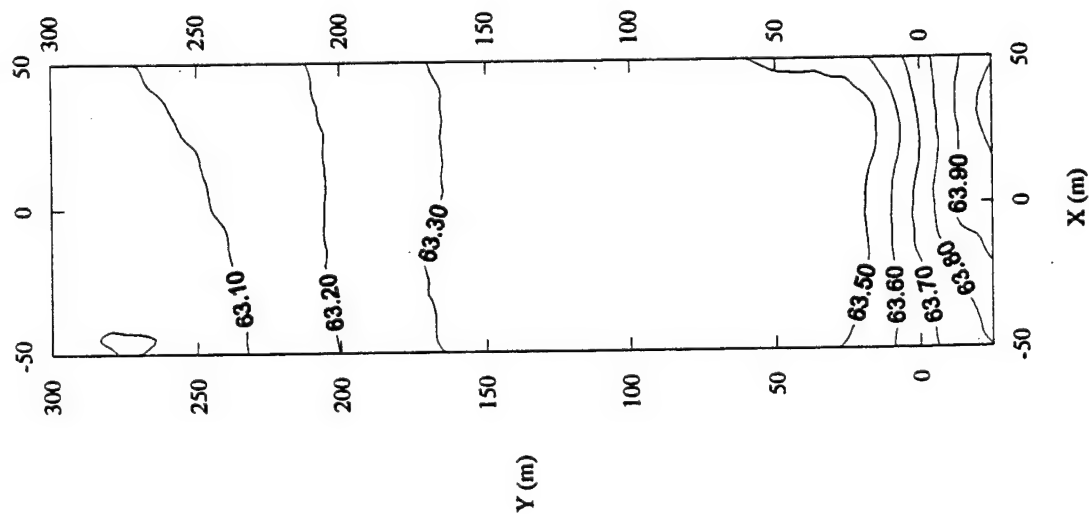
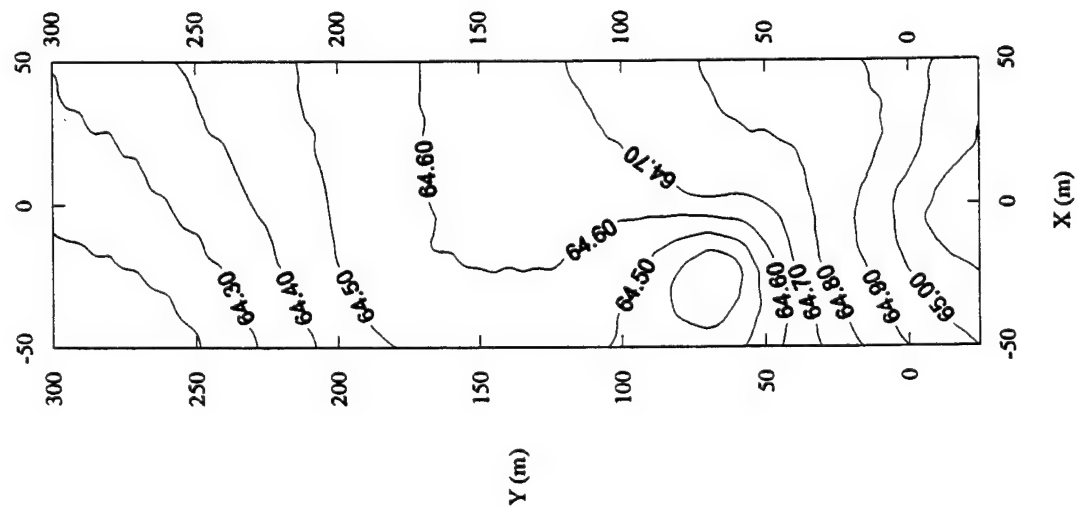


Figure A-9. Upper and Lower Kriged Heads of April 4, 1991.



Upper Screened Heads of May 10, 1991



Lower Screened Heads of May 10, 1991

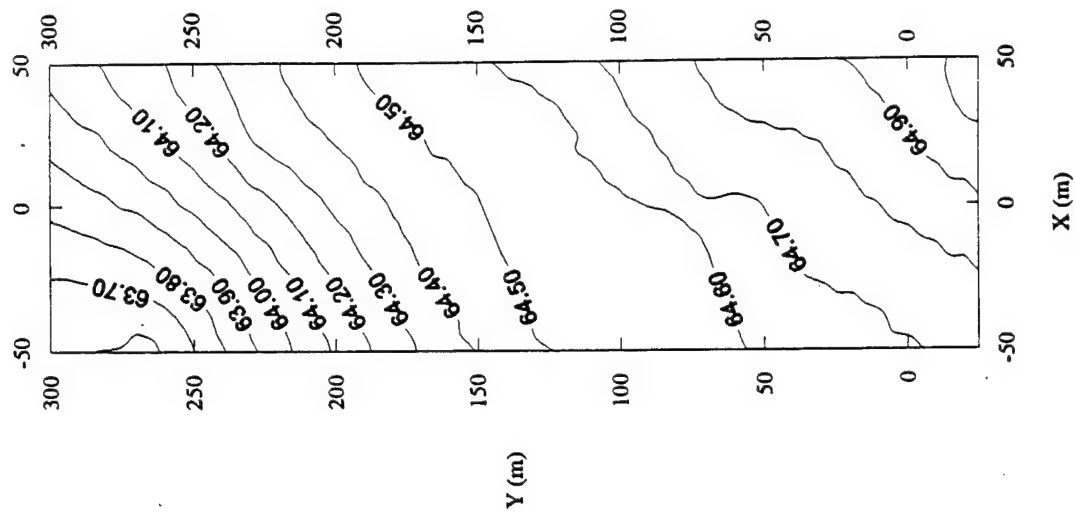
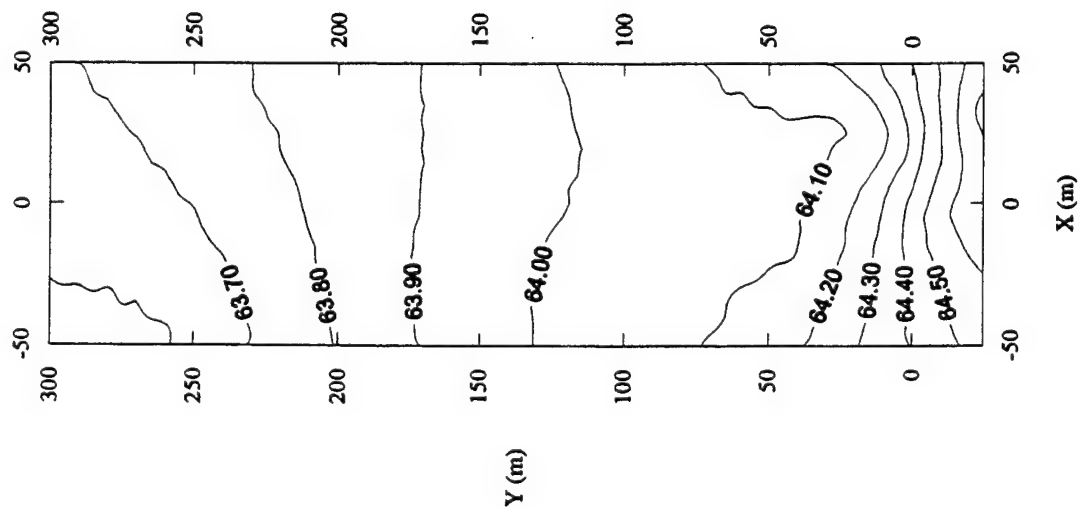


Figure A-10. Upper and Lower Kriged Heads of May 10, 1991.

Upper Screened Heads of May 20, 1991



Lower Screened Heads of May 20, 1991

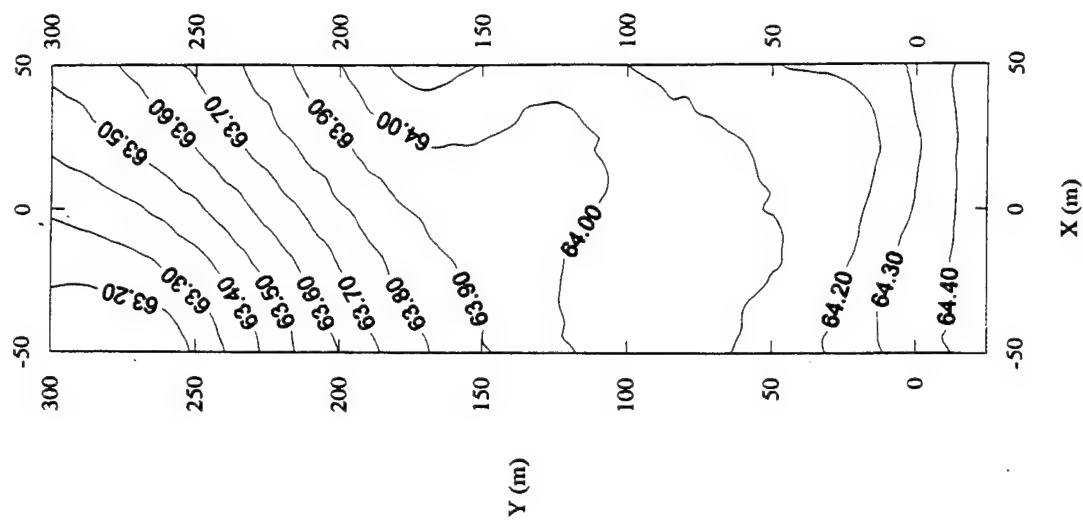
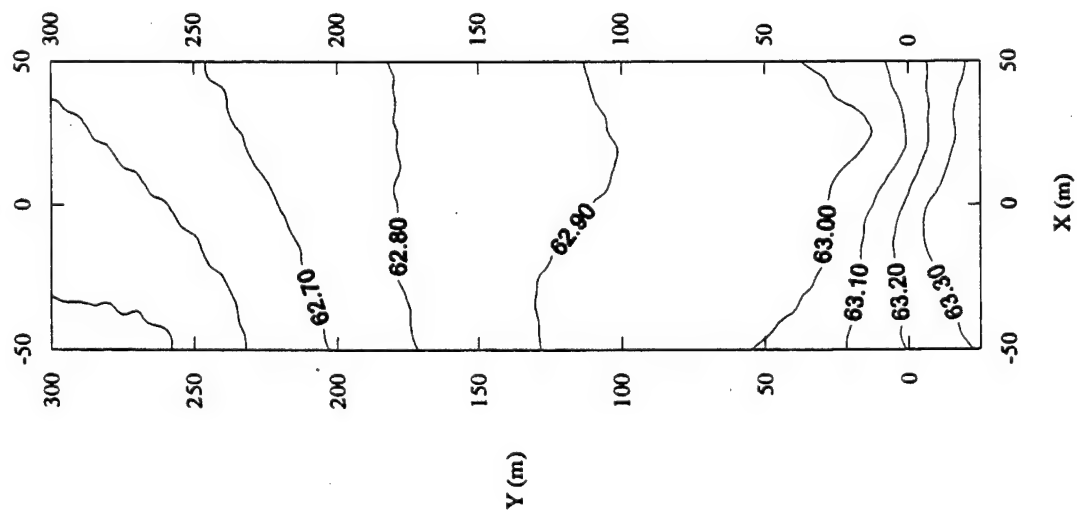


Figure A-11. Upper and Lower Kriged Heads of May 20, 1991.

Upper Screened Heads of June 13, 1991



Lower Screened Heads of June 13, 1991

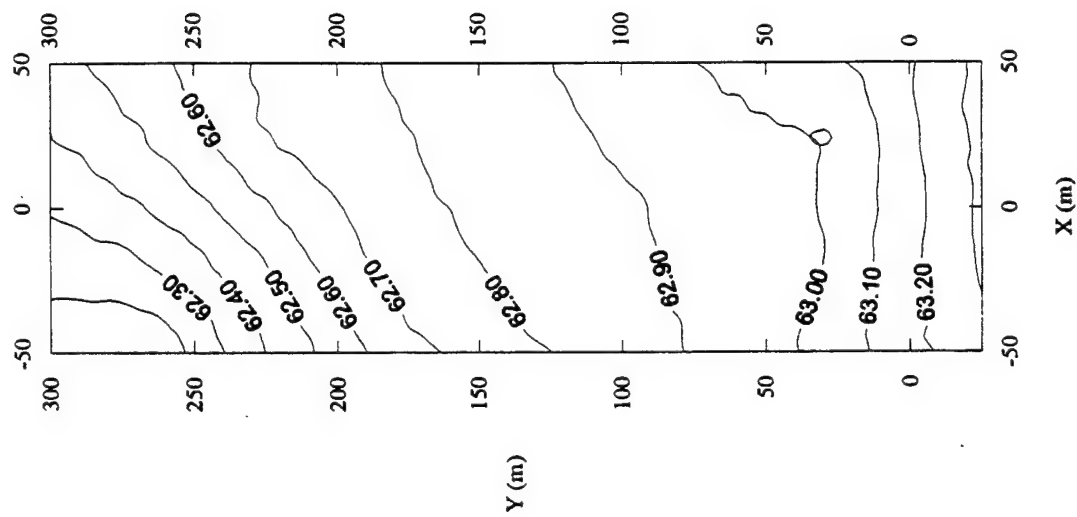
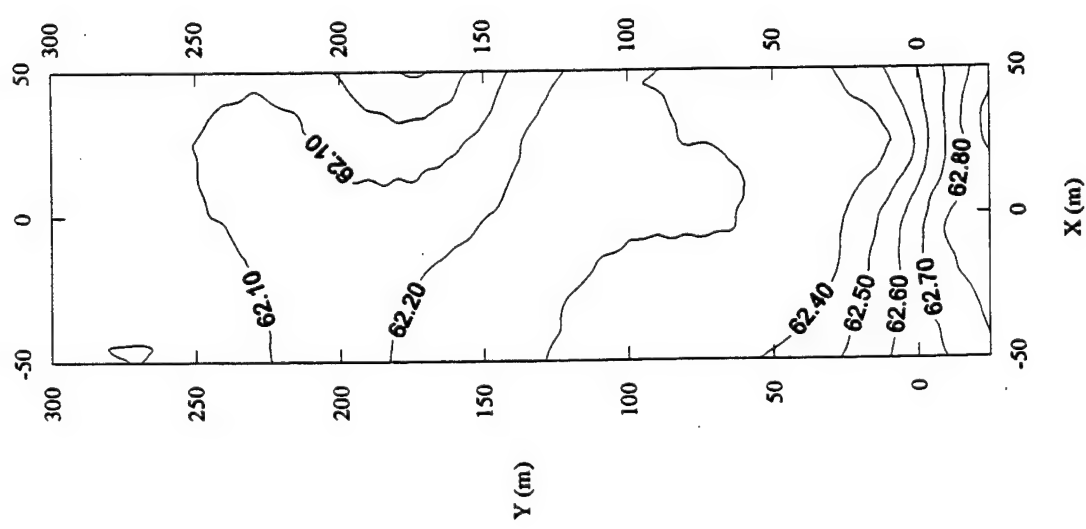


Figure A-12. Upper and Lower Kriged Heads of June 13, 1991.

Upper Screened Heads of July 9, 1991



Lower Screened Heads of July 9, 1991

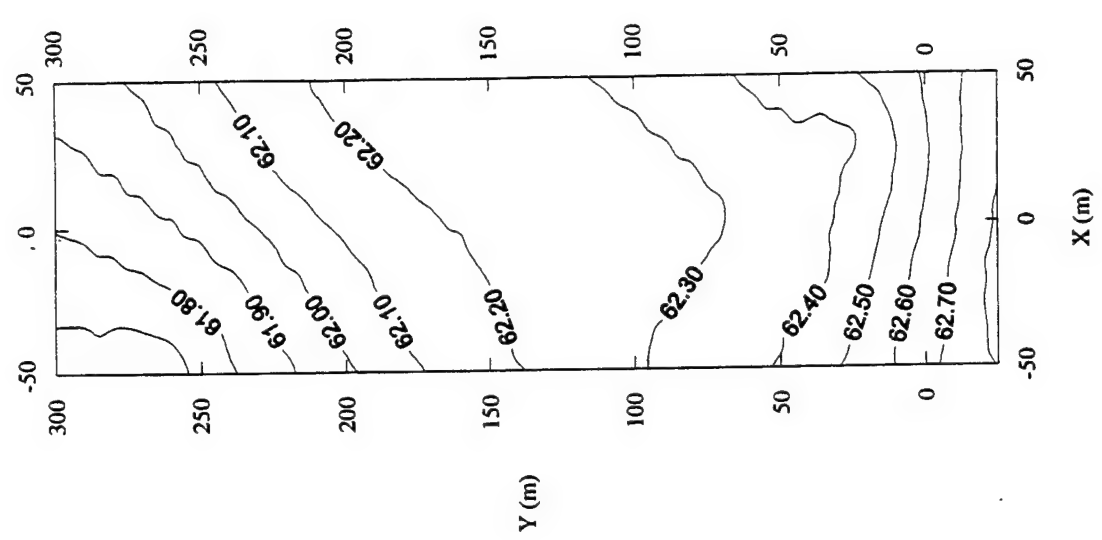
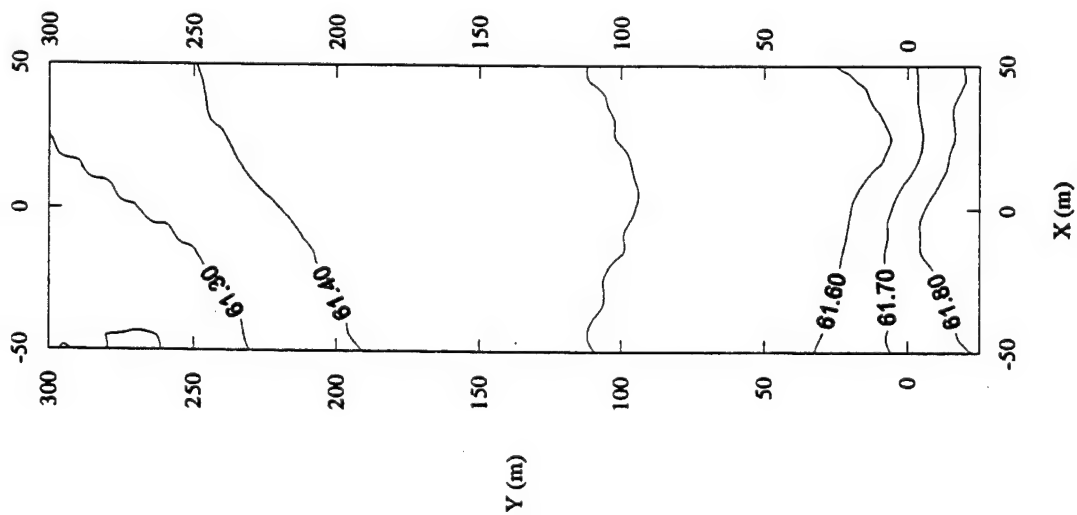


Figure A-13. Upper and Lower Kriged Heads of July 9, 1991.

Upper Screened Heads of August 19, 1991



Lower Screened Heads of August 19, 1991

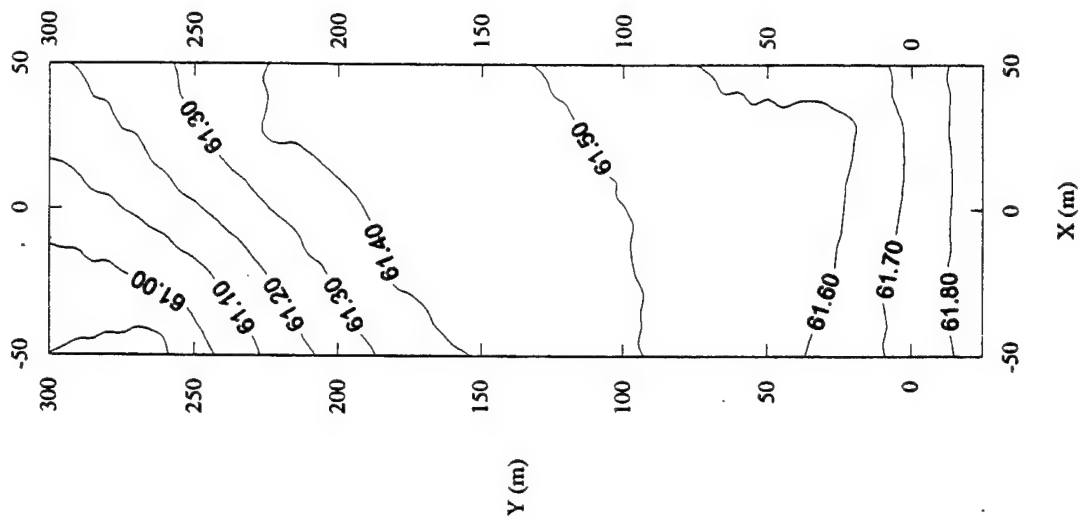
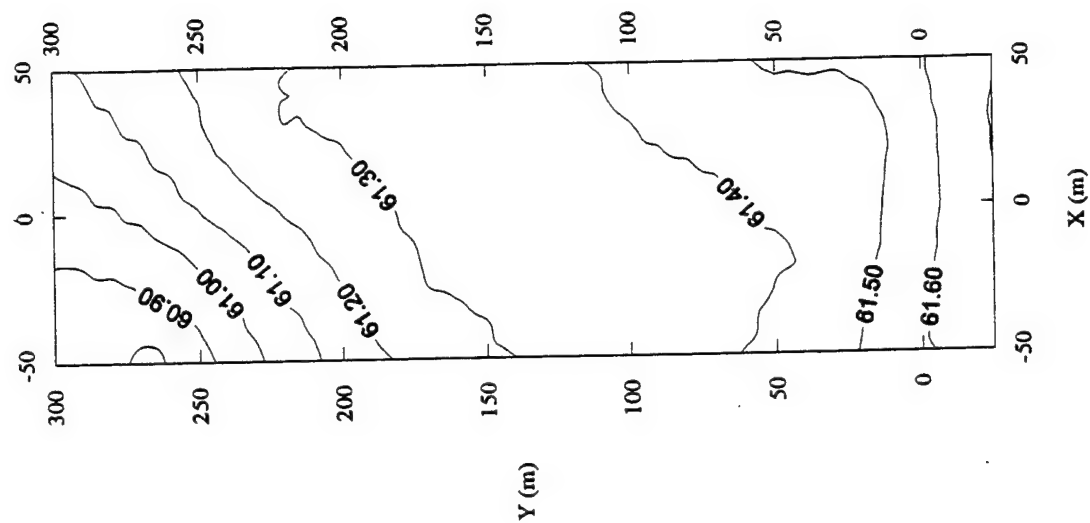


Figure A-14. Upper and Lower Kriged Heads of August 19, 1991.

Lower Screened Heads of September 11, 1991



Upper Screened Heads of September 11, 1991

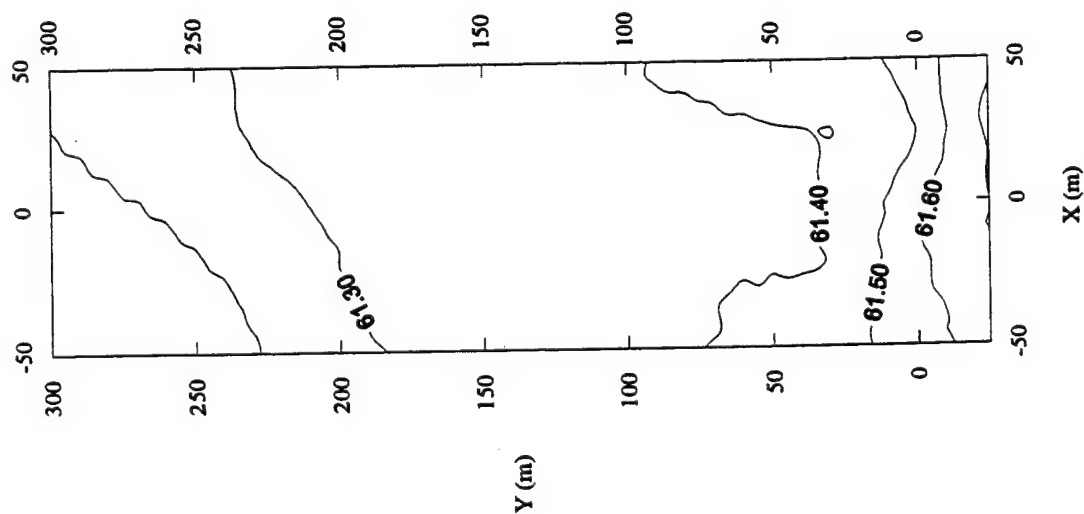


Figure A-15. Upper and Lower Kriged Heads of September 11, 1991.

## **APPENDIX B**

### **KRIGED TRANSMISSIVITY AND LEAKANCE FOR M2-8-8**

**Based on borehole flowmeter data through K81**

**(See Figure 19 for Layer 3.)**

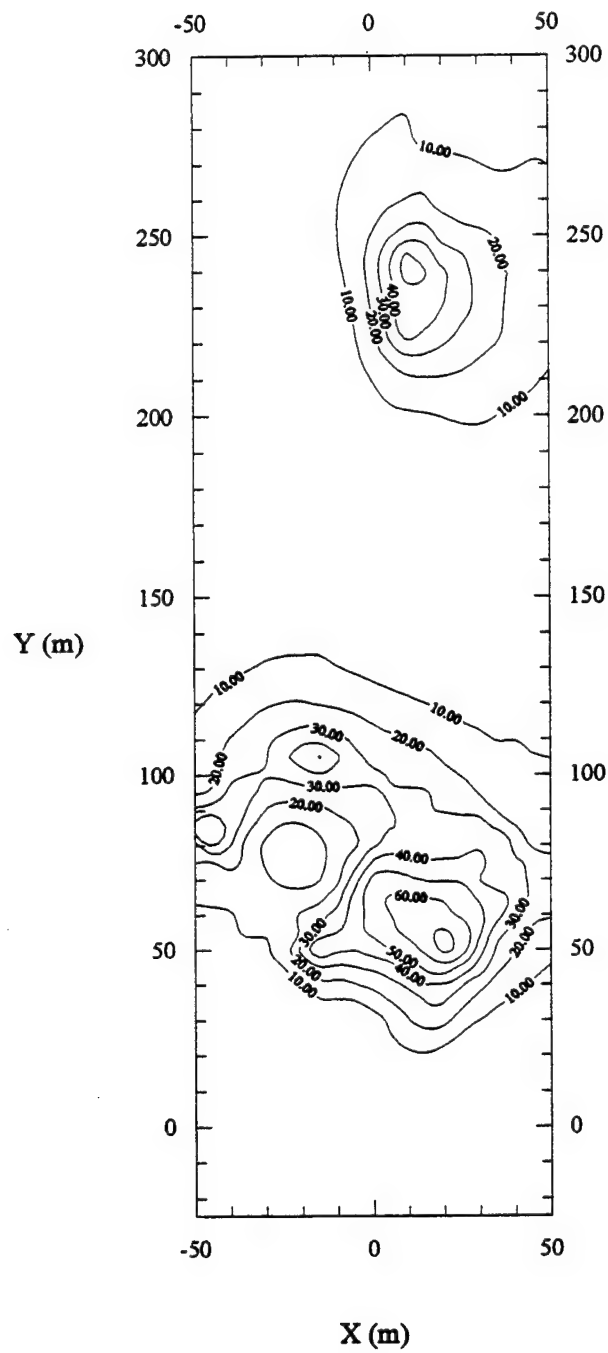


Figure B-1. Hydraulic Conductivity [m/d] of Layer 1.



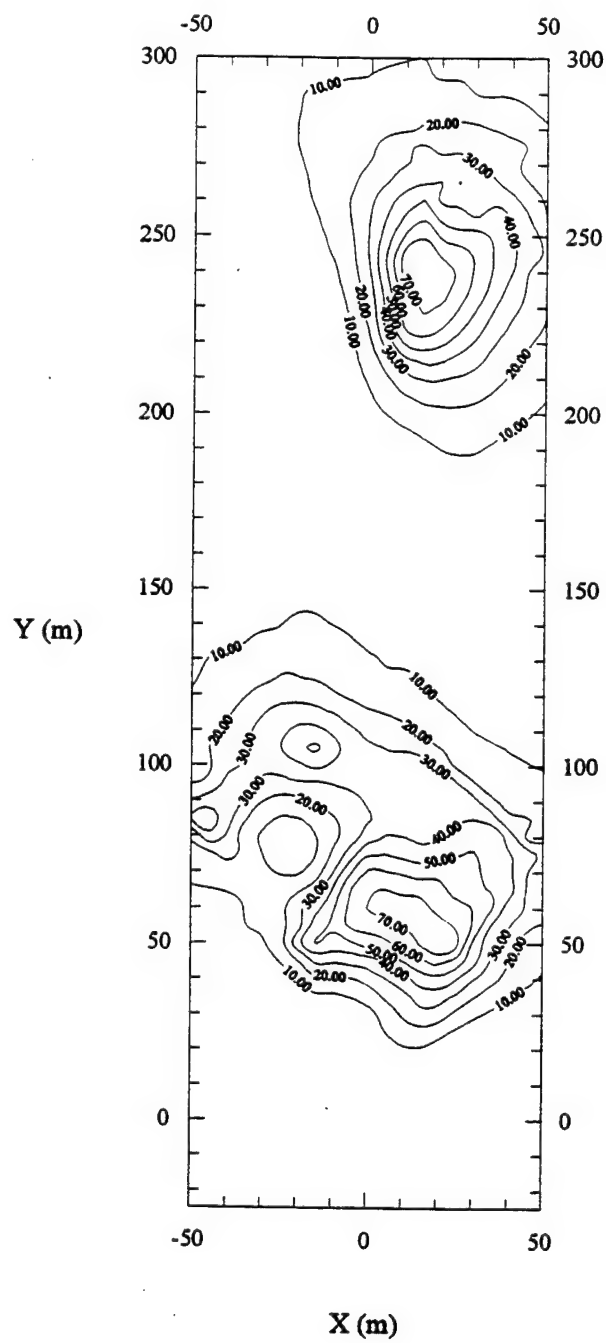


Figure B-2. Transmissivity [ $\text{m}^2/\text{d}$ ] of Layer 2.

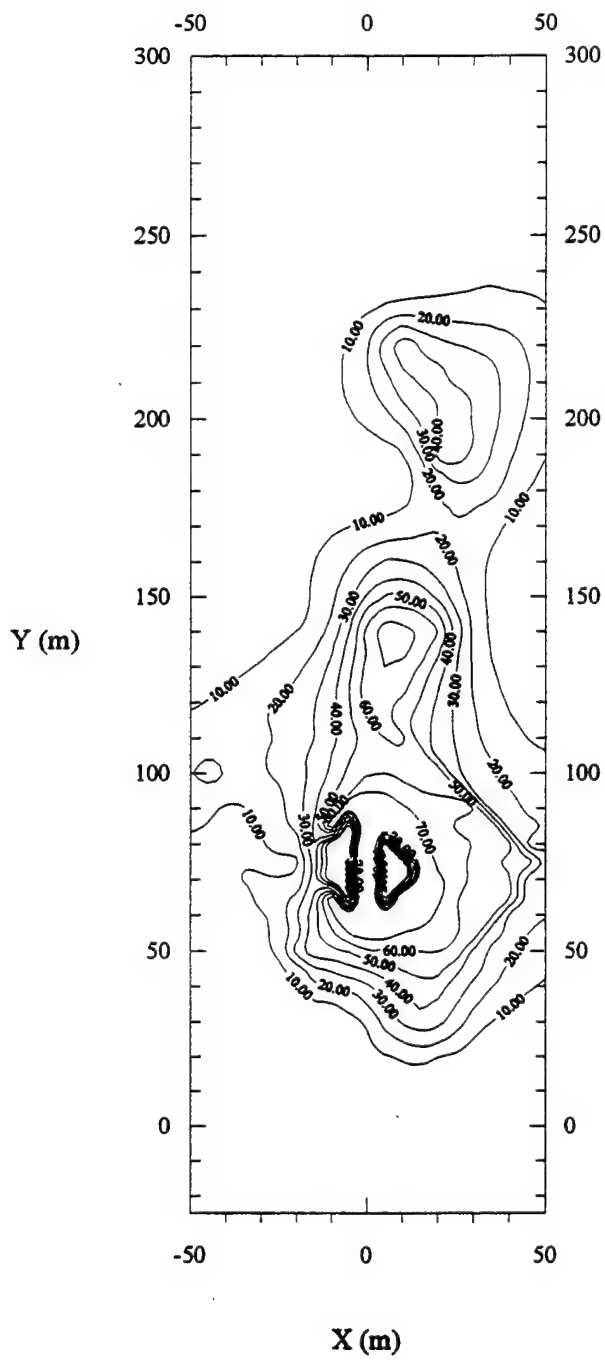


Figure B-3. Transmissivity [ $\text{m}^2/\text{d}$ ] of Layer 4.

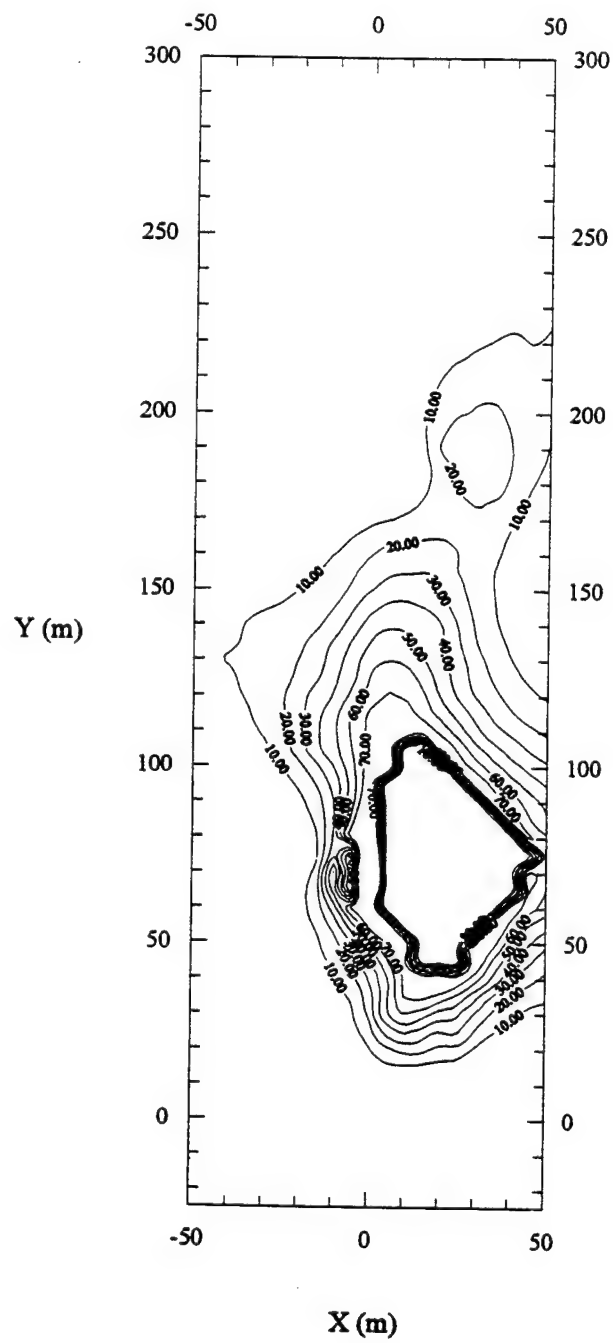


Figure B-4. Transmissivity [ $\text{m}^2/\text{d}$ ] of Layer 5.

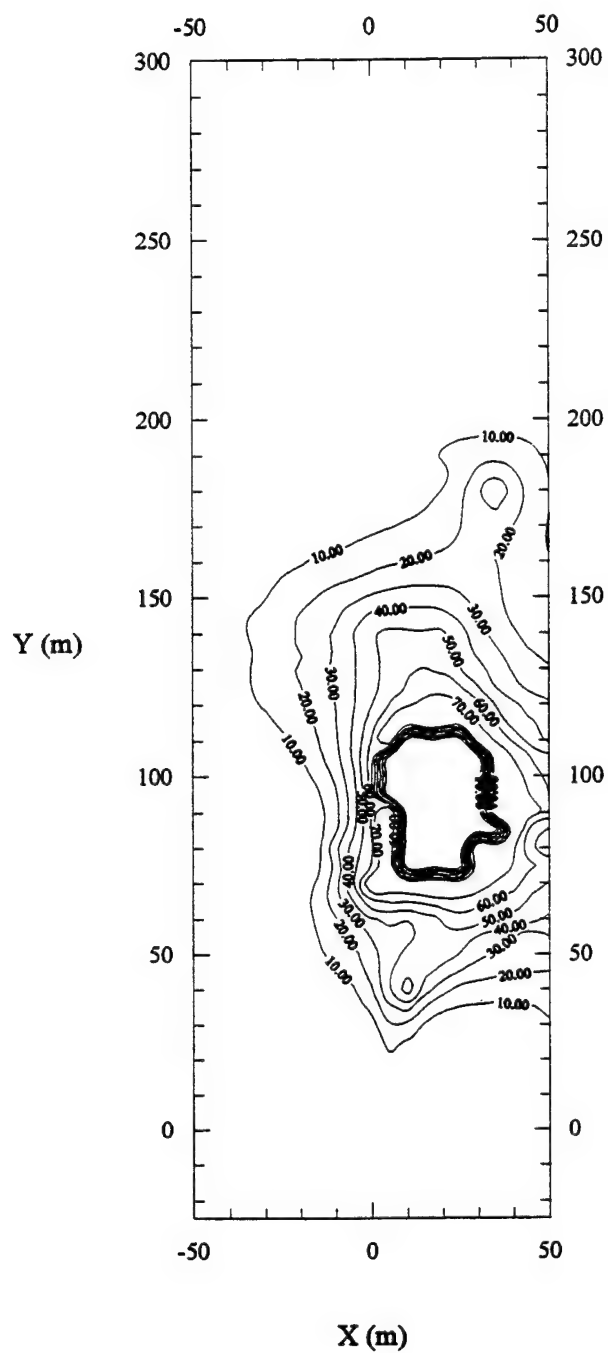


Figure B-5. Transmissivity [ $\text{m}^2/\text{d}$ ] of Layer 6.

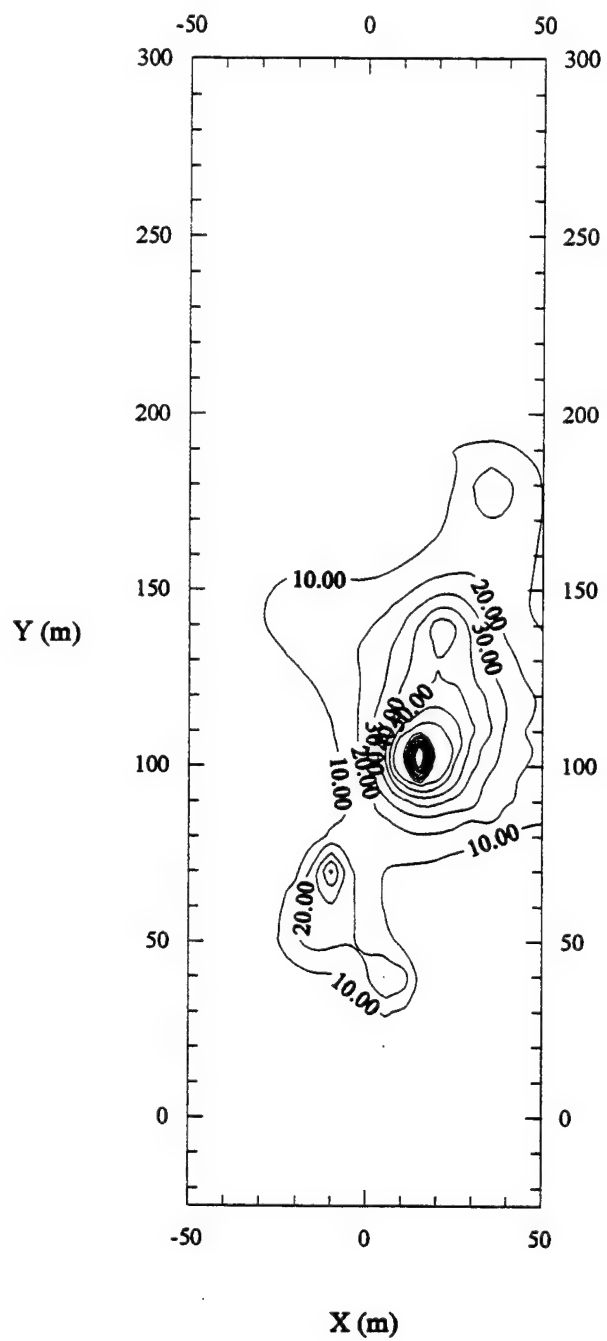


Figure B-6. Transmissivity [ $\text{m}^2/\text{d}$ ] of Layer 7.

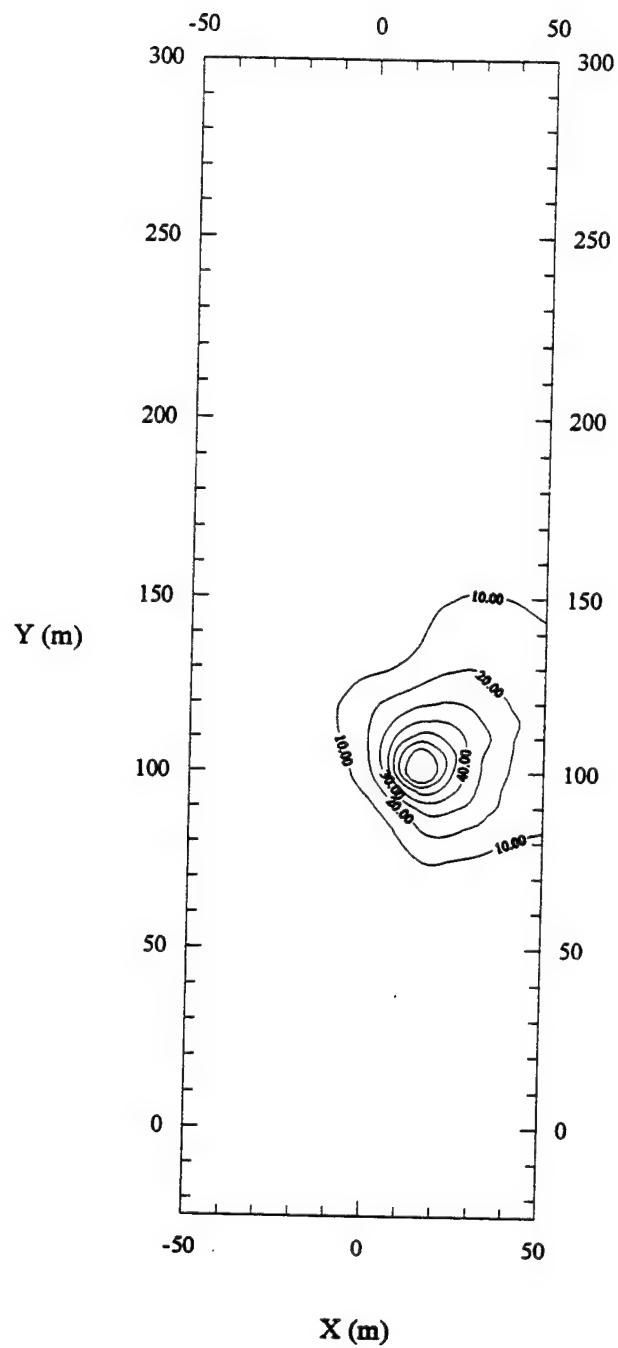


Figure B-7. Transmissivity [ $\text{m}^2/\text{d}$ ] of Layer 8.

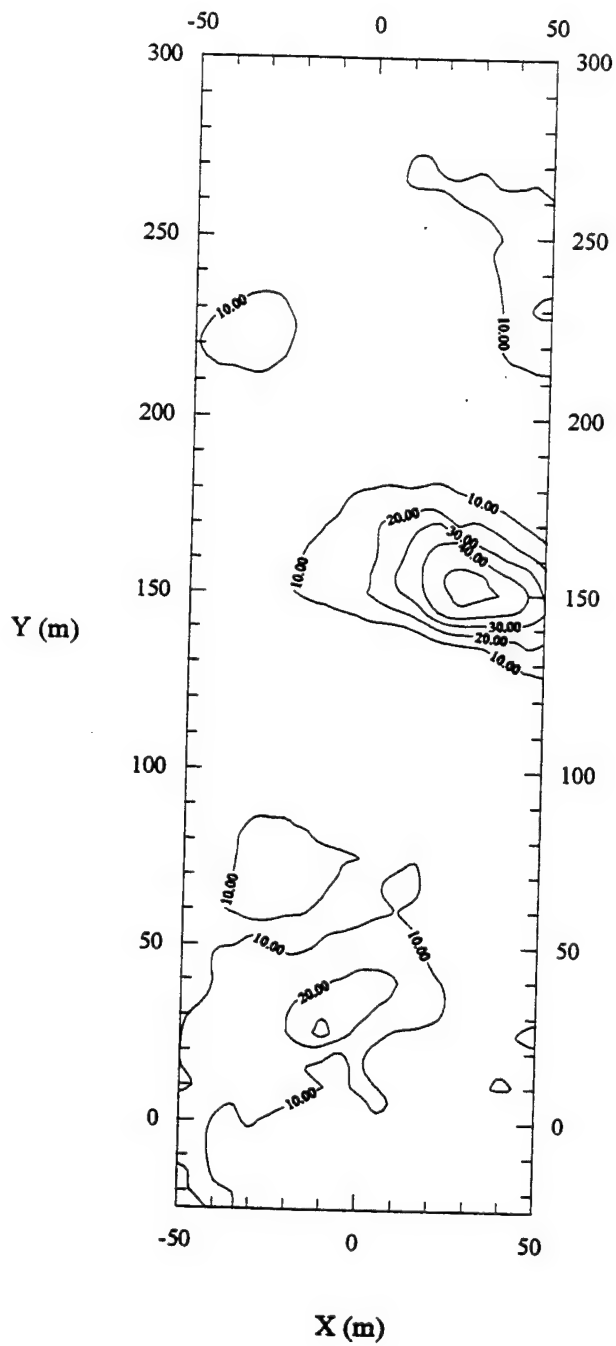


Figure B-8. Transmissivity [ $\text{m}^2/\text{d}$ ] of Layer 9.

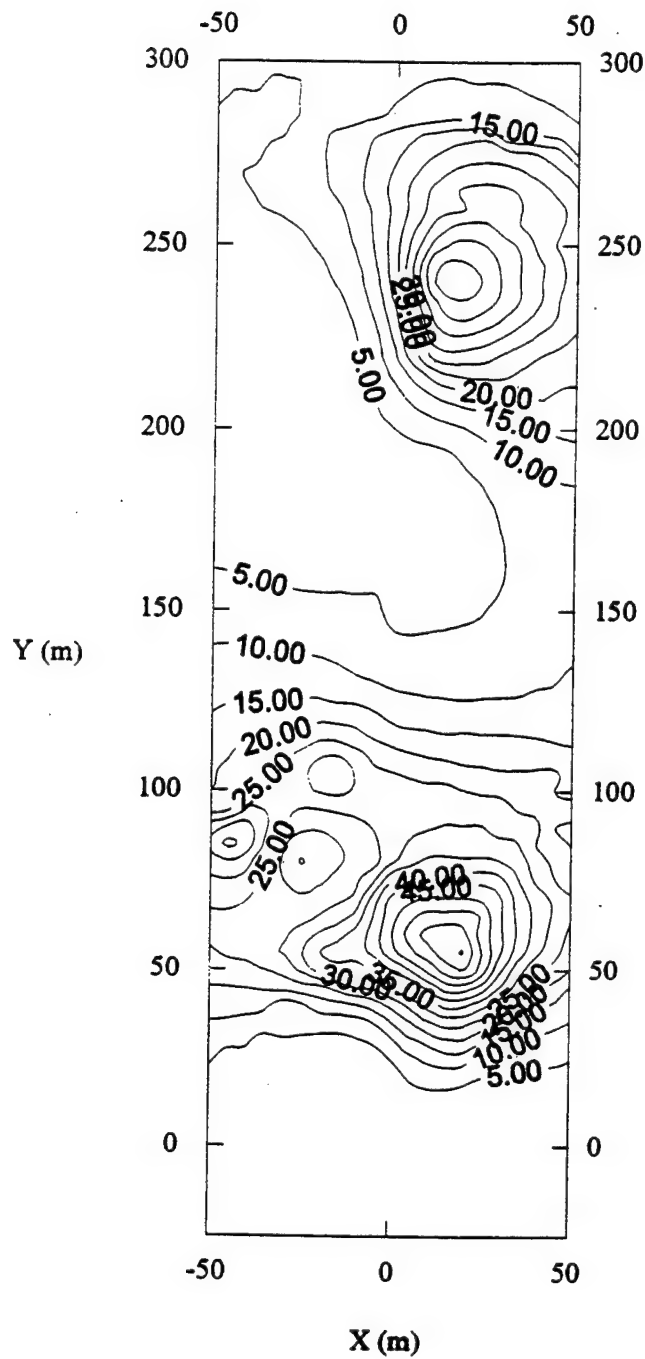


Figure B-9. Leakance  $[1/d]$  of Layer 1.



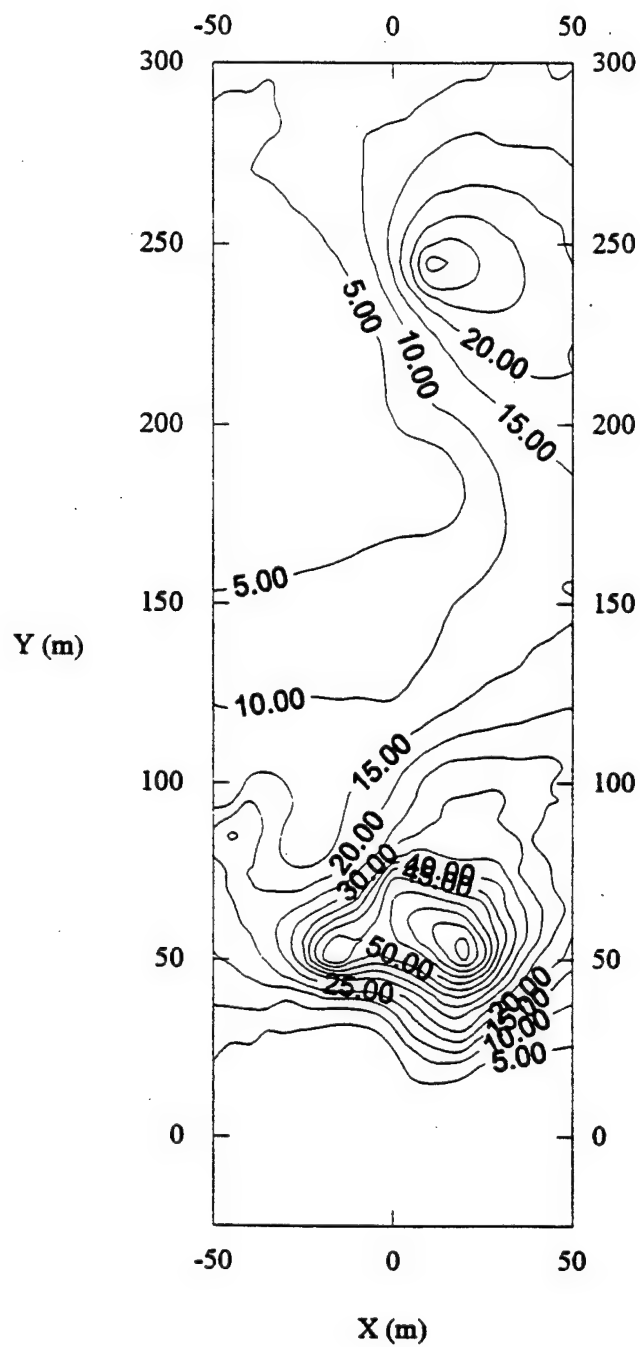


Figure B-10. Leakance [1/d] of Layer 2.

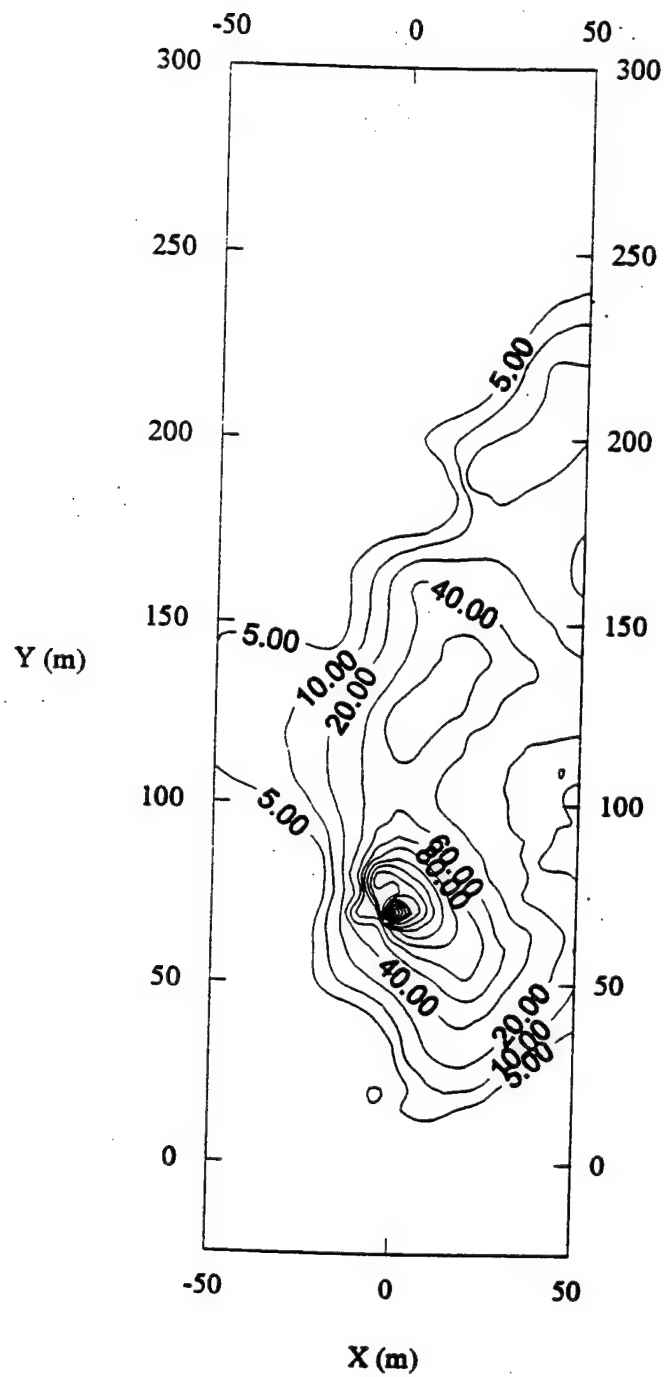


Figure B-11. Leakance  $[1/d]$  of Layer 4.

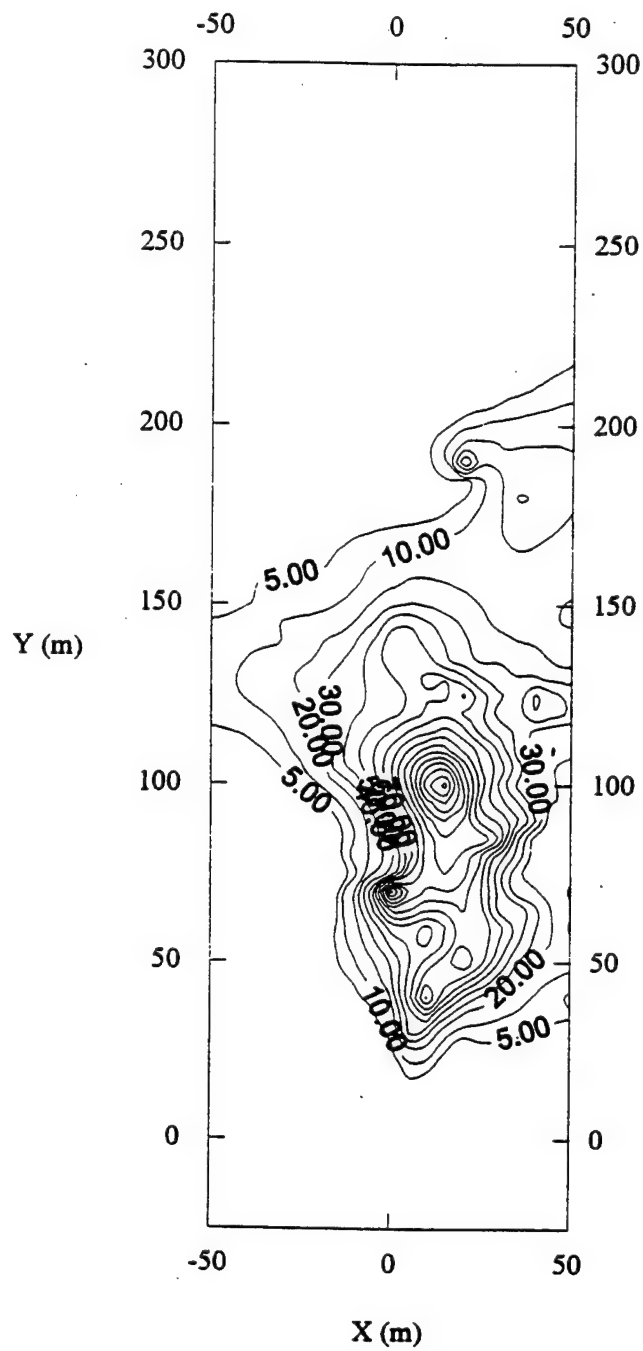


Figure B-12. Leakance [1/d] of Layer 5.

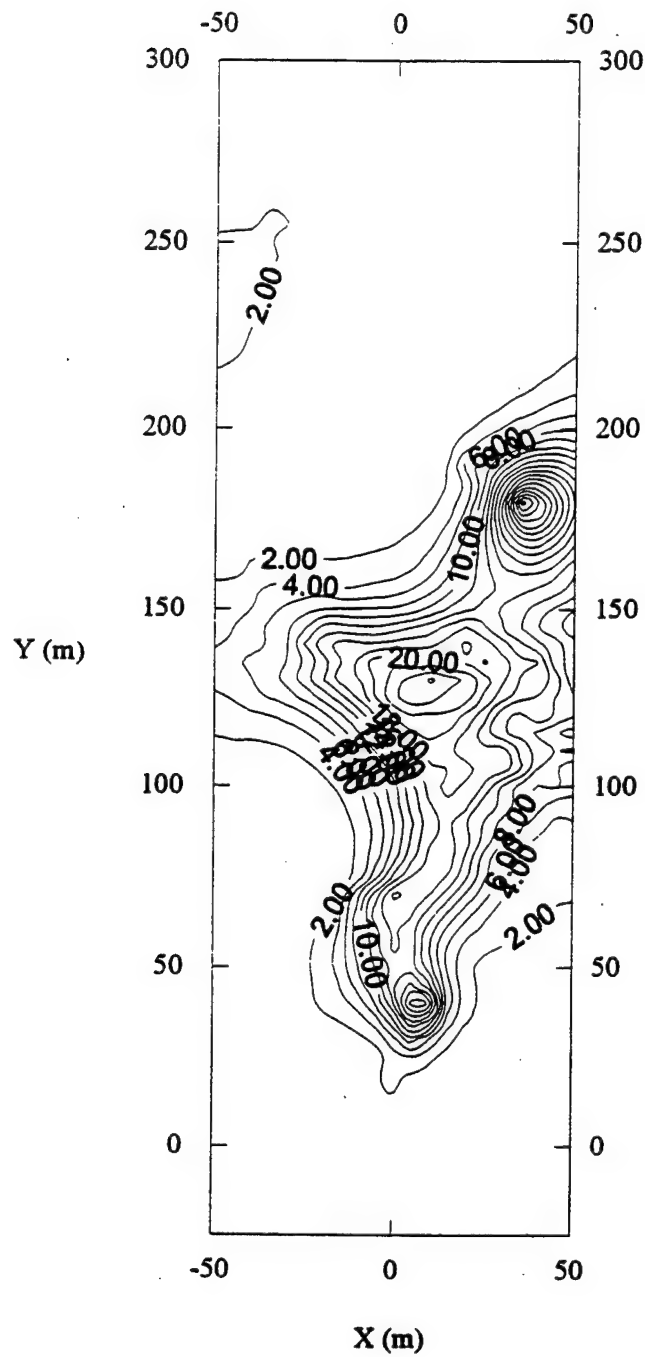


Figure B-13. Leakance  $[1/d]$  of Layer 6.

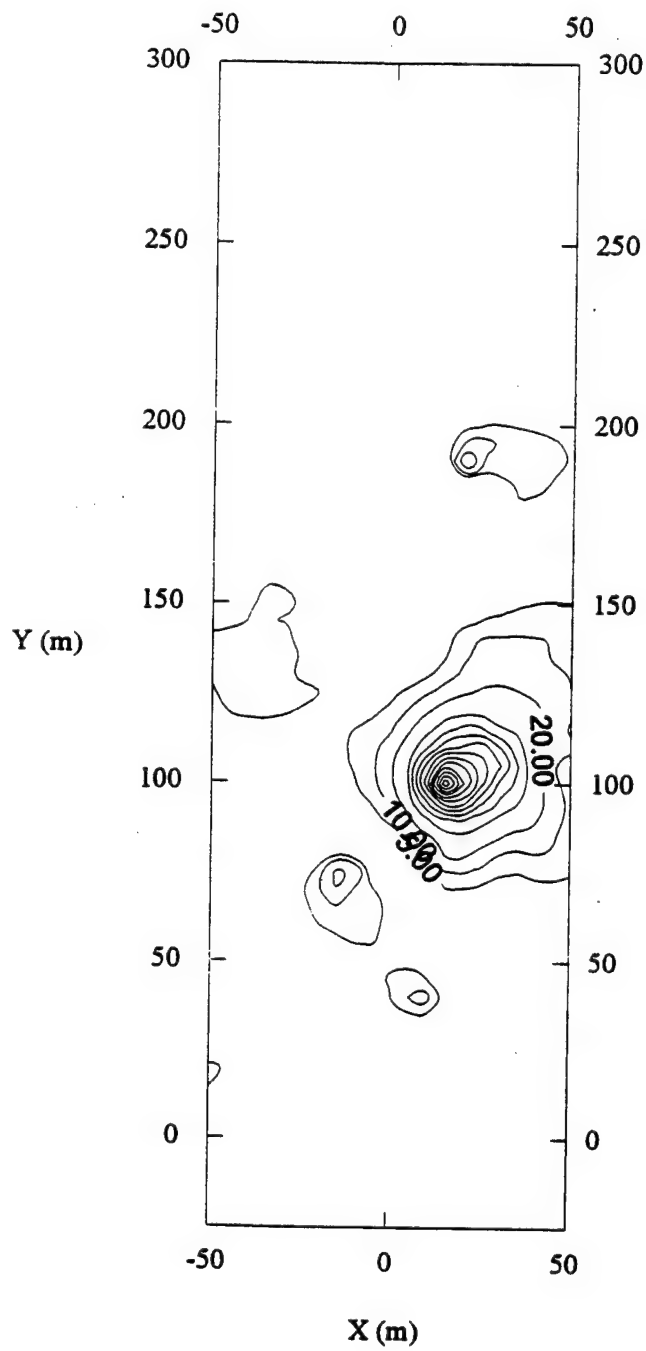


Figure B-14. Leakance  $[1/d]$  of Layer 7.

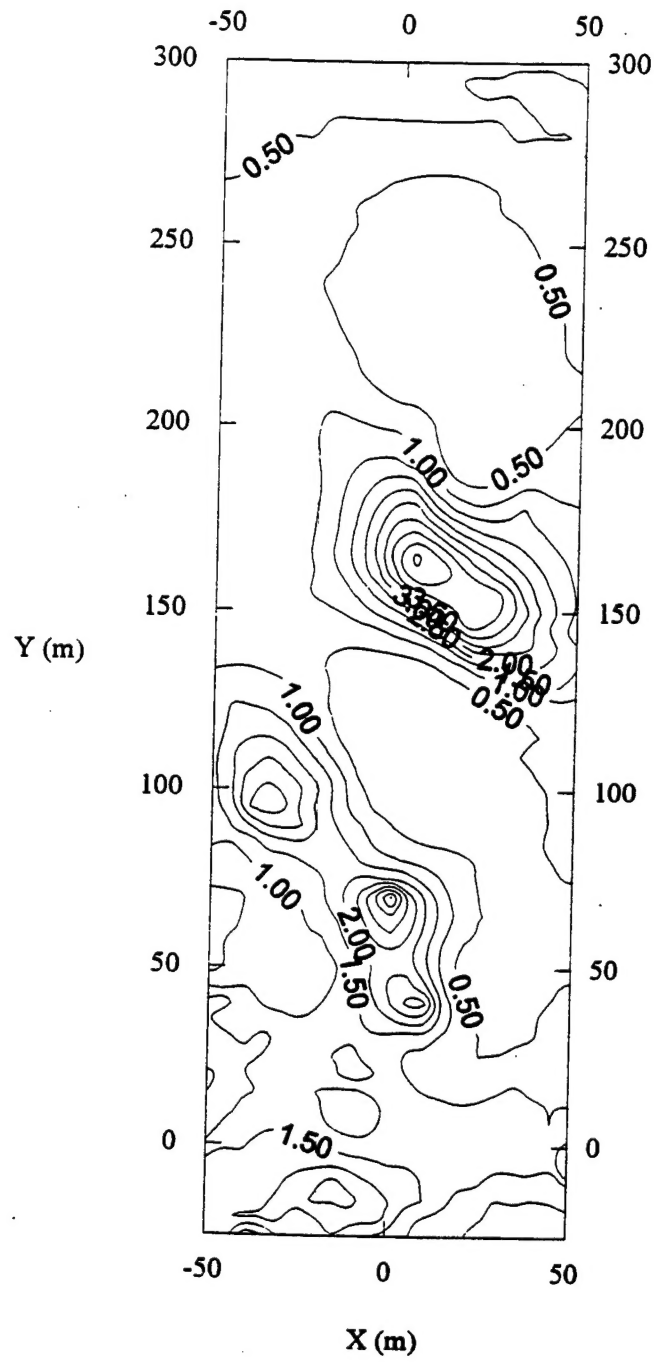


Figure B-15. Leakance  $[1/d]$  of Layer 8.

# APPENDIX C CHANGES TO MODFLOW SOURCE CODE FOR MF95

These are the changes to the MODFLOW source code to produce MF95.FOR:

- 1) In the BCF2AL subroutine, space allocation needs to be larger.

Change:

```
LCTRPY = ISUM
ISUM = ISUM+NLAY
```

To:

```
LCTRPY = ISUM
ISUM = ISUM+ISIZ
```

- 2) In the BCF2RP subroutine,

Change:

```
DIMENSION HNEW(NODES), SC1(NODES), HY(NODES), CR(NODES),
1      CC(NODES), CV(NODES), ANAME(6,11), DELR(NCOL),
1      DELC(NROW), BOT(NODES), TOP(NODES), SC2(NODES),
1      TRPY(NLAY), IBOUND(NODES), WETDRY(NODES),
1      CVWD(NODES)
```

To:

```
DIMENSION HNEW(NODES), SC1(NODES), HY(NODES), CR(NODES),
1      CC(NODES), CV(NODES), ANAME(6,11), DELR(NCOL),
1      DELC(NROW), BOT(NODES), TOP(NODES), SC2(NODES),
1      TRPY(NODES), IBOUND(NODES), WETDRY(NODES),
1      CVWD(NODES)
```

and change:

```
CALL UIDREL(TRPY,ANAME(1,8),NLAY,IN,IOUT)
CALL UIDREL(DELR,ANAME(1,9),NCOL,IN,IOUT)
CALL UIDREL(DELC,ANAME(1,10),NROW,IN,IOUT)
```

C

C2-----READ ALL PARAMETERS FOR EACH LAYER

KT=0

KB=0

```

DO 200 K=1,NLAY
KK=K
C
C2A-----FIND ADDRESS OF EACH LAYER IN THREE DIMENSION ARRAYS.
IF(LAYCON(K).EQ.1 .OR. LAYCON(K).EQ.3) KB=KB+1
IF(LAYCON(K).EQ.2 .OR. LAYCON(K).EQ.3) KT=KT+1
LOC=1+(K-1)*NIJ
LOCB=1+(KB-1)*NIJ
LOCT=1+(KT-1)*NIJ
C
C2B-----READ PRIMARY STORAGE COEFFICIENT INTO ARRAY SC1 IF TRANSIENT
IF(ISS.EQ.0)
CALL U2DREL(SC1(LOC),ANAME(1,1),NROW,NCOL,KK,IN,IOUT)

to:

CALL U1DREL(DELR,ANAME(1,9),NCOL,IN,IOUT)
CALL U1DREL(DELC,ANAME(1,10),NROW,IN,IOUT)
C
C2-----READ ALL PARAMETERS FOR EACH LAYER
KT=0
KB=0
DO 200 K=1,NLAY
KK=K
C
C2A-----FIND ADDRESS OF EACH LAYER IN THREE DIMENSION ARRAYS.
IF(LAYCON(K).EQ.1 .OR. LAYCON(K).EQ.3) KB=KB+1
IF(LAYCON(K).EQ.2 .OR. LAYCON(K).EQ.3) KT=KT+1
LOC=1+(K-1)*NIJ
LOCB=1+(KB-1)*NIJ
LOCT=1+(KT-1)*NIJ
C
C2B-----READ PRIMARY STORAGE COEFFICIENT INTO ARRAY SC1 IF TRANSIENT
CALL U2DREL(TRPY(LOC),ANAME(1,8),NROW,NCOL,KK,IN,IOUT)
IF(ISS.EQ.0)
CALL U2DREL(SC1(LOC),ANAME(1,1),NROW,NCOL,KK,IN,IOUT)

```



\*Note: The new TRPY variable is to be read by the U2DREL array reader before each SF1 array (if transient, or transmissivity if steady-state), as opposed to being read by the U1DREL array reader before DELR.

3) In BCF2FM, SBCF1C, SBCF2H, and SBCF2N, changes need to be made by changing the dimensions of TRPY (NLAY) to TRPY (NCOL, NROW, NLAY).

4) The last changes are to be made to the SBCF1C subroutine.

Change:

YX=TRPY(K)

C

C1----FOR EACH CELL CALCULATE BRANCH CONDUCTANCES FROM THAT CELL

C1----TO THE ONE ON THE RIGHT AND THE ONE IN FRONT.

DO 40 I=1,NROW

DO 40 J=1,NCOL

T1=CC(J,I,K)

to:

C YX=TRPY(K)

C

C1----FOR EACH CELL CALCULATE BRANCH CONDUCTANCES FROM THAT CELL

C1----TO THE ONE ON THE RIGHT AND THE ONE IN FRONT.

DO 40 I=1,NROW

DO 40 J=1,NCOL

T1=CC(J,I,K)

YX = TRPY(J,I,k)

This is the end of the changes to MODFLOW.